Maximum power point tracking techniques for photovoltaic water pumping system

Aashoor, Fathi

Award date:
2016

Awarding institution:
University of Bath

UNIVERSITY OF BATH

Maximum power point tracking techniques for photovoltaic water pumping system

Fathi A O Aashoor

A thesis submitted for the degree of Doctor of Philosophy

Department of Electronic and Electrical Engineering

University of Bath

May 2015

ABSTRACT

An investigation into the design of a stand-alone photovoltaic water pumping system for supplying rural areas is presented. It includes a study of system components and their modelling. The PV water pumping system comprises a solar-cell-array, DC-DC buck chopper and permanent-magnet DC motor driving a centrifugal pump. The thesis focuses on increasing energy extraction by improving maximum power point tracking (MPPT). From different MPPT techniques previously proposed, the perturb and observe (P&O) technique is developed because of its ease of implementation and low implementation cost. A modified variable step-size P&O MPPT algorithm is investigated which uses fuzzy logic to automatically adjust step-size to better track maximum power point. Two other MPPT methods are investigated: a new artificial neural network (ANN) method and fuzzy logic (FL) based method. These use PV source output power and the speed of the DC pump motor as input variables. Both generate pulse width modulation (PWM) control signals to continually adjust the buck converter to maximize power from the PV array, and thus motor speed and the water discharge rate of a centrifugal pump.

System elements are individually modelled in MATLAB/SIMULINK and then connected to assess performance under different PV irradiation levels. First, the MP&O MPPT technique is compared with the conventional P&O MPPT algorithm. The results show that the MP&O MPPT has faster dynamic response and eliminates oscillations around the MPP under steady-state conditions. The three proposed MPPT methods are implemented in the simulated PV water pumping system and compared. The results confirm that the new methods have improved energy extraction and dynamic tracking compared with simpler methods.

ACKNOWLEDGEMENTS

I am grateful to acknowledge and thank all of those who assisted me in my graduate program at the University of Bath. Frist, I would like to thank my supervisor Dr. Francis Robinson, he gave me the opportunity to conduct this research under his guidance and supervision. I received motivation, encouragement and support through the period of my research with boundless patience.

I would also like to express my sincere thanks to all my friends at University of Bath and in parts of the UK and in Libya for their constant support and encouragement.

Last, but not the least, I would like to express my deep gratitude my family, specially parents for their continuous encouragement and unlimited support. I would like to extend my thankfulness to my wife and my daughter for their support through my study. Their understanding helped me to reach my potential and complete my study. My family has been an important part and source of encouragement of this life-changing experience.

TABLE OF CONTENTS

LIST OF FIGURES

LIST OF TABLES

LIST OF SYMBOLS

η_{MPPT}	Tracking efficiency
A	Ideal diode quality factor depending on PV technology
A_L	Load friction
B_m	Viscose torque constant for rotational losses
C	Capacitor
D	Duty ratio
d	Diode
D_j	Ideal p-n diode
D_{mp}	Duty ratio corresponding to the maximum power output
dP	The total power change between two sampling periods
dV	The total voltage change between two sampling periods
e	Induced electromotive force
E_{gap}	Band-gap energy of the semiconductor used in the cell
f_s	dc/dc Converter switching frequency
G	Solar radiation
G_D	The scaling factor the duty ratio variation
G_I	The scaling factor of the PV array output current variation
G_P	The scaling factor of the PV array output power variation
G_r	Reference solar radiation
G_S	The scaling factor of the variable step-size
G_ω	The scaling factor of the rotation speed variation
I_a	Armature current of DC motor
I_C	Capacitor current
I_D	Diode internal diffusion current
I_d	Input current of converter
I_{inm}	The maximum input current of the DC/DC converter
i_L	Inductor current
$I_{MP,\,Ref}$	Maximum power point current at reference condition
I_{MPP}	Current at maximum power point or optimal current
I_o	output current of converter
I_{om}	The maximum output current of the DC/DC converter
I_{ph}	Photocurrent or light generated current
I_{PV}	Output current of the solar cell
I_{RS}	Photovoltaic cell reverse saturation current
I_S	Photovoltaic cell dark saturation current
I_{SC}	Short-circuit current of the photovoltaic model
$I_{SC,\,Ref}$	Short circuit current at reference condition
J	Moment of inertia
k	Boltzmann's constant
K_e	Back electromotive force constant of DC motor

K_I	Temperature coefficient of the cell's short circuit current
K_L	The proportional constant of the load torque
K_{SC}	PV short circuit current proportional constant
K_t	Constant of electromagnetic torque
K_V	PV open circuit voltage proportional constant
L	Inductance
L_a	Armature inductance of DC motor
η	The learning rate of the ANN
N_P	Number of connected PV cells in parallel
N_S	Number of connected PV cells in series
o_{pj}	The measured output of the outputs of the neurons
P_{actual}	The real measured power produced by the PV array
P_e	Electric power of the motor
P_{in}	Input power of the converter
P_{max}	Maximum power point
P_{out}	Output power of the converter
P_{peak}	Peak power
P_{PV}	Output power of the solar cell
q	The charge of electron
R_a	Armature resistance of DC motor
R_{opt}	Optimum operating point of the resistive load
R_S	Series resistance of the photovoltaic cell
R_{Sh}	Shunt resistance of the photovoltaic cell
S	Switch
T	Photovoltaic cell's operating temperature
T_C	Photovoltaic cell's operating temperature in kelvin
T_e	Electromagnetic torque of DC motor
T_L	Load torque
t_{off}	Off period of converter switch
t_{on}	On period of converter switch
T_p	The torque required to drive the pump
t_{pj}	The desired output of the output neurons
T_{Ref}	Photovoltaic cell reference temperature
T_S	DC/DC converter switching period
V_a	Armature voltage of DC motor
V_C	Capacitor voltage
V_D	Voltage applied across the diode terminals
V_d	Input voltage of the converter
V_{inm}	The maximum input voltage of the DC/DC converter
v_L	Inductor voltage
V_{max}	Voltage at maximum power of the PV array
$V_{MP,\,Ref}$	Maximum power point voltage at reference condition
V_{MPP}	Voltage at maximum power point or optimal voltage

V_o	Average output voltage of the converter
V_{OC}	Open-circuit voltage of the photovoltaic model
$V_{OC,\,Ref}$	Open circuit voltage at reference condition
V_{om}	The maximum output voltage of the DC/DC converter
V_{PV}	Output voltage of the solar cell
w_n	The weight on the connection between the network layers
x_x	The input of the ANN
y_n	The output of the ANN
α_{Ref}	thermal voltage timing completion factor at reference condition
γ	The momentum factor
ΔD	The duty ratio variation
ΔI_{PV}	The PV array output current variation
ΔP_{PV}	The PV array output power variation
$\Delta\omega_m$	The rotation speed variation
θ	The bias or threshold
Φ	Flux
ω_m	Rotational speed of DC motor

LIST OF ABBREVIATIONS

AC	Alternating Current
ANN	Artificial Neural Network
ANNC	Artificial Neural Network Controller
CCM	Continuous Current Mode
COG	Centre of Gravity
CV	Constant Voltage method
DC	Direct Current
dP-P&O	Improved Perturb and Observe method
emf	Electromotive force
EPP	Estimate Perturb and Perturb method
FF	Fill Factor
FIS	Fuzzy Interface System
FL	Fuzzy Logic
FLC	Fuzzy Logic Controller
GUI	Graphical User Interface
HM	Height Method
IC	Incremental Conductance
INC	Incremental Conductance
LCB	Linear Current Booster
MOM	Mean of Maximum
MP&O	Modified Perturb and Observe method
MPP	Maximum Power Point
MPPT	Maximum Power Point Tracking
MSE	Mean Square Error
OC	Open Circuit
OP&O	Optimized Perturb and Observe
P&O	Perturb and Observe
PMDCM	the Permanent Magnet Direct Current Motor
PV	Photovoltaic
PWM	Pulse Width Modulation
SC	Short Circuit

CHAPTER 1 - INTRODUCTION

Water is essential for life and for most activities of human society. Most of the human activities and needs rely upon ready access to adequate water supplies such as; ensuring food production, and protecting health, energy and the restoration of ecosystems. All societies require water for social and economic development and for sustainable development [1]. However, the UN World Water Development Report in 2003 provided an estimation of the number of people, who have no access to the water sources in forty eight countries and it was found that, two billion people are affected by water shortage, and 1.1 billion do not have sufficient drinking water [2]. Also, in the UN World Water Development Report 2014, it has been estimated that 3.5 billion people do not have their right to water satisfied and 2.5 billion people lack access to improved water supply [3]. Water pumping has throughout history been a technical challenge. There has always been a need to supply drinking water and satisfy regular agricultural demands throughout the development of civilization in human societies [4]. There is a great and urgent need to supply sustainable energy for the provision of drinking water at very low financial and environmental cost, especially in relatively poor, arid, rural regions. Without basic services, such regions are likely to become aid dependent or depopulated and unproductive, especially when expectations are raised by modern information and communications technology. Remote PV water pumping and PV power generation systems, generally, seem to be an excellent solution to assist with this problem into the future.

In this thesis, a stand-alone photovoltaic water pumping system is presented along with theoretical studies and mathematical modelling of its operation and the performance of the PV source. It also investigates in detail the maximum power point tracker, a power electronic system that extracts the maximum available power from a PV source for use in the load. To increase the system efficiency, different maximum power point tracking techniques have been investigated and improved MPPT techniques are proposed. These have been tested and assessed by developing MATLAB simulations of the systems and by making comparisons between the proposed MPPT techniques.

In the rural areas, pumping systems are needed to pump the water for domestic usage, to irrigate crops, to water cattle and animal stocks, etc. Hence a source of power is needed to operate the pumping system [5]. An AC powered system would be economic and takes minimum maintenance when the AC power is available from the nearby grid. However, in many rural areas, water sources are spread over many miles of land and the located too far away from the existing grid lines. Installation of a new transmission line and transformers at isolated locations is extremely expensive [5]. Windmills have been installed traditionally in such areas but because of the lack of proper maintenance and age, many of them are not operating now. There are many internal combustion engines that are used for a stand-alone water pumping systems nowadays. These systems have the same advantages, such as: they are portable and easy to install but they require frequent site visits for refuelling and maintenance, and in addition, the diesel is expensive and not readily available in rural areas of many developing countries and even the fuel is available within the country, transporting the fuel to remote, rural villages because there are no roads or supporting infrastructure in most of the remote villages [5].

The consumption of fossil fuels also has an environmental impact; it is considered the major cause of climate change due to their polluting effects. The energy consumption is accompanied by a release of carbon oxide (CO2) into the atmosphere and it contributes for more than of 60% of the global CO2 emitted in the atmosphere each year [6]. The increase in global demand for energy combined with the pollution concern caused by fossil fuels has encouraged scientists to search for environmentally friendly sources of energy. The problem associated with CO2 emissions can be solved through the application of renewable energy technologies, which are already cost competitive with fossil fuels in many situations [7]. Therefore, the use of renewable energy is a very attractive for water pumping systems in the rural areas of many developing countries.

Solar energy generation via PV cells is a very attractive renewable source. Its advantages include relatively light-weight, low-complexity structural requirements, although systems may extend over large areas; free and sustainable fuel source; noise free operation due to the absence of large rotating machinery or engine parts other than slow sun-tracking mechanisms; the possibility of application close to the point

of use; ease of installation; relatively predictable availability in certain geographical regions; and systems require relatively little regular maintenance [8].

Photovoltaic energy, has gained a lot of attention in recent years because it is environmentally friendly and sustainable compared to traditional energy sources. Good examples include large-scale grid-connected wind turbines, solar water heating, and off-grid stand-alone PV systems [7].
It is estimated that the PV electricity will contribute with 7% of the world electricity needs by the year 2030, and this will increase to reach 25% by the year 2050 [9].
Most of the current installed capacity of PV plants is in the United State of America (USA) and Spain. Photovoltaic is one of the fastest growing technologies in the world which has annually growth rate of 35-40% [10]. Sharp Corporation of Japan installed the first PV plant in 1963 with the capacity of 242 W which was the world largest PV plant at that time. In 2000, the cumulative global capacity of PV panels was installed is 1.5 GW which then increased with annual growth rate of 40% to reach around 70 GW at the end of 2011. From 2010 to 2011, the annual PV installations increased by 78% to each almost 30.4 GW. The global installed capacity of PV panels in 2012 was around 31.1 GW and the cumulative installed capacities become around 102.2 GW [11].

The utilization of PV water pumping systems helped both in improving the living conditions in remote areas and keeping the environment clean. The PV water pumping systems are being installed worldwide. In 1993, there were around 10 thousand systems installed, and in 1998 the number of installed systems increased up to six times to reach almost 60 thousand systems [4].

Internationally, previous studies have shown that the main rural application areas are located in Asia, Africa and Latin-American. I these locations there are available wells along with plenty of uninterrupted sunshine favouring solar PV water pumping. In Mexico around 206 PV water pumping systems were installed from 1994 to 2000, a survey where conducted to determine the user’s approval and the result was; the percentage of users agreed that PV pumping systems are very economical were around 55%, where 39% of the users said it to be economical and the rest which

represent 6% of the users considered the these systems as not economically feasible [12].

Many states in India are implementing PV water pumping systems especially the southern states where these systems found big acceptance among small farmers. The utilization potential of PV water pumping systems has a great increase in India because they provide clean and reliable power. Over a period of 5 years India put a target of installing about 50,000 PV water pumping systems from 2008 to 2012 [13].

In Namibia there are many people depending on boreholes as the main water source. There are more than 40,000 boreholes in use, from which water is pumped for households, farming and agricultural activities [12]. A comparison study has been conducted for solar and diesel water pumping systems taking into account the life-cycle costs, comprising the initial upfront cost, the operating cost maintenance costs and replacement costs. The comparison showed that even with a higher upfront cost the PV pumps can compete with diesel pumps which usually have lower upfront cost but because of ongoing diesel and intensive maintenance costs. The total cost over 20 years was around € 13,900 for a PV pumping system and around € 39,000 for a diesel pumping system at diesel price of € 0.92/Litre. However, the total cost increases further with the increase of the diesel price, and it would reach € 46,100 when the diesel price is € 1.10/Litre [12].

1.1 Photovoltaic system

The photovoltaic system consists of interconnected components designed in a way to achieve the specific target of delivering the desired electricity from a small device to the load. Photovoltaic systems are categorized by the main categories of grid-connected, stand-alone systems and hybrid system which comprises different sources of energy such as PV arrays, diesel generators and wind generators. In the grid-connected and the stand-alone systems, storage elements such as batteries or super capacitors may be adopted to store the energy during the day time when there is enough sunshine. Hybrid and stand-alone systems are used increasingly in rural areas [14, 15]. Therefore, the PV water pumping system considered in this thesis is a stand-alone system to fulfil the urgent needs of people in the rural locations.

1.1.1 Stand-alone system

The power from the photovoltaic array in the stand-alone system is directly fed to the load without connection to the utility system. The stand-alone system is considered one of the most economic ways of implementing a photovoltaic system especially for application in rural areas that have large periods of intense solar radiation and have no access to the main utility grid. Examples are communication systems, water pumping systems, lighthouses and emergency services or military applications where the auxiliary power units are needed. The stand-alone systems have some drawbacks, such as low-capacity-factor storage elements, cost and limited capacity storage batteries leading to the dissipation and waste of the surplus energy generated. The stand-alone systems have some important features as follows [14, 15]:

- As a consequence of not connecting this system to the utility grid, a storage element is needed to store the electricity during the off peak demand periods, leading to extra battery and storage cost, otherwise the generated power has to be dissipated.

- In stand-alone systems, the operational capacity must be matched to the maximum load demand.

1.2 PV water pumping system energy storage

The PV water pumping system is like any other pumping system such as wind turbine pumps: it constitutes an intermittent source of power. The system performs well during periods of intense sunlight; but the system output is susceptible to change during cloud cover, and gradually falls and rises at the beginning and end of the day. There is a total loss of output during night time when it is dark, unless a storage element is available such as a battery; or in the case of water pumping systems, a storage tank is filled and empties more slowly by the force of gravity [16].

A PV water pumping system is always categorized in two ways according to the design. The simplest approach is to connect PV system directly, consequently the system consist of a PV array directly connected to a DC motor and a pump without using battery backup. This type of systems is relatively simple and low-cost and is used for smaller application. The second configuration includes battery storage as

backup during the night [17]. Lead-acid battery technology is considered to be the most cost effective for many PV systems due to its relatively low cost and wide availability. In addition, batteries are able to satisfy transient surges of current that are much higher than the instantaneous current directly obtainable from a PV array [18]. However, this process leads to extra power loss since approximately 15-25% of the energy is lost during charging and discharging processes and the PV array must be oversized to cover the energy losses. The typical life-time of the battery in PV systems is around three to eight years, but in hot climate countries this goes down to typically two to six years since the internal corrosion dramatically increases with high ambient temperature. Furthermore, the batteries require regular maintenance and will degrade very rapidly if the electrolyte is not topped up. Therefore, these factors add significantly to the system cost and maintenance burden [7]. The battery efficiency is typically 85%, however, this reduces to below 75% in hot countries [7]. Although more efficient battery technologies are available such as lithium-ion, they are relatively expensive and charging requirements are more sophisticated. Consequently, the use of battery energy storage is not the most efficient, cost effective option for more isolated, continuously high-duty pumping. Energy in a water pumping system can be alternatively stored using water tanks to store the water to be used at night and on days when the solar radiation is insufficient to operate the system.

1.3 The proposed PV water pumping system

The Matlab Simulink water pumping system proposed in this thesis is a stand-alone type. This will be used with a water storage tank instead of using battery storage, to satisfy an isolated, remote, low maintenance and low cost water-pumping application. The system mainly comprises photovoltaic array as source, converting the sunlight into electrical energy, and a centrifugal pump load driven by permanent magnet DC motor as shown in Fig. 1.1. To achieve high efficiency system performance and to increase the amount of energy extracted from the PV array by the load during the daylight hours, a maximum power point tracker will be included in the system.

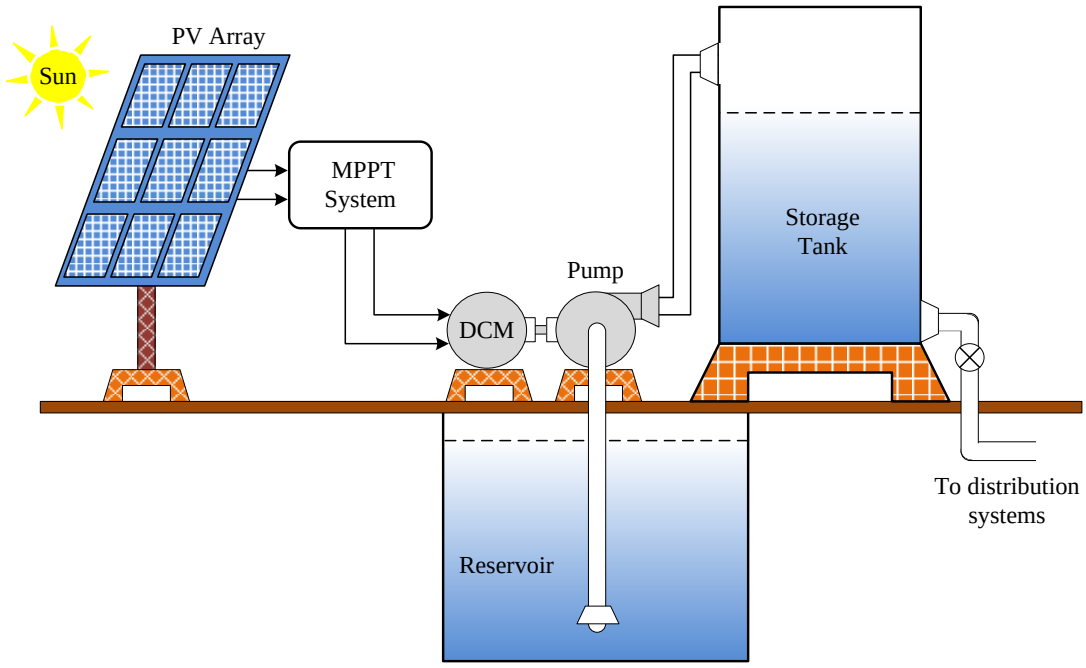

Fig. 1.1 Block diagram of the proposed stand-alone PV water pumping system

The elements of such a photovoltaic system will be described in detail in the following chapters and mathematical models will be developed to represent the behaviour of each element in a complete system simulation.

1.4 Photovoltaic Water pumps and motors

The stand-alone photovoltaic (PV) water pumping system has received increasing attention in the last 20 years because of the significant, on-going cost reductions achieved in manufacturing PV arrays. Past studies of PV energised water pumping systems have previously considered a number of suitable pumps and motors [19-23]. Two types of pumps are widely employed in PV systems: the centrifugal pump and volumetric pump. The centrifugal pump is capable of pumping a high volume of water and operating at relatively high efficiency. These pumps are used to pump the water from boreholes and from surface water reservoir and they are ideally suitable for medium to high water demands. There are two categories of centrifugal pumps are commercially available: submersible (stacked impeller) and non-submersible (vertical turbine, floating, and surface centrifugal). Similarly, there are two types of volumetric pumps are commercially available and they categorised: submersible (diaphragm) and non-submersible (piston, jack, and rotary vane). The volumetric pumps are usually used when a low flow rate is required [19]. The centrifugal

pumps have operational characteristics which well match with the PV array. However, the operational characteristics of the volumetric pumps are not a good match to the output of PV array. This is because the motor driving volumetric pump requires high starting current and they require constant current for a given head. Whereas, the PV array current varies almost linearly with the solar radiation [16].

As the maximum energy available from solar panels is in the form of slowly changing DC, the pumps are usually driven by DC motors to minimize system complexity since they can be directly connected to the PV panel or array [20]. Separately-excited and permanent magnet (PM) brushed DC motors are often recommended for PV pumping system [21-23]. The permanent magnet types however, are more popular than the separately-excited types, because the rotation of the motor is caused by the brushed commutator without inducing the surrounding magnetic field electrically. Hence there is no power consumed in field windings, which increasing the efficiency and reduces the size of the PV array of the system. The brushed motors have the disadvantage that they require frequent maintenance due to wear and clogging of the commutator and sliding brush contacts [16]. Brushless DC motors become increasingly used in PV pumping systems because they have a relatively high efficiency and require low maintenance, but the cost and complexity of the system will be significantly higher [24].

The use of other types of DC brushed and AC motors have also been investigated, such as shunt [25] and series DC motors [26], permanent magnet synchronous motors (brushless DC motors) and AC induction motors [27]. AC motors have attractive features such as high efficiency, brushless configuration, simpler geometry and rugged construction; and initial cost can be lower in the case of the cage induction motor. However, a detailed analysis of DC and AC motors used in PV pumping has been carried out in [28] and it was concluded that the efficiency and dynamic performance of permanent magnet DC motor is better than an AC single phase induction motor. Additionally, if AC motor is used an inverter is required to convert the DC output of the PV array to AC power to drive the motor. Consequently, the cost and complexity of the overall system significantly increases.

1.5 Photovoltaic efficiency and maximum power point tracking

While the photovoltaic panels may seem like a good source of electricity, their conversion efficiency is not very high. Their ability to convert sunlight energy to electrical power is relatively imperfect, with conversion efficiency typically in the range 12 ~ 20%. The range of efficiency can drop further during variable solar irradiation, panel temperature and load conditions [29]. Therefore, if the load is directly coupled to the PV array, the PV array must usually be oversized to supply the required power to the load. This leads to an over-sized expensive system. It is important to operate the PV-cells of the array at the maximum power point, MPP, or as near to it as possible, by using an electronic load-matching circuit, since this gives a worthwhile improvement in the available power in comparison with direct load connection [30]. The output current and power of a PV array depends on the terminal voltage. Moreover, the available output power of PV array fluctuates with change in ambient temperature and solar irradiation. Therefore, the operating point of most DC motor and pump systems over varying solar radiation levels would be far from the MPP of the PV array. It is a challenge to track the exact MPP with varying source and load conditions due to the non-linear voltage-current characteristic of the PV array. The overall system cost can be reduced, and operation is possible at increased efficiency and output power capacity, if the solar panel is constantly used to extract as much power as possible during day time by ensuring that the panel is always operating under optimal power delivery conditions; rather like impedance matching allows maximum power to be extracted from a voltage/signal source with appreciable internal resistance. To accomplish this, electronic maximum power-point tracker (MPPT) systems are employed. A typical MPPT system consists of a switch-mode power-converter inserted between the PV source and the load, and the duty ratio of the converter is controlled by a control algorithm to enable tracking of the MPP [8]. A large amount of research work has been carried out by different researchers and designers to investigate power converter and control methods to track the MPP of a photovoltaic module and a number of methods exist because no single method or system outperforms the others in all respects [8, 30-33].

In recent years, many different techniques or algorithms for automatically identifying and producing operation at approximately the maximum power point have been presented with practical implementations in the literature. These methods vary in

complexity, cost, range of effectiveness, hardware implementation, popularity, convergence speed, and in other respects. In [34, 35] at least nineteen distinct techniques are analysed and compared to determine their advantages and disadvantages. These are summarised in a performance table as a helpful guide for choosing the appropriate MPPT method for a specific PV system. The maximum power point tracking methods can be classified as incremental conductance (IncCond) [30], fractional short-circuit current [32], fractional open-circuit voltage [33], load current voltage maximization, ripple correlation control, hill climbing or perturb and observe (P&O) [31], neural network [36], fuzzy logic control and other MPPT methods [34, 37]. So far, the P&O method is the most commonly used technique in practice, owing to its ease of implementation in a low cost controller, and it has relatively good MPP tracking performance when compared to the other techniques. Nevertheless the P&O method fails to track the MPP effectively when radiation and temperature conditions change rapidly. The algorithm also oscillates around the MPP or near to it when the conditions slowly change or are constant. Consequently, part of the available energy is wasted [38].

Many authors have proposed different improvements to the basic P&O algorithm [39-44]. For example, the incremental conductance method is used to overcome the oscillation by comparing the incremental and instantaneous conductance of the PV array. However, the control system requirements are more complex and add appreciable cost to the whole system [45]. The fractional short-circuit current and fractional open-circuit voltage methods are simple, but both techniques share the same drawbacks. These include error due to linearization approximation and power loss caused by the extra measures and necessity to short-circuit or open-circuit the PV array for short periods [34]. The operating concept of each MPPT technique will be further discussed in detail in the next chapter along with their advantages and disadvantages.

1.6 A Simple Maximum Power Point Tracking System

A typical MPPT-PV stand-alone power system comprises photovoltaic array modules, load and step-down (Buck) switching DC/DC converter, acting as the power interface between the PV array and the load as illustrated in Fig. 1.2. The

system will be used to test the performance of proposed MPPT techniques with two load types. Three MPPT algorithms have been designed and implemented in MATLB SIMULINK in this work.

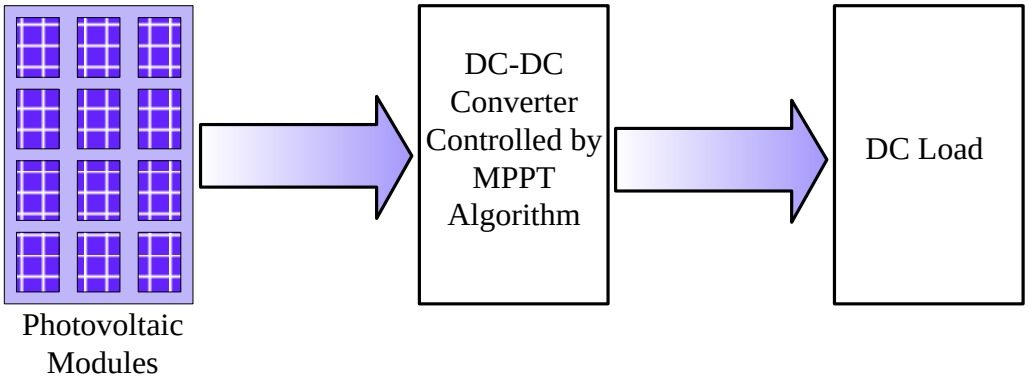

Fig. 1.2 Block Diagram of the Proposed MPPT-PV System.

The first algorithm is called the modified perturb and observe (MP&O) method. The second and third techniques involve fuzzy logic and neural network based MPPT of PV Water Pumping System. The simulation test is divided into two parts: firstly, the MP&O method has been tested in the system using a resistive load to verify its improvement compared with the conventional perturb and observe (P&O) method. Secondly, the proposed MP&O, fuzzy logic and neural network techniques are implemented in the system with a DC water pump load as shown in Fig. 1.1 to verify the improvement in the system efficiency with each technique. Moreover, a comparison has been carried out between the three proposed MPPT techniques in the same system to find the most efficient one.

1.7 Research objectives

The overall aim of this thesis is to investigate the performance of a stand-alone water pumping system. This will be energised entirely from a photovoltaic (PV) source via a power–electronic DC-DC power converter with no connection to battery energy storage or smoothing to minimise any maintenance. The system comprises a PV array, DC-DC power converter, permanent magnet DC motor and a centrifugal pump. Changing atmospheric conditions will have an effect on the output characteristics of the PV array, and the need for a maximum power point tracking system will be considered. To increase the system efficiency, the performance of

different MPPT techniques and different types of DC-DC converter will be studied and investigated. The main focus will be to investigate how to improve the MPPT in a stand-alone PV water pumping system by implementing more efficient MPPT technique. Accordingly, the research objectives of this thesis may be summarised as follows:

- Model and study the photovoltaic array output characteristics and investigate how to increase the efficiency of PV water pumping system by increasing the system's efficiency.

- Investigate and study the characteristics of motor and pump with the characteristics of the PV array of the stand-alone PV water pumping system operating without MPPT system.

- Investigate and analyse the effect of irradiation and temperature changes on the output characteristics of the PV array and investigating how to capture the maximum energy during favourable sunshine exposure and deliver the maximum power to the load.

- To study different types of DC-DC converter and investigate which converter is the most suitable for a stand-alone PV water pumping system. Also various types of MPPT techniques will be investigated to find the most efficient technique for the system.

- Optimize and develop more efficient MPPT techniques to increase the efficiency of the stand-alone PV water pumping system.

- Implement the PV water pumping system in MATLAB/SIMULINK to test the overall system efficiency using the proposed MPPT techniques in a directly connected system (without an MPPT system). Furthermore, to compare the total efficacy of the PV water pumping system using the proposed MPPT techniques under similar dynamic and steady state weather conditions, and identify the most efficient technique of all the proposed MPPT techniques.

1.8 Thesis outlines

The thesis is organised into eight chapters and the content of these is discussed below.

CHAPTER 1

This introductory chapter presents an overview of the project background, objectives, scope and a brief summary of the thesis. It presents a brief introduction to PV energy, its history and how increasing fuel cost and emissions make PV water pumping systems attractive and economically viable in remote locations. Moreover, this chapter provides brief description of the proposed stand-alone PV water pumping system and the MPPT system.

CHAPTER 2

Chapter 2 provides a review of the literature on the maximum power point tracking algorithms or methods along with their functionalities, computational flow structure, and mathematical equations. It presents and briefly explains simple panel load matching, the load switching technique, constant voltage (CV) method, perturb and observe (P&O) method, and incremental conductance (INC) method, fractional short-circuit current (SC) method, and fractional open-circuit voltage (OV) method. The issues of power fluctuations around MPP and tracking speed of MPP are discussed, and the possible improvements under different weather conditions are investigated. These improvements were mostly investigated with the P&O algorithm because of its simplicity and ease of implementation. Therefore, different techniques for optimizing the P&O algorithm have also been investigated along with their advantages and disadvantages, such as, using combined the P&O constant voltage (CV) MPPT methods, improved *dP*-P&O algorithm, optimized P&O algorithm (OP&O), modified perturb and observe (MOP&O) method and estimate perturb and perturb (EPP) method.

CHAPTER 3

Chapter 3 explains the relevant semiconductor physics and the operation of photovoltaic cells in order to understand how the photovoltaic cell converts the energy of the solar radiation to electrical energy, and shows how the PV cells are interconnected in order to build PV modules. It gives an overview of the photovoltaic

model and introduces the functional principles and the characteristics of the PV panels and illustrates how the output voltage and current of the PV array are affected by changes of irradiation and temperature.

Chapter 3 provides a discussion and investigation of the different types of DC-DC power converter used in PV MPPT systems. The chapter covers only the non-isolated converters which are commonly used in the PV stand-alone systems, such as, the Buck converter, Boost converter, Buck-Boost converter and Cuk converter. The electrical circuit and operating principle of each converter is considered in order to select the most suitable and efficient converter for a stand-alone PV water pump system implementation.

This chapter also provides a discussion of the best combination of a DC motor and load pump to be used in the proposed stand-alone PV water pumping system. The mathematical model of the load which is a permanent magnet DC motor coupled to a centrifugal pump is presented. Furthermore, the characteristics of a system involving directly connecting the load to the PV array without MPPT are presented. The problems arises from this direct connection is discussed to show the importance of the MPPT.

CHAPTER 4

This chapter introduces a fuzzy logic control (FLC) based MPPT for PV water pumping systems. It provides a brief history of fuzzy logic control development and applications, and illustrates its basic structure and the working principles. It then provides a discussion of the proposed fuzzy logic control based MPPT method for the PV water pumping system and shows the complete block diagram of the system. It also provides a detailed explanation of the proposed FLC process and illustration of operation when tracking the MPP.

CHAPTER 5

Chapter 6 proposes an artificial neural network control based MPPT for PV water pumping systems. The chapter starts with introducing the development history of the ANN and its main applications. The chapter provides a brief explanation of the working principles including the learning and testing processes of the ANN. Then the construction of the proposed ANN controller is presented and the collection of

training data sets which is used for training the proposed ANN controller is discussed in detail along with the training process.

CHAPTER 6

This chapter introduces a modified perturb and observe MP&O method with variable step-size which is implemented using fuzzy logic control. The chapter begins by introducing the limitations of the conventional P&O algorithm with a fixed step-size. It then presents how the proposed MP&O overcomes these limitations by employing a variable step-size method. The flow chart of the MP&O algorithm is presented with the adapted FLC system for adjusting the step-size, and the operating principle of the proposed MP&O method is discussed in detail.

CHAPTER 7

Chapter 7 presents the MATLAB/SIMULINK implementation of the system and describes each of the subsystems in detail, including the PV cell model, buck converter, permanent magnet DC motor connected to a centrifugal pump load and the proposed maximum power-point tracker techniques. This chapter also discusses and compares the MATLAB results for the proposed maximum power-point tracking algorithms applied to photovoltaic water pumping system. It also shows the behaviour and performance of each method in terms of time convergence, available power, and dynamic adjustment performance under similar conditions of temperature and irradiation.

CHAPTER 8

The conclusions and contribution summary of the thesis are presented. Moreover, potential research ideas for future work in this field are proposed.

CHAPTER 2 - LITERATURE REVIEW

2.1 Maximum power point tracking (MPPT)

It is very important with photovoltaic generation to operate the system at high power efficiency by ensuring that, the system is always working at the peak power point regardless of changes in load and weather conditions. In other words, transfer the maximum power to the load by matching the source impedance with the load one. To confirm that, an MPPT system has been implemented which enables the maximum power to be delivered during the operation of the solar array and which tracks the variations in maximum power caused by the changes in the atmospheric conditions. The MPPT system is basically an electronic device inserted between the PV array and the load. This device comprises two essential components, as illustrated in Fig. 2.1. A DC-DC switching power converter along with an MPPT control algorithm to operate the PV system in such way it can transfer the maximum capable power to the load.

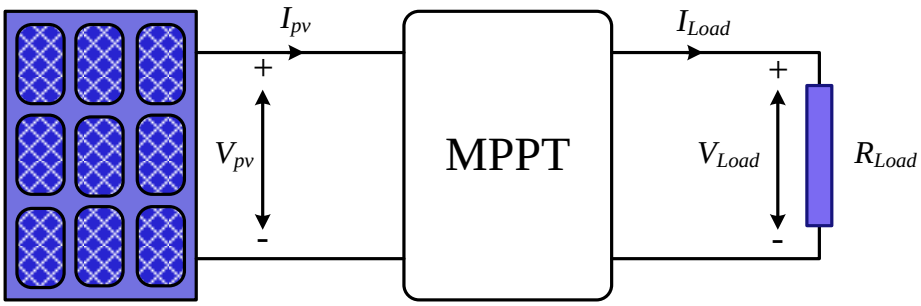

Fig. 2.1 Converter acting as a Maximum Power Point Tracker.

As the solar panel outputs power, its maximum generated power changes with the atmospheric conditions (solar radiation and temperature) and the electrical characteristic of the load may also vary. Thus, the PV array internal impedance rarely matches the load impedance. It is crucial to operate the photovoltaic generation system at the MPP or near to it to ensure the optimal use of the available solar energy. The main objective of the MPPT is to match these two parameters by adjusting the duty ratio of the power converter. As the location of the MPP on the *I-V*

curve varies in an unpredictable manner it cannot be defined beforehand due to changes of

adiation and PV panel temperature. Accordingly, the use of MPPT algorithm or calculating model is required to locate this point [46].

There are several methods to track the MPP of the photovoltaic system that have been carefully studied, developed and published over the last decades. The authors in [34, 47-51] have presented many MPPT control algorithms, some of which are addressed in the following sections. There are variations between these techniques in terms of, simplicity, sensor requirements, cost, range of efficiency, convergence speed and hardware implementation. Some MPPT algorithms outperform the others under the same operating conditions. A review and analysis of several MPPT techniques have been carried out in [38, 46] to quantify the performance of each control algorithm compared to the others.

2.2 Performance specifications of MPPT control algorithm

As noted earlier, the dynamic response, steady-state error and tracking efficiency should be considered for a successful design when evaluating the performance of a new or modified MPPT control algorithms [52].

2.2.1 Dynamic response

The response of a MPPT control algorithm needs be fast to track the MPP during the rapid changes in the atmospheric conditions (solar irradiation and temperature). The higher the tracking speed of the MPPT algorithm, the lower the loss in solar energy in the system.

2.2.2 Steady-state error

The MPPT control algorithm should stop tracking, once the MPP is located and should force the system to maintain operation at this optimal operating point as long as possible. However, this is impossible to achieve practically in an actual MPPT system because of the active perturbation process in MPPT algorithms with fixed tracking step-size and the continuous variation in solar insolation and temperature. This phenomenon has a negative impact on the PV system efficiency.

2.2.3 Tracking efficiency

Defining the tracking efficiency is a very important step, to quantify how successfully an MPPT control algorithm tracks the MPP and to what extent it contributes to increase the overall performance of the PV system compared to other methods. According to [30, 53, 54] the tracking efficiency is defined as the ratio between the actual power of the PV array and the theoretical power during the same time period. The atmospheric conditions (irradiation and temperature) are changeable and vary over a wide range. Hence, each MPPT algorithm must be evaluated over a range of different operating conditions when comparing MPPT algorithm performance. A well-designed MPPT control system should provide good performance in different atmospheric conditions. Equation (2.1) is used in a simulated VP system to calculate the tracking efficiency [55].

$$\eta_{MPPT} = \frac{1}{n}\sum_{i}^{n}\frac{P_{actual,i}}{P_{max,i}} \tag{2.1}$$

Where P_{actual} is the *i*th sample of real measured power produced by the PV array while using the MPPT control, P_{max} is the *i*th sample of true maximum power of the PV array could produce under the given solar insolation and temperature and *n* is the total number of samples.

2.3 MPPT algorithms classification

Several MPPT algorithms have been proposed for PV power systems in recent years, to locate the MPP and increase the system efficiency. The MPPT algorithms may be divided into two types, which are indirect control or “quasi tracking techniques” and direct control or “true tracking techniques” [35, 50]. In the indirect control techniques, the MPP is calculated either by measuring the voltage and current of the PV array, the solar insolation, or by the use of mathematical functions obtained from empirical data. Therefore, these techniques are incapable of tracking the MPP with varying irradiation and temperature. The indirect control techniques are look-up table technique, constant voltage technique, fractional open-circuit voltage and fractional short-circuit current. However, the true tracking techniques have the ability to find the optimum operating point even under changing atmospheric conditions, because

they do not rely on previous knowledge of or calculated data from the PV array *V-I* characteristics. The true tracking techniques are the perturbation and observation (P&O) technique, incremental conductance (INC) technique; but artificial intelligence techniques can also be included in this category, such as, fuzzy logic control (FLC) techniques and the neural network techniques. In the tracking process one or two variables are used for calculating the MPP. The fractional open-circuit voltage and fractional short-circuit current use only one variable, either the PV array output voltage or current respectively, though the P&O and INC methods need both variables to determine the MPP [35, 56].

2.3.1 Simple panel load matching

The simple panel load matching technique is one of the simplest techniques to operate a PV array close to its maximum power point. In this technique the optimum operating point of the PV array is determined either by a series of measurements under average operating conditions or theoretical calculation. The load is designed to produce the values of PV voltage and current corresponding to the MPP. There is another commonly used simple method that is widely used all over the world in PV battery charger systems, which involves choosing the average battery voltage close to the average solar panel V_{MPP} [57]. This method has the advantages of simplicity and no additional circuitry is used, therefore, the power loss between the panel and the battery is reduced and the risk of component failure is kept low for the whole system. However, the system does not take into consideration the changes of solar irradiation or temperature [58].

2.3.2 Load switching technique

The load switching technique was proposed in 1993 by Huang Yongji and Lin Deheng to optimize the output power produced by the PV array. The MPPT technique is based on the use of an array reconfiguration controller [59]. In this configuration different panels are connected in series and parallel in an appropriate manner to form a PV array. Then, the PV array is connected to a number of controllable battery cells connected in series to fulfil the load matching process as illustrated in Fig. 2.2.

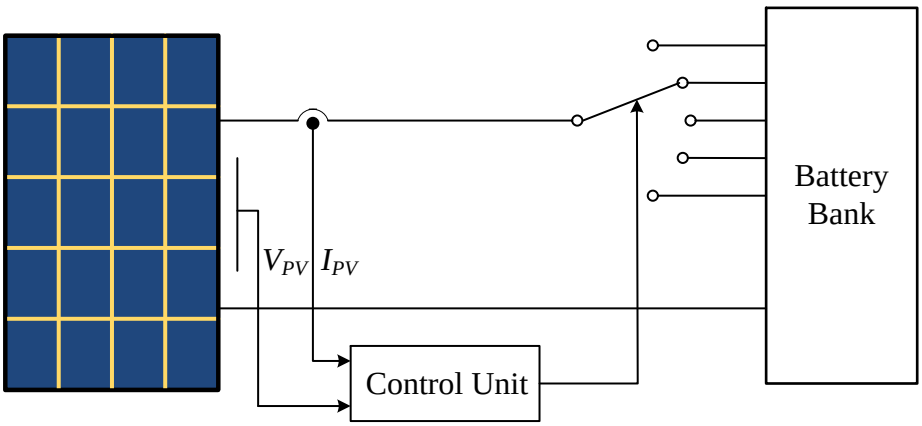

Fig. 2.2 Schematic block diagram of the load-matching method.

The group of batteries is used to store the energy produced by the PV array. The control unit detects the output of the solar array in real time, finds out the optimum operating point, and maintains operation as close as possible to this by switching the battery connection [58]. However, this technique has the drawbacks that it requires extra switching circuits and wiring, and the stepwise, switched operating voltage cannot guarantee accurate tracking of MPP. Moreover, it is difficult to keep an equal charge level on all the battery cells, hence degrading battery life in the long term [58].

2.3.3 Constant voltage method (CV)

If the PV system is implemented without a battery to tie the bus voltage to an approximately constant level, a simple control scheme of the constant voltage method can be applied as presented in [38, 60]. In this method the feedback of the PV voltage is compared with a fixed reference voltage and the resultant signal adjusts the duty ratio of the DC-DC converter to keep the operating point of the PV array at the MPP or close to it, as illustrated in Fig. 2.3. The reference voltage is set to be equal to the V_{MPP} of the characteristic PV array or to another calculated best fixed voltage.

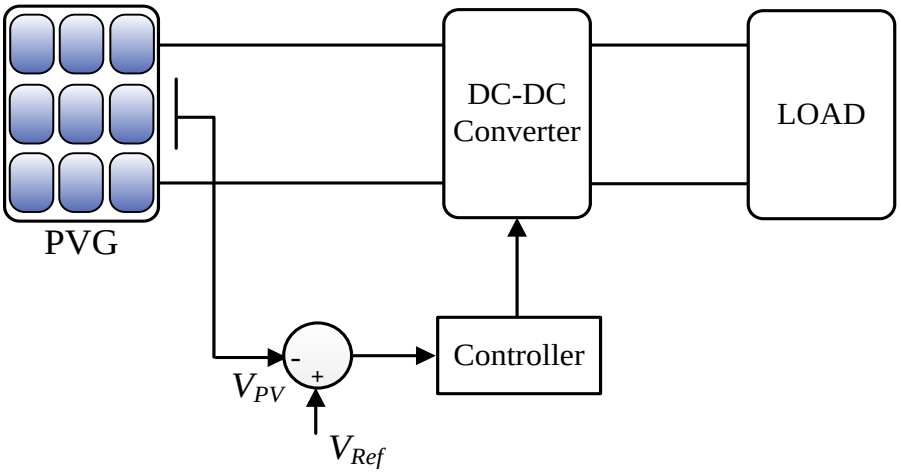

Fig. 2.3 Voltage feedback MPPT method with constant voltage reference.

This method is simple, economical and only one feedback-loop control is required. However this technique has the drawback that it does not correct for environmental variation such as change in irradiation and temperature [58].

2.3.4 Perturb and observe (P&O) algorithm

The perturb and observe algorithm is considered to be the most commonly used MPPT algorithm among the other techniques because of its simple structure and ease of implementation. It is based on the concept that on the power-voltage curve, the change in the PV array output power is equal to zero ($\Delta P_{PV} = 0$) on the top of the curve as illustrated in Fig. 2.4 [8, 31, 39, 47]. The P&O operates by periodically perturbing (incrementing or decrementing) the PV array terminal voltage or current and comparing the corresponding output power of PV array $P(n+1)$ with that at the previous perturbation $P(n)$. If the perturbation in terminal voltage leads to increase in the PV power ($\Delta P_{PV} > 0$) the perturbation should be kept in the same direction, otherwise the perturbation is moved to the opposite direction. The perturbation cycle is repeated until reaching the maximum power at ($\Delta P_{PV} = 0$). The control flow chart of P&O is shown in Fig. 2.5. There are two different ways to implement the P&O algorithm. In the conventional way a reference voltage is used as a perturbation parameter; therefore a PI controller is needed to adjust the duty ratio [39, 52, 61]. The second way is that, the duty ratio is directly perturbed and the power is measured every PWM cycle [31, 62]. The advantages of this technique are simplicity, ease of implementation and it does not require a previous knowledge of the PV array.

However, the P&O will not stop perturbing when the MPP is reached and will oscillate around it resulting in some unnecessary power loss.

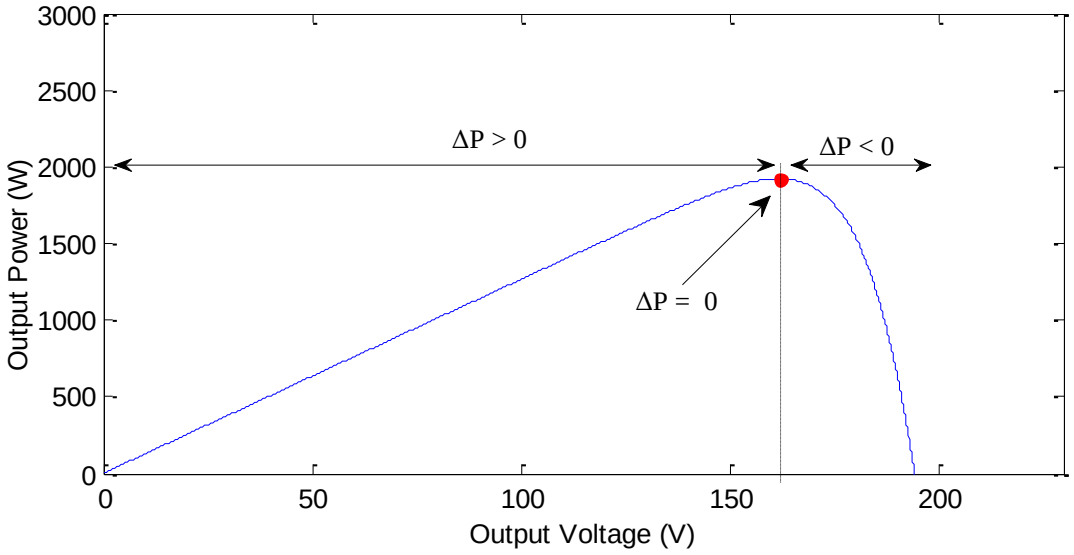

Fig. 2.4 Sign of the *dP/dV* at different positions on the power characteristic.

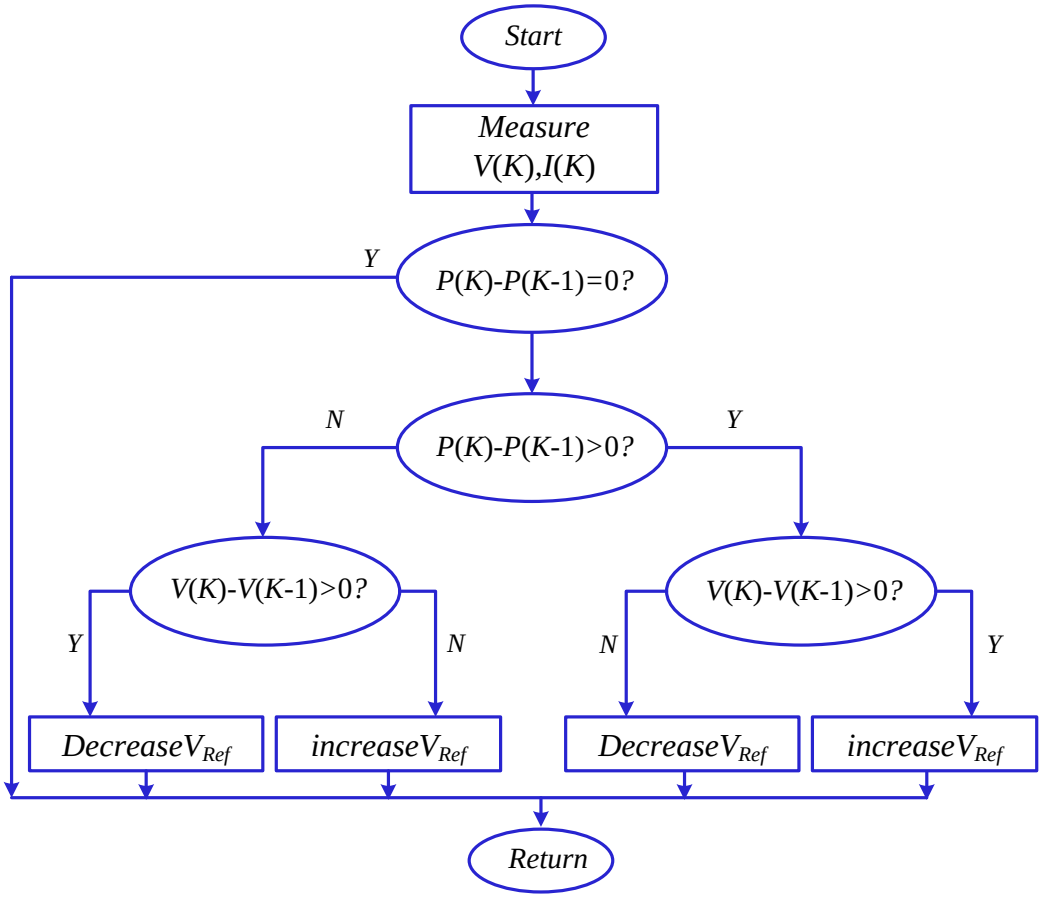

Fig. 2.5 Flowchart of the P&O algorithm.

2.3.5 Combined P&O with constant voltage (CV) MPPT method

At low irradiation levels, the conventional perturb and observe (P&O) algorithm exhibits a poor efficiency. Hence, in order overcome the limitations of the conventional P&O algorithm and increasing the tracking performance at all irradiation levels, the author in [63] has proposed a combination of a constant voltage (CV) method and modified P&O algorithm. The flowchart of the combined algorithm is shown in Fig. 2.6, and it starts operating by increasing the duty cycle until the output voltage of the PV array reaches 76% of its open circuit voltage V_{OC}, which is nearly close to the actual MPP and it is considered as the starting point of the algorithm. Therefore, the algorithm can evaluate the PV array output current, if the current value is lower than 0.7A it will switch method and if the current value is greater than 0.7A it will switch to P&O method.

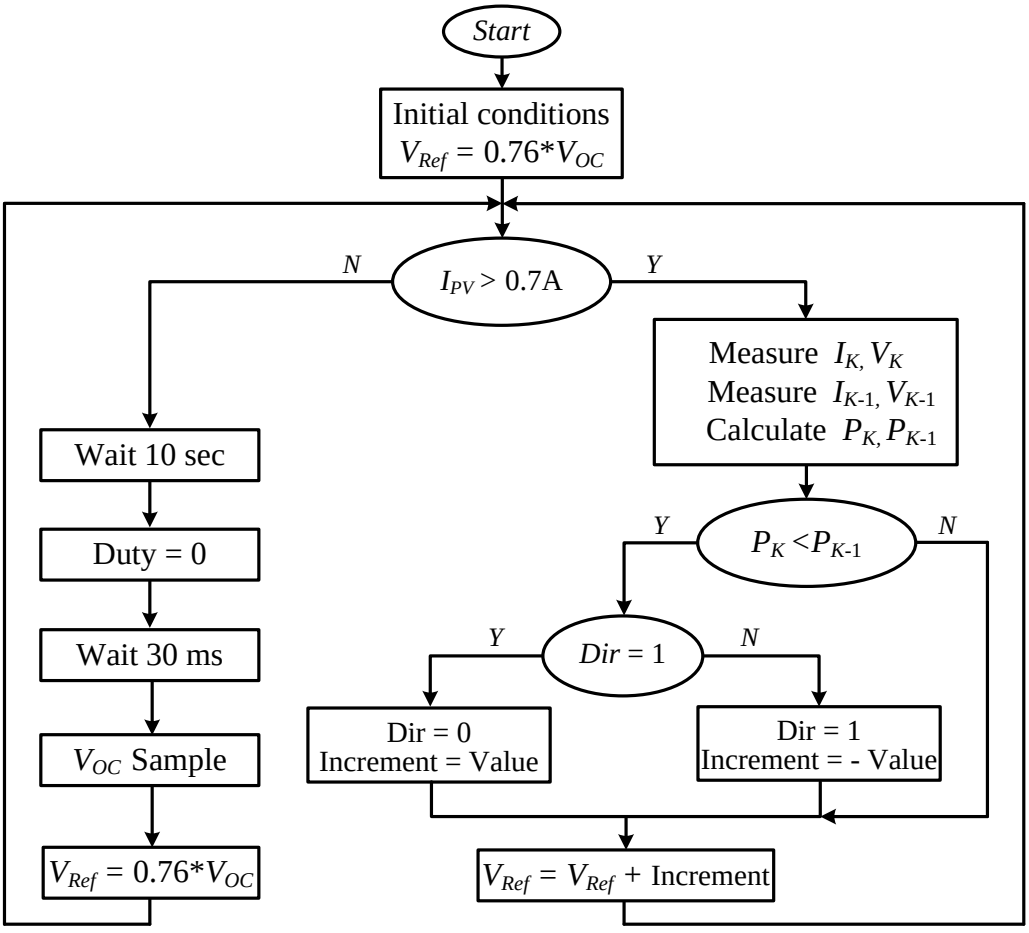

Fig. 2.6 Flowchart of the combined P&O with CV MPPT method

The simulation results proved that the algorithm can track the MPP at low and high irradiation levels and it showed higher efficiency over wide range of irradiation [63]. However, the disadvantage of this method is increasing the complexity.

2.3.6 Improved *dP*-P&O algorithm

The conventional P&O algorithm has some limitations, such as oscillations around the MPP in the steady state condition, slow tracking speed, and even confuses and tracks the MPP in the wrong direction when the irradiation rapidly changes [38]. Dezso Sera has proposed a simple improvement which is called *dP*-P&O method [64]. There is an additional block added in this method as shown in Fig. 2.8. The additional block is to perform the measurement of power in the middle of the MPPT sampling period (T) without any perturbation.

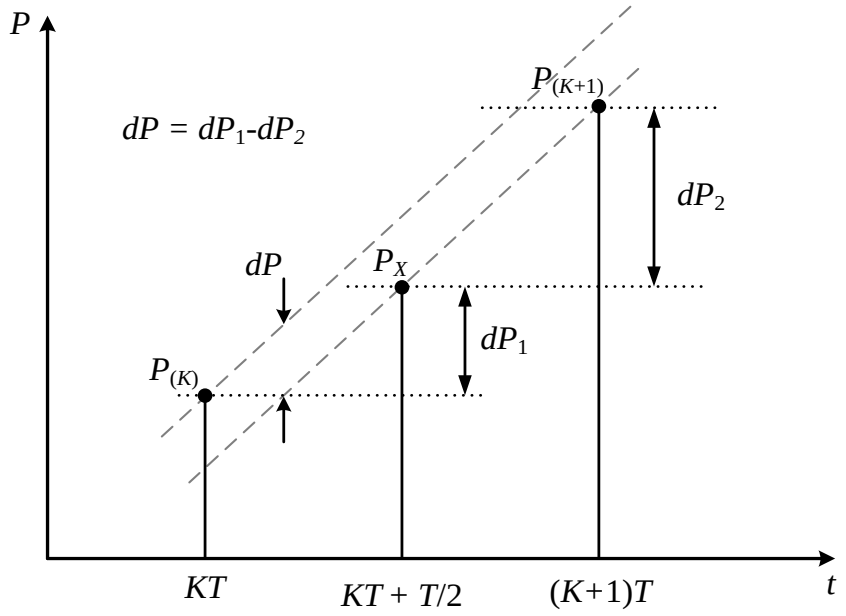

Fig. 2.7 Measurement of the power between two MPPT sampling instances

$$dP = dP_1 - dP_2 = (P_X - P_K) - (P_{K+1} - P_X) = 2P_X - P_{K+1} - P_K \quad (2.2)$$

In Fig. 2.7, $P_{(K)}$ is the power measurement at sampling instant K, $P_{(K+1)}$ is the power measurement at sampling instant (K+1), dP_1 and dP_2 are the change in power cussed by the perturbation of the MPPT and by the increase in irradiation respectively.

The change in environmental condition can be shown by the change of power between P_X and $P_{(K+1)}$ reflects as no action has been taken by the MPPT. The changes in environmental condition with a slight perturbation of the MPPT will result in the change in power dP_1 which is the power difference between P_X and $P_{(K)}$. Hence, assuming that over one sampling period of the MPPT the rate of change in the irradiation is constant, the *dP* caused purely by the MPPT command can be calculated by Equation (2.2). The performance of improved *dP*-P&O method has been experimentally validated and compared to the conventional P&O algorithm. The results proved that the improved *dP*-P&O has the ability to track the MPP in the right direction under rabidly changing irradiation unlike the conventional P&O, and increased the tracking speed [43, 64].

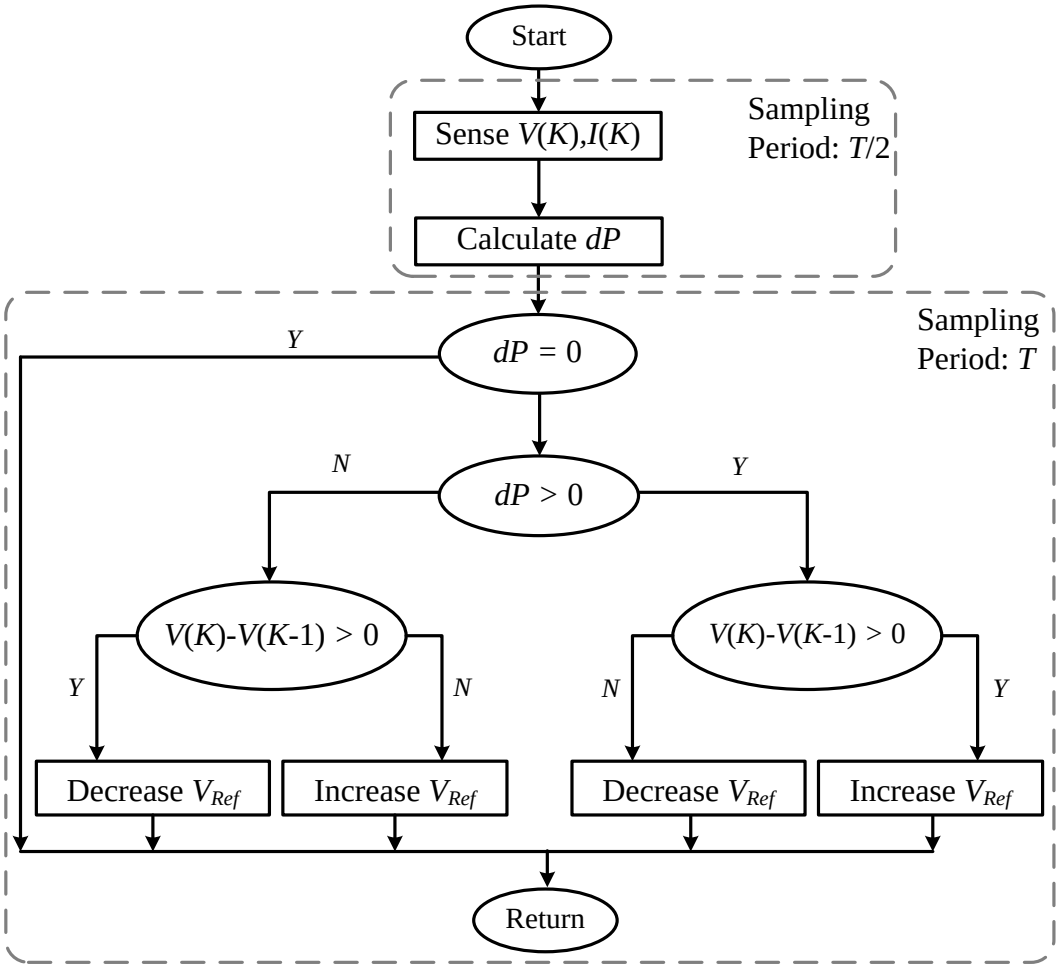

Fig. 2.8 Flowchart of the *dP*-P&O algorithm

2.3.7 Optimized P&O algorithm (OP&O)

The conventional P&O algorithm running with a fixed step-size oscillates around the MPP giving rise to the losses of some amount of available energy [65, 66]. A solution has been proposed in [65] that to have a variable step-size in which gets smaller to words the MPP. The proposed OP&O method lies in optimizing the parameters of P&O MPPT to the dynamic behaviour of the whole system compose by the specific converter and PV array adopted [65].

2.3.8 Modified perturb and observe (MOP&O) method

This method was proposed to in order to reduce the oscillation around the MPP caused by conventional P&O algorithm [67, 68]. The MOP&O operates by adding an irradiance-changing estimate process in every perturb process to measure the amount of power change caused by the change of atmospheric condition. It was verified by simulations and experimental tests that evidenced the overall performance of the MOP&O is better than the P&O. However, it slows down the tracing speed to the half of conventional P&O [68].

2.3.9 Estimate, perturb and perturb (EPP) method

The EPP method was proposed by C. Lui, B. Wu, and R. Cheung to improve the tracking speed of the MOP&O [67]. The EPP method uses one estimate mode for every two perturb modes. The EPP method was experimentally tested against the MOP&O method, and it has increased the tracking speed with keeping the same tracking accuracy [67, 68].

2.3.10 Incremental conductance (INC) method

The incremental conductance technique was proposed in 1996 by Hussein [30]. The INC method is based on the fact that, the derivative of PV array output power with respect to its output voltage is zero $(dP/dV = 0)$ at the MPP and at any irradiation and temperature level. It is negative on the right of MPP and positive on the left of the MPP as shown in Fig. 2.9 [30, 69-71].

$$\left.\begin{array}{ll} dP/dV = 0 & \text{at MPP} \\ dP/dV < 0 & \text{right of MPP} \\ dP/dV > 0 & \text{left of MPP} \end{array}\right\rangle \quad (2.3)$$

Since

$$\frac{dP}{dV} = \frac{d(IV)}{dV} = I + V\frac{dI}{dV} = I + V\frac{\Delta I}{\Delta V} \quad (2.4)$$

Equation (2.3) can be written as

$$\left.\begin{array}{ll} \Delta I/\Delta V = -I/V & \text{at MPP} \\ \Delta I/\Delta V < -I/V & \text{right of MPP} \\ \Delta I/\Delta V > -I/V & \text{left of MPP} \end{array}\right\rangle \quad (2.5)$$

As shown from the flowchart in Fig. 2.10, the MPP is reached when the instantaneous conductance (I/V) is equal to the incremental conductance ($\Delta I / \Delta V$). Once the MPP is reached, the PV array continues to operate at this point until change in ΔI is measured. This change in ΔI will correlate with the change in atmospheric condition and MPP. Hence, the algorithm increments or decrements the PV array operating voltage to track the MPP. When ($\Delta I / \Delta V < -I/V$) the algorithm is operating on the right of MPP therefore, the array operating voltage is decreased to move the operating point towards the MPP. When ($\Delta I / \Delta V > -I/V$) the algorithm is operating on the left of MPP hence the array operating voltage is increased. However, the array operating voltage does not need any change once the MPP is reached at ($\Delta I / \Delta V = -I/V$). This technique has the advantages of no oscillation around the MPP during steady-state conditions. Conversely, the INC method performs erratically during transient conditions. Also the computational time is increased due to the slowing down of the sampling frequency as a consequence of the algorithm's high complexity in contrast to the P&O technique.

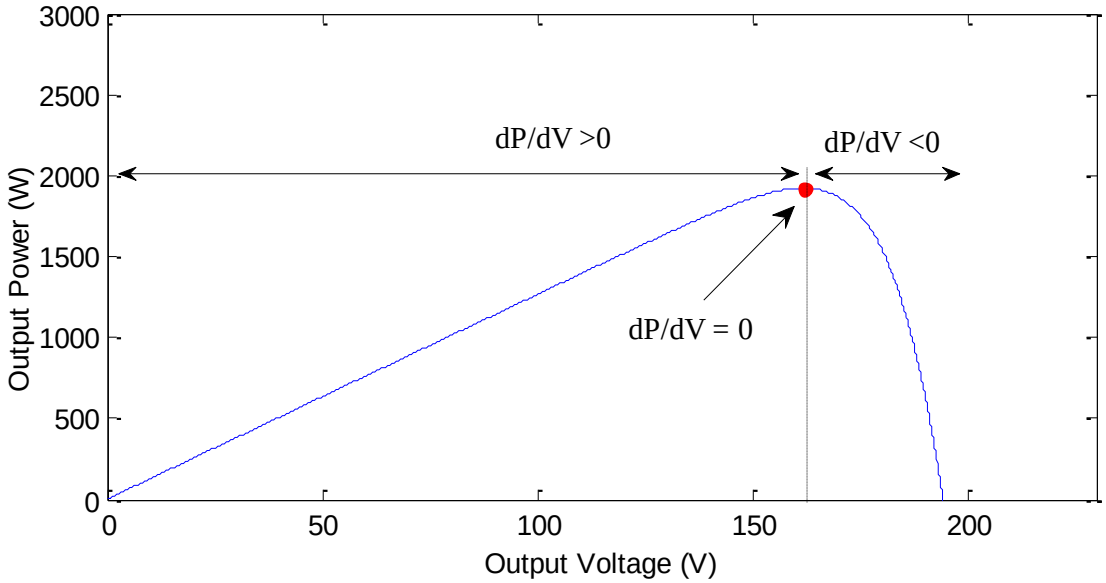

Fig. 2.9 The derivative of power with respect to voltage

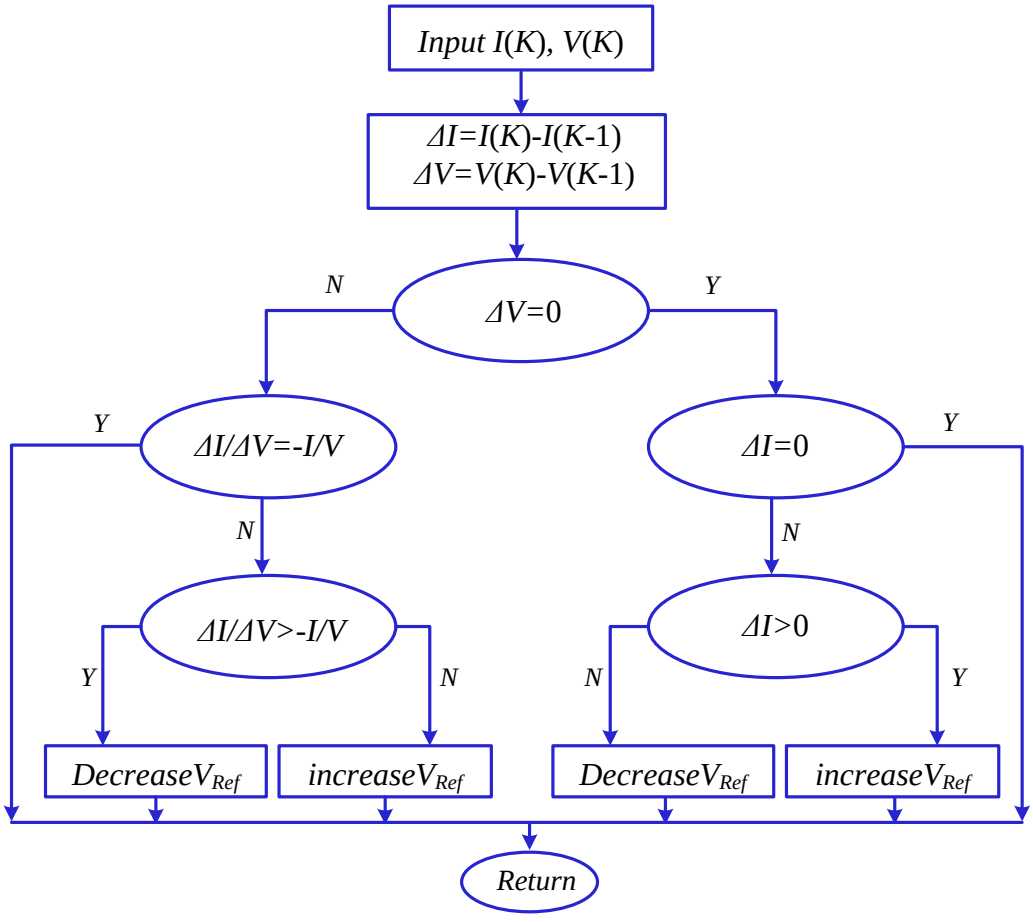

Fig. 2.10 Flowchart of the incremental conductance algorithm.

2.3.11 Fractional short-circuit current (SC)

The basis for short-circuit current method is that, the maximum operating current I_{MPP} is approximately linearly related to the short-circuit current I_{SC} under varying atmospheric conditions; in other words:

$$I_{MPP} \approx K_{SC} \cdot I_{SC} \tag{2.6}$$

Where K_{SC} is a proportional constant and it depends mainly on the metrological conditions and fill factor. The proportional constant K_{SC} is usually found to be between (75% - 92%) . The algorithm flowchart of the fractional short-circuit current is shown in Fig. 2.11. To measure I_{SC} an additional switch has to be introduced in parallel with the PV array to satisfy the short circuit condition. However the author in [72] provided another option by using a boost converter and the switch of the converter is used for short circuiting the PV array. Once K_{SC} is known and I_{SC} is measured the I_{MPP} can be calculated from Equation (2.6).

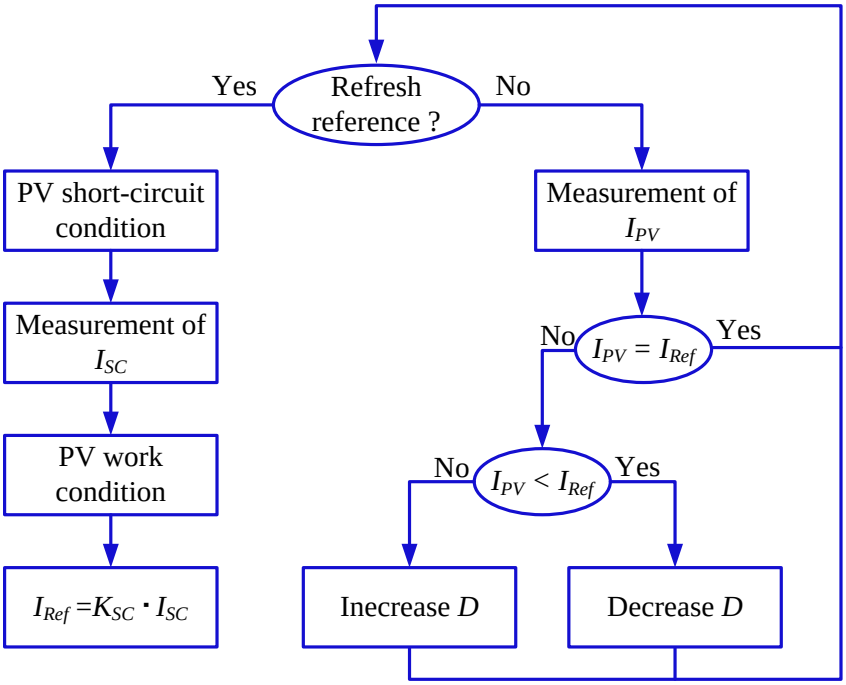

Fig. 2.11 Fractional short-circuit current algorithm flowchart.

The advantages of this method are its simplicity and low cost of implementation. On the other hand, the momentary interruption required for measuring I_{SC} leads to some loss of generated power, and the value of K_{SC} changes slightly [32, 73].

2.3.12 Fractional open-circuit voltage (OV)

The open-circuit technique is based on the fact that the ratio of PV array output voltage V_{MPP} at the maximum power point to its open circuit voltage V_{OC} is approximately constant under varying irradiation and temperature levels as shown in the Equation (2.7) [33, 74, 75].

$$V_{MPP} \approx K_V \cdot V_{OC} \tag{2.7}$$

K_V is the proportional constant which depends on the characteristic of the photovoltaic array being used. Therefore it has to be estimated by empirically determining V_{OC} and V_{MPP} for the particular PV array at different levels of temperature and irradiation. However the value of K_V has been reported to range between 71% and 80%. Fig. 2.12 shows the fractional open circuit voltage algorithm flowchart. The open circuit voltage V_{OC} is measured by momentarily interrupting the normal operation of the system. This is done by introducing a static switch in series with the PV array. Once K_V is known and V_{OC} is measured, the V_{MPP} value can be calculated from Equation (2.7) as a reference and a feed forward voltage control scheme is implemented to bring the PV array voltage to the point of peak power.

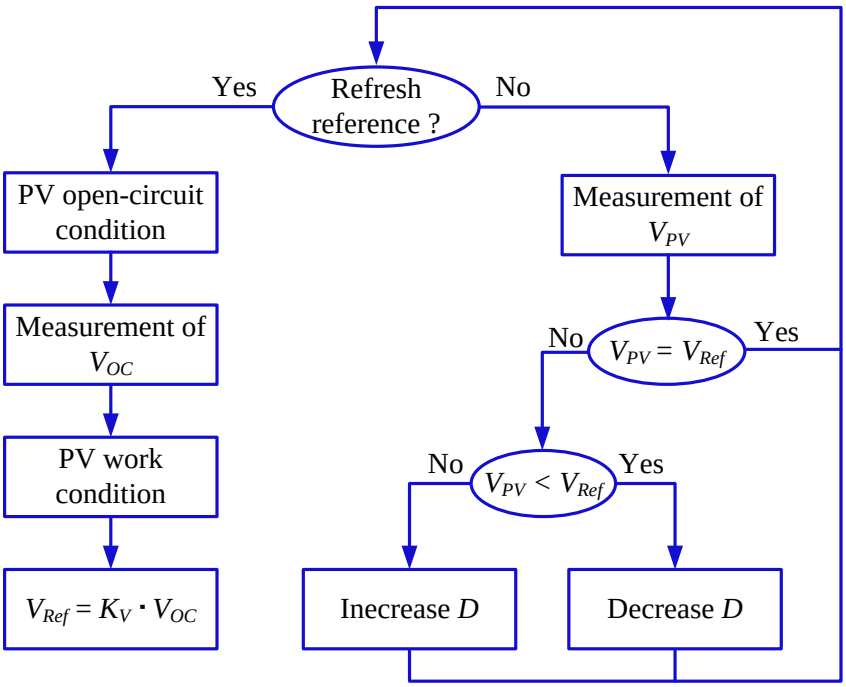

Fig. 2.12 Fractional open circuit voltage algorithm flowchart.

This method has an advantage that it is very simple, cheap to implement and it uses only one feedback loop. However, its drawback is that the interrupted system operation at the time of measuring V_{OC} results in some generated power loss. To prevent this, the authors in [76, 77] used pilot cells to obtain V_{OC}. The pilot cells are solar cells that represent the PV array's cells, which are not used to produce electricity but to obtain the characteristic parameters such as V_{OC} without interrupting the main PV system. The pilot cells must be carefully chosen to represent the characteristics of photovoltaic array. Hence, each pair of pilot cell/solar array must be calibrated, consequently, increasing the energy cost of the system

2.3.13 Discussion

Different MPPT techniques have been reviewed and discussed earlier in this chapter, and the advantages and disadvantages of these techniques have been addressed to give better understanding of each MPPT technique and its influence on the system performance. Many comparisons have been carried out amongst different MPPT techniques. The authors in [35, 38, 78] provided comparison in different aspects between the main MPPT techniques (CV, P&O, INC, SC and OV). The CV technique was the worst amongst the other MPPT techniques, because it fixes the reference voltage to a best fixed voltage value and holds it constant under any operating condition instead of following the MPP [38]. However, the CV technique is more effective than the P&O and INC techniques when the PV array is operated at low insolation levels and it has low implementation cost compared to the other MPPT techniques. The OV and SC techniques have better performance with their moderate complexity compared to the CV technique. However the P&O and INC techniques OV and SC techniques provide higher energy supply than this because the OV and SC require an additional static switch to perform the open-circuit and short circuit condition, which increases the losses and hence reduces their performance.

In the literature [38, 78] it has been highlighted that, the P&O and INC techniques are the most efficient compared to the other MPPT techniques. Moreover, the relative cost of P&O and INC techniques are not high, because they do not require additional static switches as in the OV and SC techniques. Though the INC technique has the similar performance as P&O technique, but its implementation cost is higher [78].

Also it has been reported by [39, 79, 80] that the P&O is the most widely applied method because of its low cost and ease of implementation. However, when the atmospheric condition changes slowly or constant, the P&O method oscillates around the MPP, and when theses change rapidly, this method has incorrect or slow power tracking. This is because the P&O runs with a fixed step-size [39, 63, 68].

There are several improvements that have been made to the conventional P&O method to reduce the oscillation around the MPP in the steady-state condition, as presented earlier in this chapter, such as the combined P&O with constant voltage (CV) MPPT method [63], improved *dP*-P&O algorithm [64], optimized P&O algorithm (OP&O) [65], modified perturb and observe (MOP&O) method [67], and estimate perturb and perturb (EPP) method [68]. Each of these improved techniques have reduced the oscillation around the MPP in the steady-state to different extend, but they increase the complexity. Moreover, they slow down the speed of response of the algorithm to the changing atmospheric conditions and lower the efficiency during cloudy days [39].

2.3.14 Summary

This chapter reviews and discuses several popular MPPT techniques for solar PV systems that are discussed in the literature along with their advantages and disadvantages. Besides that, this chapter presents a comparison between these techniques in terms of steady-state oscillation, tracking speed and efficiency. The comparison suggest that, on the basis of MPPT efficiency, the P&O and INC techniques have the potential to perform better the other MPPT techniques. However, because of the higher implementation cost of the INC technique, its use would not be justified by the relatively small improvement in the performance. This makes the P&O technique more attractive than the INC technique in this work.

Though the P&O is the most used techniques because of its low cost and ease of implementation, it has some limitations. The conventional P&O is usually implemented with fixed step-size by which the controlled parameter such as reference voltage or duty cycle is adjusted; large step-size values increases the losses in the steady state condition due to large oscillation around the MPP, while small step-size values slow down the tracking speed when the atmospheric conditions quickly change. To solve this problem, a trade-off between steady state accuracy and

dynamic tracking should be performed. In the literature, there are many improvements of the P&O method that have been proposed to reduce the oscillation around the MPP in steady-state condition. However, they increase the complexity, slow down the tracking speed when the atmospheric conditions rapidly change and degrade the algorithm efficiency in the cloudy days [39].

To solve this problem, a modified P&O MPPT with variable step-size is proposed in this thesis. The step-size is automatically tuned according to the variation of the atmospheric conditions, using a fuzzy logic controller.

This thesis proposes and presents the evaluation of two additional techniques using a fuzzy logic controller FLC and an artificial neural network ANN controller which are intended for the MPPT system of a PV water pumping system.

CHAPTER 3 -PV WATER PUMPING SYSTEM COMPONENTS AND DESIGN

This chapter provides an explanation of component characteristics and circuit design and the mathematical modelling of the PV water pumping system. It starts with the solar cells, reviewing the physical structure of the semiconductor of the PV cell and the basic concept of how does it convert the sun light into electrical energy. The mathematical model of the solar cell, panel and array are presented to show and analyse the effect of the atmospheric conditions on their *I-V* and *P-V* output characteristics. This chapter introduces and investigates various DC-DC converters, which are commonly used in MPPT power converter of PV systems, to select the most suitable converter for a DC motor pump load. This chapter discusses the type of DC motor and pump which will be used in the system and selecting the appropriate and efficient DC motor pump combination. The load characteristics will be analysed and discussed with the PV array characteristics when directly connected without the MPPT.

3.1 Photovoltaic Modules

3.1.1 The *p-n* junction diode

The symbol of a conventional *p-n* junction diode and its characteristics can be represented as shown in Fig. 3.1. The diode is shown below as a blackened triangle with a bar; the triangle suggests an arrow, which gives an indication of the direction in which conventional current flows easily, if a voltage V_D is applied across the diode. Under reverse bias when a voltage is applied to send the current in the reverse direction, only a very small reverse saturation current will flow. In the forward direction, the voltage drop across the diode increases with current, as illustrated in Fig. 3.1, and may be less than 1V or above, depending on whether the diode is intended for signal conditioning or power electronic applications [18].

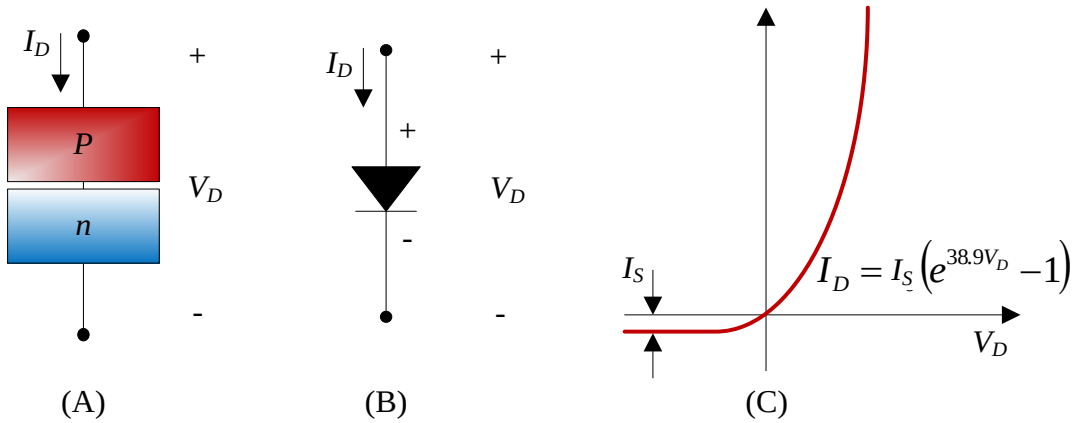

Fig. 3.1 A p–n junction diode (A) geometry, (B) symbol and (C) *I-V* characteristic curve.

3.1.2 Photovoltaic cell

The structure of solar cells is illustrated in Fig. 3.2. A semiconductor of *p*-type with a small quantity of added boron atoms forms the substrate. Then atoms of phosphorous are added to the substrate to form a *p-n* junction by applying high-temperature diffusion processing. Near the junction of the two semiconductors, the electrons from the *n*-side diffuse into the p-side leaving behind a layer of ions with positive charge in the *n*-side. In the same manner, the holes in the *p* region diffuse into the n region, which leaves behind a layer of ions with negative charge in the *p*-side. A potential barrier is formed from the rearranged positively and negatively charged ions [81].

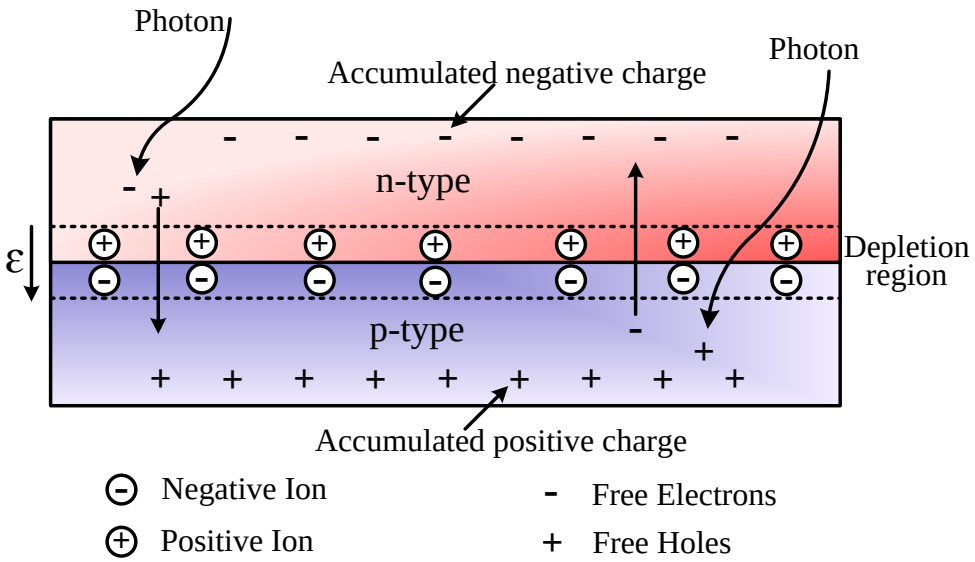

Fig. 3.2 Hole-electron pairs created by photons in p-n junction of PV cell.

This potential barrier is known as the depletion region and it is free from the mobile charge carriers. The potential barrier also prevents the motion of electrical charges as shown in Fig. 3.2. When the structure of p-n is exposed to the sunlight, the electrons in the structure will be excited because of the energy supplied by the photons, and consequently produce hole-electron pairs. These electrical charges are separated by the potential barrier at the p-n junction. At the same time the semiconductors of p-type will extract the holes and electrons will be extracted by the n-type semiconductor. At this moment if an external circuit is connected with n-type and p-type semiconductor of a solar cell as illustrated in Fig. 3.3.

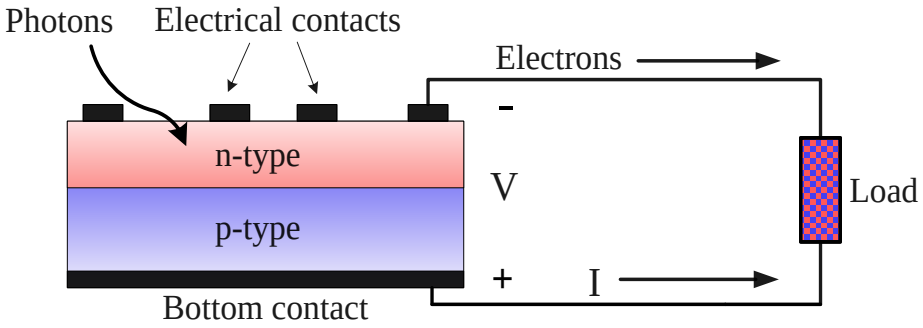

Fig. 3.3 Connecting solar with a load and conducting current.

The electrons will move through the external circuit from the n-type semiconductor to p-type in the other side to combine with the holes. This shows how the current in the external circuit is generated. Both sides of the junction are attached with metallic contact in order to collect the electrical current induced by the photons received on one side. The mono-crystalline and poly-crystalline silicon are the most common used material in PV cells. For the most practical applications the solar cells are connected in series and parallel to multiply the voltage, current and hence power. These cells are put together to form a PV module, and then encapsulated in flat glass to protect them from dust, water etc. [82-84].

3.1.3 Photovoltaic cell simplified model

There are various mathematical models that have been discussed in the literature to theoretically model photovoltaic cells. All of these models give an approximate behaviour of the solar cell. The accuracy of each model is classified according to how many internal phenomena are considered. The basic solar cell is usually represented by a p-n junction diode connected in parallel with current source. This

conventional equivalent circuit as illustrated in Fig. 3.4 [85-87]. The basic model does not provide a high range of accuracy but it shows the basic behaviour of the solar cell.

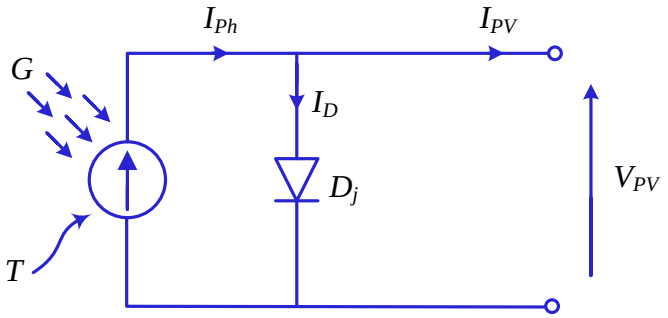

Fig. 3.4 Simple model of photovoltaic cell.

The current source represents the photocurrent produced by sunlight and the diode determines the current-voltage characteristic of the cell. The current-voltage characteristic function can be gained by applying Kirchhoff's current law in Fig. 3.4 which gives Equation (3.1).

$$I_{PV} = I_{Ph} - I_D \tag{3.1}$$

In the circuit above shown in Fig. 3.4, D_j is the ideal p-n diode, I_D the diode internal diffusion current and I_{Ph} the photocurrent, or light generated current, which is proportional to the radiation and surface temperature. The output current and voltage of the solar cell is represented by I_{PV} and V_{PV}, respectively. The diode internal diffusion current is modelled by Equation (3.2).

$$I_D = I_S \cdot \left[exp\left(\frac{q \cdot V_{PV}}{A \cdot k \cdot T_C} \right) - 1 \right] \tag{3.2}$$

Where q is the charge of electron, $1.6\times10^{-19}\,C$, A is diode ideality factor and it takes the value between 1 and 2, k is Boltzmann's constant, 1.38×10^{-23} J/K, and T_C is the cell's operating temperature in kelvin. The cell dark saturation current, I_S , varies with temperature according to Equation (3.4). The photocurrent, I_{Ph}, is related to the cell's operating temperature and solar intensity as shown in Equation (3.3).

$$I_{Ph} = \left[I_{SC} + K_I \cdot \left(T_C - T_{Rrf}\right)\right] \cdot \frac{G}{G_r} \quad (3.3)$$

Where I_{SC} is the short-circuit current, is known from the datasheet, K_I is the temperature coefficient of the cell's short circuit (Amperes/ K), T_{Ref} is the cell reference temperature in kelvin, T_{Ref} = 298 K (25 ^oC), G is the solar insolation in W/m^2 and G_r represents the reference solar radiation W/m^2, G_r = 1kW/m^2. Short circuit current is measured under the standard test condition at a reference temperature of 25 ^oC and solar radiation of 1kW/m^2 [85-87].

$$I_S = I_{RS} \cdot \left(\frac{T_C}{T_{Ref}}\right)^{\left(\frac{3}{A}\right)} . \, exp\left[\frac{q \cdot E_{gap}}{A \cdot k}\left(\frac{1}{T_{Ref}} - \frac{1}{T_C}\right)\right] \quad (3.4)$$

In Equation (3.4), I_{RS} is the cell's reverse saturation current in ampere at T_{Ref}, and the solar radiation 1kW/m^2. E_{gap} is the band-gap energy of the semiconductor used in the cell. The cell's reverse saturation current at reference temperature can be obtained by Equation (3.5) [88].

$$I_{RS} = \frac{I_{SC}}{exp\left(\frac{q \cdot V_{OC}}{A \cdot k \cdot T_{Ref}}\right) - 1} \quad (3.5)$$

Where V_{OC} is the open-circuit voltage at reference temperature T_{Ref}.

3.1.4 Photovoltaic cell general model

The general model is shown in Fig. 3.5 is more accurate because it includes the parasitic elements, shunt resistance R_{Sh} and series resistance R_S. Hence the PV cell output current I_{PV}, in Fig. 3.5 is given by Equation (3.6).

$$I_{PV} = I_{Ph} - I_S \cdot \left[exp\left(\frac{q \cdot (V_{PV} + I_{PV} \cdot R_S)}{A \cdot k \cdot T_C}\right) - 1\right] - \left(\frac{V_{PV} + I_{PV} \cdot R_S}{R_{Sh}}\right) \quad (3.6)$$

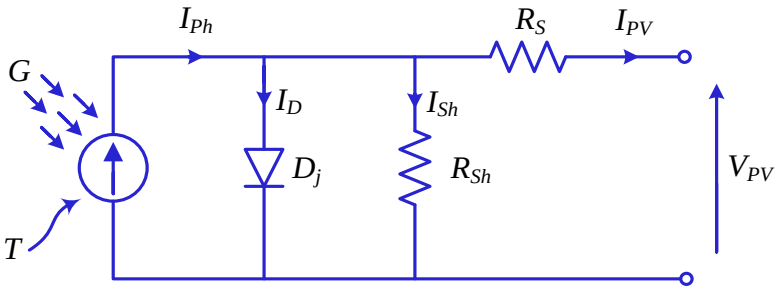

Fig. 3.5 More complete general model of photovoltaic cell.

The shunt resistance, R_{Sh}, represents the shunt leakage current to the ground due to p-n junction non-idealities and impurities near the junction. The series resistance R_S is due to the bulk resistance of the semiconductor material, the metal contact particularly the front grid and the transverse flow of current in the solar emitter to the front grid. In general the variation of R_{Sh} has no effect on the PV cell short circuit current, I_{SC}, but it reduces the PV cell open circuit voltage as shown in *I-V* characteristic and *P-V* characteristic in Fig. 3.6 and Fig. 3.7 respectively. Without leakage current to the ground the, R_{Sh}, can be assumed to be infinite. From Fig. 3.7, it can be seen that the maximum power point P_{max} in the knee, increases with the increases of R_{Sh} until some extend then the increases of R_{Sh} will have no effect on the P_{max}.

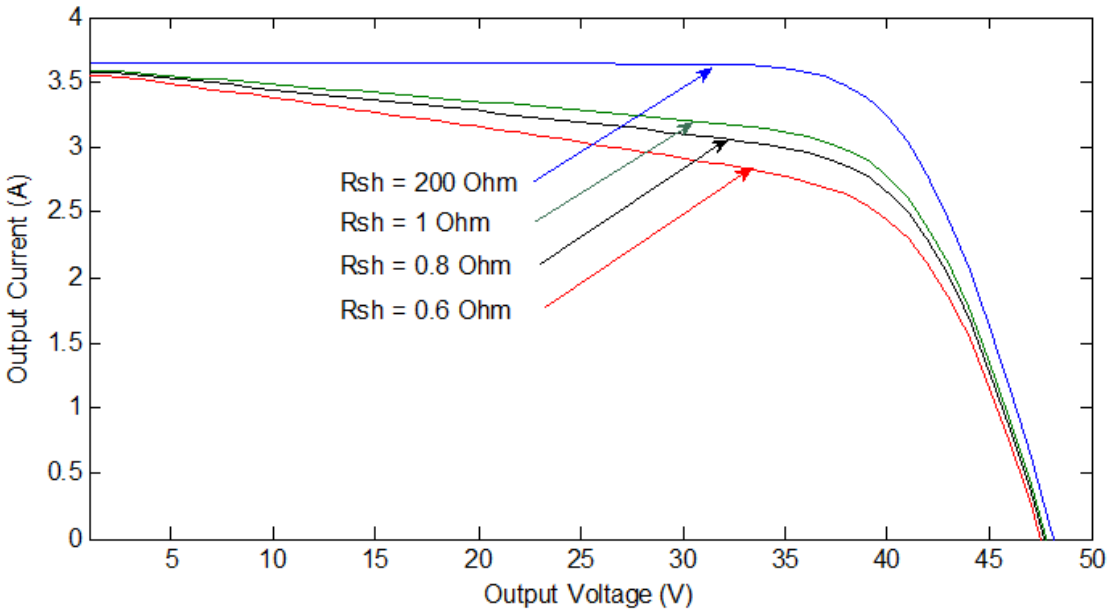

Fig. 3.6 Effect of shunt resistance on the *I-V* characteristic.

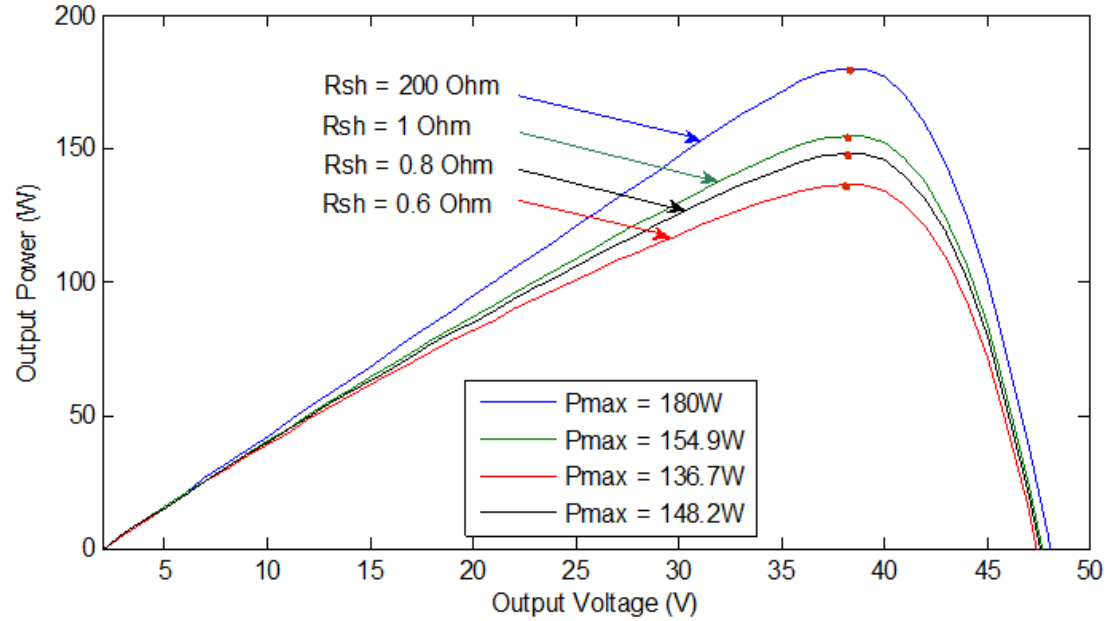

Fig. 3.7 Effect of shunt resistance on the *P-V* characteristic.

On the other hand, a small variation in R_S leads to a reduction in the short-circuit current but has no effect on the open-circuit voltage as in Fig. 3.8, therefore the maximum power changes significantly as depicted in Fig. 3.8 and Fig. 3.9 [86, 89].

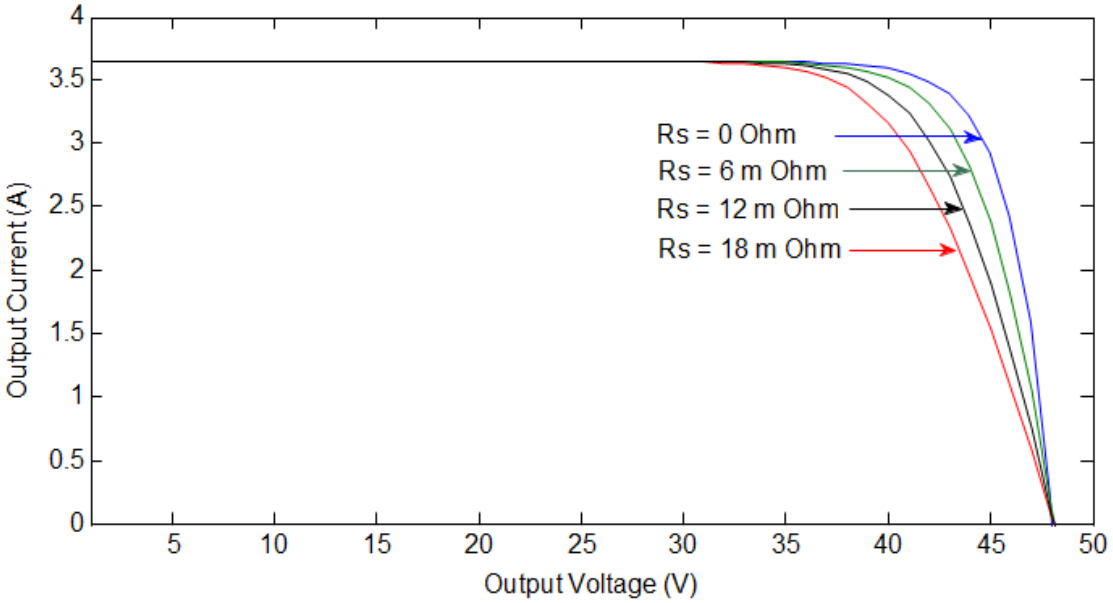

Fig. 3.8 Effect of series resistance on the *I-V* characteristic.

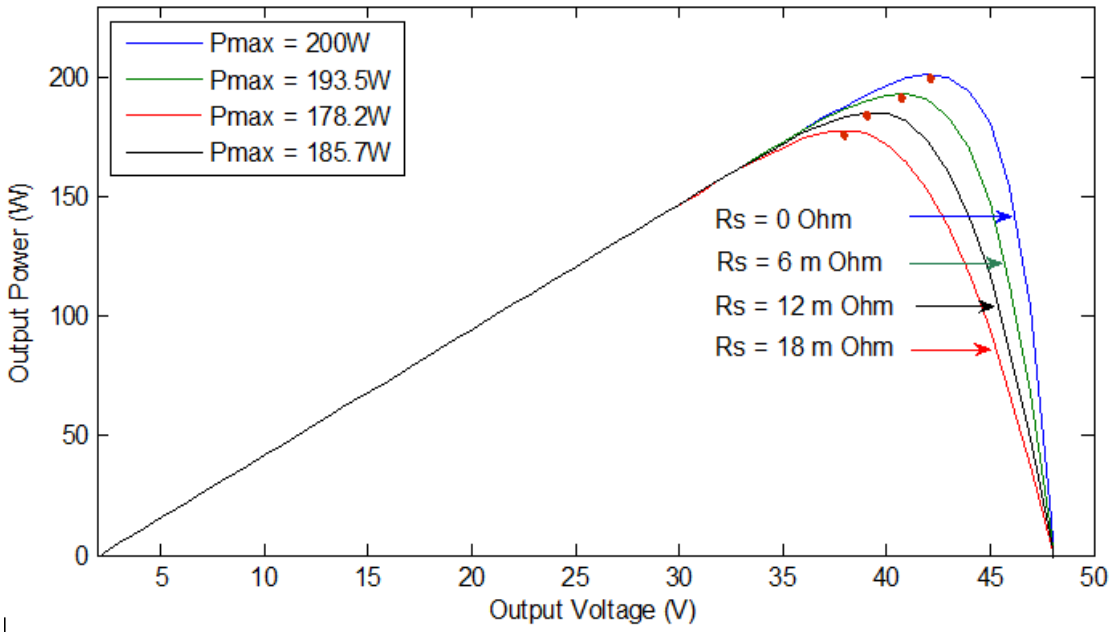

Fig. 3.9 Effect of series resistance on the *P-V* characteristic.

3.1.5 Photovoltaic cell appropriate model

As mentioned above, the small variation in R_S has a significant effect on the output power of the PV panel. On the other hand, the PV efficiency is insensitive to the variation in R_{Sh}, which can be assumed to approach infinity without leakage current. Therefore, the R_{Sh} can be neglected to give the appropriate model with suitable complexity. And the effect of R_{Sh} on the *I-V* characteristic and *P-V* characteristic of the PV array is shown in Fig. 3.6 and Fig. 3.7 respectively [86, 90]. Neglecting the shunt resistance, the model of PV cell becomes an appropriate model with suitable accuracy as shown in Fig. 3.10 and Equation (3.6) can be written as

$$I_{PV} = I_{Ph} - I_S \cdot \left[exp\left(\frac{q \cdot (V_{PV} + I_{PV} \cdot R_S)}{A \cdot k \cdot T_C} \right) - 1 \right] \qquad (3.7)$$

The value of R_S is provided in the datasheet by some manufactures. However, if is not provided, the equation of R_S can be derived by differentiating the Equation (3.7) and rearranging in terms of R_S.

$$dI_{PV} = 0 - I_S \cdot q \left(\frac{dV_{PV} + R_S \cdot dI_{PV}}{A \cdot k \cdot T_C} \right) \cdot e^{q\left(\frac{V_{PV} + R_S \cdot I_{PV}}{A \cdot k \cdot T_C} \right)} \qquad (3.8)$$

$$R_S = -\frac{dI_{PV}}{dV_{PV}} - \frac{A \cdot k \cdot T_C / q}{I_S \cdot e^{q\left(\frac{V_{PV} + R_S \cdot I_{PV}}{A \cdot k \cdot T_C}\right)}} \quad (3.9)$$

Then by evaluating the Equation (3.9) under the open circuit voltage condition when $V_{PV} = V_{OC}$ and $I_{PV} = 0$.

$$R_S = -\frac{dV_{PV}}{dI_{PV}}\Big|_{V_{OC}} - \frac{A \cdot k \cdot T_C / q}{I_S \cdot e^{q\left(\frac{V_{OC}}{A \cdot k \cdot T_C}\right)}} \quad (3.10)$$

In Equation (3.10); $\frac{dI_{PV}}{dV_{PV}}\Big|_{V_{OC}}$ is the slope of the *I-V* curve at the V_{OC}.

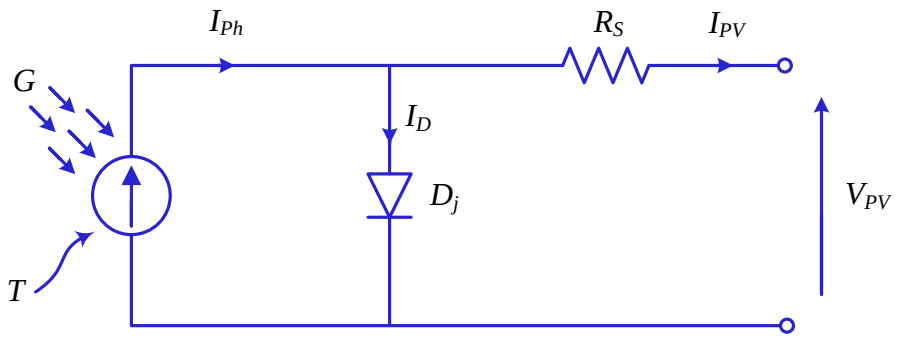

Fig. 3.10 Appropriate equivalent circuit model.

According to [91], the value of R_S can also be calculated by Equation (3.11).

$$R_S = \frac{\alpha_{Ref} \ln\left(1 - \frac{I_{MP,\,Ref}}{I_{SC,\,Ref}}\right) + V_{OC,\,Ref} - V_{MP,\,Ref}}{I_{MP,\,Ref}} \quad (3.11)$$

Where $I_{MP,\,Ref}$ is the maximum power point current at reference condition, $I_{SC,\,Ref}$ short circuit current at reference condition, $V_{MP,\,Ref}$ maximum power point voltage at reference condition $V_{OC,\,Ref}$ open circuit voltage at reference condition and α_{Ref} is the thermal voltage timing completion factor at reference condition and can be calculated by Equation (3.12).

$$\alpha_{Ref} = \frac{2V_{MP,\,Ref} - V_{OC,\,Ref}}{\frac{I_{SC,\,Ref}}{I_{SC,\,Ref} - I_{MP,\,Ref}} + \ln\left(1 - \frac{I_{MP,\,Ref}}{I_{SC,\,Ref}}\right)} \tag{3.12}$$

It is possible for the Equation (3.7) of *I-V* characteristics to be solved. However, the inclusion of a series resistance in the model makes finding a solution complex. Although the answer can be found by using Newton's method [92].

The Newton's method is described as follows:

$$x_{n+} = x_n - \frac{f(x_n)}{f'(x_n)} \tag{3.13}$$

$f'(x)$ is the derivative of the function, $f(x) = 0$, x_n is present value, and x_{n+1} is a next value.

Rewriting the Equation (3.7) yields the following equation:

$$f(I_{PV}) = I_{Ph} - I_{PV} - I_s \cdot \left[exp\left(\frac{q \cdot (V_{PV} + I_{PV} \cdot R_S)}{A \cdot k \cdot T_C}\right) - 1\right] = 0 \tag{3.14}$$

Substituting Equation (3.12) into (3.11) yields the following equation, and the output current I_{PV} is computed iteratively by using Newton's equation:

$$I_{PV(n+1)} = I_{PV(n)} - \frac{I_{Ph} - I_{PV(n)} - I_S \cdot \left[exp\left(\frac{q \cdot \left(V_{PV} + I_{PV(n)} \cdot R_S\right)}{A \cdot k \cdot T_C}\right) - 1\right]}{-1 - I_S \cdot \left(\frac{q \cdot R_S}{A \cdot k \cdot T_C}\right) . exp\left(\frac{q \cdot \left(V_{PV} + I_{PV(n)} \cdot R_S\right)}{A \cdot k \cdot T_C}\right)} \tag{3.15}$$

By using MATLAB, the function in Appendix A.1.1 can be computed numerically to obtain the net output current from the PV cells. Although, finding the value of $I_{PV(n)}$ never takes more than four interactions, it usually converges within three iterations. To ensure convergence of the results, the MATLAB function script in this thesis performs the calculation five times iteratively. For the script of this MATLAB function please refer to Appendix A.1.1.

3.1.6 Characteristics of *I-V*

The electrical performance of the solar cell is always described by two factors, the short circuit current I_{SC} and the open circuit voltage V_{OC}. The I_{SC} is the point where the curve intersects with the vertical axis and it is the maximum possible current in the circuit and it is expressed in amps. This is measured by connecting the positive and negative terminals of the cell together. When the terminals are shorted the output voltage of the circuit is zero.

V_{OC} is the point where the curve intersects with the horizontal axis and represents the maximum possible output voltage from the circuit. This occurs when the PV cells are connected to a very large resistance or in case of no load. Under the condition of open circuit the current is zero.

The power drawn by the photovoltaic module at any point along the curves are shown in Fig. 3.6 and Fig. 3.8 is expressed in watts. Since the voltage is zero under a short circuit current condition and the current is zero under the open circuit, the output power will be zero at these points.

3.1.7 Fill factor (*FF*)

The fill factor of photovoltaic generator is defined as the ratio of output power at MPP to the power result from multiplying V_{OC} by I_{SC} as in the Equation (3.17). It determines the shape of the photovoltaic generator characteristic as shown in Fig. 3.11. The fill factor plays an important role when comparing the performance of different photovoltaic cells. A high fill factor is equal to a high quality cell which has low internal losses.

$$FF = \frac{I_{MPP} \cdot V_{MPP}}{I_{SC} \cdot V_{OC}} = \frac{Area\ B}{Area\ A} \tag{3.16}$$

After simple multiplication the following equation results

$$I_{SC} \cdot V_{OC}\ FF = I_{MPP} \cdot V_{MPP} = P_{max} \tag{3.17}$$

Where I_{MPP} is the current at MPP and V_{MPP} is the voltage at MPP. The fill factor ranges from material to material and it can be seen that it is always < 1. The closer

the fill factor is to unity the better the operation of PV cell. The factors which affect (*FF*) are the shunt and series resistances of the photovoltaic generator as shown above in Fig. 3.6 to Fig. 3.9. A good fill factor is between (0.6-0.8) [89].

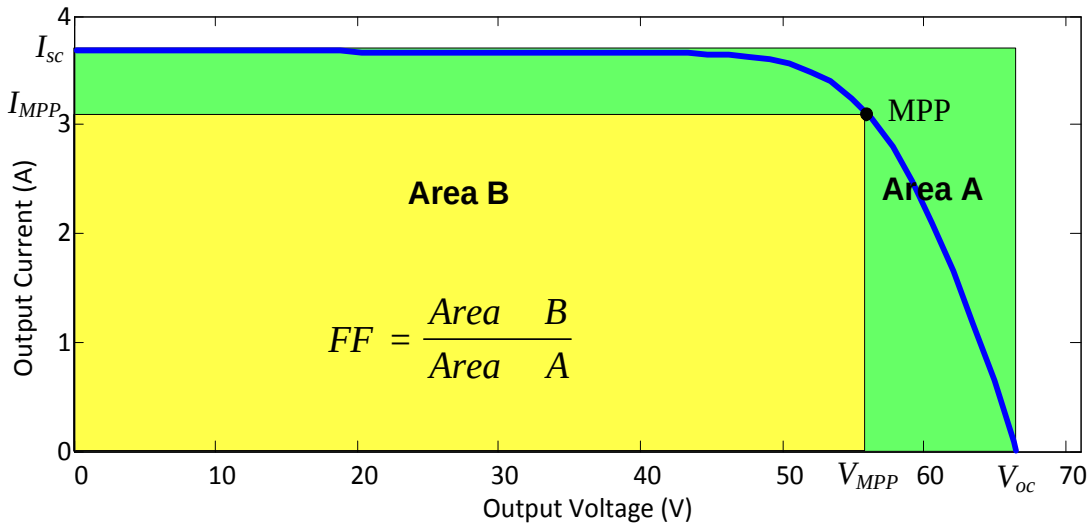

Fig. 3.11 Photovoltaic module characteristics showing the fill factor.

3.1.8 Effect of temperature

The panel temperature is considered one of the important parameters due to its effect on the output power of photovoltaic panel [93, 94].

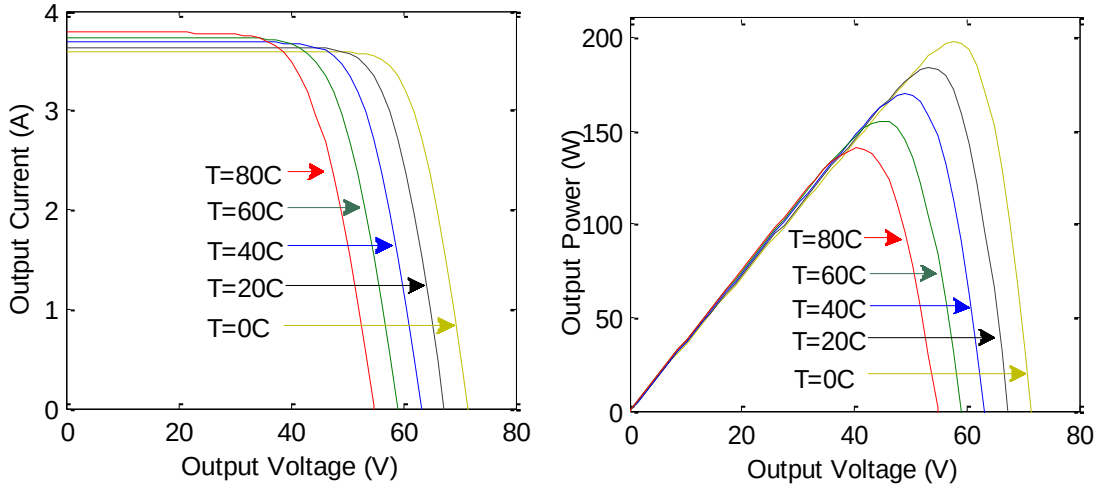

Fig. 3.12 Effect of temperature on the *I-V* and *P-V* characteristic at constant irradiance.

The open circuit voltage V_{OC} is highly influenced by the increase in the panel temperature as shown in the Fig. 3.12. As the temperature increases with a fixed irradiation level it results in a slight increase in the short circuit current I_{SC}, because the band gap energy decreases and more photons have enough energy to create electron-hole pairs. On the other hand, the increase of temperature have an obvious reduction in the PV panel output power due to the drop in the open circuit voltage V_{OC} and the fill factor; therefore the module efficiency is reduced [94].

3.1.9 Effect of irradiation

At constant temperature the change in irradiation has a clear effect on the PV output maximum power as illustrated in Fig. 3.13 [93, 94]. It is obvious that as the irradiation level increases the PV output voltage and current increases with it. In general, the increment in the irradiation level leads to a theoretical increment in the maximum power voltage when there is no change in the cell temperature. On the other hand, the short circuit current I_{SC} depends totally and linearly on the irradiance level; therefore the maximum power current is changed as shown in Fig. 3.13 [94].

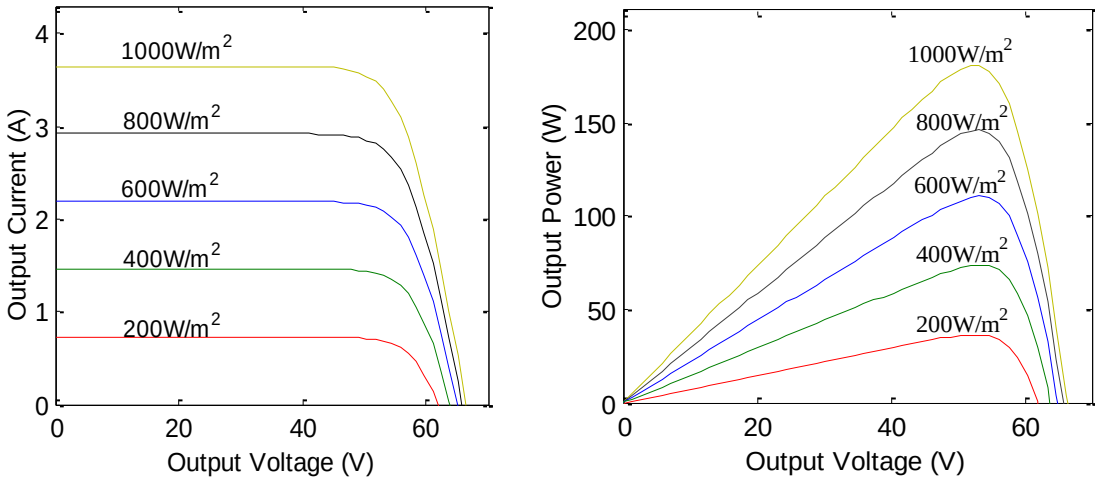

Fig. 3.13 Effect of irradiance on the *I-V* and *P-V* characteristic at constant temperature.

3.1.10 PV module and array module

The typical output power of solar cells in general is very low. It is normally less than 2W at 0.5V. Therefore, the photovoltaic cells are connected in particular configurations so as to form an array which is called a photovoltaic module. In general, the modules consist of group of cells connected in series and parallel to

provide the desired output power and voltage as depicted in Fig. 3.14. In addition to that, for a photovoltaic system a group of several PV modules are connected in parallel and series in form of PV array to generate the required voltage and current values for the system. When two or more solar panels are wired in series, the same current flows through each panel and the output voltage is the sum of the voltages generated by each panel. Hence, Equation (3.7) can be written as

$$I_{PV} = N_P \cdot I_{Ph} - N_P \cdot I_S \cdot \left[exp\left(\frac{q}{A \cdot K \cdot T_C} \left(\frac{V_{PV}}{N_S} + I_{PV} \cdot \frac{R_S}{N_P} \right) \right) - 1 \right] \quad (3.18)$$

In contrast, when the solar panels are wired in parallel the output current becomes the sum of the currents from each panel, and the output voltage remains the same.

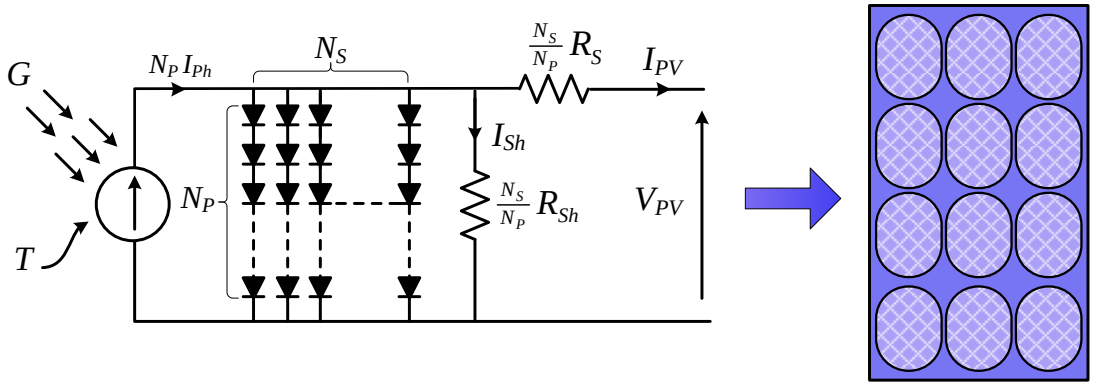

Fig. 3.14 Solar model in parallel and series branches.

3.1.11 Solar I-V characteristics with resistive load

As can be seen in Fig. 3.15, the operating characteristic of a solar cell consists of two main regions: the voltage source region and current source region. The voltage source region is located at the right of *I-V* curve and the internal impedance of the solar cell in this region is low. Where the current source region is located on the left of the *I-V* curve and the internal impedance in this region is high. Additionally, it can be observed from the *I-V* curve, that the output current remains almost constant while the terminal voltage changes in the current source region. But in the voltage source region over wide range of output current the terminal voltage has only slight changed.

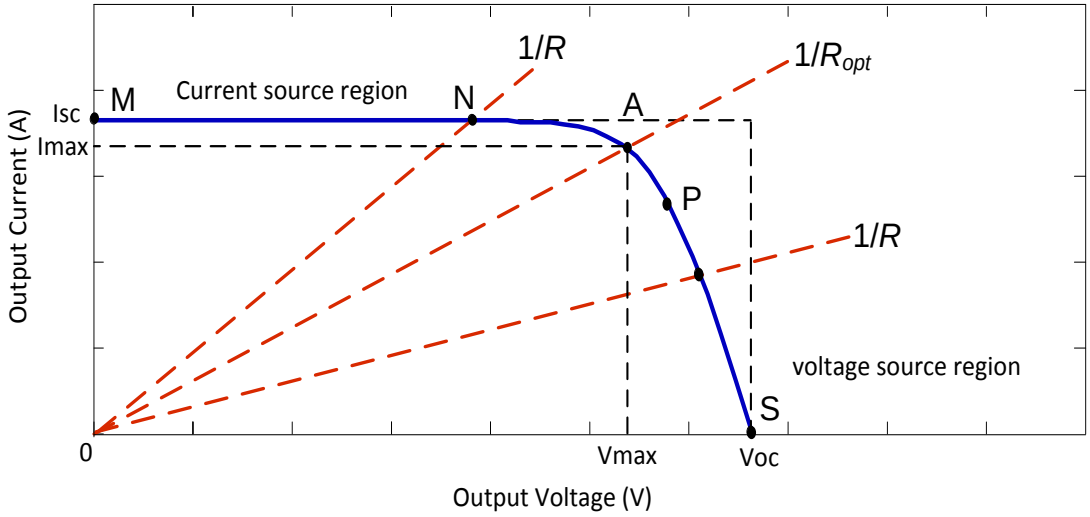

Fig. 3.15 Intersection of the I_{PV}-V_{PV} characteristic curve and the load characteristic.

When a fixed resistive load (R) is connected directly to the PV cell's terminals, the operating point is determined by the intersection of the solar cell I-V characteristic with the I-V characteristic of the load. As shown in the Fig. 3.15, the characteristic of the resistive load is a straight line with a slope, $I/V = 1/R$ [95, 96]. Additionally, the power delivered to the load depends only on the resistance value. If the load resistance is small, the cell operates in the current source region MN of the curve, almost near to the short circuit current. Alternatively, if the load resistance is large, the cell operates on the voltage source region PS of the curve, almost near to the open circuit voltage [97].

From Fig. 3.15 it is clear that, the operating point may not be at the point (A) which is the maximum power point (MPP) of the PV array. Furthermore, the output characteristics of PV cells are nonlinear, and the optimum operating point constantly varies with changes in the environmental conditions of solar irradiation and cell temperature. The effects of solar irradiation and cell temperature on the P-V and I-V characteristics are shown in Fig. 3.12 and Fig. 3.13 respectively.

Fig. 3.13 shows that, output power of the PV array varies dramatically with little shift in the maximum operating voltage when the irradiation changes. Therefore, the MPP shifts with insolation change. Fig. 3.12 represents that, the MPP moves in large range along the X-axis due to the variation in the PV array's temperature [95, 96]. Additionally, they are highly coupled under ordinary operating conditions. Hence, it is impossible to encounter one without the other. An increase in the insolation on PV

cell will be accompanied by an increase in the cell temperature. Since the MPP depends on factors that are not constant and cannot be controlled, i.e. solar irradiation and temperature, a device capable of tracking the MPP and maintain the operation at this point is needed. A maximum power point tracker is a device capable of tracking the MPP, and this device consists of DC-DC power converter its duty cycle adjusted by MPPT controller.

3.2 DC-DC converters

The switch mode DC-DC converter is considered the main part of a MPPT system. These are widely used to convert unregulated DC inputs into a controlled DC output at a desired voltage and current levels in DC power supplies and DC motor drives [98]. The same converter is used for a MPPT to provide load matching for the maximum power transfer by regulating the input voltage at the PV array MPP by controlling the duty ratio (*D*).

If the photovoltaic panel is directly connected to a load, its operating point will be defined by the intersection of the load and photovoltaic generation curves as shown in Fig. 3.15. Therefore, there is a unique point where the both curves intersect each other, exactly at a MPP. The generation curve nonlinearly changes with the change of the radiation (*G*) and temperature (*T*), while the load curve has a different characteristic according to the type of load is connected to the photovoltaic module. Hence, DC-DC converters are used to interface the photovoltaic module with the load, in order to ensure the photovoltaic module is always operating at the maximum power point. This is done by controlling the converter duty ratio (*D*) with maximum power point tracking algorithms (MPPT).

3.3 Topologies

There are several types of DC-DC converters. They are generally categorized into two types: isolated and non-isolated converters. In the isolated topologies a small high frequency electrical isolation transformer is used to provide the DC isolation between the input and output of the DC converter; and step up or down of the output voltage is achieved by changing the transformer turns ratio. These types of converter are used in switch mode power supply [99]. The flyback, half bridge and full bridge are the most commonly used topologies for majority of the applications [5]. Also these types of topology are used in PV grid-tied system when electrical isolation is needed for safety reasons, and to eliminate the possibility of coupling DC to AC grid. Non-isolated converters do not have an isolation transformer. They are very often used in DC motor drives [98]. Non-isolated converters are classified into three types: step up (boost), step down (buck), and step up & step down (buck-boost).

3.3.1 Buck converter

In this type of DC-DC converter, the average output voltage V_o produced is always lower than the DC input voltage. The buck converter is used for voltage step-down in PV applications, such as for charging batteries and in water pumping systems. The basic circuit of the step-down converter as illustrated bellow in Fig. 3.16 [98]. The diode (*d*) is used to enhance the output filtering effect and prevent the switch from absorbing or dissipating the inductive energy because this would lead to overheating the switch. In addition to that, there is an inductor and capacitor at the output of the converter which forms a low-pass filter to attenuate the output voltage fluctuation.

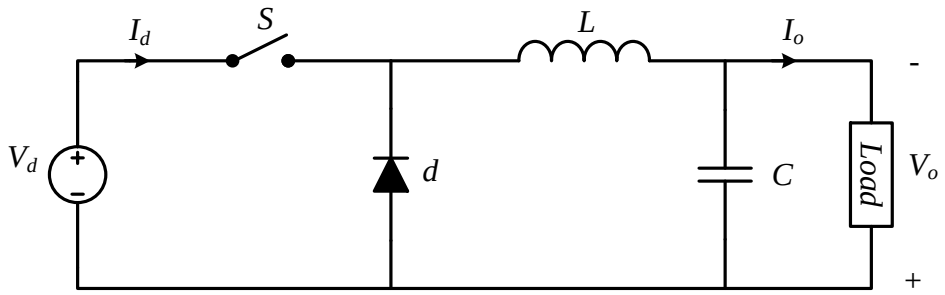

Fig. 3.16 Step-down Buck converter.

Fig. 3.19 illustrate the wave forms of the inductor current (i_L) and voltage (v_L) of the step-down converter operating in a continuous conduction mode.

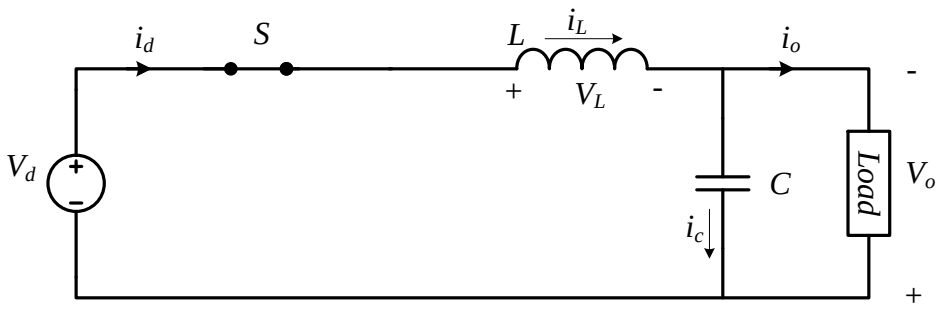

Fig. 3.17 Step-down Buck converter switch closed.

At the time duration when the switch *S* is on as shown in Fig. 3.17, the diode *d* becomes reverse biased and the input voltage V_d appears across the inductor leading to linear increase in the inductor current i_L. In addition, the capacitor *C* is charged in the same cycle [98, 100, 101].

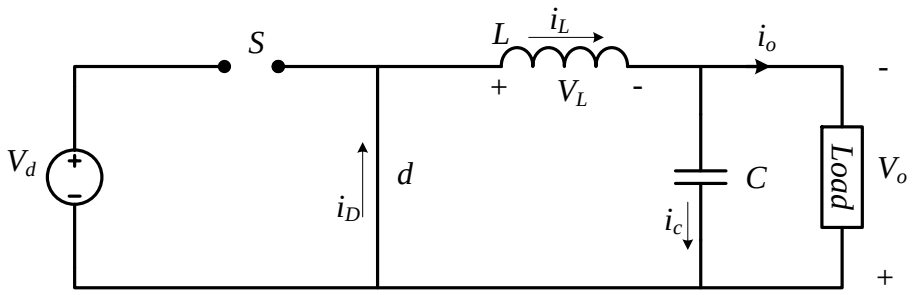

Fig. 3.18 Step-down Buck converter switch open.

When the switch *S* is turned off as shown in Fig. 3.18, the diode *d* becomes forward biased and the voltage across the inductor is reversed $v_L = -V_o$. Therefore, current in the inductor freewheel through the diode and starts decreasing linearly. In this cycle the capacitor is charged by the inductor energy.

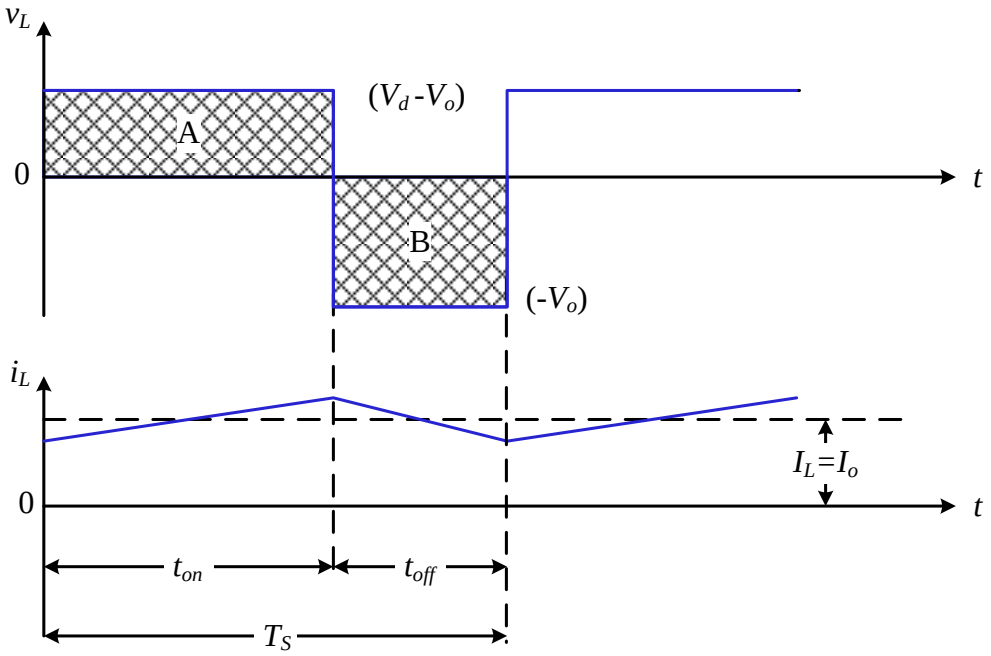

Fig. 3.19 Step-down converter wave form of the inductor current and voltage in continuous current mode.

The waveform must repeat from one time period to the next during steady-state operation. The relation between the input and output voltage, input and output current and the duty ratio *D* can be defined by Equation (3.19) and (3.20) [101].

$$\frac{V_o}{V_d} = \frac{t_{on}}{T_S} = D \qquad (3.19)$$

$$\frac{I_o}{I_d} = \frac{1}{D} \quad (3.20)$$

$$L = \frac{V_s\,(1 - D)}{2\Delta I_s\, f_s} \quad (3.21)$$

$$C = \frac{\Delta I_o}{8\Delta V_o f_s} \quad (3.22)$$

In Equations (3.19) and (3.20) T_S is the switching period, or time period of square pulse that controls the electronics switch *S*, t_{on} is the on time of controlling square-wave, I_o is the converter output current, I_d is the converter input current.

3.3.2 Boost converter

Example applications of boost converter operation are the regenerative braking circuit of DC motors and in regulated DC power supplies. In this type of converter the output voltage is always greater than the input voltage. Therefore the step up converter can be applied to MPPT systems where the output voltage needs to be greater than the input voltage. Such as in a grid-connected system where the boost converter maintains a high output voltage even if the PV array voltage falls to low values. The circuit topology of the step-up converter as illustrated in Fig. 3.20 [98].

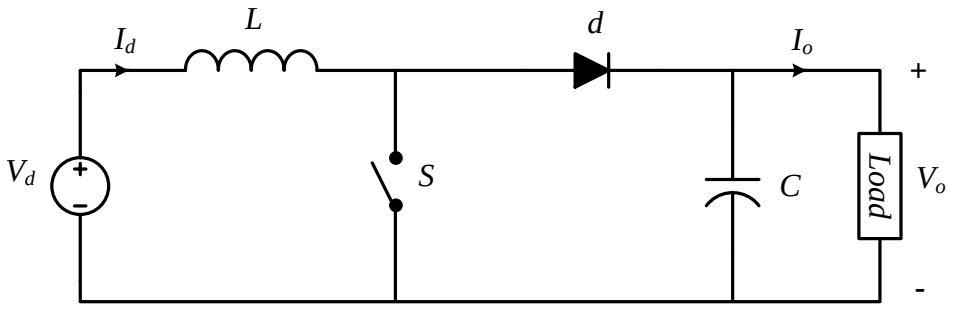

Fig. 3.20 Step-up boost converter.

When the switch *S* is on the diode *d* is reverse based. Consequently, the current in the inductor *L* rises linearly due to the input voltage source, and in this case the output stage is isolated and the capacitor *C* is partially discharged supplying the current

load. When the switch is off during the second interval the diode is conducting, and during this time the output stage receives energy from both the inductor and the input source. The wave form of the inductor current during continuous conduction mode is shown below in Fig. 3.21 where the inductor current flows continuously, i.e. $I_L(t) > 0$ [98, 100, 101].

When the converter is operating at steady-state condition, the duty ratio, D, can be expressed by Equation (3.23) [101].

$$D = 1 - \frac{V_d}{V_o} \qquad (3.23)$$

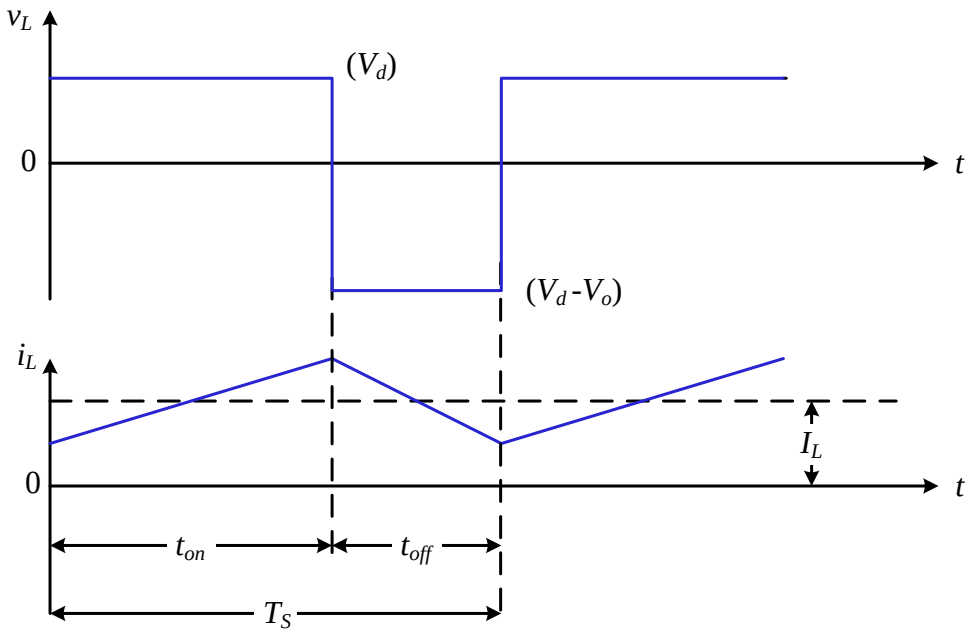

Fig. 3.21 Step-up converter wave form of the inductor current and voltage in continuous current mode.

Where D denotes the duty ratio, V_d and V_o denotes the input and the output voltages of the converter, respectively. From the above equation it can be seen that, the increase in the duty ratio D will increase the value of the output voltage, V_o. In addition the change in the duty ratio results in change in the input and the output current of the converter. The filter inductor and capacitor to operate the converter in the continuous conduction mode can be calculated by the following equations;

$$L = \frac{V_d D}{2\Delta I_L f_s} \quad (3.24)$$

$$C = \frac{I_o D}{\Delta V_o f_s} \quad (3.25)$$

3.3.3 Buck-Boost converter

A Buck-Boost converter is cascade connection of two basic converters, the buck converter and boost converter. The Buck-Boost converter provides an output voltage can be higher or lower than the input voltage. Also this type of converter produces a negative polarity output with respect to the common terminal of the input voltage [98]. The main application of Buck-boost converter is in regulated DC power supplies. Fig. 3.22 shows the circuit topology of Buck-Boost converter [100, 101].

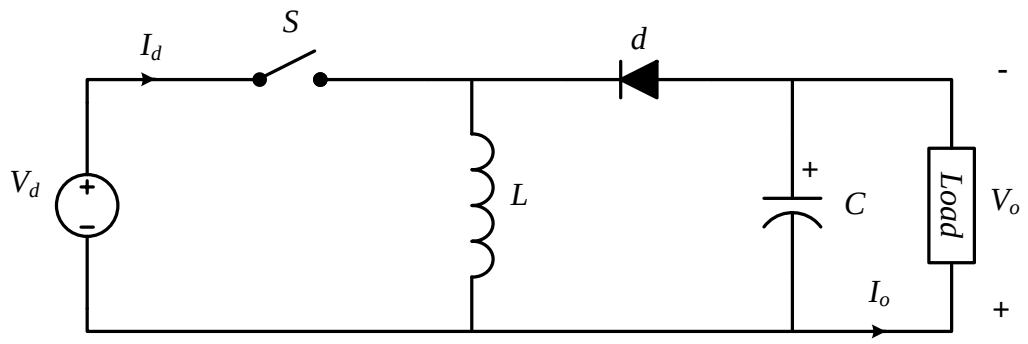

Fig. 3.22 Buck-boost converter.

In the equivalent circuit shown in Fig. 3.22 when the switch *S* is turned on during the first time interval t_{on} of the switching period T_S, the diode *d* is reverse based and input provides energy to the inductor causing the inductor current i_L to increase as illustrated in Fig. 3.23. When the switch is off during the second time interval t_{off}, the diode is forward biased so the energy stored in the inductor is transferred to the load. In this case the inductor current i_L is forced to flow backwards through the load and results in a negative polarity in the converter output voltage.

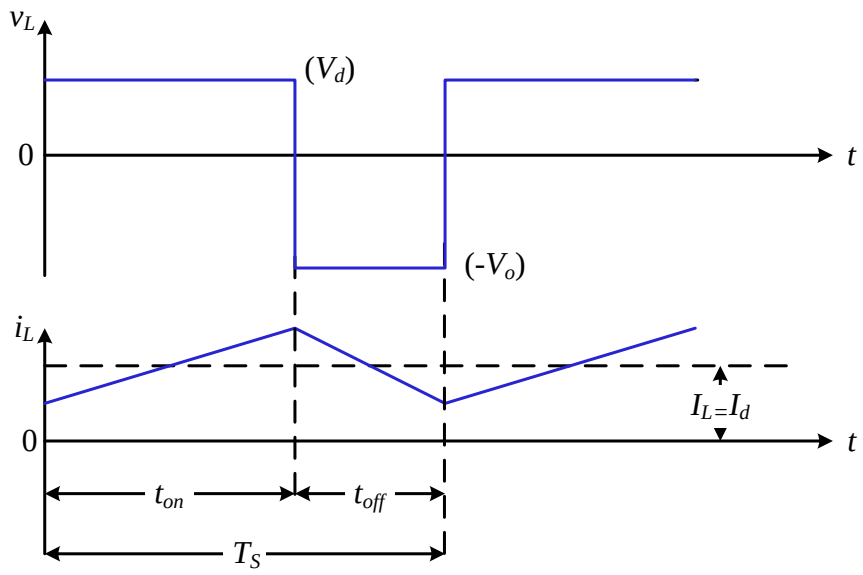

Fig. 3.23 Step-down converter waveform of the inductor current and voltage in continuous current mode.

During the steady-state condition the relation between the output voltage V_o and the duty ratio of the converter can be defined by the following equation.

$$\frac{V_o}{V_d} = \frac{D}{1-D} \tag{3.26}$$

From the above equation the output voltage could be higher or lower than the input voltage according to the value of the duty ratio. For the duty ratio condition $D > 0.5$, the output is higher than the input as in a boost converter. If $D < 0.5$ the output is lower than the input as in a buck converter.

$$L = \frac{(1-D)^2 R}{2 f_s} \tag{3.27}$$

$$C = \frac{D}{R f_s (\Delta V_o / V_o)} \tag{3.28}$$

3.3.4 Cuk Converter

The Cuk converter can be obtained by using the duality principle on the circuit of a Buck-Boost topology. The circuit diagram of Cuk converter is shown in Fig. 3.24. It is clear that the input circuit of Cuk converter is a Boost converter and the output circuit is seen to be a Buck converter [102]. Hence the Cuk converter is similar to the Buck-Boost converter, it provides a negative polarity regulated output voltage with respect to its terminal of the input voltage [98].

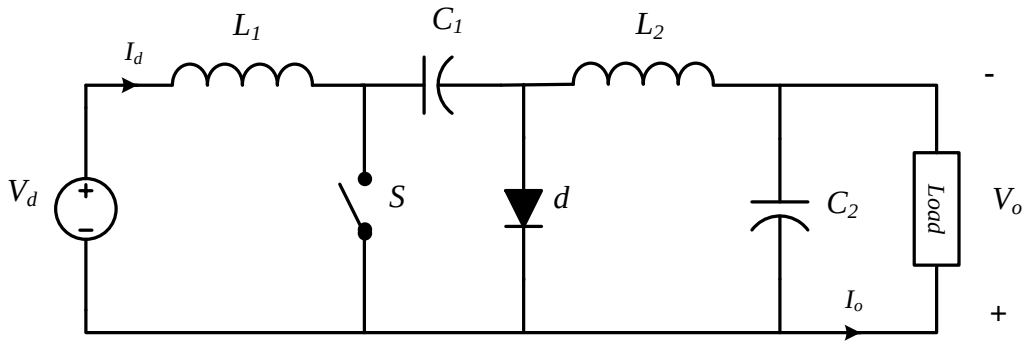

Fig. 3.24 Cuk converter.

In steady-state operation, the average voltage of the inductor is zero, therefore by applying Kirchoff's voltage law to the circuit shown in Fig. 3.24.

$$V_{C1} = V_d + V_o \tag{3.29}$$

Cuk converter shows two different operating modes. The first mode obtained when the switch *S* is off. In this case the diode *d* is conducting as shown in Fig. 3.25. Therefore, the capacitor C_1 is charged by the input V_d through the inductor L_1. The energy stored in the inductor L_2 feeds the load. Hence, the following relationship is obtained [98, 102].

$$I_{C1} = I_{L1} \tag{3.30}$$

The second mode of operation exists when the switch *S* is on. The diode *d* is not conducting because it is reverse-based due to C_1. The capacitor C_1 discharges through the switch *S*, transferring its energy to the load and L_2. Assume the inductor currents are ripple free, because the inductors are large enough. Therefore, the following relationship is obtained [98, 102].

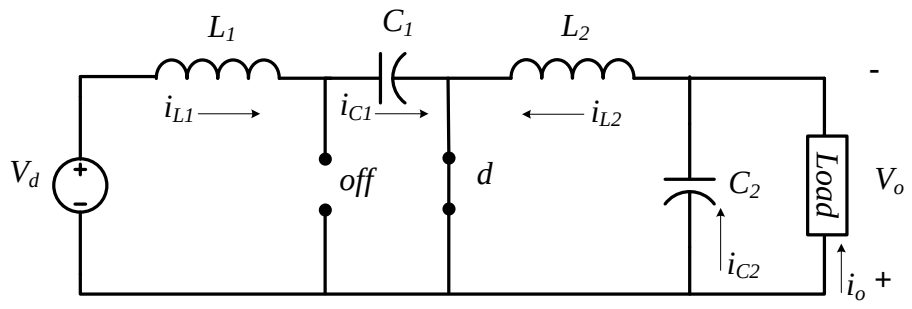

Fig. 3.25 Cuk converter when the switch is off.

$$-I_{C1} = I_{L2} \tag{3.31}$$

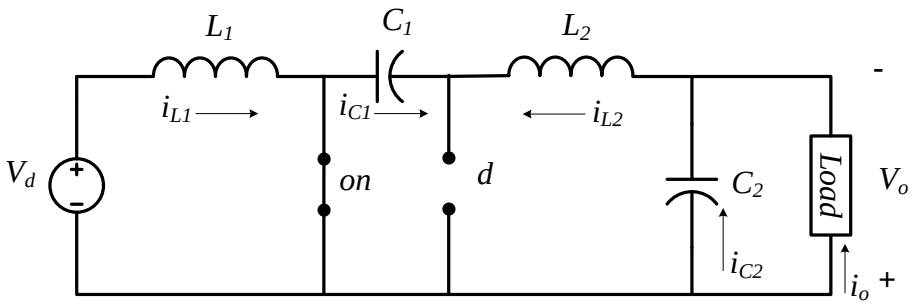

Fig. 3.26 Cuk converter when the switch is on.

For one time period of operation, the average capacitor current is zero. Therefore, by rearranging the Equations (3.30) and (3.31) yields [98],

$$\left[I_{C1}|_{S_{on}}\right] \cdot DT_S + \left[I_{C1}|_{S_{off}}\right] \cdot (1 - D)T_S = 0 \tag{3.32}$$

$$-I_{L2} \cdot DT_S + I_{L1} \cdot (1 - D)T_S = 0 \tag{3.33}$$

$$\frac{I_{L1}}{I_{L2}} = \frac{D}{1 - D} \tag{3.34}$$

Where D is the duty ratio of the converter and it is the ratio of the conduction time t_{on} to the switching period T_S. The value of D changes between 0 and 1 [98].

Assuming the converter is ideal in other words there are no losses. Therefore, the input power of the converter P_{in} is equal to the output power P_{out} [98].

$$P_{in} = P_{out} \tag{3.35}$$

$$V_d \cdot I_{L1} = V_o \cdot I_{L2} \tag{3.36}$$

$$\frac{I_{L1}}{I_{L2}} = \frac{V_o}{V_d} \tag{3.37}$$

Combining the Equations (3.34) and (3.37), the following relation is obtained [98].

$$\frac{V_o}{V_d} = \frac{D}{1-D} \tag{3.38}$$

- If $0 < D < 0.5$ the output is smaller than the input.
- If $D = 0.5$ the output is the same as the input.
- If $0.5 < D < 1$ the output is larger than the input.

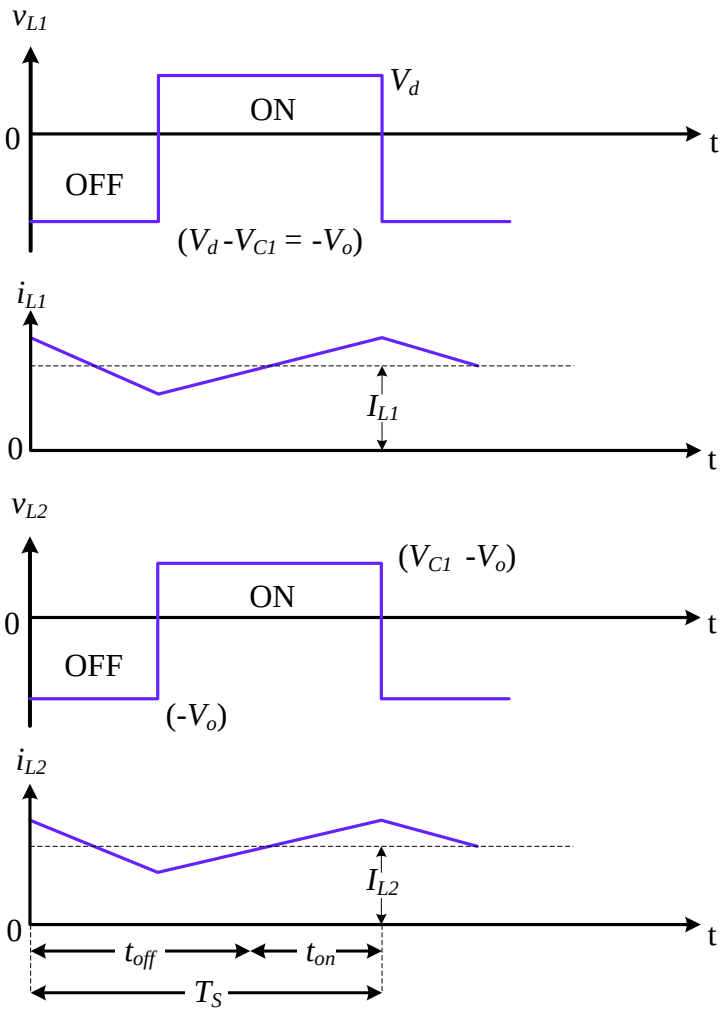

Fig. 3.27 Cuk converter waveforms.

3.3.5 Discussion

In the literature, many types of DC-DC converters have been studied to see which converter is suitable for the MPPT stage of the PV system. In the literature [61, 103-107], a comparative analysis from different viewpoints has been made between some commonly used topologies to track the maximum power of the PV array. Some of them are known as single inductor types, such as the Buck, Boost, CSC and Buck-Boost; and also several are defined as two inductor types, such as SEPIC, Zeta and Cuk converters. Reference [107] showed that, the Buck-Boost converter has the advantage over individual Buck and Boost converters of following the MPP at all times, under any conditions of solar global radiation, cell temperature and connected load. However, the individual Boost and Buck types are the most efficient converters for a given price. The author in [106] found that each topology has its pros and cons in comparison to the others. For example, some of them present low current ripple such as SEPIC and Cuk converter and may provide input-output isolation. The DC-DC converter family in general has no theory for the designer to decide which converter is the most suitable for tracking the maximum power. Consequently, designers often choose the simplest DC-DC converters such as the Buck or the Boost.

For water pumping systems, the output voltage needs to be stepped down, unlike in the grid connected systems, in order to provide a higher starting current for a pump motor. Therefore, the Cuk, SEPIC, Buck-Boost and Buck converters are a good choice since step-down or step up voltage conversion may be performed by converter transistor duty-cycle adjustment. The Cuk and SEPIC converters have the advantage that their input current is continuous, and they can draw ripple free current from a PV array [5]. However, Cuk, SEPIC and Buck-Boost converters have a higher number of passive components and high current, voltage and switched power stresses in the switch or transistor compared to the Buck converter. This also affects the whole system efficiency [108], since the switched current and voltage are higher for the same output power as an individual buck or boost. Also, the higher voltage devices required generally switch less rapidly and have higher on-state voltage, which further increases conduction and switching losses. Therefore, in this work it was decided to use a Buck converter because of its higher efficiency, less complex control

requirements, more robust and predictable operating characteristics than other topologies.

For photovoltaic applications such as battery charging systems and water pumping systems, an output voltage lower than the source voltage is generally needed. Hence, step-down converters are usually preferred such as the buck converter. The author in [109] concluded that, the buck converter is the most suitable topology if the load comprises a DC motor. This allows the maximum available power to be used during the starting stage of the motor when it can be represented by a very small resistor. Accordingly, the buck converter would be the most suitable topology amongst the other DC-DC topologies. Additionally, the step-down converter outperforms the boost type in the ability of easily controlling output voltage and currents during turn-on and turn-off and under output fault conditions. It also shows better loop stability and dynamic response to control actions.

3.4 DC motor and pump

Employing DC motors to PV pumping systems instead of AC motors have been the object of many studies and it was concluded that DC motors can be directly coupled to the PV array. Therefore, the overall system cost and complexity will significantly reduce. A permanent magnet DC motor is proposed in this work. The permanent magnet DC motors are reliable, efficient and require low maintenance [99]. In addition, the PMDCM coupled with centrifugal pump have suitable matching characteristics with the PV array characteristics and has low starting torque compared to the other PV electro-mechanical systems.

3.4.1 PMDC motor modelling

The equivalent circuit of the permanent magnet DC motor is shown in Fig. 3.28 [99], where R_a is the armature winding resistance (Ω), L_a is the armature self-inductance (H), I_a is the motor armature current (A) and V_a is the applied voltage (V).

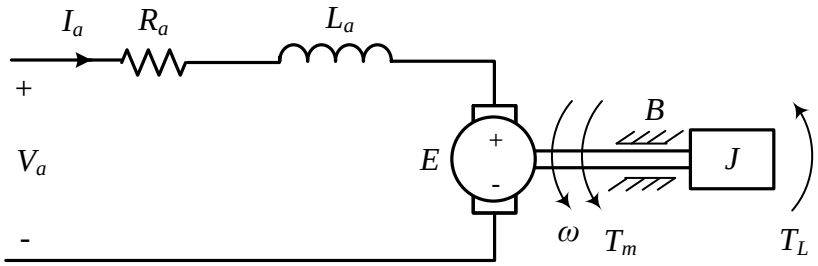

Fig. 3.28 Circuit model for DC permanent magnet motor with pump load.

From the equivalent circuit shown in Fig. 3.28, the armature DC voltage can be calculated by using Equation (3.39).

$$V_a = R_a I_a + L_a \frac{dI_a}{dt} + e \tag{3.39}$$

e is the induced voltage when the motor is turning, and it is known as a back emf, or a counter electromotive force. The induced voltage e is proportional to the angular

speed of the rotor ω_m, the constant proportionality, K_e, and the field flux Φ as given by Equation (3.40).

$$e = K_e \Phi \, \omega_m \tag{3.40}$$

In the case of separately exited motors with constant field voltage or permanent magnet motors the field flux remains constant. Accordingly, Equation (3.40) becomes;

$$e = K_e \omega_m \tag{3.41}$$

Hence Equation (3.39) becomes;

$$V_a = R_a \, I_a + L_a \frac{dI_a}{dt} + K_e \omega_m \tag{3.42}$$

The torque balance equation is given by

$$T_e = J \, \frac{d\omega_m}{dt} + B_m \omega_m + T_L \tag{3.43}$$

Where J is the moment of inertia, B_m is the viscous torque constant for rotational losses, T_e and T_L are the electromagnetic torque and the load torque respectively. The electromagnetic torque T_e is equal to the product of the torque constant K_t and the current through the armature winding as given by:

$$T_e = K_t \, I_a \tag{3.44}$$

Therefore Equation (3.43) can be rewritten as:

$$K_t \, I_a = J \, \frac{d\omega_m}{dt} + B_m \omega_m + T_L \tag{3.45}$$

For a constant flux machine the torque constant is equal to the back emf constant (K_e) [110]. Also the torque developed by the armature can be written as in Equation (3.46).

$$T_e = \frac{P_e}{\omega_m} = \frac{e\, I_a}{\omega_m} = \frac{K_e \omega_m\, I_a}{\omega_m} = K_t\, I_a \qquad (3.46)$$

Where P_e is the electric power of the motor and $B_m\,\omega_m$ represent the rotational losses torque.

In a steady-state condition, Equations (3.39) and (3.43) become:

$$V_a = R_a\, I_a + E \qquad (3.47)$$

$$K_t\, I_a = B_m \omega_m + T_L \qquad (3.48)$$

3.4.2 Direct Coupling of the DC Motor

Coupling the DC motor directly to the PV array in the water pumping system without interfacing circuitry gives a severe system efficiency disadvantage because of the deviation of the operating point away from the optimal point, as illustrated in Fig. 3.29.

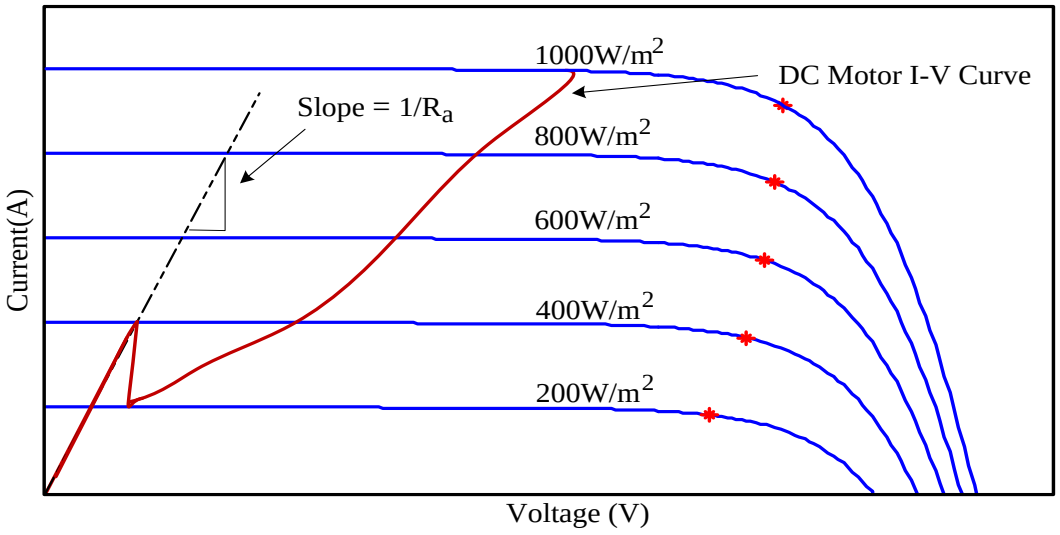

Fig. 3.29 PV *I-V* curves at different irradiation levels and a DC motor *I-V* curve.

It is clear that the motor would not start operating unless the 400W/m^2 of irradiation is reached. However, when the motor starts to run the 200W/m^2 of irradiation is sufficient to maintain the minimum operation. This means that the system cannot utilize a fair amount of morning insolation just because there is not enough starting

torque. Therefore, the motor may operate under locked condition for a long time and this causes the input electrical energy converts to heat instead to mechanical output, resulting in shortening the life of the motor. There is a device, is called a linear current booster (LCB) that is designed to overcome this problem [5]. In addition, in direct coupling when the irradiance or the PV array operating temperature changes there are only few conditions where the operating of the DC motor is near to the maximum operating point [111]. The operating point of the PV array can be moved to the maximum power point by using a DC-DC converter as an interface. The converter has the ability to change the input resistance by changing the duty ratio [111].

3.4.3 Interfacing the PV array to the DC water pumping load

This section presents how to maximize the power delivered from the PV array to the load at all insolation levels. A buck converter without the output filter, which is essentially a step-down converter, also known as a chopper, inserted between the PV array and the load as shown in Fig. 3.30.

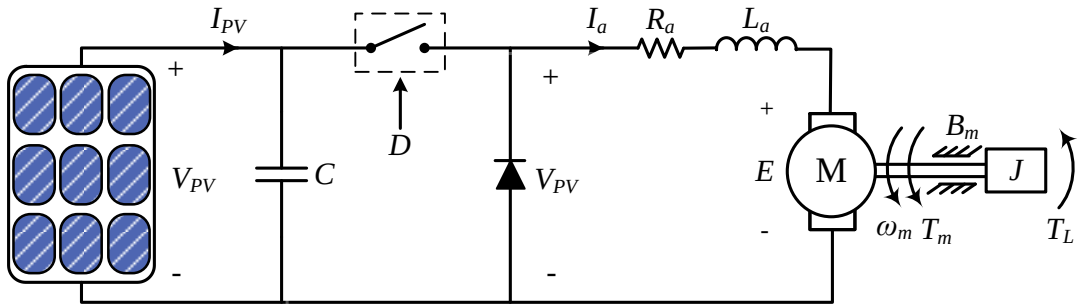

Fig. 3.30 PV array supplying DC pump through step-down converter.

In block diagram shown above, the maximum power can be transferred to the load by the chopper when it is driven with optimal duty ratio *D*. The peak power P_{peak} delivered to the load under steady-state conditions at any solar insolation levels can be derived using Equation (3.49).

$$P_{peak} = R_a I_a^2 + E I_a \tag{3.49}$$

The duty ratio is expressed in terms of the motor speed to define how the motor speed is affected by changing the buck chopper duty ratio. Therefore, Equation (4.11) can be expressed in terms of the speed. From Equations (4.8) and (4.10), the torque developed by the motor under steady-state condition is given by either Equation (3.50) or (3.51).

$$\frac{E\,I_a}{\omega_m} = B_m\omega_m + T_L \tag{3.50}$$

$$E\,I_a = B_m\omega_m{}^2 + T_L\omega_m \tag{3.51}$$

Similarly from Equation (3.48), the armature current is given by

$$I_a = \frac{B_m\omega_m + T_L}{K_t} \tag{3.52}$$

Substituting Equations (3.51) and (3.52) into (3.49) yields,

$$P_{peak} = \left(\frac{B_m\omega_m + T_L}{K_t}\right)^2 R_a + B_m\omega_m{}^2 + T_L\omega_m \tag{3.53}$$

$$P_{peak} = \frac{R_a}{K_t^2}\left(B_m{}^2\omega_m{}^2 + 2B_m\omega_m\, T_L + T_L{}^2\right) + B_m\omega_m{}^2 + T_L\omega_m \tag{3.54}$$

Equation (3.54) results in a polynomial whose order depends on the type of load torque T_L. Equation (3.54) is solved for ω_m for various insolation levels taking the real and the positive values. To determine the variation of the duty ratio D with the speed ω_m corresponding to peak powers associated with different levels of solar insolation, the output voltage V_o of the buck chopper is calculated from

$$V_o = R_a\, I_a + E = R_a\, I_a + K_e\omega_m \tag{3.55}$$

Where ω_m is the speed corresponding to maximum power point of Equation (3.54) and then I_a can be obtained by substituting this value of ω_m into Equation (3.52).

Since the buck converter is operating in the continuous conduction mode, its duty ratio is defined by the Equation (3.56).

$$D = \frac{V_o}{V_d} \tag{3.56}$$

Then at different insolation levels the duty ratio D is calculated by:

$$D = \frac{V_o}{V_{max}} \tag{3.57}$$

Where V_o is given by Equation (3.55) and V_{max} is the voltage at maximum power of the solar panel for different insolation.

For a constant type of load torque, Equation (3.54) is a second order polynomial given by

$$\left(\frac{{B_m}^2 R_a}{K_t^2} + B_m\right)\omega_m{}^2 + \left(\frac{2B_m T_L R_a}{K_t^2} + T_L\right)\omega_m + \frac{{T_L}^2 R_a}{K_t^2} - P_{peak} = 0 \tag{3.58}$$

3.4.4 Centrifugal pump load

Although the volumetric pump and the centrifugal pump are widely used in PV pumping systems, it was reported in [112] that a load composed of a DC motor driving a constant volume pump represents a non-matched load for a PV array because the motor driving a constant volume pump requires a nearly constant current. However, it was found in [113] the PV array energy utilized by the centrifugal pump is much higher than by the volumetric pump, because the centrifugal pump works for longer periods even for low insolation levels and its load characteristic is well matched to the maximum power locus of the PV array. Also centrifugal pumps are inexpensive, simple, require low maintenance and are available in a wide range of flow rates and heads. Therefore a centrifugal pump is considered in this work.

The centrifugal pump load develops speed-dependant torques. The speed-torque characteristics of centrifugal pump including friction torque are approximately given by the Equation (4.21) [21].

$$T_p = T_L = A_L \, K_L \omega_m^{1.8} \tag{3.59}$$

T_p is the torque required to drive the pump, A_L is the load friction (Nm) and K_L The proportional constant of the load torque N.m/(rad/sec)^2.
Since the load torque $T_L = T_p$, hence Equation (3.54) becomes:

$$\left(\frac{B_m^2 R_a}{K_t^2} + B_m\right)\omega_m^2 + \left(\frac{2B_m(T_p)R_a}{K_t^2} + (T_p)\right)\omega_m + \frac{(T_p)^2 R_a}{K_t^2} - P_{peak} = 0 \tag{3.60}$$

By substituting Equation (3.59) into (3.60) yields,

$$\left(\frac{K_L^2 R_a}{K_t^2}\right)\omega_m^4 + \left(\frac{2B_m K_L R_a}{K_t^2} + K_L\right)\omega_m^3 + \left(\frac{B_m^2 R_a}{K_t^2} + B_m\right)\omega_m^2 - P_{peak} = 0 \tag{3.61}$$

Equation (3.61) is implemented in MATLAB to calculate the rotation speed of the motor ω_m for a given value of peak power P_{peak}. For the MATLAB script of this equation please refer to Appendix A.1.2.

3.5 Summary

In this chapter, the model development for the component parts of the proposed PV water pumping system are discussed. The component parts are: PV array, power electronic interfacing device (DC-DC converter), permanent DC motor and centrifugal pump load.

The chapter begins with the physical structure of PV cells along with the fundamental concept and principles of converting the solar energy to electrical energy. The modeling of equivalent electrical circuit of PV cell presented and discussed. The model is implemented using MATLAB to study the PV characteristics. Furthermore, the low output power of the single cell is discussed and

how to connect number of cells in series and parallel to form a PV panel and array to meet the desired load power. The effect of temperature and solar radiation on the I-V and P-V characteristics of PV cell also discusses this chapter to show the importance of MPPT in the PV system.

This chapter introduces and investigates various DC-DC converters used in the MPPT of PV systems. As the PV system is proposed in this work is a stand-alone system therefore, the focus was on the non-isolated converter: Buck converter, Boost converter, Buck-Boost converter and Cuk Converter. The electrical circuits of these converters were presented and operating concept of each convert was thoroughly discussed. And then followed by a discussion mentioning advantages and disadvantages of each converter and which the most reliable converter to be implemented in the PV water pumping system. It was concluded that, the DC-DC buck converter is the suitable converter if the load comprises a DC motor and it will be simulated in the MATLAB using the SimPowerSystems block-set.

The chapter discusses the DC motor and load pump used in proposed PV water pumping system. The DC motor type chosen is a permanent magnet brushed motor hence it can be directly coupled to the PV array without inverter and it is efficient, require low maintenance. The mathematical model of the PMDC motor is presented and the problem of the motor directly connected to the PV array discussed. The load pump driven by the PMDC motor is a centrifugal pump this is because it is inexpensive, requires low maintenance, and available in a wide range of flow rates and heads. Additionally, the centrifugal pump works for longer periods even for low insolation levels and its load characteristic is well matched to the maximum power locus of the PV array. Mathematical equations also are derived in this chapter to be implemented in MATLAB/SIMULINK using various functional blocks develop the PMDC motor and the pump models.

CHAPTER 4 - FUZZY LOGIC CONTROLLER

4.1 Fuzzy logic

Fuzzy logic is based on a mathematical model which deals with uncertainty and imprecise, ambiguous, noisy, or missing input information. It compares an analog input signal to a predetermined logic variable membership function or fuzzy sets, that correspond to values in the range 0 and 1. Fuzzy logic is implemented in a control system to emulate human-like decisions in control. FL techniques have been widely used in a wide range of engineering applications due to their heuristic nature associated with simplicity and effectiveness for both linear and nonlinear systems [114]. It can be implemented in software, hardware or a combination of both. Fuzzy sets are considered as the brain of the fuzzy control system which in turn is responsible for converting analog input values into a scale of 0 to 1.

The concept of fuzzy logic was first known 40 years ago, since the fundamental theory was introduced by Zadeh in 1965 [115, 116]. However, the theory of FL was not applied to control system until ten years later, because of insufficient small computer capability before that time. In the early 70's, the theory began to produce results when it was applied in a practical application to control an automatic steam engine by Mamdani in 1974 [117]. In 1976, an industrial application to control cement kilns was developed in Denmark by Blue Circle Cement and SIRA and the system started working in 1982 [118]. Over the past few decades fuzzy logic controllers have been successfully applied to many industrial applications. Starting from 1980s it was implemented in applications such as industrial manufacturing, banks, automatic control, automobile protection, banks, and to control consumer products: washing machines, dish washers, televisions, air conditioners, rice cookers and video cameras[119].

Some of the essential characteristics of FL are listed below [120]:

- In fuzzy logic, exact reasoning is viewed as a limiting case of approximate reasoning.
- In fuzzy logic, everything is a matter of degree.

- In fuzzy logic, knowledge is interpreted a collection of elastic or, equivalently, fuzzy constraint on a collection of variables.
- Interface is viewed as a process of propagation of elastic constraints.
- Any logic system can be fuzzified.

There are two main characteristics of fuzzy systems that give them better performance for specific applications.

- Fuzzy systems are suitable for uncertain or approximate reasoning, especially for a system with a mathematical model that is difficult to derive.
- Fuzzy logic allows decision making with estimated values under incomplete or uncertain information.

4.2 Fuzzy Logic Controller Structure

The general structure of a fuzzy controller and its main parts is shown in Fig. 4.1. The fuzzy logic controller consists of four components: fuzzification interface, knowledge base, interface engine, and defuzzification interface [121].

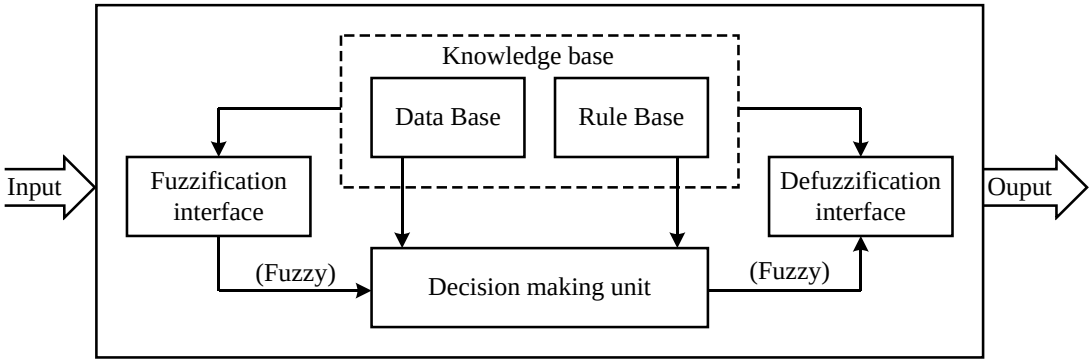

Fig. 4.1 general structure of fuzzy interface system.

The fuzzifier transforms crisp inputs into the fuzzy subsets to obtain degrees of memberships and represent them with linguistic variables, which in turn are used to activate rules. The fuzzy inference engine process those data to obtain the desired output. The defuzzifier converts those fuzzy outputs to crisp variables to complete the desired fuzzy logic control objectives.

Every fuzzy set can be represented by its membership function. In practice the membership functions can have a number of different shapes depending on the

application. They can be triangular, trapezoidal, Gaussian, bell-shaped, sigmoidal or S-curve. Some popular waveforms of the membership functions are shown in Fig. 4.2 [121, 122].

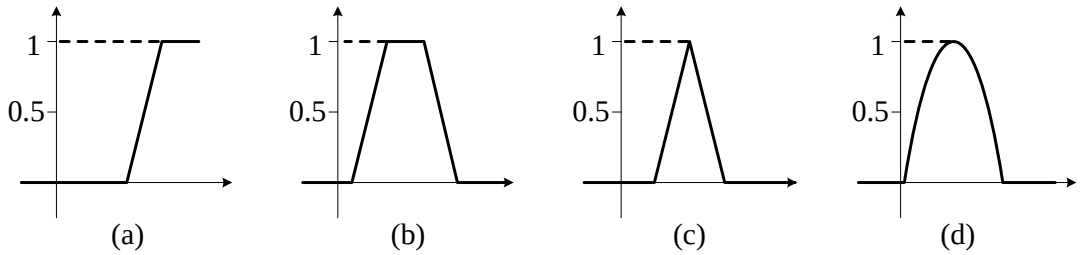

Fig. 4.2 different graphs of membership functions (a) monotonic (b) trapezoidal (d) triangular (c) Gaussian.

Trapezoidal or triangular membership functions are usually used in systems that require significant dynamic variation in a short period of time. A Gaussian or S-curve membership function is always selected if the system requires very high control accuracy [121].

4.2.1 Knowledge base

The knowledge base is the heart of the fuzzy control system. It is the inference basis for fuzzy control. The knowledge base, defines all relevant language control rules and parameters. The derivation of fuzzy control rules can be performed in four modes. These four modes are not mutually exclusive, and it is necessary to combine them to obtain an effective system [122, 123].

- Expert experience and control engineering knowledge: the fuzzy control rule is based on information obtained from the controlled system.
- Operators' control actions: observation of human controller's actions in terms of input-output operating data.
- Based on the fuzzy model of process: linguistic description of the dynamic characteristics of a process.
- Based on learning: ability to modify control rules such as self-organizing controller such as neural network and genetic algorithm.

The number of base rules can be defined based on the number of membership in the fuzzy set and the inputs. For example if the system contains two inputs and each of

them contains three memberships then the total base rules will be 3*3 = 9 base rule. The higher the number of memberships, the better the system efficiency will be, but the system implementation will become more complex [122].

4.2.2 Fuzzy interface procedure

There are several techniques for performing the fuzzy interface process, such as, the Mamdani method, Takagi-Sugeno_Kang (TSK) method, Tsukamot method and Larsen method. The Mamdani and TSK methods are the most commonly used methods in fuzzy controllers [121, 122]. However, the Mamdani method is usually more popular for most control engineering applications because this method is computationally more efficient and has better interpolative properties than the other interface methods [124].

A. Mamdani method

The Mamdani method is the most widely used fuzzy interface strategy. Since it was proposed in 1975, by Professor Ebrahim Mamdani of London University who built one of the fuzzy systems to control a combination of steam engine and boiler. In Mamdani‘s method a set of fuzzy if-then rules was applied, and these were supplied by experienced human operators [125].

Mamdani fuzzy logic uses the linguistic variables to describe the process states and uses these variables as inputs to control rules. The terms of the linguistic variables are fuzzy sets with certain shape. Mamdani fuzzy logic usually uses the trapezoidal or triangular fuzzy set but other shapes are possible. The fuzzy interface process of the Mamdani method can be formed in four steps [125]:

- Fuzzification
- Rule evaluation
- Aggregation of the rule outputs
- Defuzzification

To clarify the fuzzy interface working process of the Mamdani method, a simple two-input one-output problem that includes three rules is examined:

Rule 1: IF X is A_3 OR Y is B_1 THEN z is C_1

Rule 2: IF X is A_2 AND Y is B_2 THEN z is C_2

Rule 3: IF X is A_1 THEN z is C_3

Step 1: Fuzzification

Fuzzification is the first step in fuzzy logic processing, in which the crisp quantities are converted to fuzzy inputs. The transformation process of fuzzy values is represented by the membership function [122, 125].

There might be some error, when measuring the voltage, current, temperature, solar insolation, etc., in most real applications. This will result in vague data. Therefore, the vagueness can be represented by the membership functions. Fig. 4.3 shows the fuzzification stage of the example. Firstly, take the crisp inputs, $x1$ and $y1$, and determine the degree to which these inputs belong to each of the appropriate fuzzy sets. According to Fig. 4.3 the following are obtained [122, 125]:

$$\mu A1(x) = 0.5,\ \mu A2(x) = 0.2,\ \mu B1(y) = 0.1,\ \mu B1(y) = 0.7$$

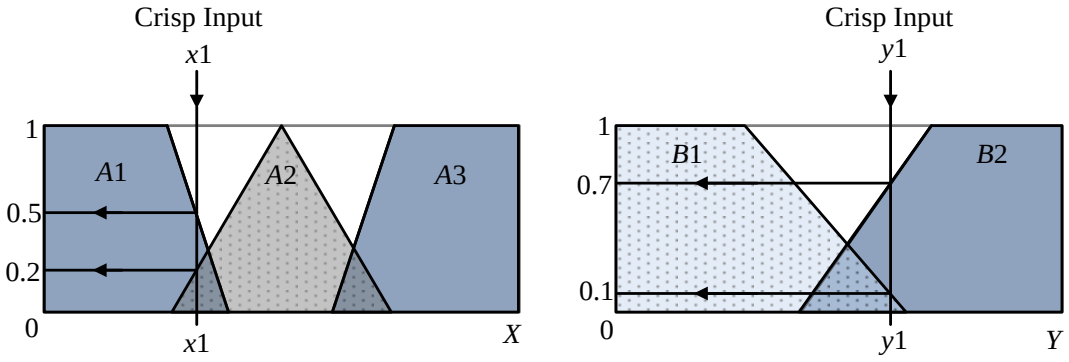

Fig. 4.3 Fuzzification.

Step 2: Rule evaluation

In this step the fuzzified inputs are applied to the antecedents of the fuzzy rule, then applying the fuzzy operator to fuzzy rule that has multiple antecedents to resolve the antecedents to a single number between 0 and 1. The fuzzy operator (AND or OR) is used to obtain this signal number. If the OR fuzzy operation is used, thus the classical fuzzy operation union is used [125]:

$$\mu A \cup B(x) = max\ [\mu A(x),\ \mu B(x)] \qquad (4.1)$$

Similarly, in order to evaluate the conjunction of the rule antecedents, the AND fuzzy operation intersection is applied as in Equation (6.2).

$$\mu A \cap B(x) = min\ [\mu A(x),\ \mu B(x)] \tag{4.2}$$

Fig. 4.4 illustrates the rule evaluations. The most common method of correlating the rule consequent with the truth value of the rule antecedent is the clipping method. In this method, the consequent membership function is being cut at the level of the antecedent truth. Since the top of the membership function is sliced, the clipped fuzzy set loses some information. However, clipping method is widely used because it involves less complex and faster mathematics, generates an aggregated output surface that is easier to defuzzify [122, 125].

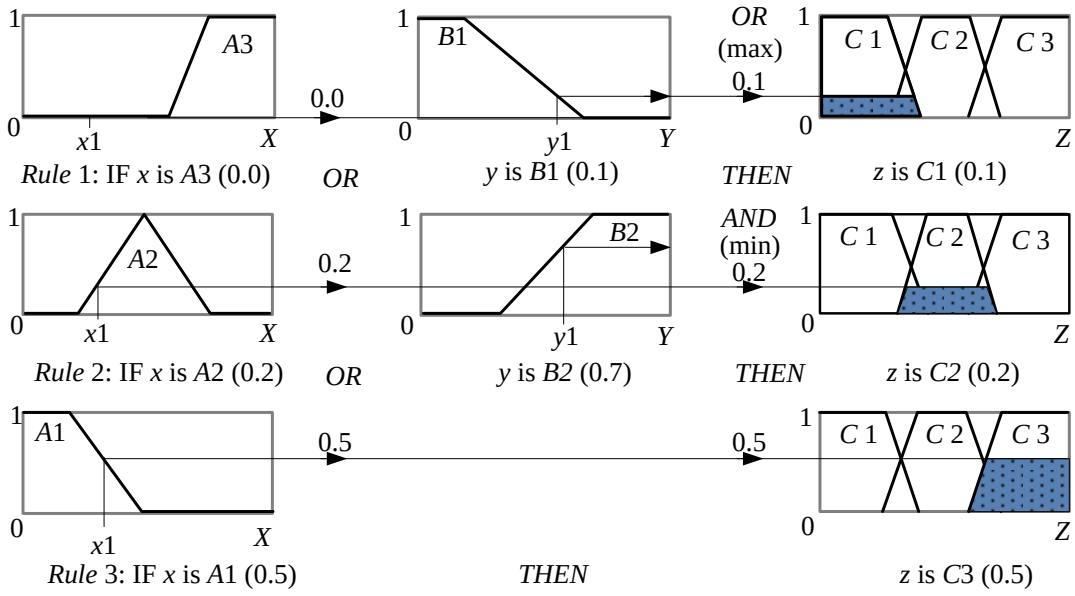

Fig. 4.4 Rule evaluation in Mamdani method.

There is another method which generally loses less information by providing a better approach for preserving the original shape of the fuzzy set, which is called scaling. In this method, the original membership function of the rule consequent is adjusted by multiplying all its membership degrees by the truth value of the rule antecedent [122]. The clipping and scaling methods are shown in Fig. 4.5.

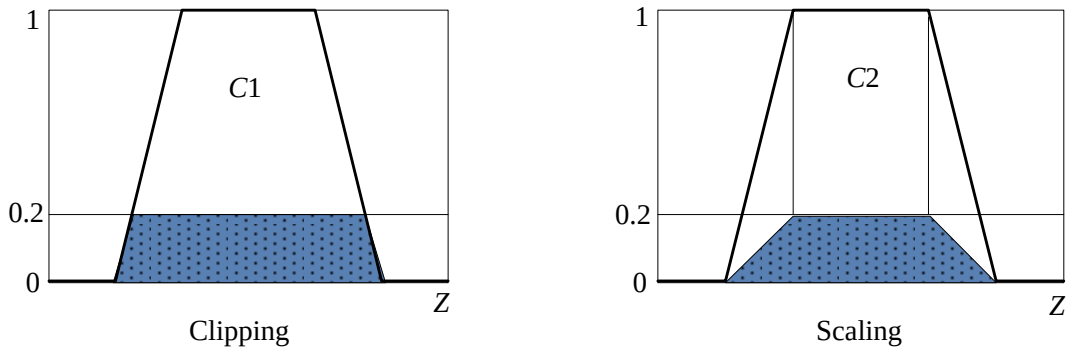

Fig. 4.5 Clipping and scaling examples.

Step 3: Aggregation of the rule outputs

After finding the output of each rule, the aggregation process is applied to unify all the rules outputs to become one output. The input to the aggregation process is the combination of truncated or scaled consequent membership function, and the output is the combined output fuzzy set. Fig. 4.6 shows the aggregation of the rule outputs [122].

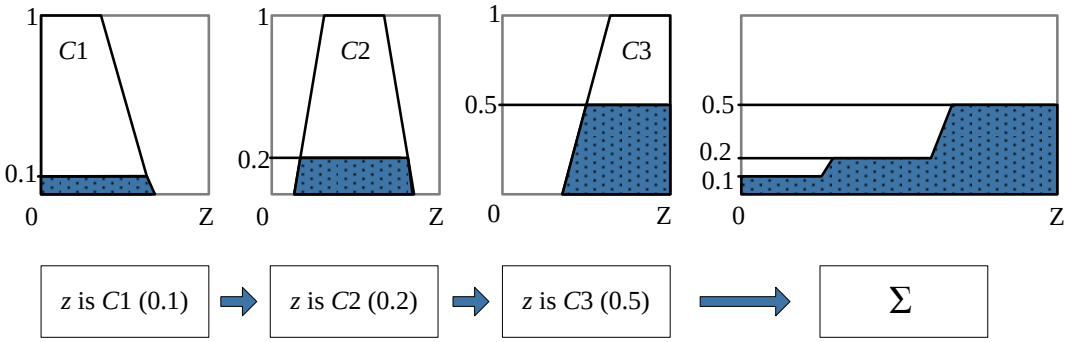

Fig. 4.6 Aggregation of the rule outputs.

Step 4: Defuzzification

The Defuzzification is the last step in the process of the fuzzy inference, and its reverse of the fuzzification process. The output of the fuzzy inference process result from the combination of the control inputs and it is still linguistic variable. However, the final output of the fuzzy control has to be a crisp number. Hence the defuzzification process is needed to convert the fuzzy output back to the crisp output to be available for real application controllers [119, 123].

There are several defuzzification techniques which are used, but there is one systemic procedure for selecting a good defuzzification strategy. Selection of the defuzzification technique relies on the system or the application characteristics [126]. The following three defuzzification techniques are the most commonly used techniques:

- **Mean of maximum method (MOM)**

The MOM defuzzification strategy computes the average value of all the control actions whose membership functions reach the maximum. In the case of a discrete universe, the control action can be expressed by Equation (4.3) [126].

$$MOM = \sum_{i=1}^{l} \frac{w_j}{l} \tag{4.3}$$

In Equation (4.3), w_j is the support value when the membership function reaches the maximum value $\mu_z(w_j)$, and l is the number of support values.

- **Height method (HM)**

The HM defuzzification method can only be applied when the output membership function is an aggregated union result of symmetrical functions [121]. In the HM method, the first step involves evaluating the centroid of each output membership function for each rule and then the final output is calculated as the average of individual centroids weighted by their heights (degree of membership) as in the Equation (4.4) [127].

$$Z = \frac{\sum_{j=1}^{n} w_j \cdot \mu(w_j)}{\sum_{j=1}^{n} \mu(w_j)} \tag{4.4}$$

- **Centre of gravity method (COG)**

The centre of gravity method is the most widely used defuzzification technique in real applications. The advantage of COG method is the defuzzified values tend to move smoothly around the output fuzzy region [119]. The COG technique is a basic

general defuzzification technique that computes the value of the abscissa of the centre of gravity of the area below the membership. The output of COG can be represented by Equation (4.5) [119, 123].

$$COG = \frac{\sum_{j=1}^{n} w_j \cdot \mu_z(w_j)}{\sum_{j=1}^{n} \mu_z(w_j)} \tag{4.5}$$

Where *n* is the number of quantization levels of the output. According to Fig. 4.7, the COG is calculated as a follows:

$$COG = \frac{(0 + 10 + 20)\times 0.1 + (30+40 +50+60)\times 0.2 + (70 +80+ 90+100)\times 0.5}{0.1 +0.1 +0.1 +0.2 +0.2 +0.2 +0.2 +0.5 +0.5 +0.5 +0.5} = 67.4$$

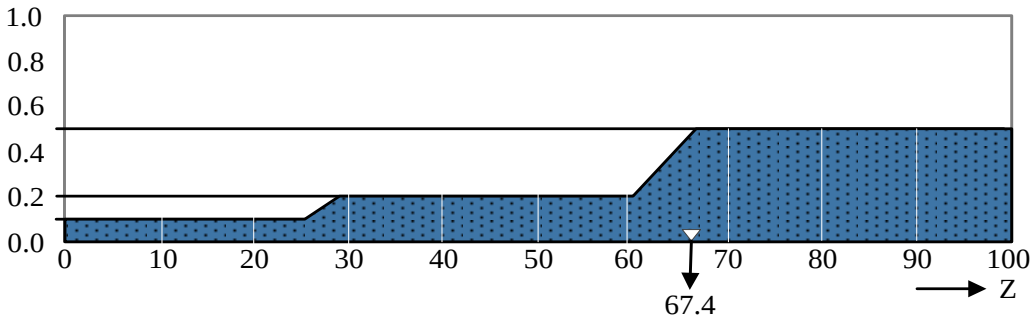

Fig. 4.7 Defuzzification example.

4.3 Fuzzy logic controller based MPPT of PV water pumping system

This section presents the proposed fuzzy logic controller for MPPT of the PV supplied DC water pump. The variation of solar radiation is the most important factor in the MPPT of PV system. It is changing periodically and nonlinearly, hence an FLC based MPPT is proposed to solve the problem and to deliver the maximum available power of the PV array to the load. A schematic of the photovoltaic array and water pumping system used to investigate the fuzzy logic controller performance is shown in Fig. 4.8. The system comprises a PV array, buck converter, fuzzy based MPPT control unit and DC permanent magnet motor coupled to a centrifugal pump. The power produced by the PV array is supplied to the DC motor through a buck converter. The change in output power of the PV array, ΔP_{PV}, and the change in rotation speed of the pump, $\Delta\omega_m$, are used as input variables of the fuzzy control unit to determine the duty-ratio, D, control signal for the buck converter.

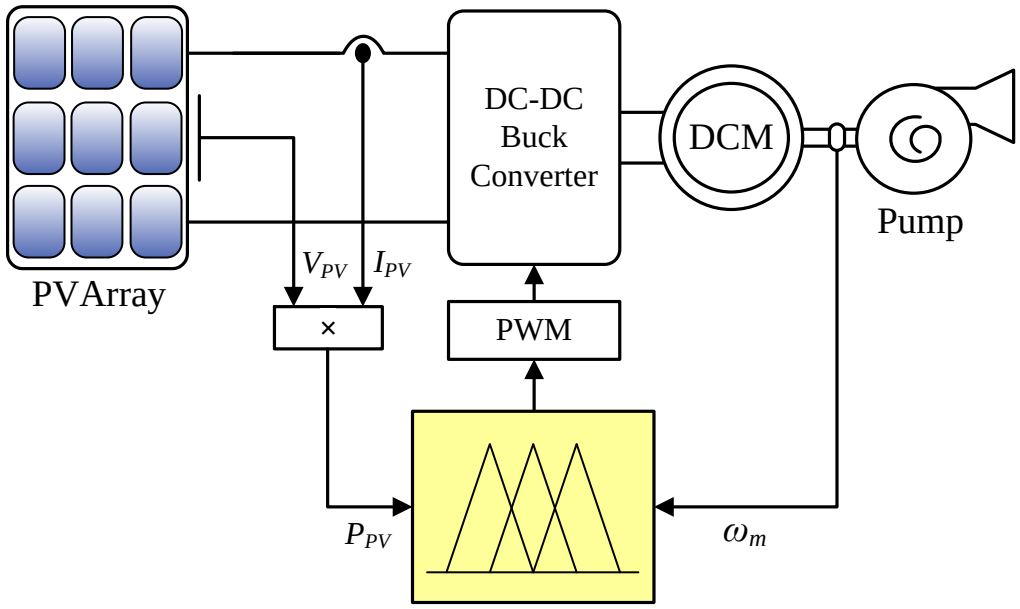

Fig. 4.8 Schematic diagram of the proposed MPPT water pumping system based FLC.

4.3.1 Fuzzy logic controller

The control objective is to track the maximum power point and maintain the system operating on this point at all levels of temperature and solar irradiation, which will lead consequently to maximizing the dc motor speed and the water discharge rate of the coupled centrifugal pump. At the time when output power of the PV array is

maximum, the hydraulic power, $P_P = K_T \omega_m^3$, is maximum. Consequently, the rotational speed, ω_m, is a maximum at the maximum power point. By making use of the relation between the PV array output power and the rotational speed, a fuzzy logic controller has been proposed to adjust the buck converter duty ratio which adapts online the PV array output power to maximize the rotational speed, which in turn increases the water discharge of the centrifugal water pump.

In the fuzzification stage, numerical input variables are calculated or converted into linguistic variables based on subsets called membership function [27, 128], [16]. The proposed FLC MPPT method has two input variables and one output variable as shown in Fig. 4.9. The input variables are the PV array output power variation ΔP_{PV} (k) and rotation speed variation $\Delta\omega_m$ (k) at sampling instant k. The output variable is the duty ratio D of the buck converter. The input variables $\Delta P_{PV}(k)$ and $\Delta\omega_m$ (k) are expressed by Equation (7.5) and Equation (7.6) respectively.

$$\Delta\omega_m(k) = G_\omega(\omega_m(k) - \omega_m(k\text{-}1)) \quad (4.6)$$

$$\Delta P_{PV}(k) = G_P(P_{PV}(k) - P_{PV}(k\text{-}1)) \quad (4.7)$$

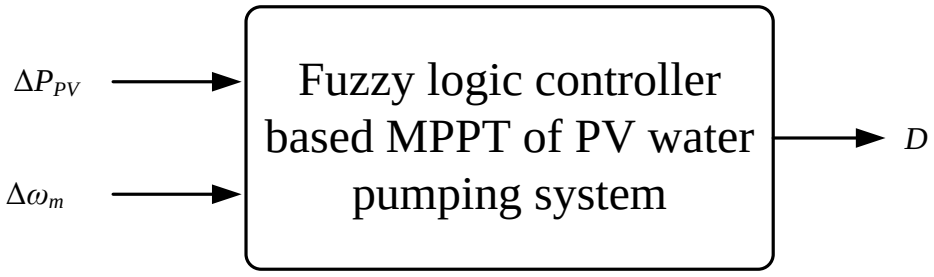

Fig. 4.9 General diagram of the proposed FLC of water pumping MPPT.

In (7.5) and (7.6), G_ω and G_P are scaling factors used to normalize the $\Delta\omega_m$ (k) and ΔP_{PV} (k), respectively. The scaling factors play an important role in optimizing performance and can be chosen using trial and error. The membership functions of the both inputs and output variables are represented by symmetric triangular functions and defined in common normalized range of (-1, 1). The membership functions of the input variables ΔP_{PV} and $\Delta\omega_m$ which are assigned for fuzzy sets have the same shape and range, and they are shown in

Fig. 4.10. The membership function of the output variable also has the same number of sets as the input variables, and is shown in Fig. 4.10. The membership function of both inputs and output variables are assigned five sets, including positive big (PB), positive small (PS), zero (ZO), negative big (NS), and negative small (NB).

Fuzzy rules comprise a set of rules in linguistic form which associate the fuzzy inputs with the fuzzy output. These are based on an expert knowledge and understanding of the system behaviour that is required to achieve the control objectives. The fuzzy control rules have been set up using a set of IF-THEN statements that contain all information for the controlled parameters. The fuzzy control rule includes 25 rules as described in
Table 4.1. These rules are used for the control of the buck converter such that the maximum power is achieved at the output of the PV array. The fuzzy rules are designed to incorporate the following considerations keeping in view the overall tracking performance.

1. If a positive variation in the rotation speed is accompanied with a positive variation of PV array output power, then the chopper duty ratio should be increased. Otherwise if the variation of PV array output power is negative, then chopper ratio should be decreased.

2. If the rotation speed variation is zero or sufficiently close to zero which means that its maximum is reached, then there should be no change in the chopper ratio.

3. If a negative variation in the rotation speed is accompanied with a positive variation in PV array output power, then the chopper duty ratio should be decreased. Otherwise if the variation of PV array output power is positive, then chopper ratio should be increased.

In the defuzzification stage and inference mechanism the output of fuzzy logic control is converted from linguistic variables to numerical variables. The inference mechanism determines the matching degree of the current fuzzy input with respect to each rule and the controller has to resolve the conflict between different rules being obeyed at the same time and decides which rules are to be obeyed according to the input field. Then the obeyed rules are combined to form the control actions. There are

different methods of defuzzifying an outcome fuzzy set. The method used for this is called Centre of Gravity (COG) or centroid. The idea of (COG) is to find the variable value of the centre of gravity of the composite membership function for the fuzzy value [129].

The crisp value of the output variable $\Delta D(k)$ is computed by Equation (4.5).

$$D(k) = D(k\text{-}1) + G_D\, \Delta D(k) \tag{4.8}$$

Where G_D is the output scaling factor of the fuzzy logic controller and $D(k)$ is the final output signal sent to the system.

Table 4.1 Fuzzy rules base

If $\Delta\omega_m > 0$ If $\Delta P > 0$ D(K) = D(K-1) +ΔD Else D(K) =D(K-1) - ΔD End	If $\Delta\omega_m$ is PB and ΔP is PB then ΔD is PB
	If $\Delta\omega_m$ is PB and ΔP is PS then ΔD is PB
	If $\Delta\omega_m$ is PB and ΔP is NB then ΔD is NB
	If $\Delta\omega_m$ is PB and ΔP is NS then ΔD is NB
	If $\Delta\omega_m$ is PB and ΔP is ZO then ΔD is NS
	If $\Delta\omega_m$ is PS and ΔP is PB then ΔD is PS
	If $\Delta\omega_m$ is PS and ΔP is PS then ΔD is PS
	If $\Delta\omega_m$ is PS and ΔP is NB then ΔD is NS
	If $\Delta\omega_m$ is PS and ΔP is NS then ΔD is NS
	If $\Delta\omega_m$ is PS and ΔP is ZO then ΔD is NS
If $\Delta\omega_m = 0$ D(K) = D(K-1)	If $\Delta\omega_m$ is ZO and ΔP is PB then ΔD is PB
	If $\Delta\omega_m$ is ZO and ΔP is PS then ΔD is PB
	If $\Delta\omega_m$ is ZO and ΔP is ZO then ΔD is ZO
	If $\Delta\omega_m$ is ZO and ΔP is NB then ΔD is NB
	If $\Delta\omega_m$ is ZO and ΔP is NS then ΔD is NB
If $\Delta\omega_m < 0$ If ΔP > 0 D(K) = D(K-1) -ΔD Else D(K) = D(K-1) + ΔD End	If $\Delta\omega_m$ is NB and ΔP is PB then ΔD is NB
	If $\Delta\omega_m$ is NB and ΔP is PS then ΔD is NB
	If $\Delta\omega_m$ is NB and ΔP is NB then ΔD is PB
	If $\Delta\omega_m$ is NB and ΔP is NS then ΔD is PB
	If $\Delta\omega_m$ is NB and ΔP is ZO then ΔD is PS
	If $\Delta\omega_m$ is NS and ΔP is PB then ΔD is NS
	If $\Delta\omega_m$ is NS and ΔP is PS then ΔD is NS
	If $\Delta\omega_m$ is NS and ΔP is NB then ΔD is PS
	If $\Delta\omega_m$ is NS and ΔP is NS then ΔD is PS
	If $\Delta\omega_m$ is NS and ΔP is ZO then ΔD is PS

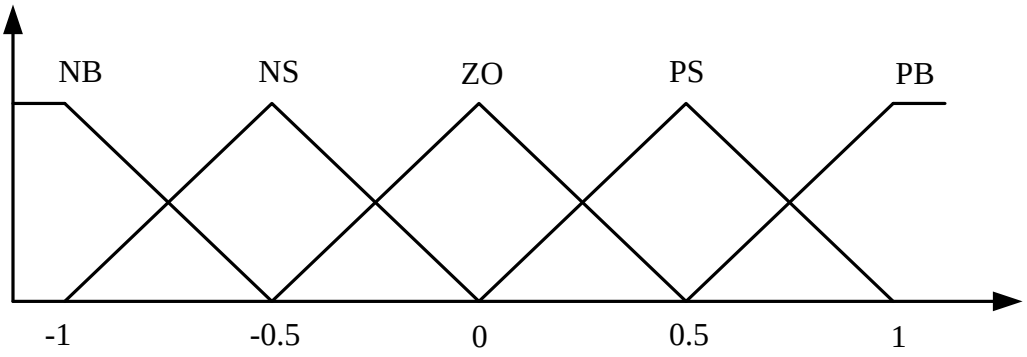

Fig. 4.10 Membership functions of the 1st input variable (ΔP_{PV}), 2nd input variable ($\Delta\omega_m$) and the output variable (ΔD).

4.4 Summary

This chapter presents a discussion of the selection of the strategy and modelling of the proposed fuzzy logic based MPPT control for the PV water pumping system. The chapter begins with a brief introduction about the fuzzy logic development history and applications. Next it provides an overview of fuzzy controller basic structure with brief illustration of its main components which are: the fuzzification interference, knowledge base, interface engine, and defuzzification interference. The fuzzy interface process has also been discussed and explained however, there are several methods for performing the fuzzy interface process, the Mamdani method was thoroughly explained and used in this work. This is because the Mamdani method is computationally more efficient and has better interpolative properties than the other interface methods.

The design of the proposed fuzzy logic based MPPT controller for the PV water pumping system is also discussed in this chapter and illustrated with a the complete schematic diagram of the system. The proposed FLC is designed to track the maximum power of the PV array and deliver it to pump load under variable temperature and insolation conditions. The controller uses the variation of the PV array output power ΔP_{PV} and variation of the motor-pump rotational speed $\Delta\omega_m$ as the input variables to continuously adjust the buck converter's duty ratio, which constitutes the output variable of the control, to maintain system operating at the MPP.

CHAPTER 5 - ARTIFICIAL NEURAL NETWORK

5.1 Artificial neural network

The concept of artificial neural network (ANN) analysis was developed almost 60 years ago. However, applications software has only been developed in the last 30 years to handle practical problems. It is an artificial network that mimics human biological neural network behaviour. Recently, ANN applications have rapidly increased in various fields as the key solution to solving highly complex problems [130, 131]. The ANNs have supporting characteristics to become successful such as, simplicity and relatively high speed response. The ANNs operate like a black-box model. It does not require detailed information about the system. They effectively learn the relationship between the input and the output variables by making use of trends in previously recorded data. Also ANNs have the ability to work with highly nonlinear relationships, can work with numerical or analogue data, are relatively robust in terms of finding best-fit solutions, and the user does not require sophisticated mathematical knowledge [131].

5.1.1 Mathematical model of the neuron

Most of the of the neural network models that have been proposed within different theory over the years share the common building block, known as a neuron and the network interconnection structure [132]. The well-known and the most used example of the model of neuron, initially proposed by McCulloch and Pitts, is illustrated in Fig. 5.1.

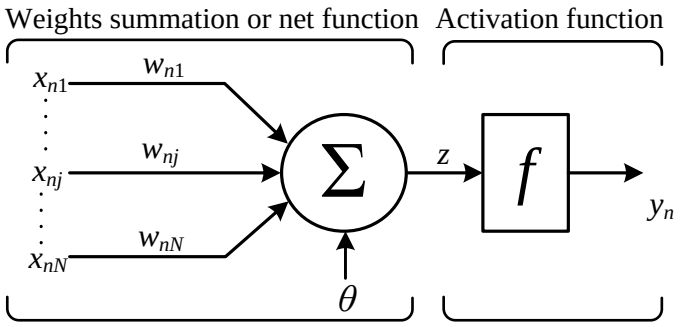

Fig. 5.1 Basic artificial neuron.

The neuron shown in Fig. 5.1, consists of two parts: the net function and the activation function. The net function determines how the network inputs ((x_{nj}; $1 \leq j \leq N$)) are combined inside the neuron. In this Fig. 5.1, a weighted linear combination is described by Equation (6.6).

$$z = \sum_{j=1}^{N} w_{nj}\, x_{nj} + \theta \tag{5.1}$$

Where the parameters ((x_{nj}; $1 \leq j \leq N$)) are known as synaptic weights and θ is called the bias (or threshold) and is used to model the threshold. There are other different types of input combination of network have been proposed in the literature [132, 133]. The output of the neuron is denoted by y_n in Fig. 5.1 and is computed through the activation function. There are several types of transfer function that are used as activation functions, such as sigmoidal (or log-sigmoid), hyperbolic tan (or tan-sigmoid), linear (bipolar), threshold and Gaussian etc [134]. The selection of activation function plays an important role in the neural network design. However, the sigmoidal, hyperbolic and linear function activations are the most commonly used function amongst the others. Examples of linear, sigmoidal and hyperbolic transfer function are shown in Fig. 5.2 (a), (b) and (c) respectively [135-137]. The linear function is described by Equation (6.7), sigmoidal function is described by Equation (6.8) and hyperbolic tangent sigmoid function is described by Equation (6.9)

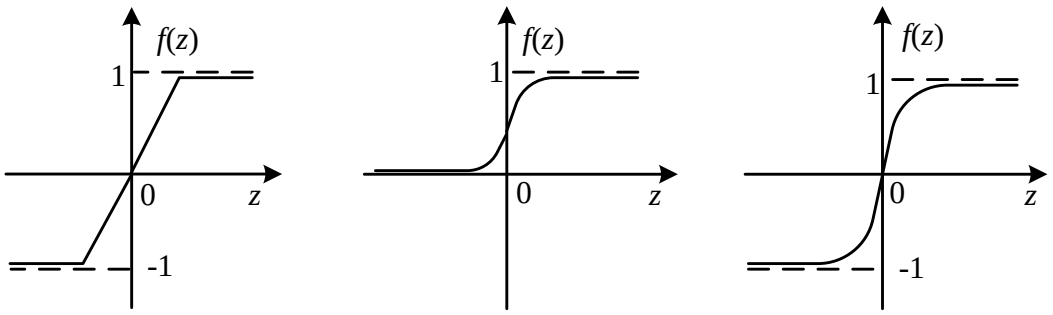

(a) Linear bipolar (b) Sigmoidal or log-sigmoid (c) Hyperbolic tan or tansig

Fig. 5.2 Transfer function

$$y_n = f(z) \tag{5.2}$$

$$f(z) = \frac{1}{1 + exp^{-z}} \tag{5.3}$$

$$f(z) = \frac{2}{1 - e^{-2z}} - 1 \tag{5.4}$$

5.1.2 Training methods

In all prediction methods a training dataset is used. The dataset comprises a sub-set of the data that we wish to model. The training can be classified into two types according to the use of the output values during the training process [138, 139]. Firstly, supervised training, in which the training set contains the input features of the system and the output data which has been predetermined by another method such as human decisions or experimental measurement. The supervised training scheme is shown in Fig. 5.3. In this method, the learning algorithm attempts to find a functional mapping between the inputs and outputs by using the training data to determine the parameters (weights and thresholds) of the prediction technique.

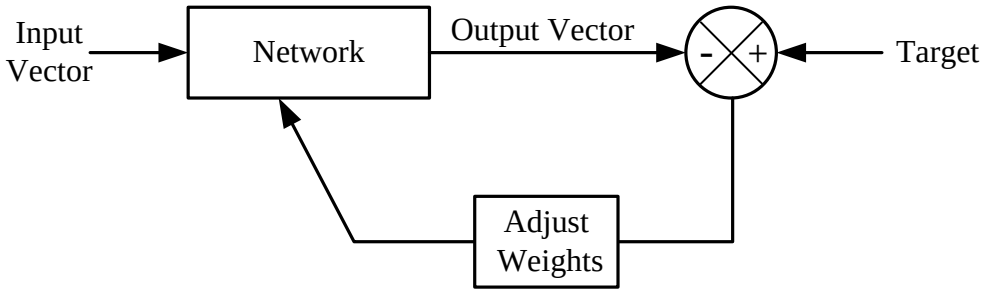

Fig. 5.3 Supervise training scheme.

The performance of the ANN model is monitored by the use of a “performance” or “error” function during the training process. This function provides a comparison between the predictions of the ANN model and the actual output values. The training process performed by iteratively decreasing in the error function and continuously until a predetermined value is reached. After training, the trained ANN model is evaluated by application of a “test dataset”, containing new data to determine how

well the model performs. A model which performs well when working on new data is said to have good generalisation [139].

Secondly, unsupervised learning or self-organized learning, in this type of training only the input training data is available. Unsupervised training techniques are often faster than for supervised methods, but unsupervised methods are often only the initial stage in a two (or more) stages training process, later stages involving supervised learning, the first training stage uses an unsupervised process to determine locations and sizes of the basic functions [139]. The schematic diagram of the unsupervised learning method is shown in Fig. 5.4.

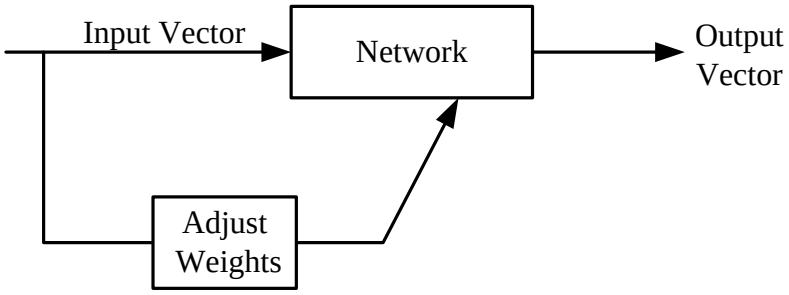

Fig. 5.4 unsupervised training scheme.

The training method used in this work is the supervised training by feedforward network.

There are several existing types of training algorithms such as backpropagation algorithm, Delta-bar-Delta, Quasi-Newton algorithm, conjugate gradient algorithm, Kohonen training and Levenberg-Marquardt algorithm [140, 141]. For training the multilayer feedforward network, the Levenberg-Marquardt method is generally recommended due to its robustness, and it provides fast convergence and it is not necessary for the user to initialize any strange design parameters [140].

5.2 ANN control based MPPT of PV Water Pumping System

The complete combined system of artificial neural network ANN controller with a PV water pumping system is illustrated in Fig. 5.5. From the schematic diagram shown below, the inputs of the proposed ANN controller are the PV array output power P_{PV} and the motor rotational speed ω_m and the output of ANN controller is the buck converter control signal. To enables delivering the maximum power of the PV array to the pump load at different solar insolation levels the duty ratio of the buck converter is adjusted accordingly by the ANN controller. The ANN controller design and training will be discussed in more detail in the later sections.

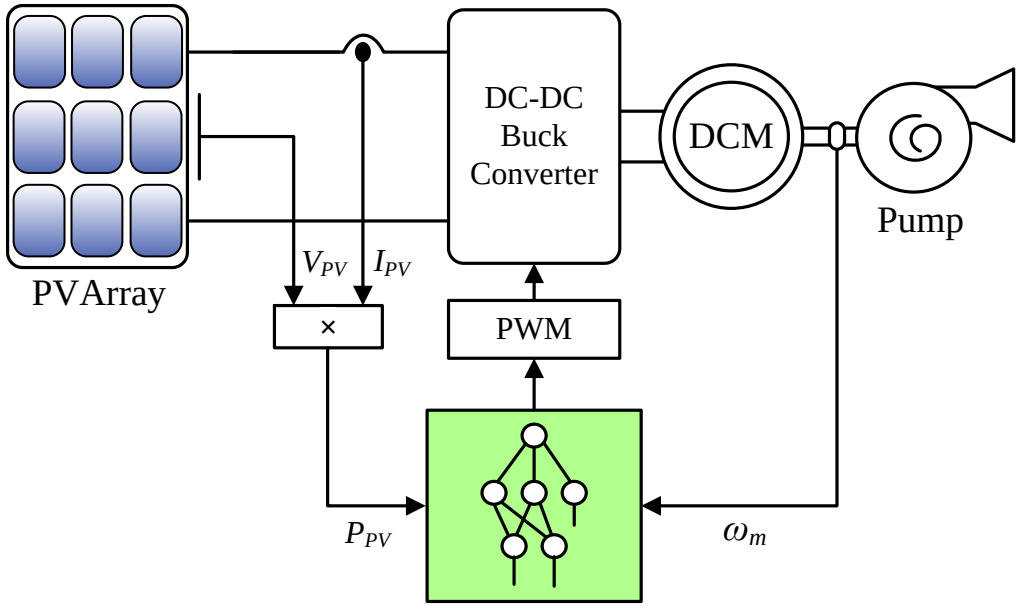

Fig. 5.5 Schematic diagram of the proposed PV water pumping system based ANNC.

5.2.1 Neural network MPPT controller architecture

The proposed ANN in this thesis is a feedforward neural network comprising three layers three layers namely input layer, hidden layer and the output layer is considered for the online estimation of the duty ratio. The configuration of the proposed three-layer feedforward neural network is illustrated in Fig. 5.6. The structure of multilayer feedforward networks are mostly determined by experience, and according to the previous studies there is no a valid formula that is appropriate for different situations [142]. The author in [143] reported that, the ANN in the default setting has 10 neurons in the hidden layer. Increasing the number of neurons in the hidden layer

increases the power of the network, but requires more commutation and is likely to produce overfitting. There are two categories from which to select the architecture of the ANN techniques as in [142, 144]. The first category begins with a small network and gradually adding connections or nodes as needed. In the second category, a big network is selected, and then reduced by gradually eliminating the unnecessary connections or nodes. The first category was used in this study to map the relationship between the duty ratio and the PV power and the motor speed. The input layer consists of a two dimensional vector, PV array output power and the DC motor speed. The output layer of the proposed ANN comprises a one dimensional vector, which is the controlling signal of the buck chopper *D*.

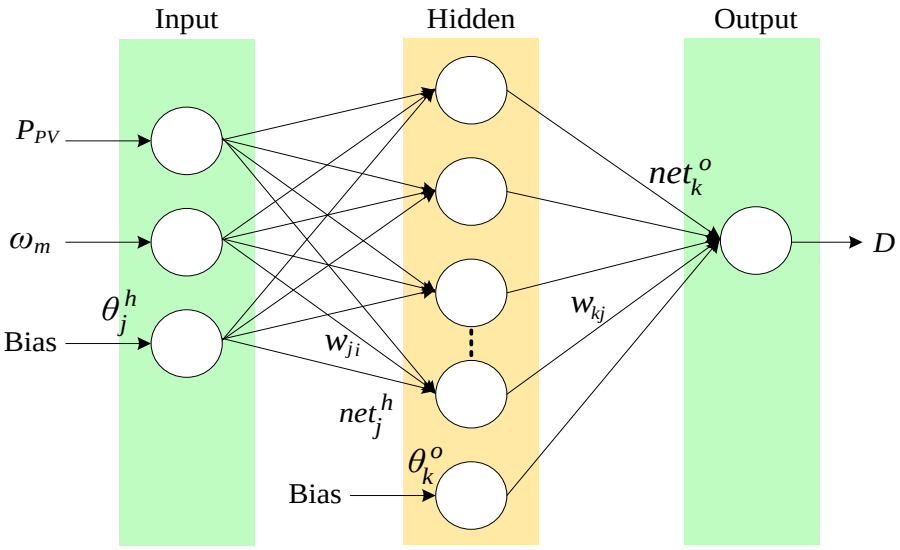

Fig. 5.6 Feedforward neural network.

The outputs of the input layer are weighted and summed together, and then a bias is added to the sum of the weighted inputs. Finally the summation of the weighted inputs and the bias are passed through the transfer function *f*. A hyperbolic tangent sigmoid transfer function was used as an activation function to calculate the hidden layer output. For the neurons of the output layer of the proposed neural network a linear transfer function was used to provide a wide range of solutions [137, 145].

The collected data for training should be first normalized before being applied to the input layer as the input vector.

$$x_n = \left(x_{n_1},\, x_{n_2},\, x_{n_3},\, \ldots, x_{n_n}\, x_n\right)^T$$

When the weight vectors of the input layer are multiplied to the hidden layer and added to the bias vector, the net input for the *j*th hidden unit is

$$net_j^h = \sum_{i=1}^{n} \left(w_{nji}\, x_{ni} + \theta_j^h \right) \tag{5.5}$$

Where w_{nji} is the weight on the connection from the *i*th input unit to the *j*th hidden layer, and θ_j^h is the bias for each joint from the input layer to the output layer, which is mainly used to improve the learning speed during network training process. Now the output value from the hidden layer is

$$y_{n\ j}^{\ h} = f_1 \left(\sum_{i=1}^{n} w_{nji}\, x_{ni} + \theta_j^h \right) \tag{5.6}$$

The net input to the neurons in the output layer becomes

$$net_k^o = \sum_{j=1}^{N_h} w_{nkj}\, y_j^h + \theta_k^o \tag{5.7}$$

Where w_{nki} is the output weight connecting the *i*th input unit to the *k*th output unit and θ_k^o is the threshold value for neuron in the output layer. The output of the neurons in the output layer is

$$y_{n\ k}^{\ o} = f_2 \left(\sum_{j=1}^{N_h} w_{nkj}\, y_j^h + \theta_k^o \right) \tag{5.8}$$

5.2.2 Training the network

The training process determines the connection weights of the neural network. The training method used in this work is the supervised method. Therefore, a set of input output pairs of the training patterns or training data are required to accomplish the training process. The set of input output training data is shown in Appendix C in Table C.1 to Table C.4.

The input data set is PV array maximum output power P_{max} and the rotational speed of the DC motor $\omega_{m,}$ whereas the output data set is the corresponding duty ratio D of the buck chopper. The data for P_{max} has been obtained from the MATLAB function shown in Appendix A.1.1 , the data for ω_m has been obtained from the MATLAB script shown in Appendix A.1.2 and the data for D has been obtained from the MATLAB script shown in Appendix A.1.3.

The training data has been obtained by varying the solar radiation level from 50W/m^2 to 1200W/m^2 in increments of 10W/m^2. While the PV surface temperature is added by 5^{o}C per step from 0 to 70 ^{o}C, and the corresponding duty ratio is calculated for each case.

A neural network toolbox in MATLAB software has been used to achieve the training process, during the network training all the computations are achieved offline. The backpropagation algorithm with the Levenberg-Marquardt optimization method is used in this work; this type is considered one of the most widely used algorithms for training the feedforward ANN because of the ease of implementation, robustness and stability. The learning stage of the network is performed by updating the weights and biases using a backpropagation algorithm with the Levenberg-Marquardt optimization method in order to minimize a mean squared error performance index E, given by Equation 7.13. The smaller the mean square error is, the better the performance and accuracy the network will achieve in real life.

$$E_p = \frac{1}{2} \cdot \sum_j \left(t_{pj} - o_{pj}\right)^2 \tag{5.9}$$

Where P is the index of the output neurons, o_{pj} is the measured output of the outputs and t_{pj} is the desired output of the output neurons.

The overall performance of a multilayer perceptron neural network measured as mean square error (MSE), can be calculated by Equation (7.14).

$$E = \sum_{p=1}^{m} E_p \tag{5.10}$$

In this work, the connection weights are updated by the following formula:

$$w_{nji}(n+1) = w_{ji}(n) - \eta\left(\frac{\partial E_n}{\partial w_{nji}(n)}\right) + \gamma\left(w_{nji}(n) - w_{nji}(n-1)\right) \tag{5.11}$$

$$w_{noj}(n+1) = w_{noj}(n) - \eta\left(\frac{\partial E_n}{\partial w_{noj}(n)}\right) + \gamma\left(w_{noj}(n) - w_{noj}(n-1)\right) \tag{5.12}$$

Where η is the learning rate, which is used to adjust the weights between layers and γ is the momentum factor, which is added to the last variation of weights on the variation of weights, in order to reduce the vibration and avoid the problem of slow convergence speed in the learning process of the weights [146]. The steps involved to perform the training process of the neural network are as follows:

Step 1 Initialize weight of neural network with small random values.

Step 2 Apply the input vector (PV array output power P_{PV} and the DC motor speed ω_m) to the neural network and calculate the corresponding output value (controlling signal of the buck chopper D).

Step 3 Compare the actual outputs with the desired outputs (duty ratio D) and determine the measure of error.

Step 4 Determine the amount by which each weight is to be changed (Equations 7.9 - 7.17) and update all the connection weights of the neural network.

Step 5 Repeat steps 2 to 4 with all training vectors until the error E for the vectors in the training set is reduced to an acceptable value.

5.2.3 Neural network model in MATLAB

Fig. 5.7 shows the neural network diagram as implemented in MATLAB, as stated earlier, the neural network model shows multiple layers of neurons with nonlinear transfer functions to allow the network to learn nonlinear and linear relationships

between the input and corresponding output values. This is a two layer feedforward configuration.

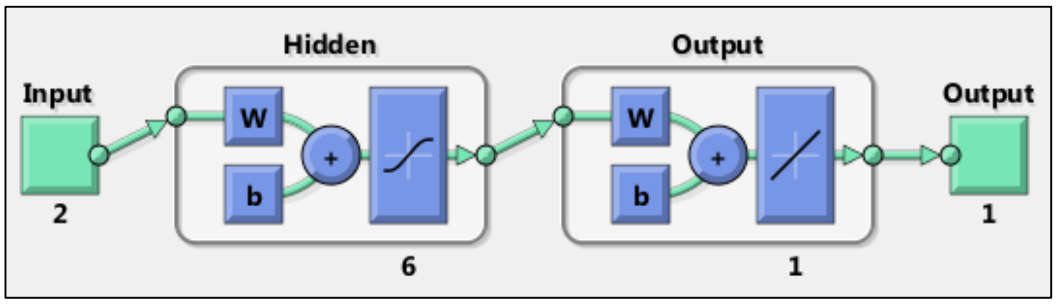

Fig. 5.7 The training network model in MATLAB.

After the network weights and biases have been adjusted, the network is ready for training for function approximation. To accomplish the training process a set of inputs and target outputs data is required. The training data in this work has been divided into three parts, of which 70% is used for training, 15% for validation, and 15% for testing. The weights and biases of the network are iteratively adjusted during the training process to minimize the network output error. The average square error against different epoch for training process and the regression plot are shown in Fig. 5.8 and Fig. 5.9 respectively.

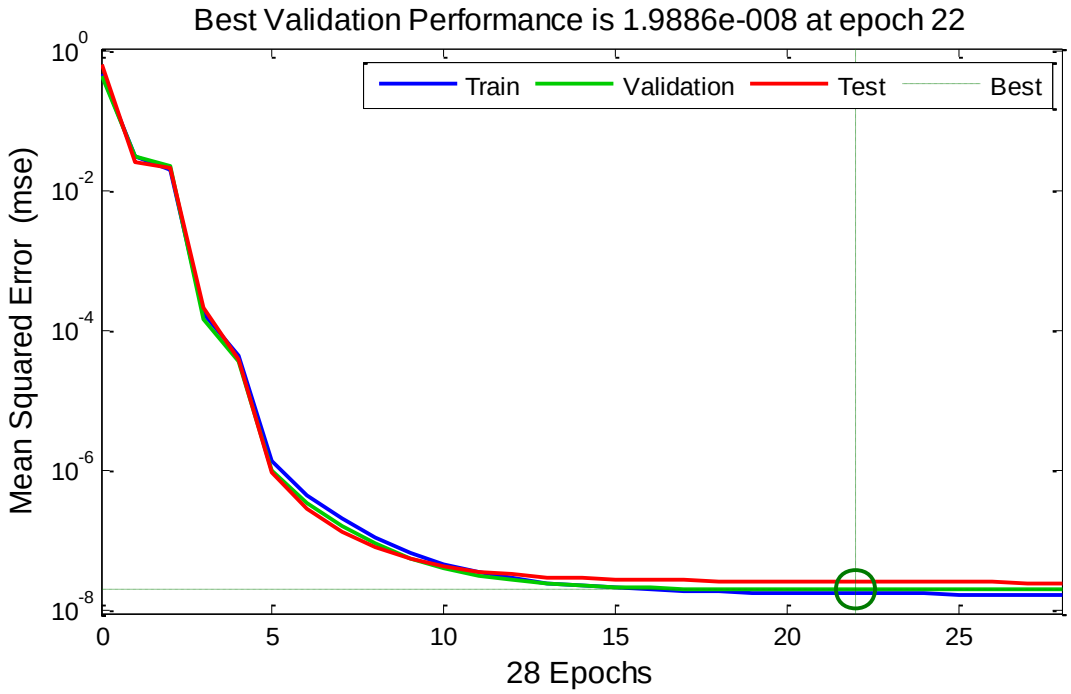

Fig. 5.8 Training result of ANN block.

To examine the network response, the test data set are put through the network and will perform a linear regression between the network outputs and the corresponding targets. Then, a regression analysis is carried out between the network response and the corresponding targets. Next, the output (predicted duty ratio) and the corresponding targets (calculated duty ratio) of the network are passed to the linear regression analysis function. It yields three different parameters as shown in Fig. 5.9 a, b, c and d.

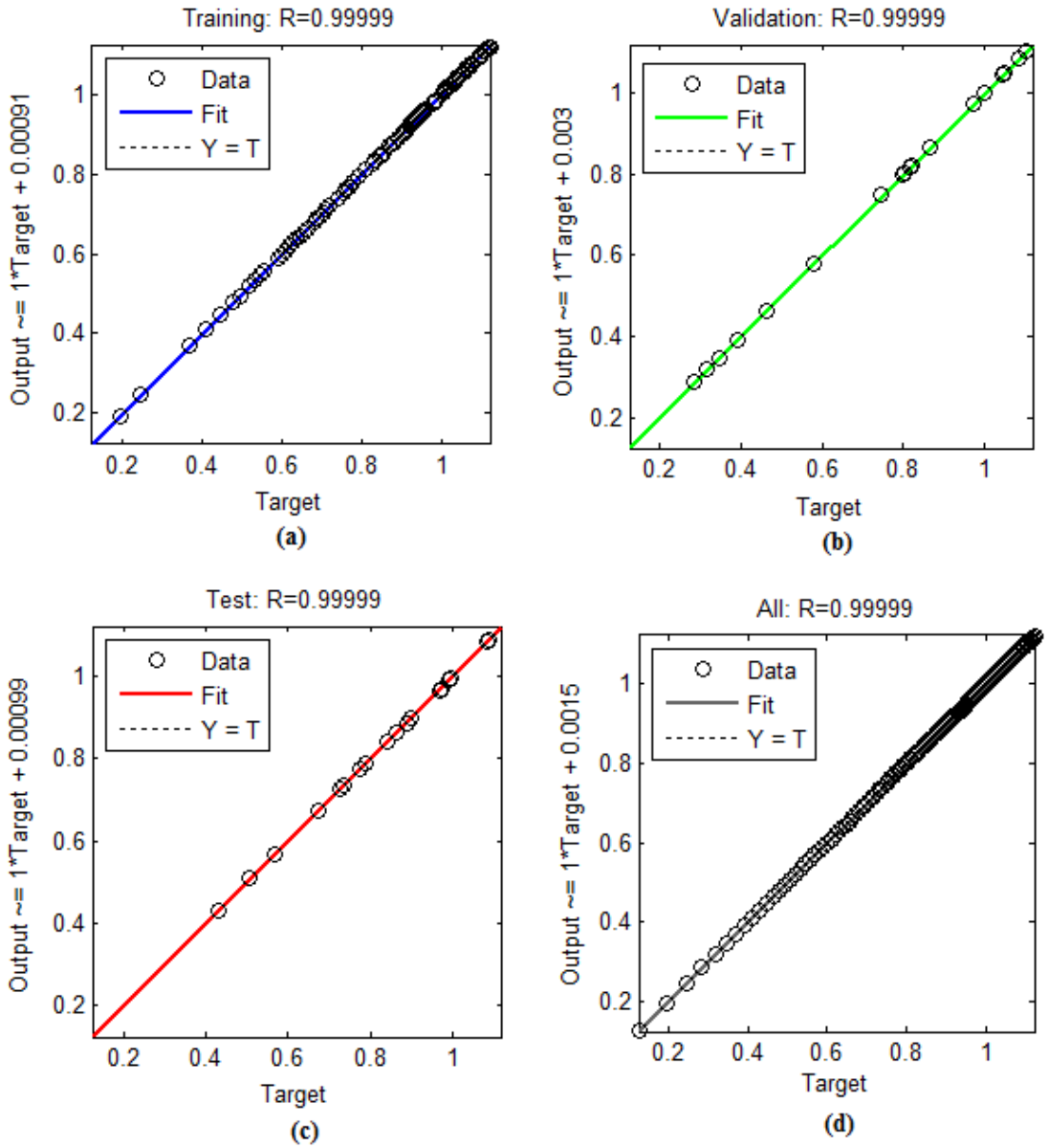

Fig. 5.9 The network performance analysis

The parameter R represents the correlation between the target output and the predicted output by network and the ideal value of R equals one. From Fig. 5.9 (a),

(b), (c) and (d) it is clear that the points are almost located on the line of best regression, which means the both networks predict the duty ratio for training data set very well.

Finally, after selecting an appropriate neural network size, a satisfactory result was obtained for a three layer feedforward neural network comprising (input, hidden and output layers). The number of nodes of the hidden layer is determined empirically applying the first category as indicated in section 5.2.1. It was found that, the 6 hidden nodes gave the most precise estimation and the result for this case is shown in Fig. 5.8. Furthermore, the neural network construction in the MATLAB simulation tool is illustrated in Fig. 5.7. The input layer has 2 nodes, the hidden layer has 6 nodes and the output layer has 1 node.

5.3 Summary

This chapter discusses the configuration of the proposed artificial neural network based MPPT control for the PV water pumping system. The chapter begins with a brief introduction of the history of ANN development and ANN applications. The basic structure of the well-known and the most commonly used mathematical model of a single neuron, which was propose by McCulloch and Pitts, was illustrated and discussed. The working principles including learning and testing of ANN are also discussed in this chapter.

The complete combined system of the proposed ANN MPPT controller with a PV water pumping system is also provided and illustrates the input and output variables of the proposed controller. The controller finds the optimal value of the buck converter's duty cycle corresponding to the MPP, starting from the sensed the motor rotational speed ω_m and the PV array output power P_{PV}, which tracks the atmospheric conditions. The proposed controller is an off-line ANN, trained using a backpropagation algorithm with the Levenberg-Marquardt optimization method, and is utilized for estimation of duty cycle for the feedforward loop. The training data set is determined by using MATLAB software to simulate the PV array, using parameters to build the PV array model which were supplied in the manufacture's datasheet. In every case of the specific irradiance and temperature values used, the

PV maximum power and the motor speed are recorded to provide the input data for the ANN. The duty cycle also is recorded at the MPP for the output data of the ANN. The MATLAB software is used for training the net. The graph of the convergence error has been provided to verify the precision of estimation.

CHAPTER 6 - PROPOSED VARIABLE STEP-SIZE P&O ALGORITHM

6.1 Problem related with the fixed step-size P&O algorithm

The P&O algorithm is widely used in PV generation systems because of its ease of implementation and low cost. However, its main limitation is the compromise between fast dynamic response and the oscillation at steady-state. Generally the P&O MPPT algorithm is run with a fixed step-size. If this step-size is set to be large, the algorithm will have faster response to dynamic conditions to track the MPP. However, the algorithm with large step-size results in excessive oscillation about the true MPP in steady-state conditions, leading to lower power extraction efficiency. This situation is reversed when the P&O MPPT is running with smaller step-size. Therefore, tracking the MPP with fixed step-size does not provide a satisfactory trade-off between steady-state oscillation and dynamic-condition. The efficiency of the P&O algorithm depends on the step-size. In particular, it is difficult to find an optimal step-size to obtain fast dynamic response with small little oscillation in the steady-state.

Choosing a step-size of the P&O algorithm has always been very critical since it can significantly affect the overall performance of the algorithm. Therefore, the proposed modified P&O MPPT algorithm with variable step-size improves the dynamics speed and eliminates the steady-state oscillations.

6.2 Proposed Variable Step-size P&O algorithm

The proposed MPPT algorithm is based on the conventional P&O algorithm, but a fuzzy logic controller block is used to provide a variable step-size to overcome the limitation that exists in the implementations of the conventional P&O algorithm. The flow chart of the proposed modified P&O algorithm with variable step-size is illustrated in Fig. 6.1.

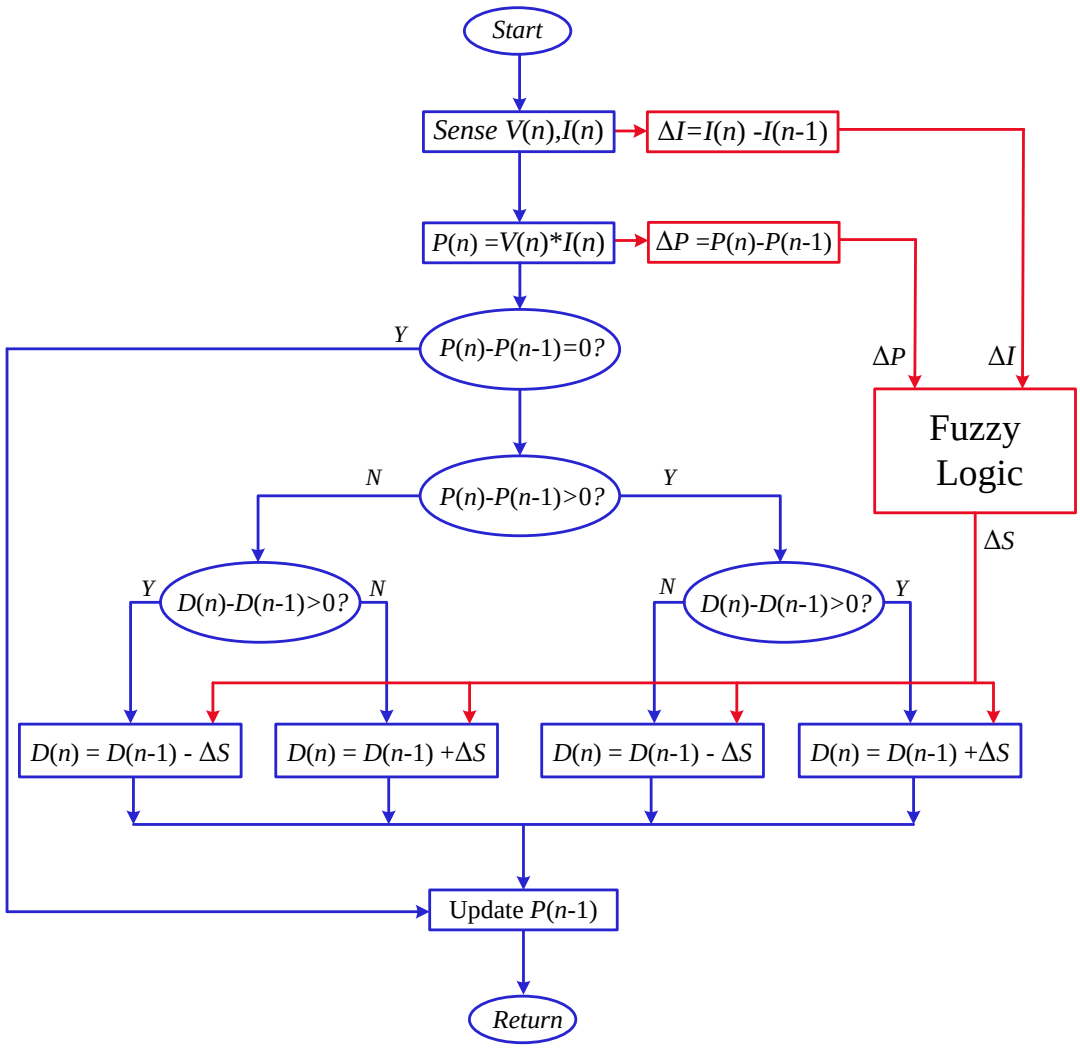

Fig. 6.1 Block diagram of the proposed P&O with variable step-size.

The inputs to the fuzzy logic controller are the change in the PV array power ΔP_{PV} and the change in the PV array current ΔI_{PV}, and controller adjusts the step-size ΔS for the P&O algorithm according to the existing solar irradiation and temperature. As the FLC uses the measurement of the PV array voltage and current as input signals, it can share the same sensors with the P&O to reduce the controller implementation cost and complexity.

The principle of the conventional P&O has already been introduced in 2.3.4, it operates by periodically perturbing the PV output voltage V_{PV} and calculates the change in the PV output power P_{PV} by comparing the instantaneous power with that of the previous perturbation cycle. If the change in the power is positive, the perturbation will continue in the same direction in the next perturbation cycle,

otherwise the perturbation will move to the opposite direction. By repeating this process, the operating point will gradually move towards the maximum power point.

The perturbation variable chosen in the proposed algorithm is the duty-cycle, hence no PI controller is needed and the duty-cycle is perturbed by adding or subtracting the step-size according to the change in the PV output power. However, the step-size is not fixed and it is calculated by the adapted FLC block.

The principle of the of the adopted FLC block is to adjust the value of the step-size according to the position of the operating point. The FLC sets the step-size to a large value when the operating point is far away from the MPP conversely, if the operating point is close to the MPP, the step-size value is adjusted to small value. This process continues until the MPP is reached, hence the FLC sets the step-size to zero value. Therefore, this ensures that a fast dynamic response and eliminates the oscillations around the MPP when a steady-state is reached.

6.2.1 Fuzzy logic control (FLC) used as variable step-size.

The fuzzy logic controller FLC is used to continuously vary the step-size. The proposed fuzzy logic controller is based on prior expert knowledge of the system. Fig. 6.2 shows the block diagram of the proposed FLC variable step-size and its main structure. It consists of four sections, Fuzzification, Inference engine, Defuzzification and Rule-Base. In this study, the FLC constructed with two input variables and one output. The input variables of the FLC are the variation of the output power of PV array, ΔP_{PV}, and the variation of the output current of the PV array, ΔI_{PV}, whereas the output variable of the FLC is the variation of the step-size ΔS which is sent to the P&O algorithm.

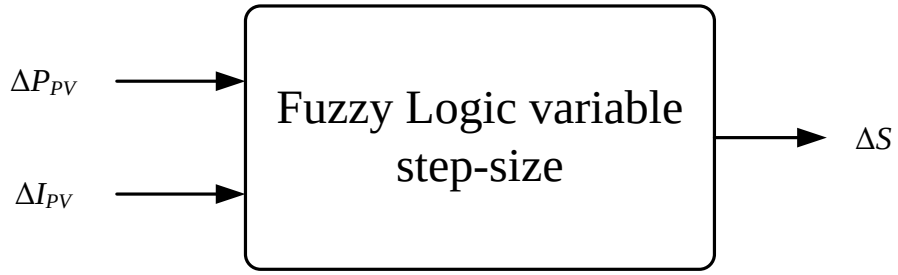

Fig. 6.2 General diagram of the proposed FLC variable step-size calculator.

The fuzzy process inputs can be measured or computed from the current and voltage of the solar array. The input variables, ΔP_{PV} and ΔI_{PV}, of the proposed fuzzy logic variable step-size can be calculated by the following equations, where $P_{PV}(k)$ and $I_{PV}(k)$ are the PV array power and current respectively and $V_{PV}(k)$ is the PV array voltage.

$$P_{PV}(k) = V_{PV}(k) * I_{PV}(k) \tag{6.1}$$

$$\Delta P_{PV}(k) = G_P \left(P_{PV}(k) - P_{PV}(k\text{-}1)\right) \tag{6.2}$$

$$\Delta I_{PV}(k) = G_I \left(I_{PV}(k) - I_{PV}(k\text{-}1)\right) \tag{6.3}$$

To simplify the control calculation, the values of variation of the output power of PV array ΔP_{PV} and the variation of the output current of the PV array ΔI_{PV} can be normalized before the fuzzification process by using the scaling factors G_P and G_I respectively as shown in Equation (6.2) and (6.3) hence the scope of PV array power change ΔP_{PV} and the PV array current change ΔI_{PV} will be between –1 to 1.

The membership function of the input and the output variables used in this model have the same shape and is shown in Fig. 6.3. All the membership functions are expressed with a triangular function and they consist of five fuzzy subsets which are denoted by NB (negative big), NS (negative small), ZZ (zero), PS (positive small) and PB (positive big)

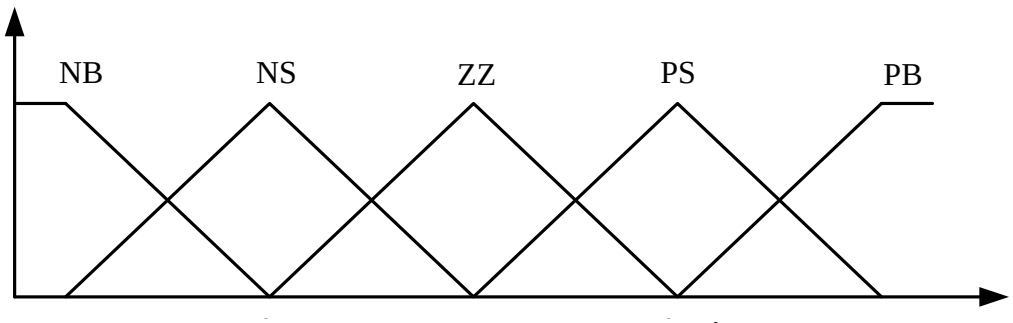

Fig. 6.3 Membership functions of the 1st input variable (ΔP_{PV}), 2nd input variable (ΔI_{PV}) and the output variable (ΔS).

The fuzzy rule base is a collection of if-then rules which all the information is available for the controlled parameters. Since the number of membership function of each input is 5, then the fuzzy inference rules of the FLC consist of 25 rules as

illustrated in Table 6.1. These rules are used to determine the output of the controller (the variable step-size for the P&O algorithm) to track the maximum power point and stop iterating once this point is reached.
Mamdani's method is used as a fuzzy interface method with max-min operation combined with fuzzy law in this work.

After the rules have been evaluated, the output of fuzzy controller is still a fuzzy set. However, the actual system usually requires a non-fuzzy value of control. Hence the process of defuzzification is required to as the last step to calculate the crisp output of the proposed fuzzy control. The output of the proposed FLC is defuzzified using centre of gravity (COG) method to calculate ΔS [147].

Table 6.1 Fuzzy rules base

ΔI_{PV} \ ΔP_{PV}	**NB**	**NS**	**ZZ**	**PS**	**PB**
NB	PB	PS	**ZZ**	NS	NB
NS	PB	PS	**ZZ**	NS	NB
ZZ	PS	PS	**ZZ**	NS	NS
PS	NP	NS	**ZZ**	PS	PB
PB	NP	NS	**ZZ**	PS	PB

6.3 Summary

The modified P&O algorithm with variable step-size was proposed and thoroughly discussed in this chapter as a way to overcome the limitation of the conventional P&O algorithm and to increase its overall efficiency especially under unstable weather conditions. The main limitation of the conventional P&O algorithm is that selecting an optimum value of the step-size that is a good compromise between fast dynamic response and steady-state stability is difficult. To improve the tracking speed and eliminating the steady-state oscillation, a FLC block is adapted to the P&O algorithm to adjust the step-size according to the position of the operating point from

the MPP. The complete flow chart of the proposed P&O algorithm was illustrated with the adapted FLC block for adjusting the step-size and the operating principle was presented and thoroughly explained. Moreover, the FLC components were presented with rule base table explaining how the step-size value adjusted to update the control variable (duty-cycle) to track the MPP.

The modified P&O algorithm will be first implemented in a simulation of a PV system with a resistive load, using a MATLAB/SIMULINK system model. This will allow its performance to be compared against the conventional P&O algorithm under different irradiation levels. Furthermore, the MP&O algorithm will be implemented in the PV water pumping system to evaluate and compare the performance of the algorithm against the other two proposed MPPT techniques.

CHAPTER 7 - SIMULATION AND RESULTS

This chapter describes how the SIMULINK models of the proposed PV power systems are implemented to test and verify the functionality of the proposed MPPT controls. In this thesis, two different PV systems are implemented in MATLAB/SIMULINK environment. The first system is implemented with a resistive load to evaluate the effectiveness and the advantages of the modified P&O. The second PV system is also simulated in MATLAB, but the resistive load was replaced with a DC water pump load to demonstrate the feasibility and performance of the proposed Fuzzy logic controller based on MPPT of water pumping system and artificial neural network. Furthermore, a comparison has been carried out between the proposed controllers and the directly coupled water pump system by way of simulation results. In this work, the simulation is run with variable-step solver for the sake of accuracy and to prevent the solver from infinitely looping on the m-file. The solver integration method used was the (ode23) [148].

7.1 System design and simulation

The system has been modelled and simulated in MATLAB/SIMULINK. The complete SIMULINK model of the proposed system is illustrated in Fig. 7.1. The modelled system consists mainly of PV array model, DC/DC buck converter model used to interface PV output to the resistive load to track the maximum power of the PV array. To perform the tracking of maximum power, a modified perturbation and observation algorithm has been implemented.

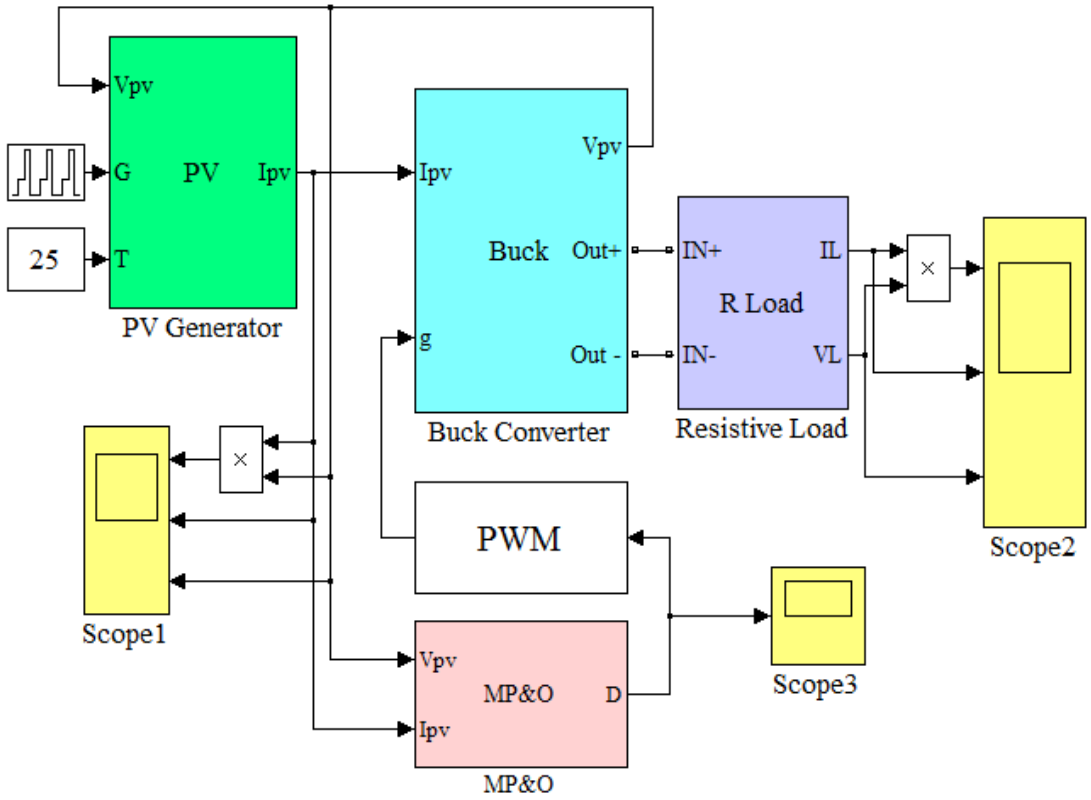

Fig. 7.1 SIMULINK model of PV system with MPPT algorithm.

7.1.1 PV model simulation and validation

The PV model simulator was implemented in MATLAB as M-file code based on Equation (3.15). The code has been masked in Embedded MATLAB Function electrically build as a voltage controlled current source and the overall block can be seen in Fig. 7.2. The temperature *T*, isolation *G* and PV voltage V_{PV} are fed to the Embedded MATLAB Function and the output is the current produced by the panel.

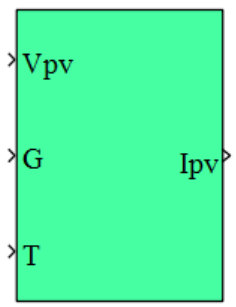

Fig. 7.2 SIMULINK model of PV Panel.

The PV panel used in the simulation is shown in Fig. 7.3. It is 96 SANYO HIT180 180W panels connected in 12×8 matrix. To validate the model, usually standard conditions specified at irradiation of (G = 1000 kW/m^2) and temperature of (T = 25^{o}C).

Fig. 7.3 Picture of 96 SANYO HIT180-180W PV module [48].

The basic performance differs from one PV panel to other, therefore typical parameters are generally given in a datasheet. The datasheet provide salient parameters regarding the characteristic and performance of PV panel under standard test conditions. The parameters of PV panel used in this work are listed in the Table 7.1.

Table 7.1 Electrical characteristics data of PV module taken from the datasheet [38]

Electrical Characteristics of SANYO HIT180W	
Rated Power (P_{max})	180 W
Maximum Power Voltage (V_{pm})	54.0 V
Maximum Power Current (I_{pm})	3.33 A
Open-Circuit Voltage (V_{oc})	66.4 V
Short-Circuit Current (I_{sc})	3.65 A
Temperature Coefficient (P_{max})	-0.33% / °C
Temperature Coefficient (V_{oc})	-0.173 V / °C
Temperature Coefficient (I_{sc})	1.10 mA / °C
Cell Efficiency	17.8%
Module Efficiency	15.5%
Series Resistance (R_S)	0.3345Ω

The current-voltage relation curves of the simulated module are shown in Fig. 7.5. The importance of the simulated model is that to reflect the influence of the temperature and insolation on the output characteristic of the PV array. To verify and validate the functionality of the simulated model, the system in Fig. 7.4 is implemented.

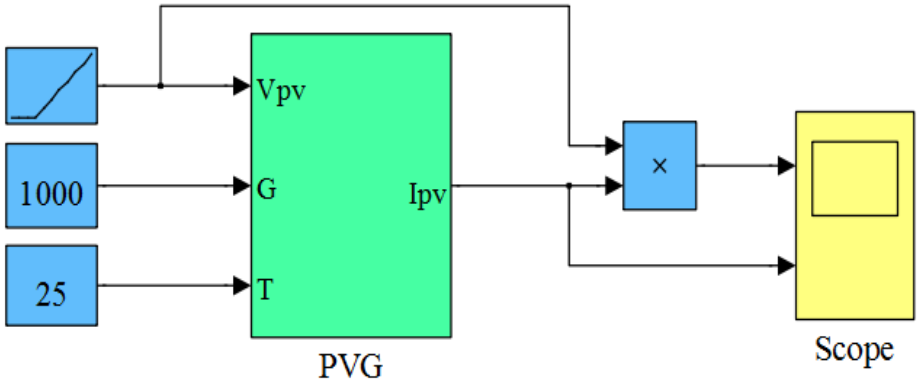

Fig. 7.4 SIMULINK test system of PV modules.

The output characteristics of the simulated model have been compared with the characteristics provided by the manufacture's datasheet as illustrated in Fig. 7.5. To further test the accuracy of the model, it was simulated under different insolation levels and the results of the *I-V* characteristics are shown in Fig. 7.6. The model provides a high degree of accuracy in simulating the behaviour of a PV panel.

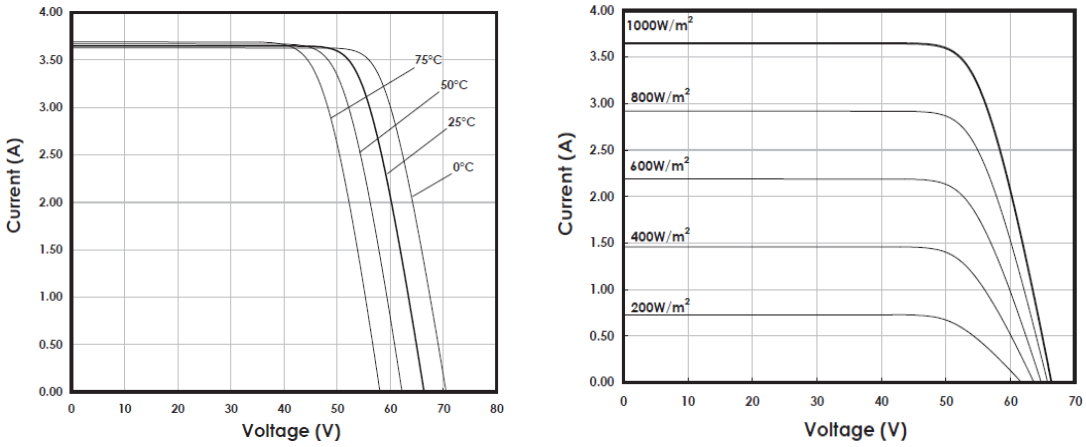

Fig. 7.5 Real product Output characteristic of SANYO HIT180.

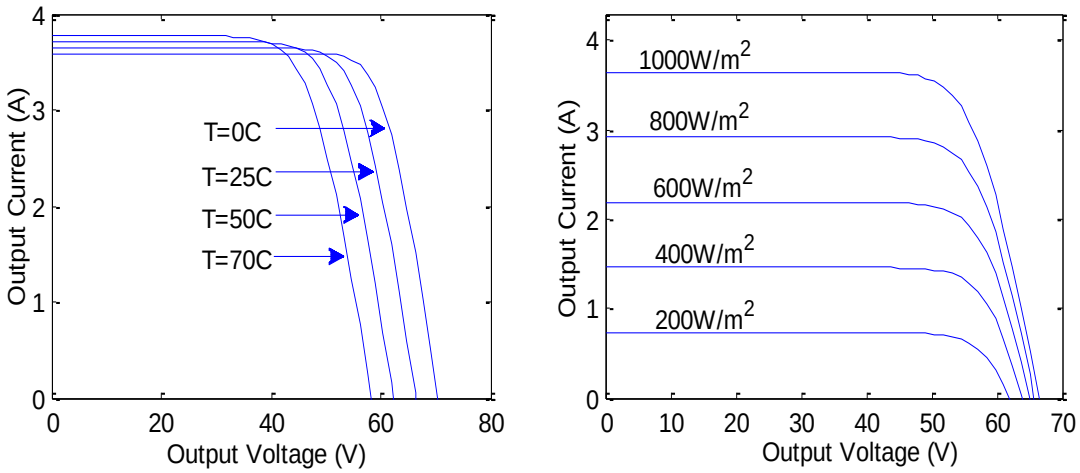

Fig. 7.6 Output characteristic of the simulated module.

7.1.2 Buck converter design

The buck converter is conducted in MATLAB and simulated using SimPowerSystems blocks and the circuit diagram is depicted in Fig. 7.7. The converter consists of IGBT switch and freewheeling diode. Additionally, input and output filters are included. The inductor is responsible for reducing the output current ripple; the larger the value of the inductor, the smaller the value of the ripple.

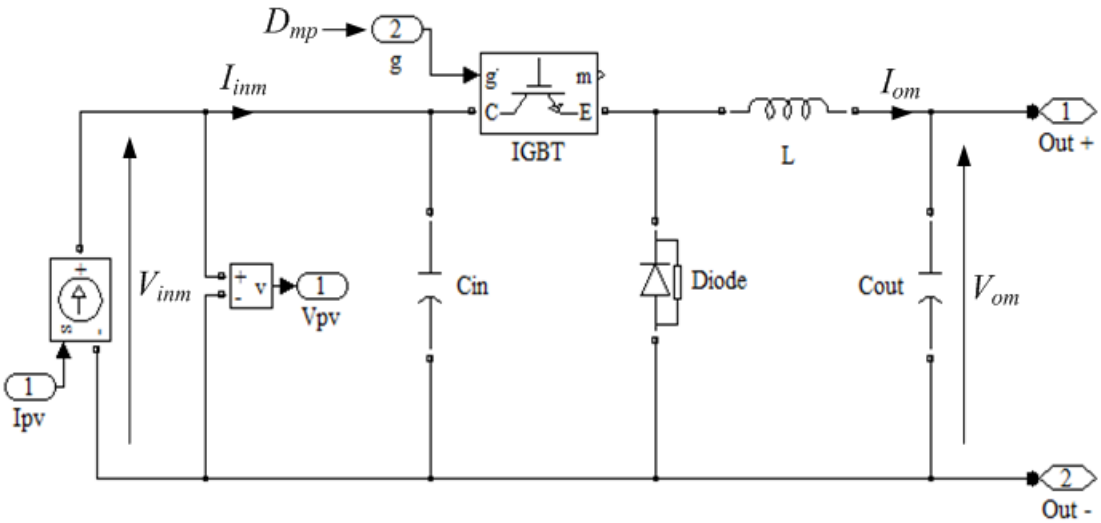

Fig. 7.7 Simulation model of DC-DC Buck Converter.

The simulation model of the switching mode buck converter can be masked by the SIMULINK and simplified into only one block as shown in Fig. 7.8.

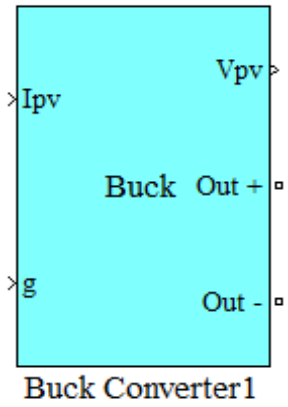

Fig. 7.8 One block representation of Buck Converter.

There are two inputs and three outputs in the Buck converter subsystem block shown in Fig. 7.8. The input terminal *g* represents the gate signal from the Pulse Width Modulation block, I_{pv} and V_{pv} are the input current and input voltage respectively, *Out+* is the secondary positive output of the buck converter, and *Out-* is the secondary negative output of the buck converter.

7.1.3 Buck converter parameters scaling

As the output power delivered by the PV array will vary with temperature and irradiation, it is necessary to initially assume a fixed operating voltage when determining the parameters of the buck converter to be used.

The proposed buck converter, which maintains the output voltage of the PV array at the maximum power point, has a target output voltage of around 24V. In this work, a maximum voltage of 54V is the maximum output voltage of the PV array used. This operating voltage is used for selecting the initial duty cycle and for choosing the appropriate values of the buck converter elements.

The block diagram of step-down (buck) converter as presented in Fig. 7.7. The maximum input voltage V_{inm} of the converter is 54.0V as listed below in Table 7.2 and it is equal to the maximum output voltage of the PV array. The maximum output voltage of the converter is V_{om} has been chosen to be 24V. Consequently, the converter duty ratio D_{mp} corresponding to the maximum power output is calculated by the Equation (7.1). The parameters values of the buck converter are listed in the Table 7.2, whereas I_{inm}, I_{om} are the maximum input and the maximum output currents of the buck converter respectively, and f_s is the converter switching frequency.

$$D_{mp} = \frac{V_{om}}{V_{inm}} \quad (7.1)$$

Table 7.2 Buck converter parameters

Maximum input Voltage	(V_{inm})	54.0V
Maximum output Voltage	(V_{om})	24.0V
Maximum input Current	(I_{inm})	3.33A
Maximum output Current	(I_{om})	7.5A
Duty ratio corresponding to the maximum power output	(D_{mp})	44.4%
Switching frequency	(f_s)	20KHz

- **Input filter**

The input capacitor is used to reduce the converter input voltage ripple and determines the amount of peak current drawn from the source. The input capacitor can be calculated Equation (7.2) with maximum voltage ripple of 2% [8].

$$C_{in} = \frac{I_{inm}\left(1 - D_{mp}\right)}{\Delta V_{inm} f_s} \quad (7.2)$$

$$C_{in} = \frac{3.33(1 - 0.44)}{0.02 \times 54 \times 10 \times 10^3} = 172.666\mu F$$

- **Output filter**

The output filter comprises inductor L and capacitor C_{out} .

1) *Inductor*

The buck converter inductor value required to operate the converter in the continuous conduction mode can be calculated by Equation (7.3).

$$L = \frac{V_{om}\left(1 - D_{mp}\right)}{2\Delta I_{om} f_s} \quad (7.3)$$

$$L = \frac{24(1 - 0.44)}{2 \times 0.02 \times 7.5 \times 10 \times 10^3} = 4.48mH$$

2) *Capacitor*

The output capacitor value is calculated by the Equation (7.4) assuming the voltage ripple (2%) to give the desired peak to peak output voltage ripple [8].

$$C_{out} = \frac{D_{mp}\, I_{om}}{\Delta V_{om} f_s} \tag{7.4}$$

$$C_{out} = \frac{0.44 \times 7.5}{0.02 \times 24 \times 10 \times 10^3} = 687.5\mu F$$

7.1.4 The MP&O Controller

The modified adaptive perturb and observe (MP&O) algorithm, which was introduced in chapter 5.1, was implemented in MATLAB/SIMULINK as illustrated in Fig. 7.9. The MP&O comprises two blokes, the conventional P&O algorithm and Fuzzy Logic Controller (FLC). The conventional P&O was implemented in a similar manner as the PV panel. It was written as M-file code in an embedded MATLAB function, the MATLAB script is shown in Appendix A.1.1.

The Fuzzy Logic Controller was implemented in MATLAB/SIMULINK using the available Fuzzy Logic Toolbox. The FLC was designed using an effective Graphical User Interface (GUI) tool provided by the fuzzy logic toolbox in MATLAB/ SIMULINK to facilitate the design of the Fuzzy logic controller. This is called the Fuzzy Interface system (FIS) editor as illustrated in Appendix B.1 in Fig. B.1. The FIS editor is used to design the fuzzy logic controller. Input and output signals are determined by choosing the desired shape and number of membership functions in the Membership Function Editor as shown in Appendix B.1 in Fig. B.2.

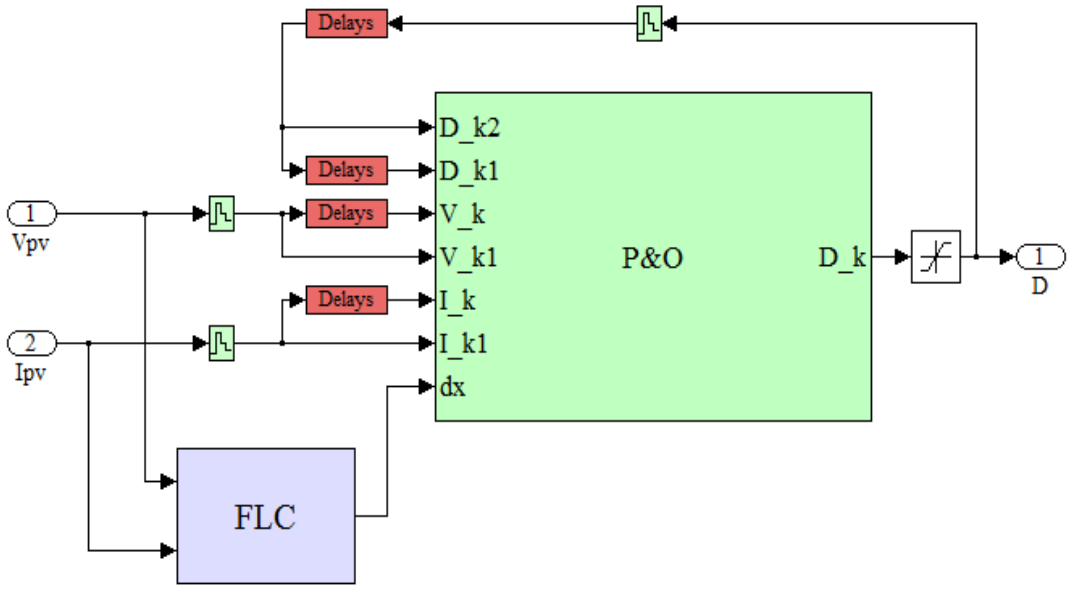

Fig. 7.9 SIMULINK model of the MP&O controller.

Fuzzy rules are a set of rules that the fuzzy controller works to. These rules can be determined in the Rule Editor as shown in Appendix B.1 in Fig. B.3.

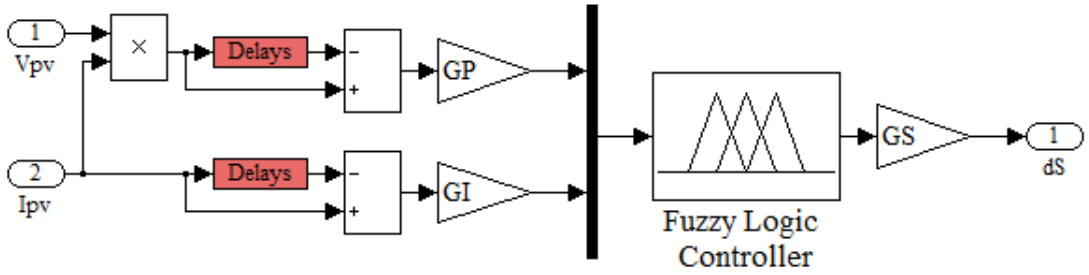

Fig. 7.10 FLC SIMULINK block for step-size tuning.

Fuzzy logic control parameters	
The scaling factor of the PV array output power variation (G_P)	0.42
The scaling factor of the PV array output current variation (G_I)	1.2
The scaling factor of the variable step-size (G_S)	0.4

Rules can be added, deleted using the appropriate button. Once the FLC has been designed, the FIS editor is saved as a (fis) file. The fis file is exported to the MATLAB workspace and the name of the file is entered in the Fuzzy logic control block in SIMULINK shown in Fig. 7.10.

The SIMULINK model of the proposed MP&O can also be further integrated into one model block as in Fig. 7.11.

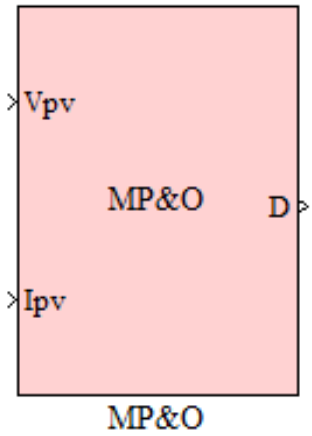

Fig. 7.11 One block representation of MP&O.

7.2 Simulation results of the P&O and MP&O MPPT techniques

The simulations offer a valuable opportunity to verify the feasibility and the performance of the proposed modified variable step-size P&O algorithm. For evaluation and comparison analysis, the simulation studies were carried out under steady-state and dynamic conditions for the proposed MP&O and conventional P&O, by configuring the simulations under exactly the same conditions.

The main focus is how fast the MPP is being tracked during the dynamic state and the power ripple caused by oscillations around the MPP in the steady-state condition. For conventional P&O, the value of duty ratio step-change will determine the convergence speed (time to reach steady-state) and the oscillation during steady-state operation. According to [149] a 0.02 step-size gave the best maximum power efficiency and the author in [150] stated that, the optimum range of the step-size is between 0.01 to 0.07. Therefore, two fixed duty ratio step changes are used, 0.01 and 0.04, to compare the performance of the conventional P&O with the MP&O.

In reality, the output power of a photovoltaic cell is mainly influenced by ambient temperature and solar irradiation, although the change in ambient temperature has a slow influence on the PV cell and it is not directly related to the speed of dynamic response. Therefore the cell working temperature is fixed at 25^{o}C in all simulations. However, in practice the clouds sometimes move very quickly leading to a sudden change in the PV panel output power. Consequently, the algorithm has to be tested

under different irradiation levels to verify the speed of tracking. The PV panel is configured to produce 180W with an open-circuit voltage of 66.4V at 1000 W/m^2 solar irradiance. The simulation time was 4.0 seconds. At the time of 1.0s, the irradiation level was abruptly decreased from 1000 W/m^2 to 700 W/m^2, then increased to 900 W/m^2 at 2.0s, and then decreased back at 3.0s to reach 700 W/m^2 again as shown in Fig. 7.12.

7.2.1 Conventional perturb & observe algorithm (P&O)

For good comparisons between the conventional perturb and observe (P&O) method and the modified one (MP&O), the behaviour of P&O will be presented by the simulation results in this section. Fig. 7.13 to Fig. 7.16 show the dynamic performance of the PV current, PV voltage, PV power, and duty ratio of the conventional P&O with fixed step-change of 0.01 when the solar irradiation changes as shown in Fig. 7.12. The simulation can be described as follows: At the beginning, it can be observed from Fig. 7.16 that, the P&O MPPT manages to adjust the duty ratio, *D,* until the maximum power output is reached. The operating power points deviate from the peak power when the irradiation suddenly changes at the moments of 1.0s, 2.0s and 3.0s. The P&O readjusts the control variables to bring the maximum power operating point back. The MPPT responds to the irradiation change through controlling the PWM input of the DC-DC buck converter by adjusting its duty ratio *D* in fixed increment steps of 0.01. However, the simulation results demonstrate oscillation in the duty ratio waveform during the steady-state as shown in Fig. 7.16. This is because the P&O MPPT uses a fixed step-size to adjust the duty ratio. Therefore, when the MPP is reached the duty ratio keeps fluctuating around this point instead of stopping at it. The oscillation in the duty ratio results in oscillation in the output current, voltage, and power of PV array respectively as shown in Fig. 7.13, Fig. 7.14 and Fig. 7.15.

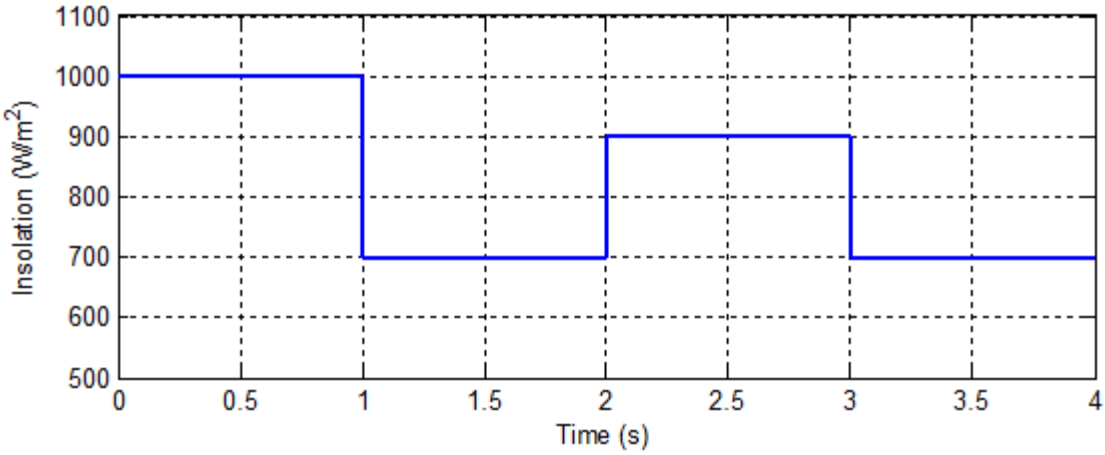

Fig. 7.12 Solar Irradiation.

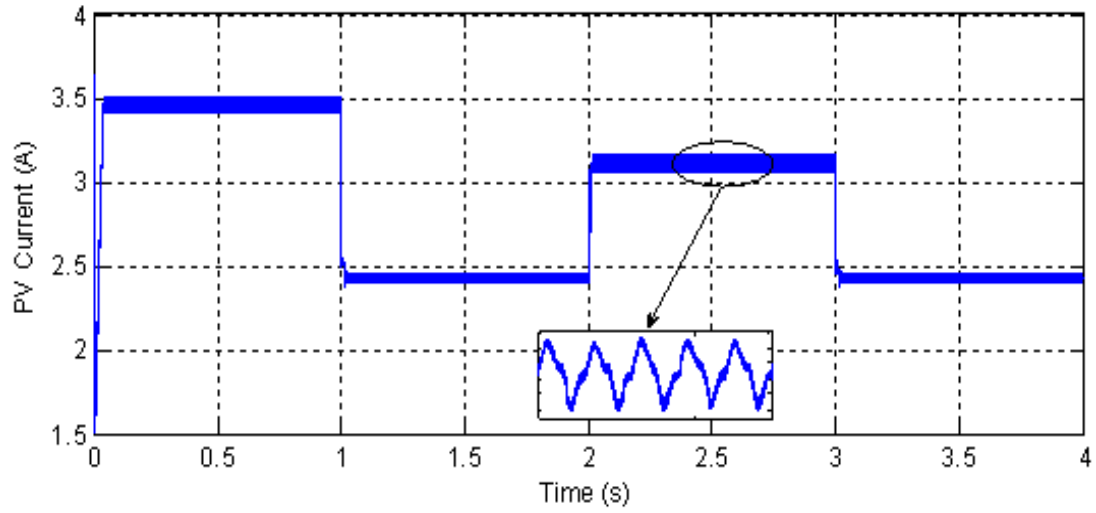

Fig. 7.13 PV array output current using P&O algorithm with fixed step size of 0.01.

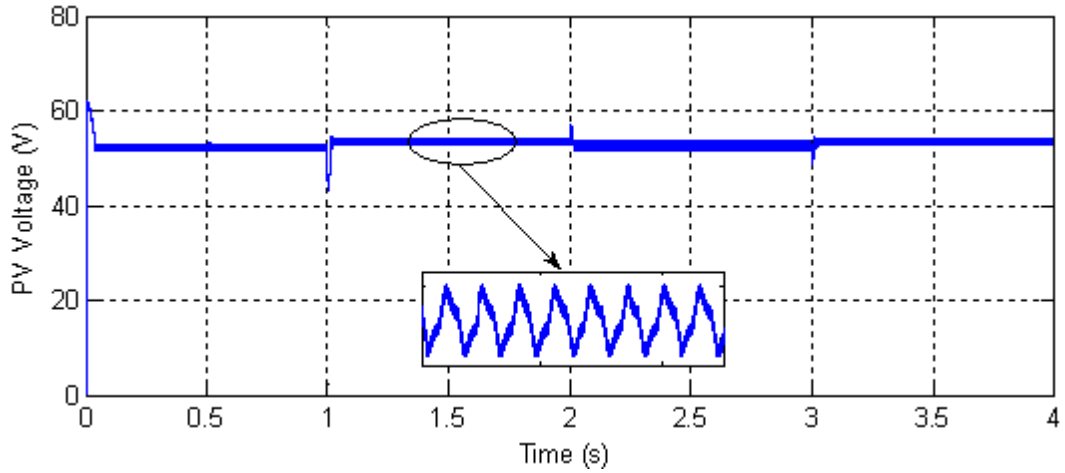

Fig. 7.14 PV array output voltage using P&O algorithm with fixed step size of 0.01.

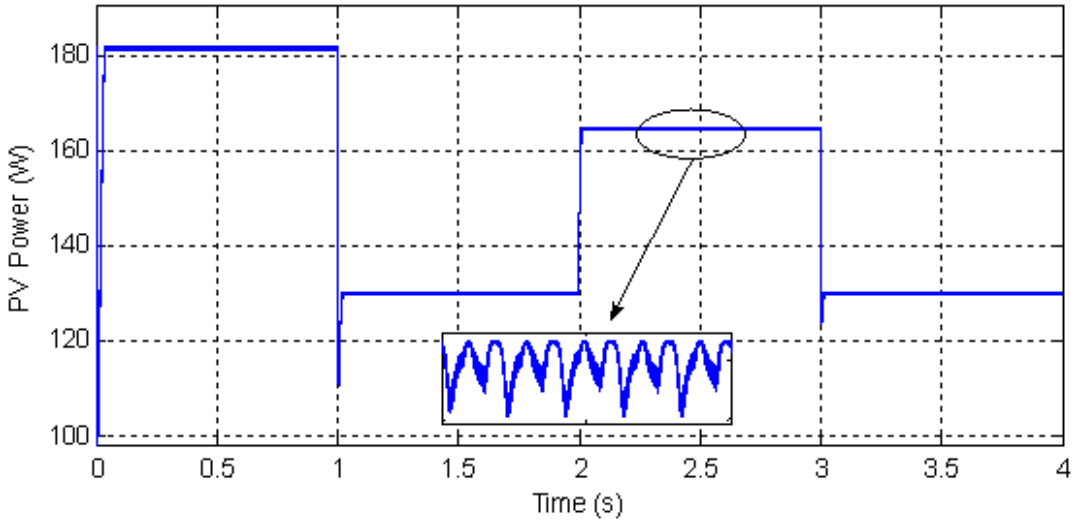

Fig. 7.15 PV array output power using P&O algorithm with fixed step size of 0.01.

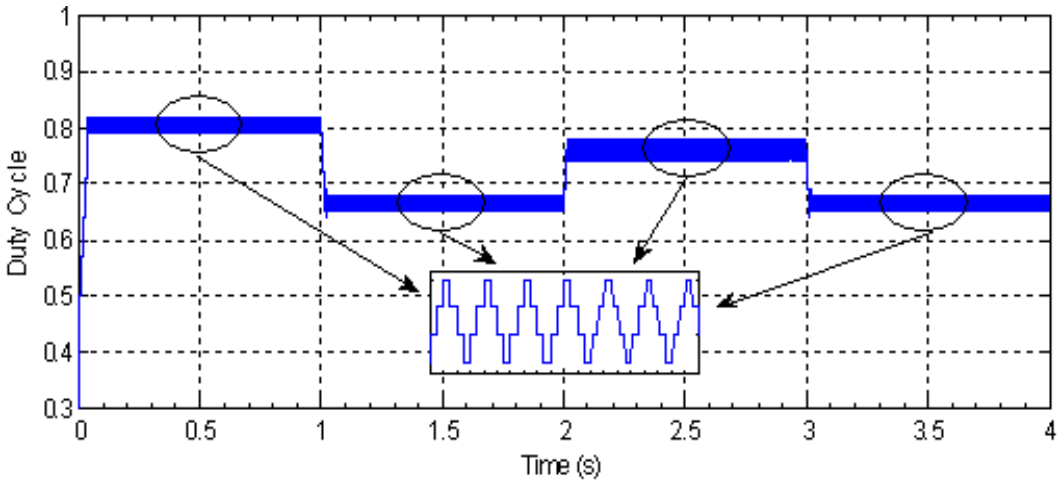

Fig. 7.16 Duty ratio waveform of P&O algorithm with fixed step size of 0.01.

7.2.2 Modified perturb & observe algorithm (MP&O)

The proposed modified perturb and observe algorithm (MP&O) was introduced and discussed earlier in section 5.1. The MP&O is based on a standard perturb and observe technique P&O. It was modified using a fuzzy logic control to provide variable step-size in order to improve the trade-off between steady-state and dynamic state performance. Simulation results based on MP&O are introduced and analysed in this section. To test the performance of the proposed method and to perform a good comparison, the simulations are carried out under the same conditions as the previous simulations with the conventional P&O control algorithm. The PV current, voltage and power and the duty ratio waveforms of the MP&O MPPT are shown in

Fig. 7.17 to Fig. 7.20. The simulation results can be described as follows: At the beginning, the proposed MP&O MPPT succeeds in performing a quick adjustment of the duty ratio *D* such that a stable maximum point of the output power is reached. Once the maximum power point is reached, the MP&O MPPT stops adjusting the duty ratio *D* and maintains operation at this point, unless it detects any change in the PV power. Fig. 7.19 shows that, the operating power points move away from the peak power point, due to the sudden change in the irradiation at the moments of 1.0s, 2.0s and 3.0s as shown in Fig. 7.12. Hence, the MP&O MPPT starts to readjusts the duty ratio *D* to track the new maximum power operating point and keep operating on this point.

The simulation results show good performance of the proposed MP&O MPPT technique. Fig. 7.19 shows that, the MP&O accurately tracked the maximum power point under varying irradiation levels. The simulation results show good performance in the steady-state condition. Fig. 7.19 shows that the oscillation around the peak power point has been eliminated in the steady-state. This is because the MP&O MPPT stops changing the duty ratio *D* once the maximum power point is reached as illustrated in Fig. 7.20.

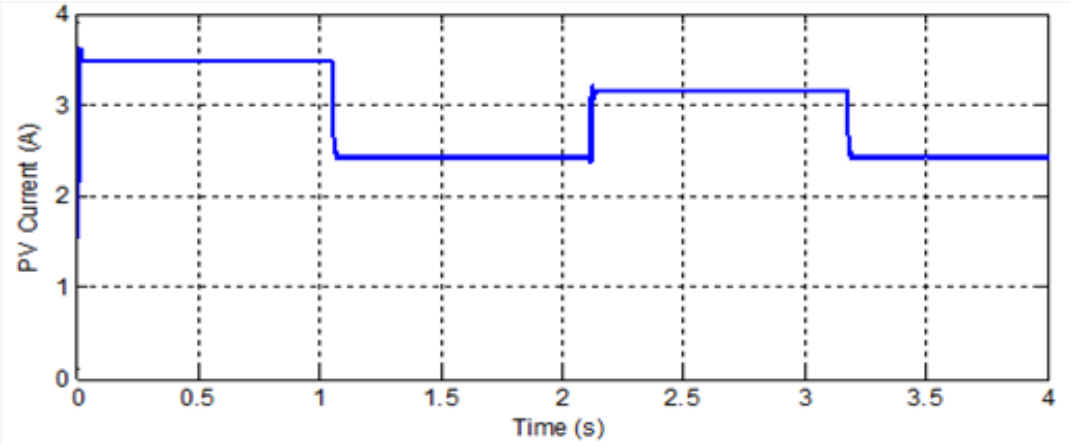

Fig. 7.17 PV array output current using MP&O algorithm.

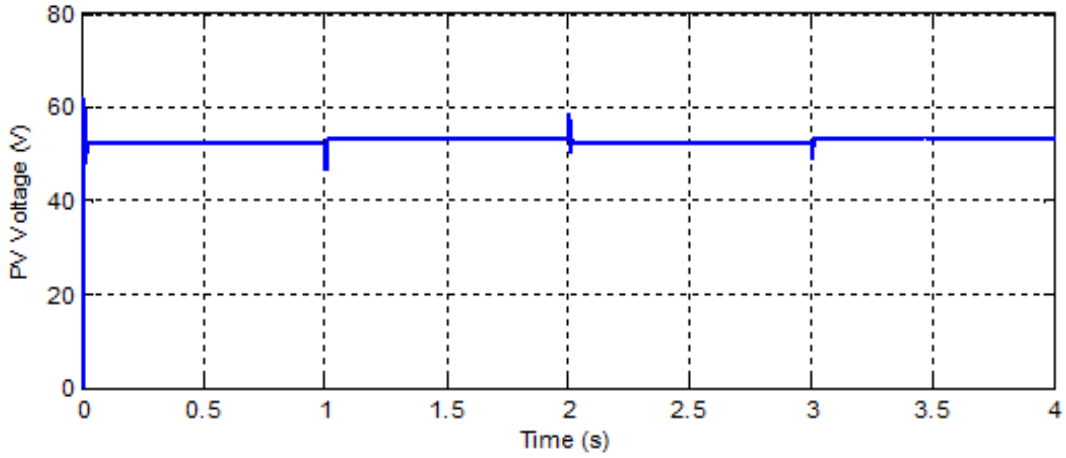

Fig. 7.18 PV array output voltage using MP&O algorithm.

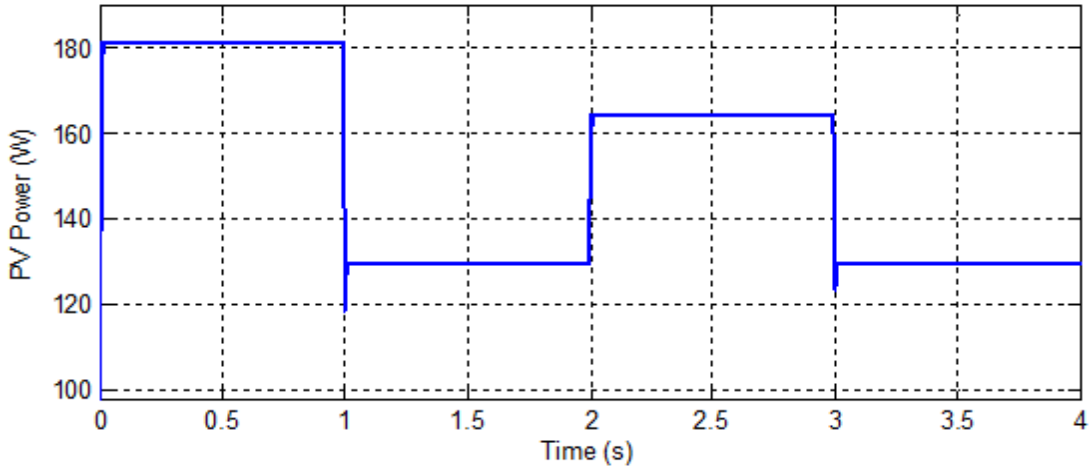

Fig. 7.19 PV array output power using MP&O algorithm.

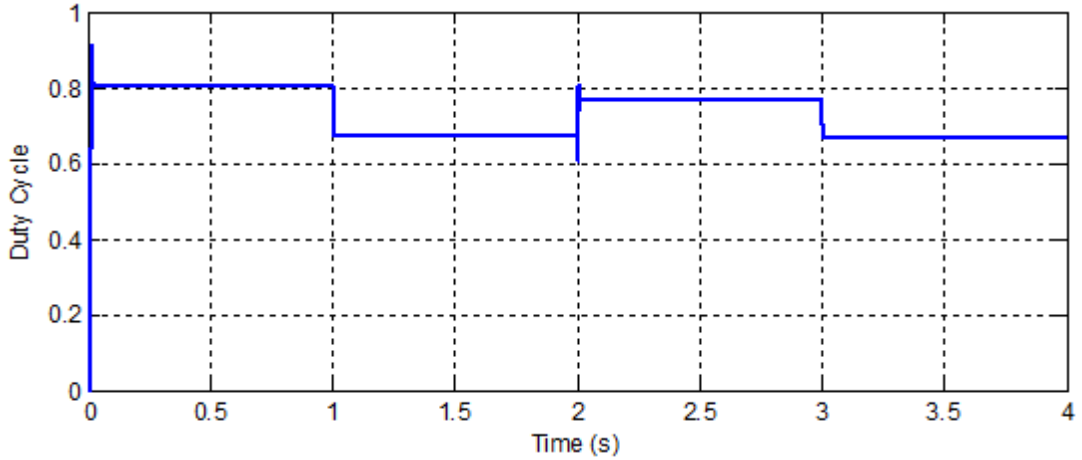

Fig. 7.20 Duty ratio waveform of MP&O algorithm.

7.2.3 Comparative performance between MP&O and M&P

In this section, a comparative analysis between MP&O and P&O is carried out to show the performance of the both techniques in the same condition. The comparative study considers two important features: the maximum power point tracking speed and steady-state oscillation. To show the performance of the proposed MP&O MPPT algorithm with the P&O MPPT algorithm in the steady-state and dynamic condition, the P&O was tested with two different duty ratio step-sizes, 0.01 and 0.04. The output performance of the proposed MP&O MPPT and the P&O MPPT with fixed step-size of 0.01 and 0.04 under three step changes of in irradiation levels. The irradiation was abruptly changed from 1000 to 700 W/m^2 at 1s and then increased to 900 W/m^2 at 2s and then decreased back to 700 W/m^2 at 3s as shown in Fig. 7.12.

Compared with the P&O MPPT with fixed step-size of 0.01, the P&O MPPT with fixed step-size of 0.04 shows a good dynamic performance, it can converge faster to the steady-state but the oscillation in the steady-state is much higher. The tracking time of P&O MPPT with fixed step-size of 0.04 under an irradiation step change is only several MPPT sampling periods. It takes 0.015s to reach the MPP, while the P&O MPPT with fixed step size of 0.01 takes 0.037s to track the MPP as shown in Fig. 7.22. The dynamic performance of the P&O MPPT algorithm can be further improved with a larger step-size. However, this will have a negative effect on the MPPT efficiency. Fig. 7.21 to Fig. 7.24 prove that the proposed MP&O MPPT method with variable step-size can eliminate the need to perform a complicated trade-off between the steady-state and dynamic performance. Fig. 7.23 shows that the steady-state oscillation has been totally eliminated in the case of the MP&O and the output power of PV array is above 179.9 W. In addition the proposed MP&O MPPT provides faster dynamic response than the P&O MPPT at both step sizes of 0.01 and 0.04, as shown in Fig. 7.22 and Fig. 7.24. The efficiency of the MP&O MPPT method is clearly improved in comparison with P&O MPPT method with both step sizes of 0.01 and 0.04. Table 7.3 provides a summary of tracking performance for the MP&O MPPT and P&O MPPT methods with different levels of illumination. Furthermore, the tracking efficiency comparison of the proposed MP&O with the P&O algorithm with step size of 0.04 and 0.01 is displayed in Fig. 7.25. However it should be noted that the efficiency is calculated based on a

simulation that represented a short operating time. In practice, the PV array will operate all day. Hence the oscillation effect will be accumulated, and as a result the total efficiency of the MP&O method will be higher than the P&O method.

In order to compare the performance of the MP&O against the conventional P&O in tracking the maximum power, the simulation power of the PV array is compared to the calculated power at the theoretical MPP for the same level of solar irradiation. The PV array power is the multiplication of the PV array current from Equation (3.15) and its corresponding voltage. The MPPT efficiency was evaluated using Equation (7.5).

$$\eta_{MPPT} = \frac{P_{PV}}{P_{max}} \times 100\% \tag{7.5}$$

Where P_{PV} is the simulated maximum power and P_{max} is the calculated maximum power.

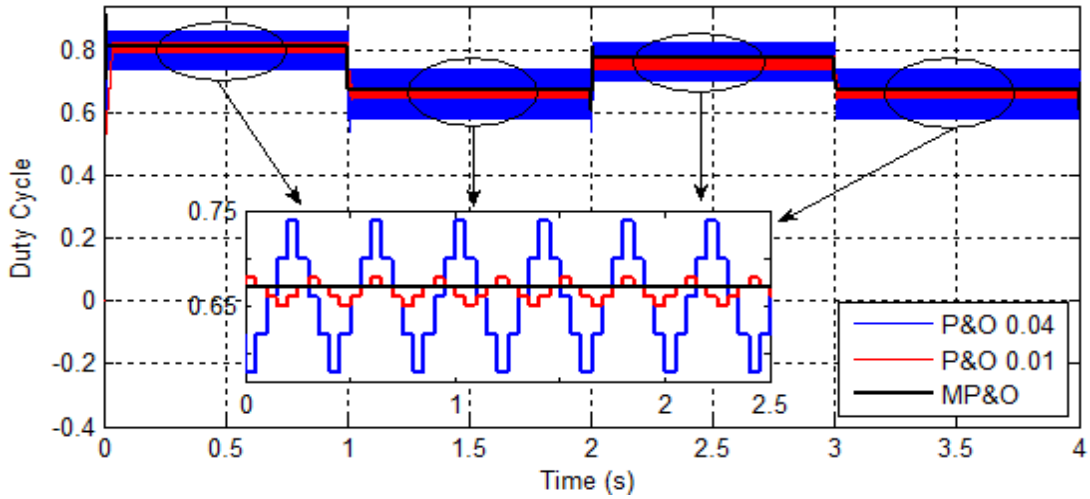

Fig. 7.21 Duty ratio waveform: steady-state comparison of the proposed MP&O with the P&O algorithm with step size of 0.04 and 0.01.

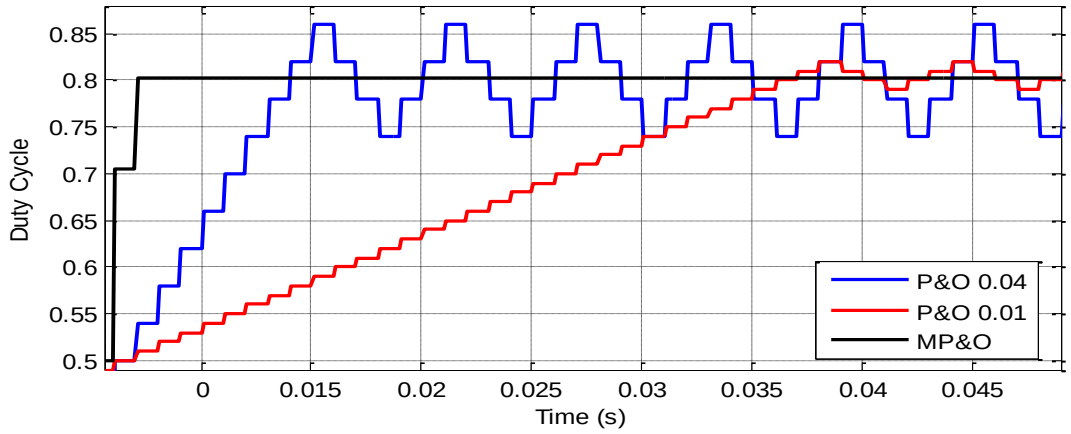

Fig. 7.22 Duty ratio: dynamic response comparison of the proposed MP&O with the P&O algorithm with step size of 0.04 and 0.01.

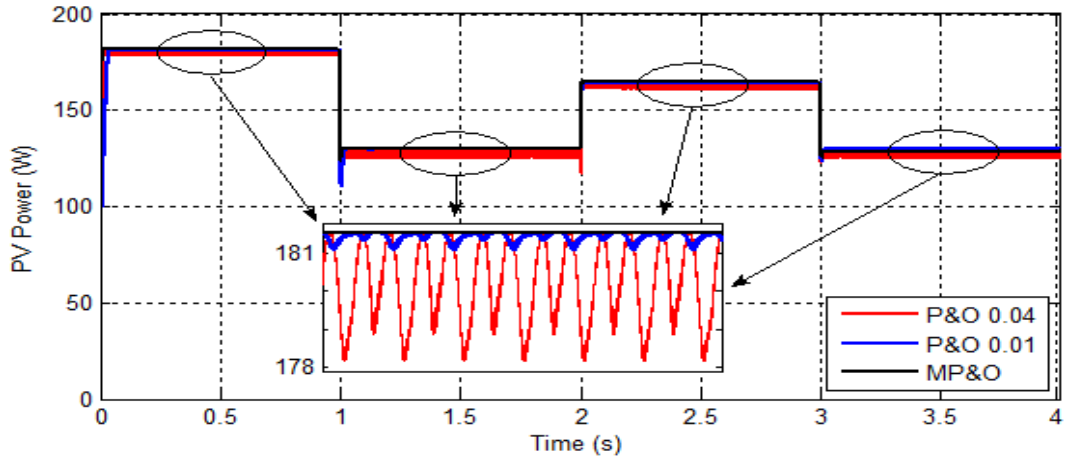

Fig. 7.23 PV output power: steady-state comparison of the proposed MP&O with the P&O algorithm with step size of 0.04 and 0.01.

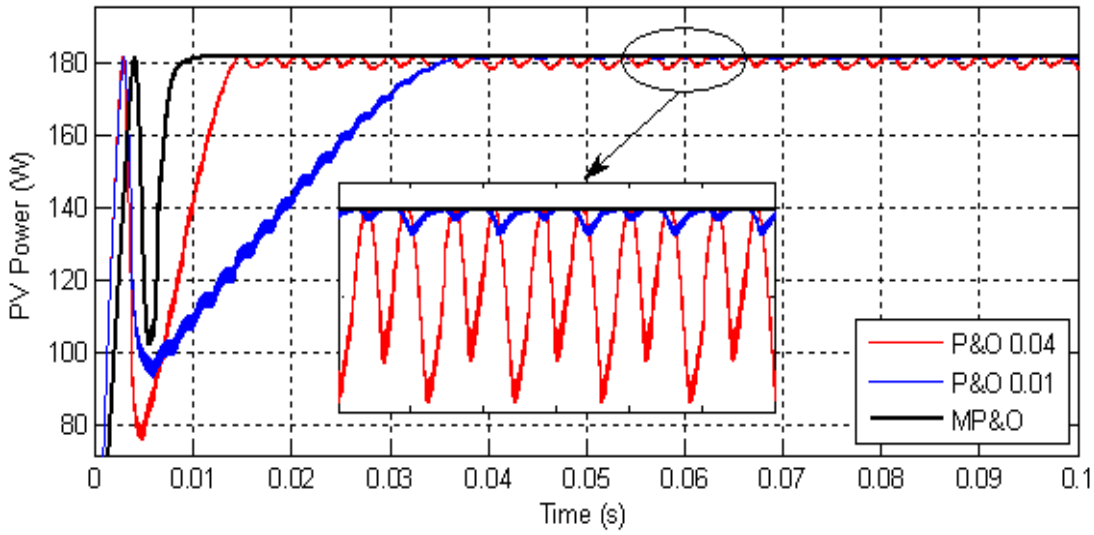

Fig. 7.24 PV output power: dynamic response comparison of the proposed MP&O with the P&O algorithm with step size of 0.04 and 0.01.

Table 7.3 Tracking performance comparison between P&O MPPT and MP&O MPPT methods.

Irradiation / MPPT	G (W/m2)	1000	700	900	700
	P_{max} (W)	180	129.8	164.5	129.8
P&O with step-size = 0.04	P_{PV} (W)	178.9	127.8	163.4	127.8
	Efficiency η (%)	99.38	99.33	98.45	99.33
	Tracking Time (s)	0.015	0.012	0.008	0.004
	Steady-state power oscillation	V-High	V-High	V-High	V-High
P&O with step-size = 0.01	P_{PV} (W)	179.3	128.1	163.8	128.1
	Efficiency η (%)	99.61	99.57	98.69	99.57
	Tracking Time (s)	0.0366	0.016	0.011	0.01
	Steady-state power oscillation	High	High	High	High
MP&O	P_{PV} (W)	179.9	129	164.35	129
	Efficiency η (%)	99.94	99.90	99.38	99.90
	Tracking Time (s)	0.01	0.005	0.004	0.002
	Steady-state power oscillation	None	None	None	None

Tracking time, is the time that the MPPT control takes to reach the maximum power point when the solar irradiation changes.

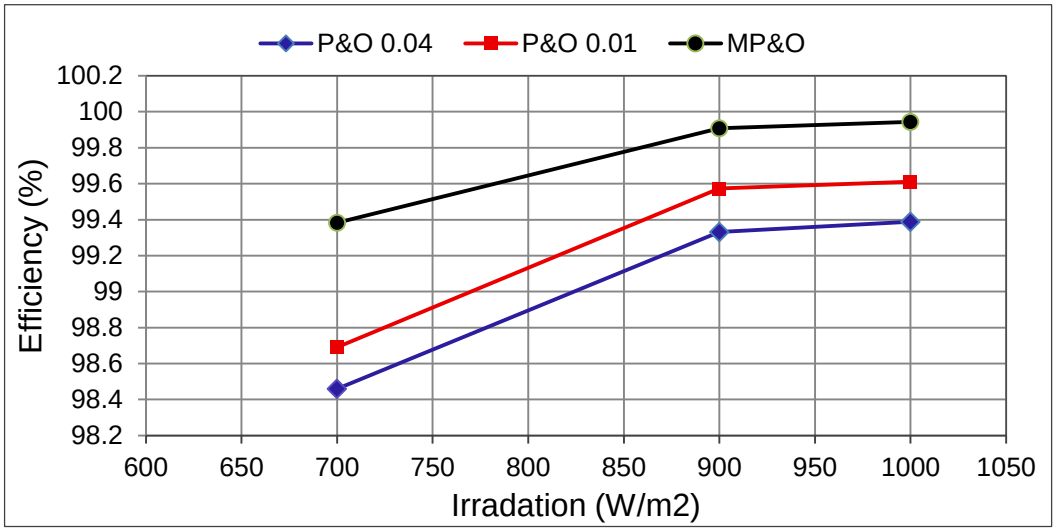

Fig. 7.25 Tracking efficiency: comparison of the proposed MP&O with the P&O algorithm with step size of 0.04 and 0.01.

7.3 Simulation of PV water pumping system with MPPT controllers

The SIMULINK/MATLAB software is used for simulation of the photovoltaic water pumping system. The complete simulation model of the system consists of some masked blocks connected together as shown in Fig. 7.26. The simulation was conducted by connecting a PV model, through a controlled buck chopper, to PM DCM driving a centrifugal pump load. Also a MPPT control unit is included. The system was simulated to verify the functionality and performance of the proposed fuzzy logic controller based on a MPPT water pumping system, and also an ANN controller based on a MPPT water pumping system. Each block in the system will be discussed in detail in the later sections, except that the SIMULINK blocks of the PV array and DC-DC buck converter will be implemented as simulated in sections 7.1.1 and 7.1.2, respectively. The buck converter was implemented without the output filter because it is feeding an inductive load.

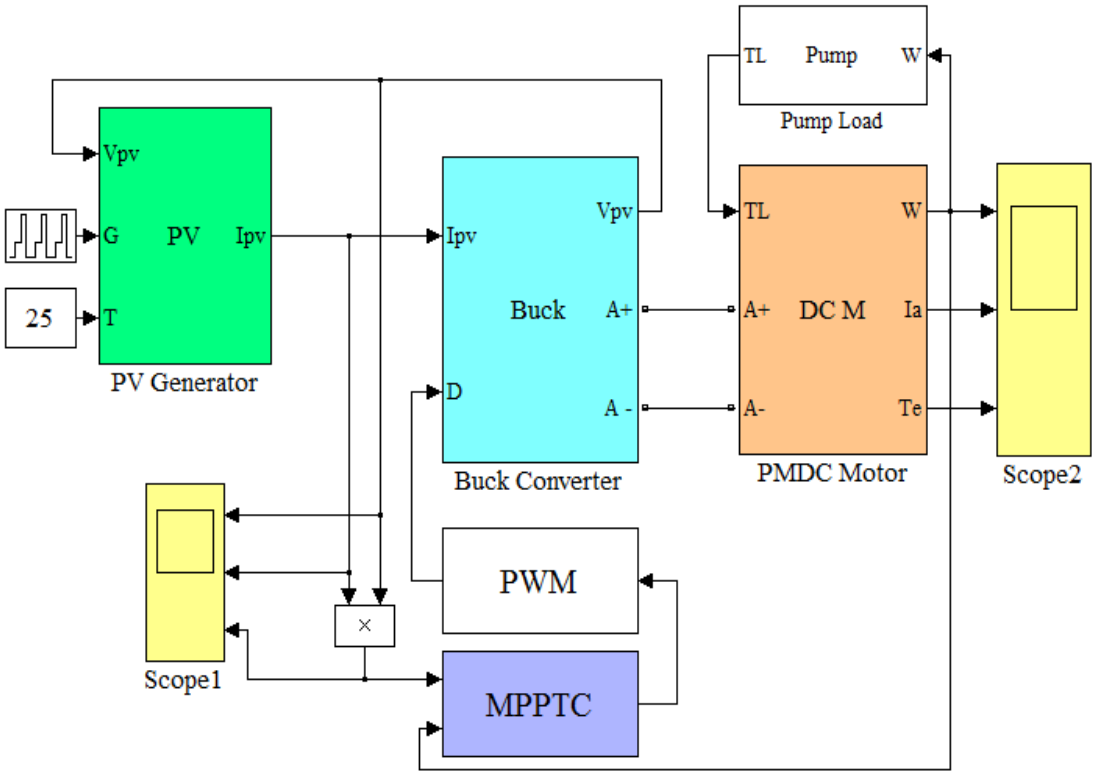

Fig. 7.26 SIMULINK model of PV water pumping system with MPPT controller.

7.3.1 Permanent magnet DC motor model

The PMDCM simulation model is built in MATLAB environment using the SimPowerSystems and SIMULINK library as shown in Fig. 7.27. The PMDCM model implements Equations (3.42) and (3.43).

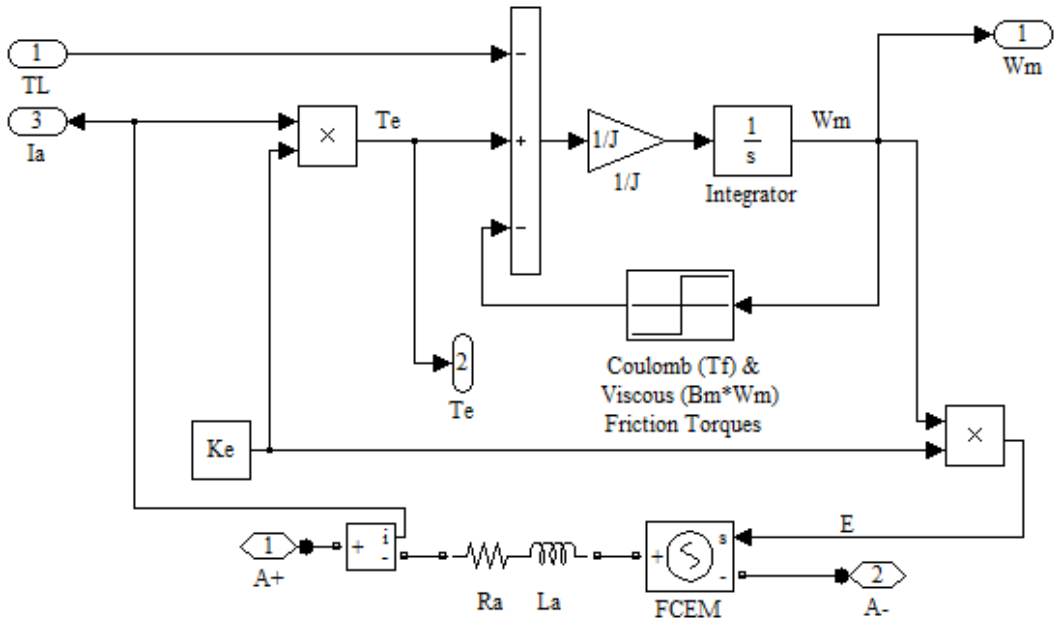

Fig. 7.27 SIMULINK model of PMDC Motor.

7.3.2 Centrifugal pump load

The centrifugal pump was simulated in MATLAB/SIMULINK by implementing Equations (3.59) using various functional blocks. The details of the centrifugal pump model are shown in Fig. 7.28 (a) and it can be further simplified into one model block as in Fig. 7.28 (b).

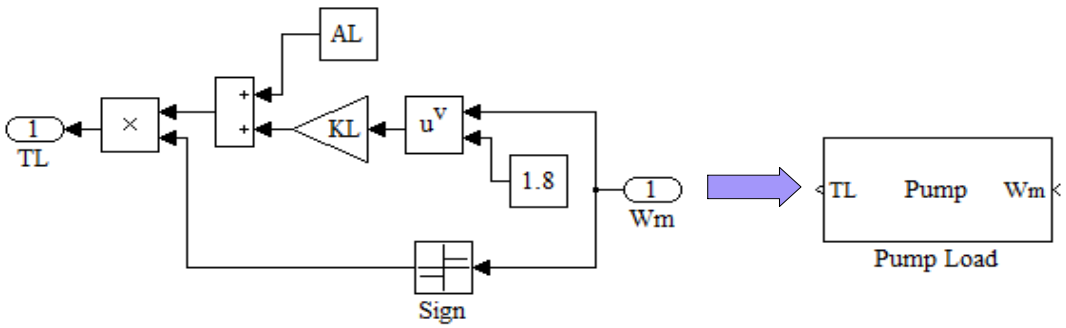

(a) (b)

Fig. 7.28 SIMULINK model of centrifugal pump load.

The pump block has one input and one output terminals; the motor speed ω_m is fed into the pump as an input which in turn outputs load torque T_L.

7.3.3 Fuzzy logic controller based on MPPT operation of water pumping system

The FLC is based on an MPPT operation for the water pumping system and is implemented in MATLAB/SIMULINK. The control model is shown in Fig. 7.29. The fuzzy control rule has been completed in MATLAB FIS as discussed in section 4.3. The detailed design of the Fuzzy Interface system (FIS) editor, Membership Function Editor and Rule Editor are as shown in the Appendix D.1 from Fig. D.4 Fig. D.8, respectively. The FLC uses the PV array Power P_{pv} and the pump ω_m as input signals and produces duty ratio D as a control signal for the buck converter.

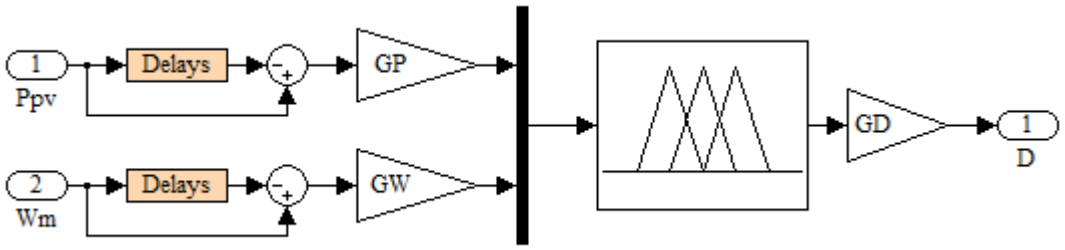

Fig. 7.29 SIMULINK block of FLC based on MPPT operation of water pumping system.

Fuzzy logic control parameters	
The scaling factor of the PV array output power variation (G_P)	0.58
The scaling factor of the rotation speed variation (G_ω)	0.18
The scaling factor the duty ratio variation (G_D)	0.0186

7.3.4 ANN controller based on MPPT of water pumping system

This section discusses the simulation of the neural network for MPPT operation of the water pumping system. The training and simulation work of the neural network has been carried out using MATLAB to identify the duty ratio of the buck chopper corresponding to the MPP from data of the PV array power and DC motor speed. The MATLAB/SIMULINK model of the trained neural network is illustrated in Fig. 7.30.

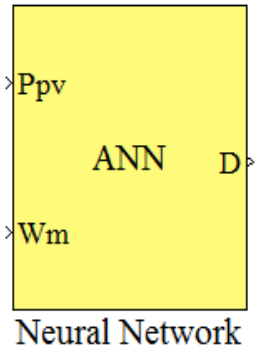

Fig. 7.30 SIMULINK block of neural network based on MPPT of water pumping system.

The neural network block has two inputs, the PV array power P_{PV} and the motor speed ω_m and it outputs the control signal D of the buck chopper. The simulated neural network consists of 1 input layer, 1 hidden layer and 1 output layer. Each layer has a set of input and base. To calculate the output of the hidden layer, a hyperbolic tangent sigmoid transfer function was used as an activation function and a linear transfer function was used for the neurons of the output layer. The weights of each layer are multiplied with the input signals in each neuron. The MATLAB simulation of the ANN layers, weighted input and bias are represented in the Appendix E.1.1 from Fig. E.9 to Fig. E.12. In the neural network control, one output signal is needed to control the switching of the buck chopper, therefore the output layer has only one neuron as shown in Fig. E.12.

7.4 Simulation results of the PV water pumping system using the MP&O, FLC and ANN MPPT techniques

The MATLAB\SIMULINK software is used for simulation of the photovoltaic water pumping system. The system was simulated to verify the functionality and performance of the proposed ANN based MPPT, FLC based MPPT and MP&O algorithm, and to quantify how the proposed controllers contribute to an increase in the system efficiency compared with directly (without MPPT controller) connecting the PV array to the pump-drive system. The effectiveness of the three proposed methods to handle weather condition changes especially the change of solar irradiation is evaluated through different levels of solar irradiation. Some other researchers consider the performance of some proposed MPPT techniques during load variation. However, the PV system implemented in this thesis is a stand-alone

system where the load has insignificant variation, unlike in a grid-tied system. Therefore, the load variation has not been taken into account for testing the performance of the proposed three MPPT methods. Also, a comparison has been carried out among the three proposed methods and each method has been compared with the calculated results. The comparison has been carried out in the same PV water pumping system and under the same weather conditions to quantify how much each method contributes to improve the efficiency of the PV system. The PV water pumping system SIMULINK model used to test the proposed MPPT techniques is shown in Fig. 7.26. The parameters of each block used in this system are listed in Table 7.4.

Table 7.4 Parameters of dc permanent motor, load, and PV array

DC PM Motor data	
Rated motor voltage (V_a)	120V
Rated motor current (I_a)	9.2A
Rated motor speed (ω)	157.079 (rad/sec)
Armature resistance (R_a)	1.5Ω
Armature inductance (L_a)	0.2H
Voltage constant (K_e)	0.67609 V/(rad/sec)
Torque constant (K_T)	0.67609 Nm/A
Motor friction (A_m)	0.2 Nm
Load pump data	
Moment of inertia (J)	0.02365 Kg.m^2
Viscous friction coefficient (B)	0.002387 Nm/(rad/sec)
Load torque constant (K_e)	0.00039 Nm/(rad/sec)
Load friction (A_L)	0.3 Nm
PV module data (Sunpower E19/240 Solar Panels)	
Rated Power (P_{max})	240 W
Maximum Power Voltage (V_{pm})	40.5 V
Maximum Power Current (I_{pm})	5.93 A
Open-Circuit Voltage (V_{oc})	48.6 V
Short-Circuit Current (I_{sc})	6.30 A
Series Resistance (R_S)	0.2746Ω

To better assess the overall performance of the PV water pumping system, the combined SIMULINK model shown in Fig. 7.26 is subjected to slow and rapid changes in solar insolation using the three proposed MPPT controllers, to display the behaviour of the MPPT controllers during the passing of clouds. The solar irradiation was started from 800 W/m^2 and then changed from 800 W/m^2 to 600 W/m^2, 600 W/m^2 to 400 W/m^2, 400 W/m^2 to 700 W/m^2 and 700 W/m^2 to 550 W/m^2 at the time instants 1.0s, 2.0s, 3.0s and 4.0s, respectively.

7.4.1 Directly connected PV water pumping system

In the directly connected PV water pumping system, the PV array has been directly connected to the pump load without using a MPPT system. The system was subjected to a sudden change in solar irradiation as shown in Fig. 7.31. The simulation results for the directly connected system are shown in Fig. 7.32 to Fig. 7.37, which illustrate the PV array output current, voltage, power and the rotational speed of the motor respectively.

The simulation waveforms show that the directly connected system is operating far from the maximum power point at all irradiation levels. Fig. 7.32 illustrates that the PV array current is greater than the optimum current. However, the voltage waveform in Fig. 7.33 shows that the operating voltage of the PV array is less than the optimum voltage. As a result of this, the system deviates from the maximum operating power all the time as shown in Fig. 7.34. The system is operating at a power point much less than the maximum power point. Therefore, some of the energy will be dissipated and the pump motor is running at a speed which is less than the maximum possible speed as shown in Fig. 7.35. This reduces the amount of water being discharged from the pump, hence, the system is operating at a relatively poor efficiency of 85.41%. For more clarification, Fig. 7.36 and Fig. 7.37 illustrate the location of the operating power points of the directly connected system relative to the MPP on the *P-V* and *I-V* curves, respectively, for various insolation levels.

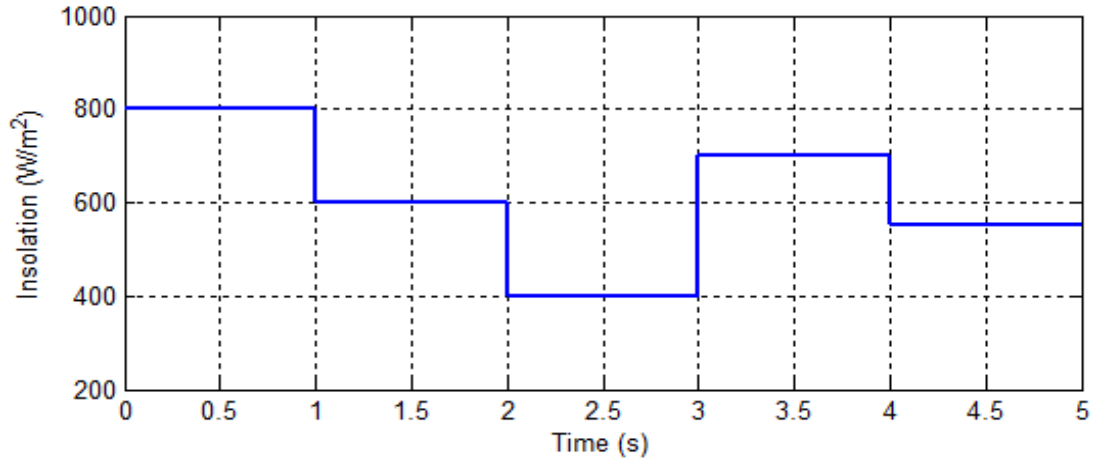

Fig. 7.31 Solar Irradiation.

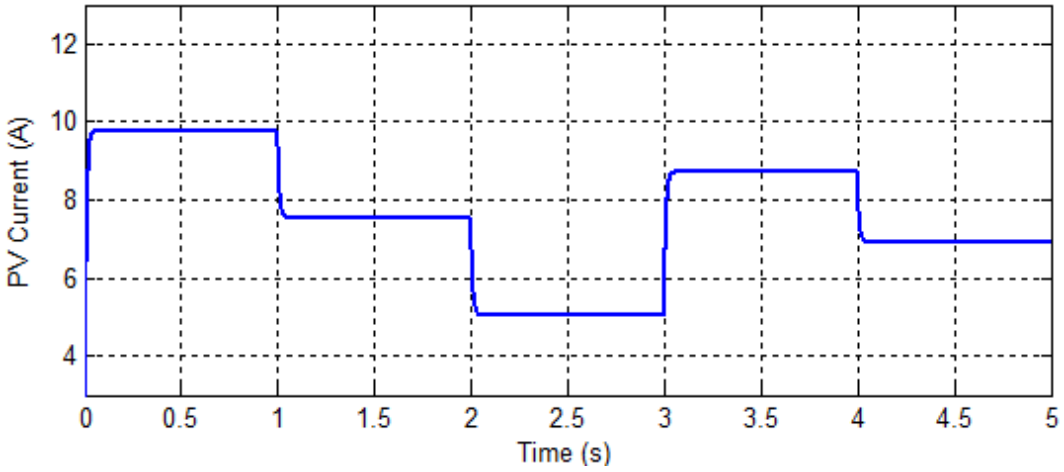

Fig. 7.32 PV array output current without MPPT controller under varying irradiation.

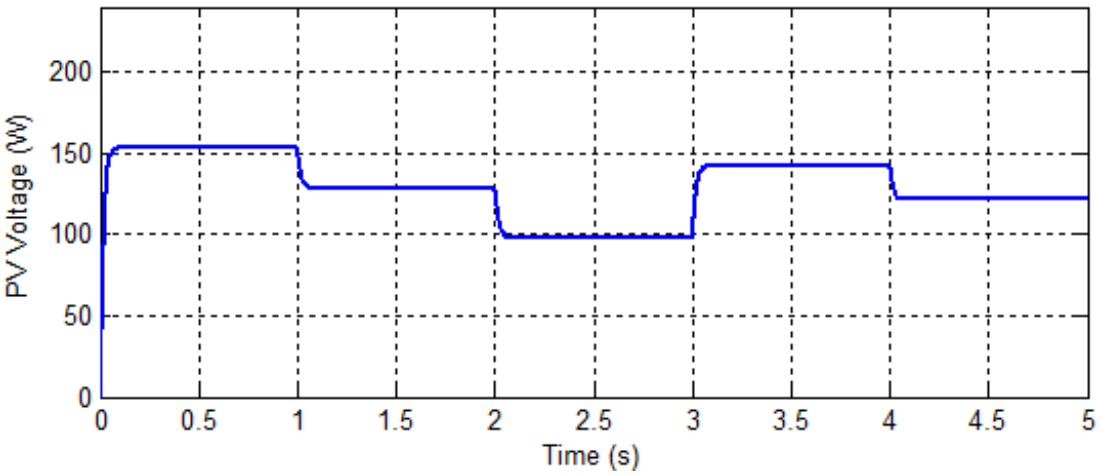

Fig. 7.33 PV array output voltage under varying irradiation without MPPT controller.

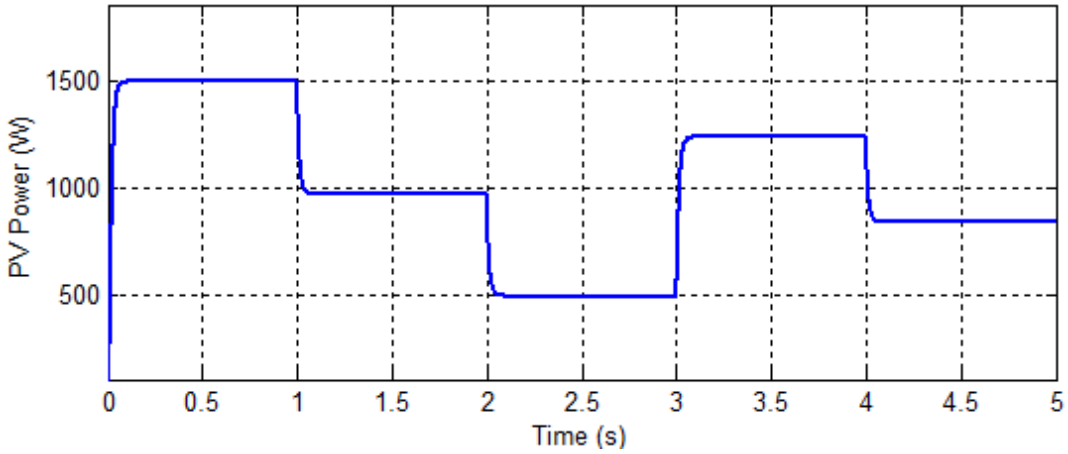

Fig. 7.34 PV array output power varying irradiation without using MPPT controller.

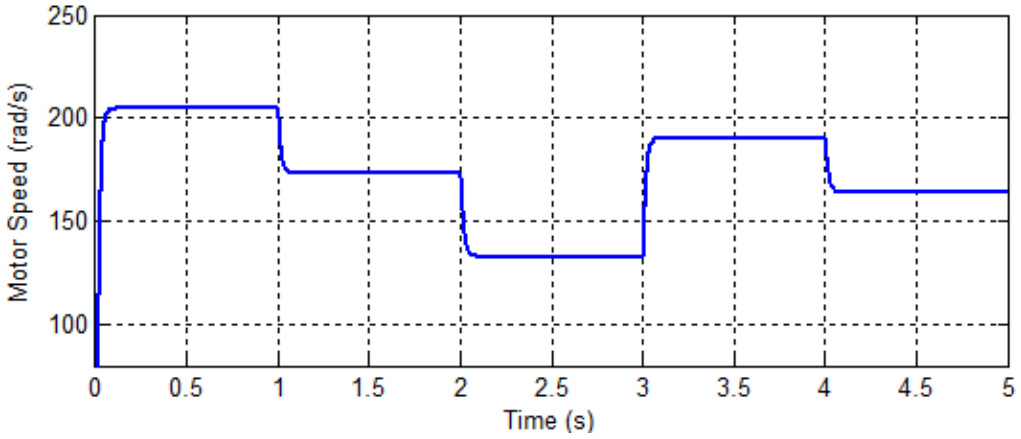

Fig. 7.35 Rotational speed under varying irradiation levels without MPPT controller.

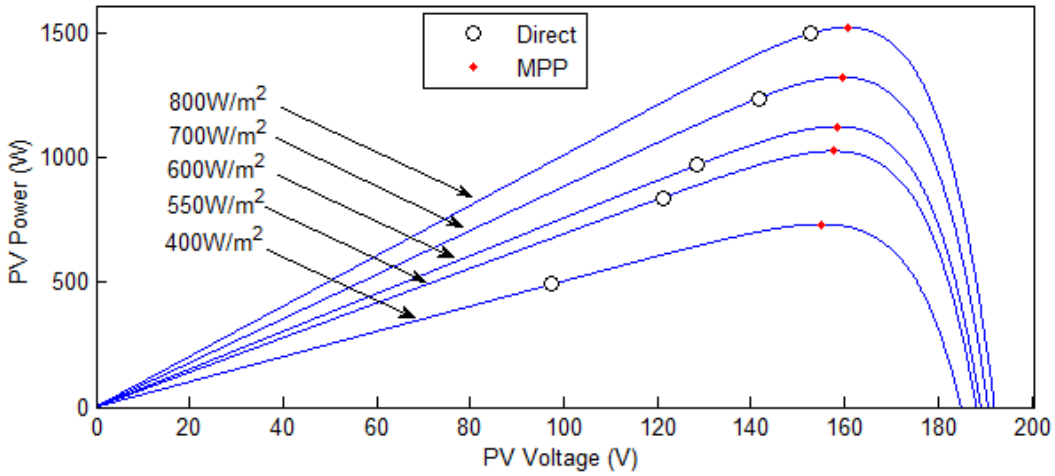

Fig. 7.36 The operating points of PV system without MPPT controller on the *P-V* curves under different irradiation levels.

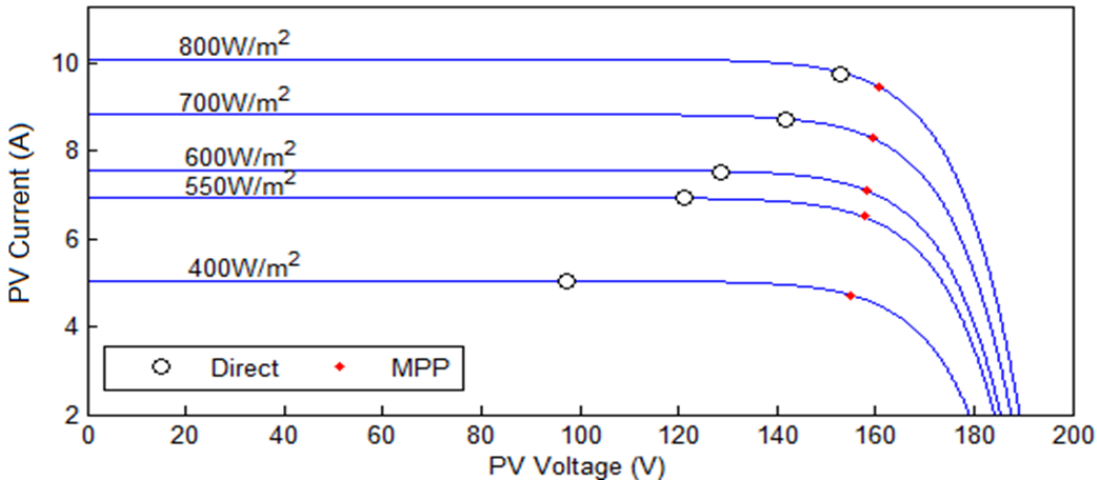

Fig. 7.37 The operating points of PV system without MPPT controller on the *I-V* curves under different irradiation levels.

7.4.2 MP&O MPPT method

The MP&O has already been discussed, and implemented in the PV system with a resistive load in section 7.2 to test its performance against the conventional P&O. The proposed MP&O presented better performance compared to the conventional P&O in both, the steady-state and the dynamic condition. In this section the MP&O is implemented in the PV water pumping system shown in Fig. 7.26 to show the quantity of power extracted compared to the directly connected system and to verify its functionality compared with the proposed FLC and ANN methods. To test the performance of the MP&O in the PV water pumping system under changing weather conditions, the solar irradiation was sharply stepped up and down as shown in Fig. 7.31. The simulated results of MATLAB/SIMULINK of the PV array current, voltage and power are displayed in Fig. 7.38 to Fig. 7.40, respectively. The pump motor speed is displayed in Fig. 7.41 and the MP&O output signal (duty ratio) is displayed in Fig. 7.42. At the beginning, starting with the 800 W/m^2 irradiation, the PV power extracted by the directly connected system is lower than the maximum available power. However, the MP&O succeeded in tracking the MPP and maintains operation at this point. From the simulation results it is obvious that PV array current and voltage change when the PV system is subjected to change in the irradiation. Therefore, the MPP of the PV array changes as shown in Fig. 7.40. The MP&O starts to respond to the change in the PV power by adjusting the duty ratio as shown in Fig. 7.42 to track the new MPP and to force the system to operate at this point. But the

directly connected system fails to track the MPP and deviates all the time from this point as shown in Fig. 7.40. Moreover the pump motor speed gained by MP&O is much greater than that gained by the directly connected system as displayed Fig. 7.41. Increasing the pump motor speed will increase the amount of water being discharged from the pump hence the total efficiency of the system will be maximized. Fig. 7.43 and Fig. 7.44 display the tracking performance and the accuracy of the MPP on the *P-V* and *I-V* curves, respectively, while using the MP&O.

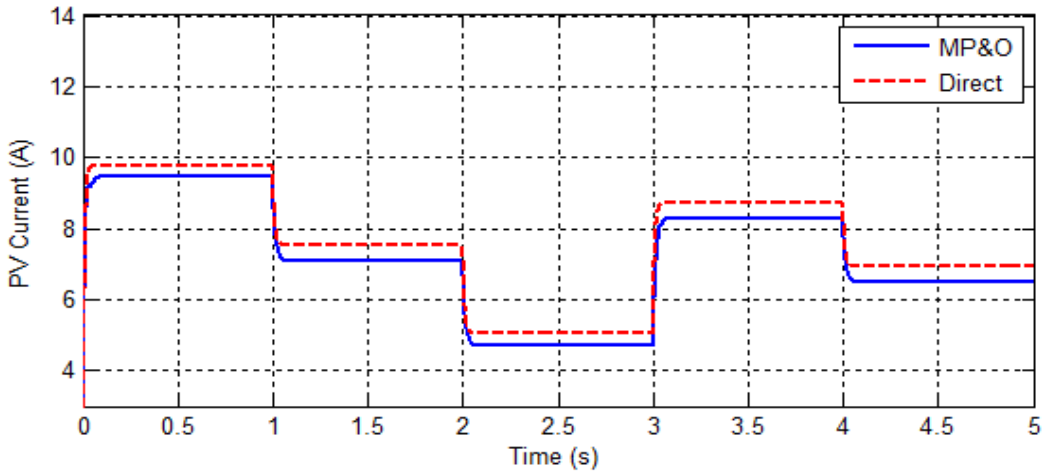

Fig. 7.38 PV array output current under varying irradiation levels for MP&O MPPT.

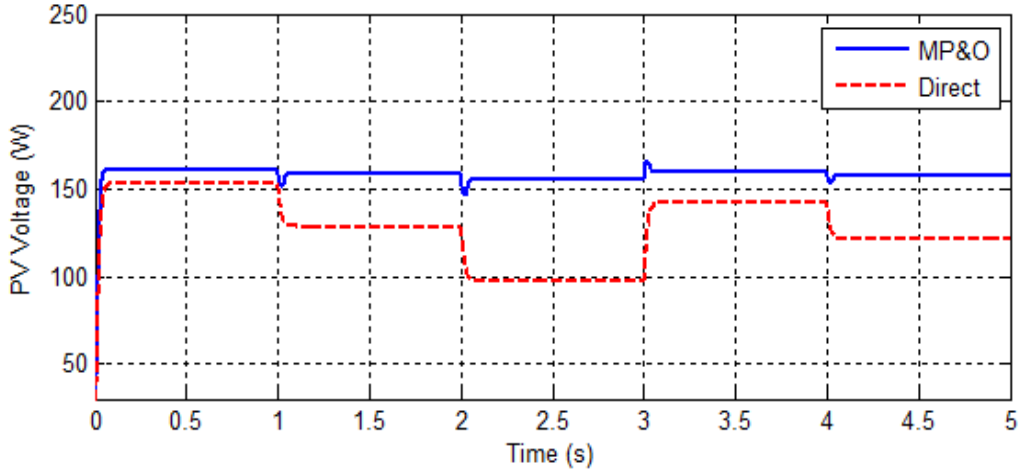

Fig. 7.39 PV array output voltage under varying irradiation levels for MP&O MPPT.

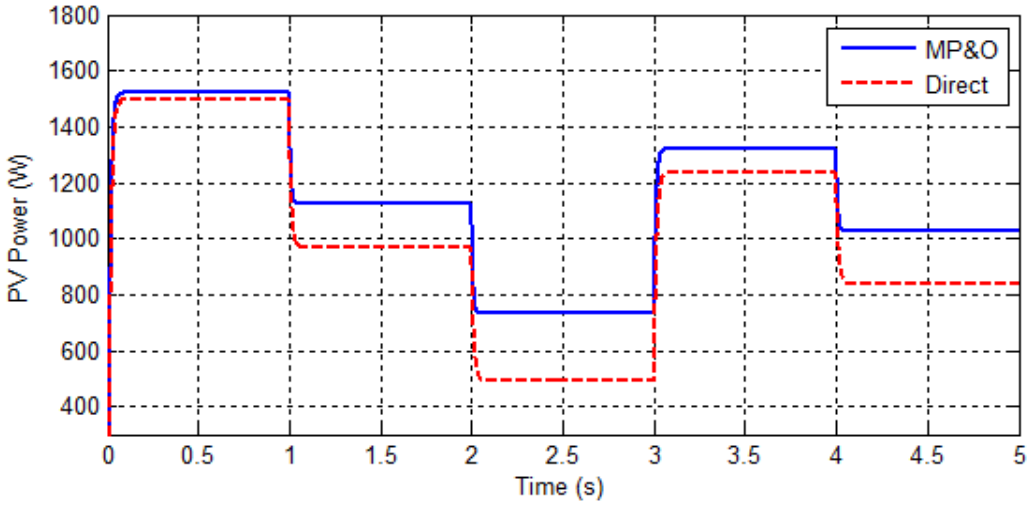

Fig. 7.40 PV array output power under varying irradiation levels for MP&O MPPT.

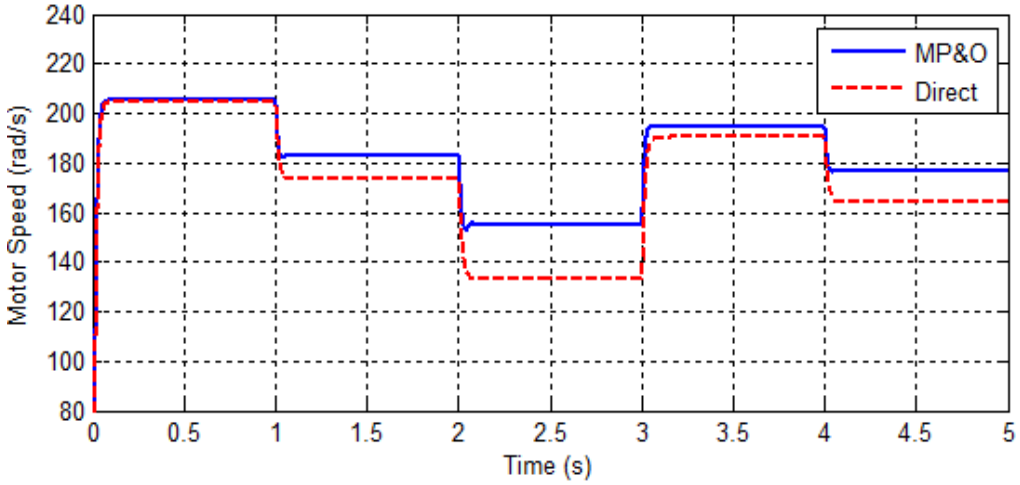

Fig. 7.41 Rotational speed under varying irradiation levels for MP&O MPPT.

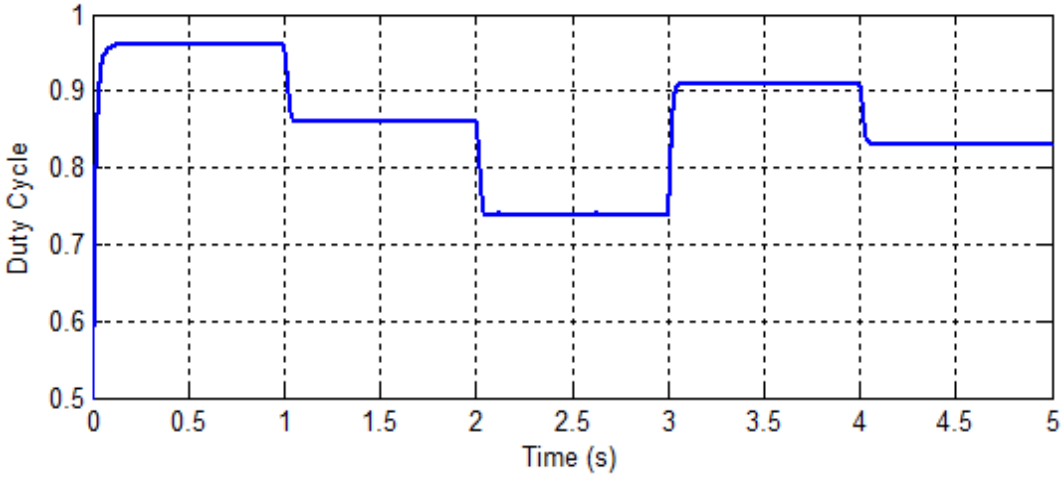

Fig. 7.42 Duty ratio waveform of MP&O MPPT algorithm.

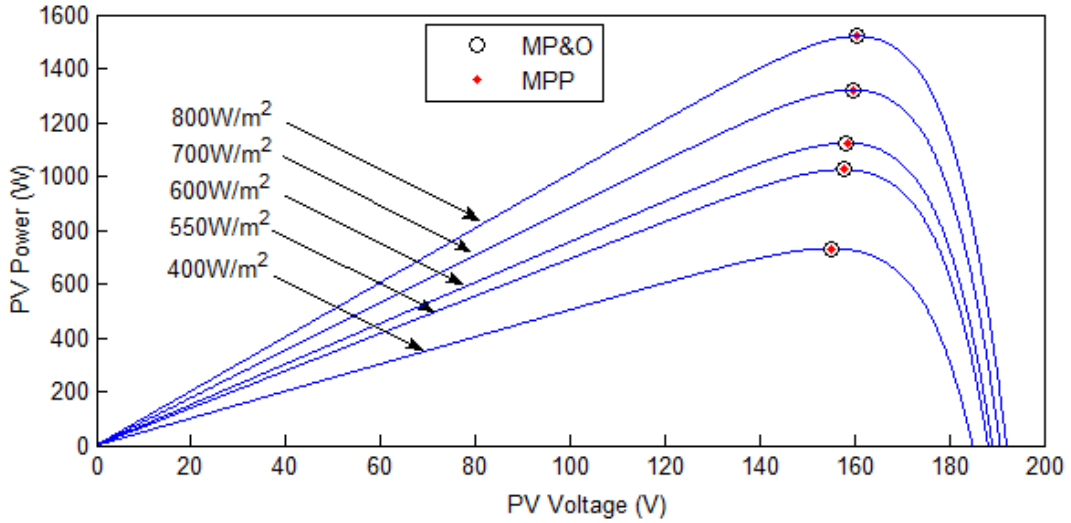

Fig. 7.43 The operating points of PV system using MP&O MPPT controller on the *P-V* curves under different irradiation levels.

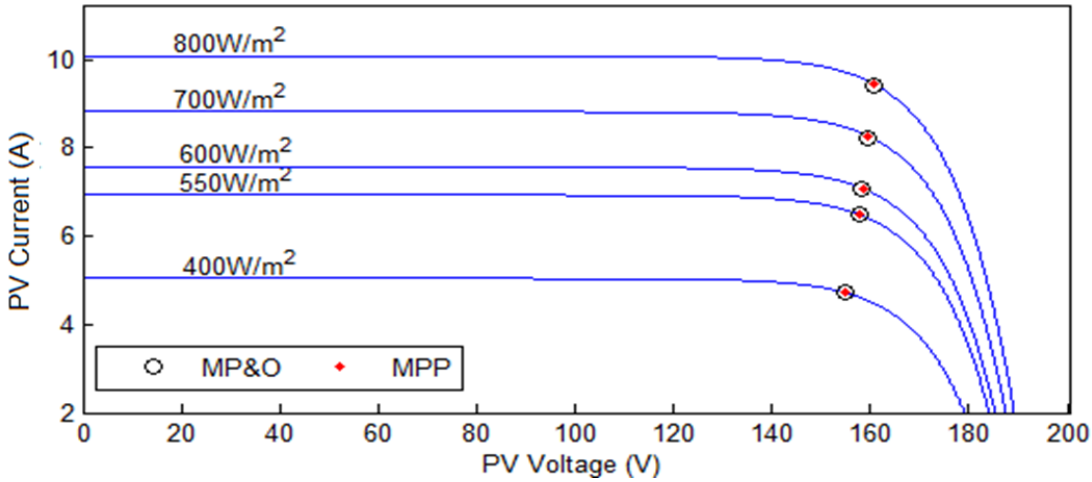

Fig. 7.44 The operating points of PV system using MP&O MPPT controller on the *I-V* curves under different irradiation levels.

7.4.3 FLC based MPPT of PV water pumping system

The FLC is modelled in MATLAB/SIMULINK, as discussed in section 7.3.3, and implemented in the simulated system shown in Fig. 7.26. The solar irradiation was abruptly changed up and down, as shown in Fig. 7.31, to test the performance and show the significant improvement in the power extraction of the system using the FLC MPPT compared with the directly connected system. Simulation results plotted in Fig. 7.45 to Fig. 7.48 present the variation of PV current, voltage and power and the motor speed with the change of irradiation, respectively, for both the FLC and directly connected systems. Fig. 7.49 shows how the output signal of the FLC (duty

ratio) changes to track the moving optimum operating power point caused by irradiation change. It is obvious that, PV array current, voltage and power vary with the variation of solar irradiation in both systems, whether using FLC or directly connected options. However the system with FLC adjusts the duty ratio of the buck chopper, as shown in Fig. 7.49, to track the new MPP of the PV array. The location of operating power points of PV system with FLC on the *P-V* and *I-V* curves are shown in Fig. 7.50 and Fig. 7.51, respectively. The PV power response obtained from the PV array closely matches the theoretically calculated results in all cases of irradiation. From the simulation results it is evident that the proposed FLC technique gives improved performance over the directly connected system in all cases of rapid change in the irradiation. As a result, the quantity of the daily pumped water gained by the proposed FLC MPPT method is higher than that pumped by directly connected system.

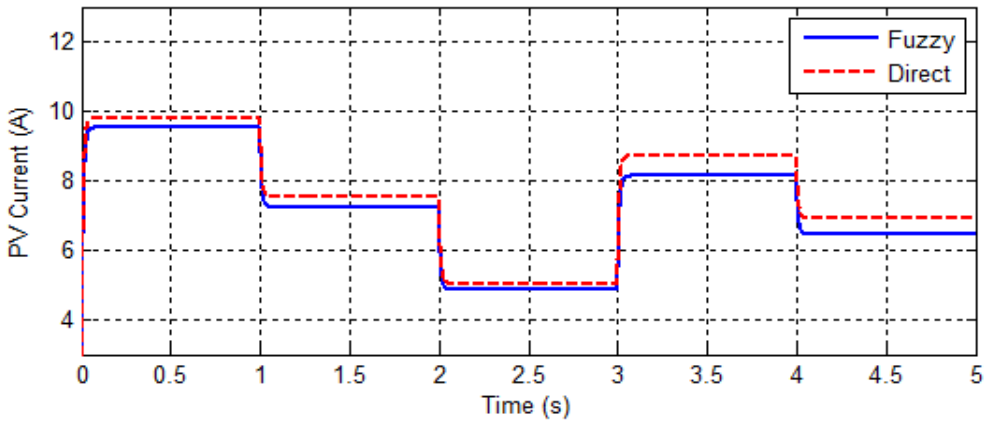

Fig. 7.45 PV array output current under varying irradiation levels for FLC MPPT.

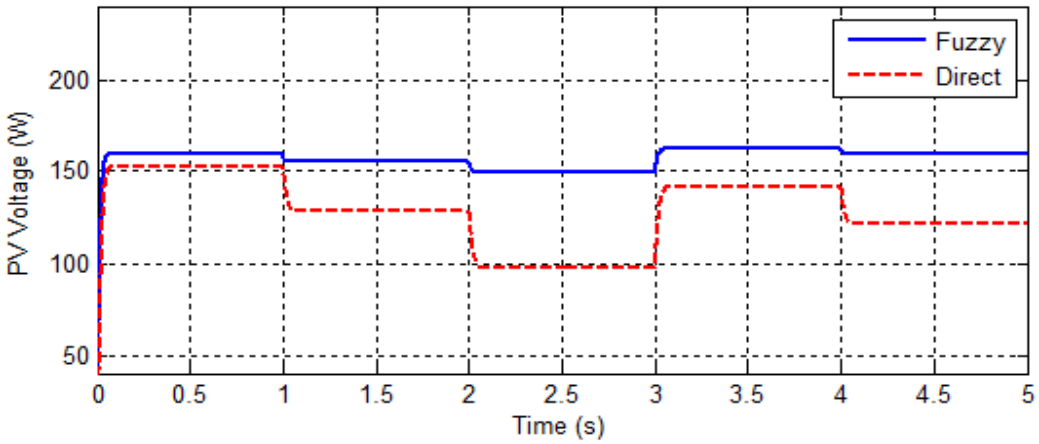

Fig. 7.46 PV array output voltage under varying irradiation levels for FLC MPPT.

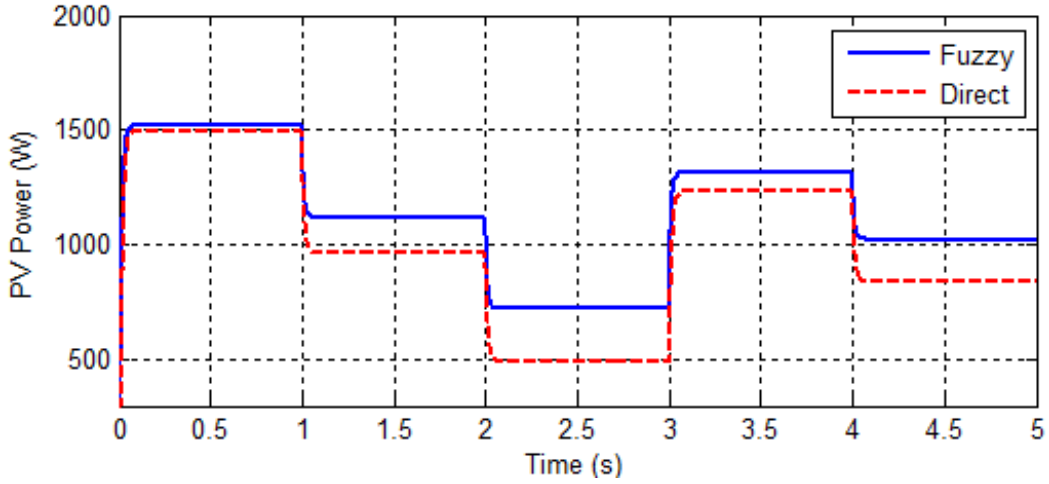

Fig. 7.47 PV array output power under varying irradiation levels for FLC MPPT.

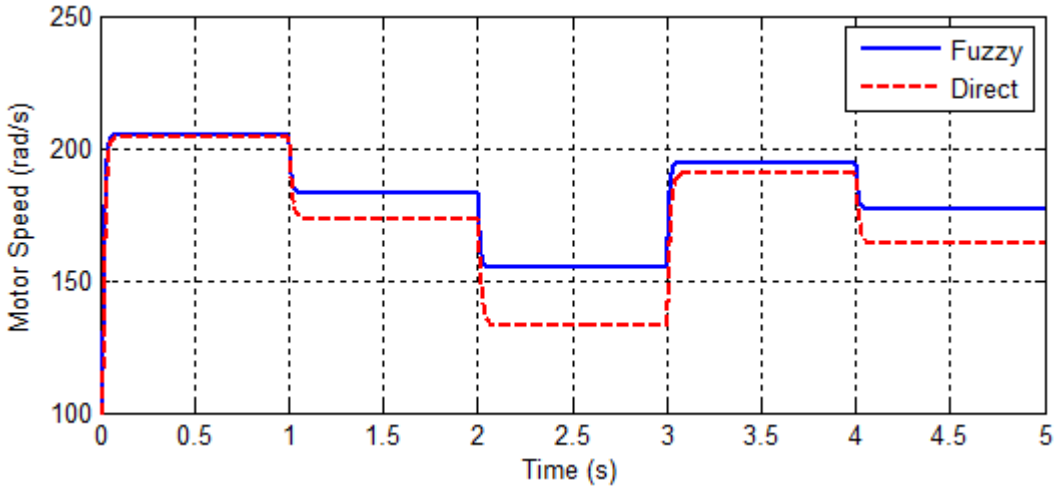

Fig. 7.48 Rotational speed under varying irradiation levels for FLC MPPT.

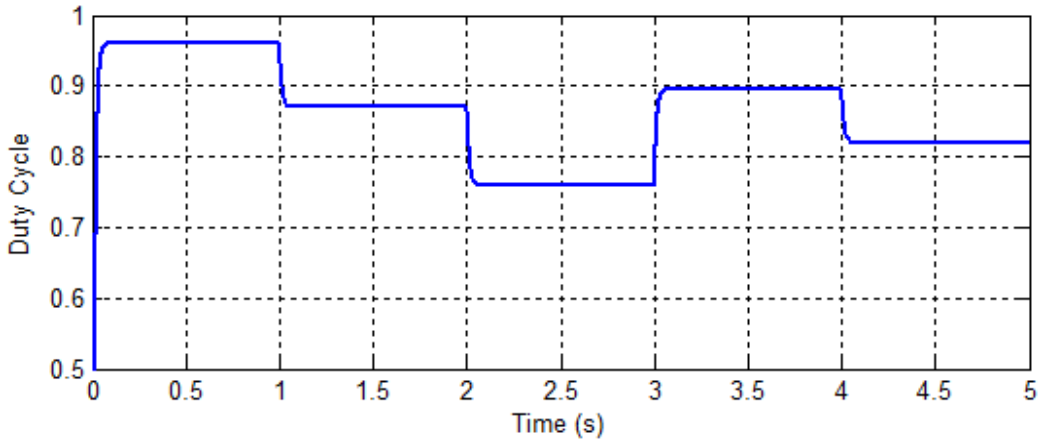

Fig. 7.49 Duty ratio waveform of FLC MPPT.

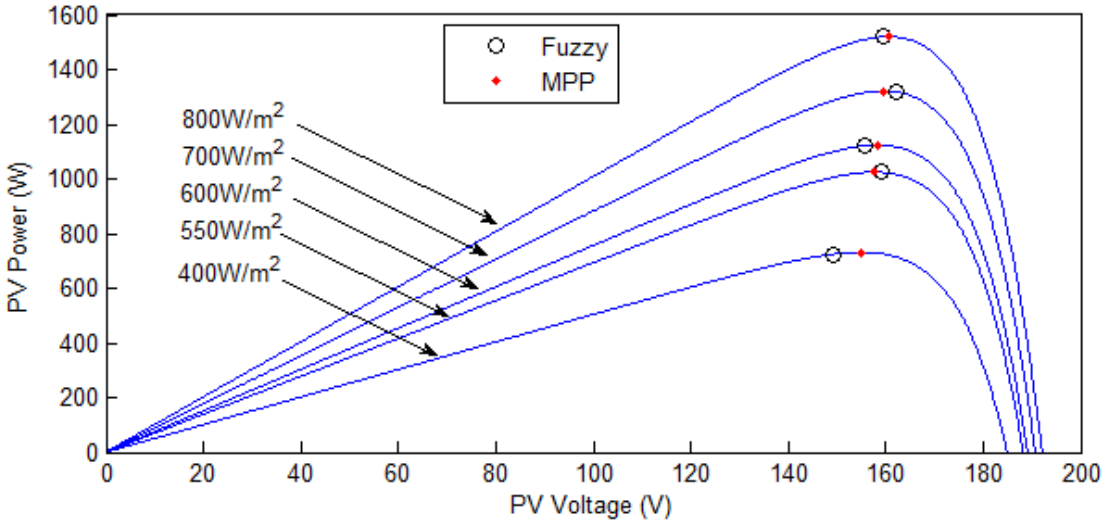

Fig. 7.50 The operating points of PV system using FL MPPT controller on the *P-V* curves under different irradiation levels.

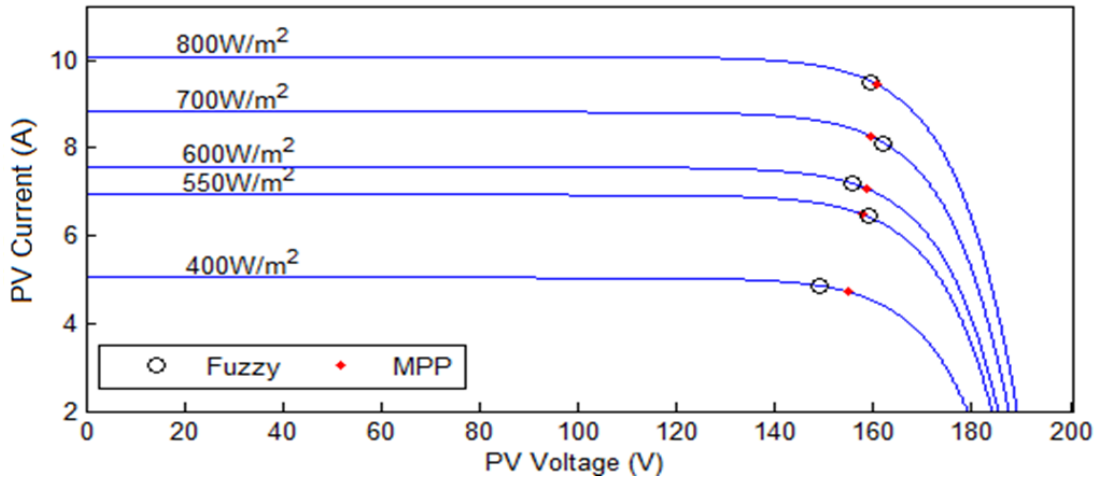

Fig. 7.51 The operating points of PV system using FL MPPT controller on the *I-V* curves under different irradiation levels.

7.4.4 ANN based MPPT of PV water pumping system

The ANN MPPT was trained with a set of input and target data until satisfactory results were gained as explained in section 5.2. Then a SIMULINK diagram was generated for the ANN as shown in Fig. 7.30 and implemented into the PV water pumping system shown in Fig. 7.26, to test the functionality and performance of the ANN controller in the PV system. It was exposed to sudden change in the irritation levels as shown in Fig. 7.31. The simulation results of the PV water pumping system with ANN MPPT controller compared with the direct connected system are shown in

Fig. 7.52 to Fig. 7.55. The simulation results show the PV current produced by directly connected system is greater than that produced with ANN controller. However, the PV voltage and power are higher when using the ANN controller at all levels of irradiation as shown in Fig. 7.53 and Fig. 7.54. This gives an indication that, the direct connected system is operating far from the MPP all the time. Therefore, when the irradiation changes the ANN controller adjusts the duty ratio, as shown in Fig. 7.56, to decrease the PV current operating point and increase the PV voltage operating point until they reach the operating points that are corresponding to MPP. Fig. 7.55 shows how the ANN controller has achieved an improvement in the pump motor speed and nearly match the optimum speed in all cases of solar irradiation. The performance and the operating points of the ANN controller on the *P-V* and *I-V* curves under different solar irradiation levels are shown Fig. 7.57 and Fig. 7.58, respectively.

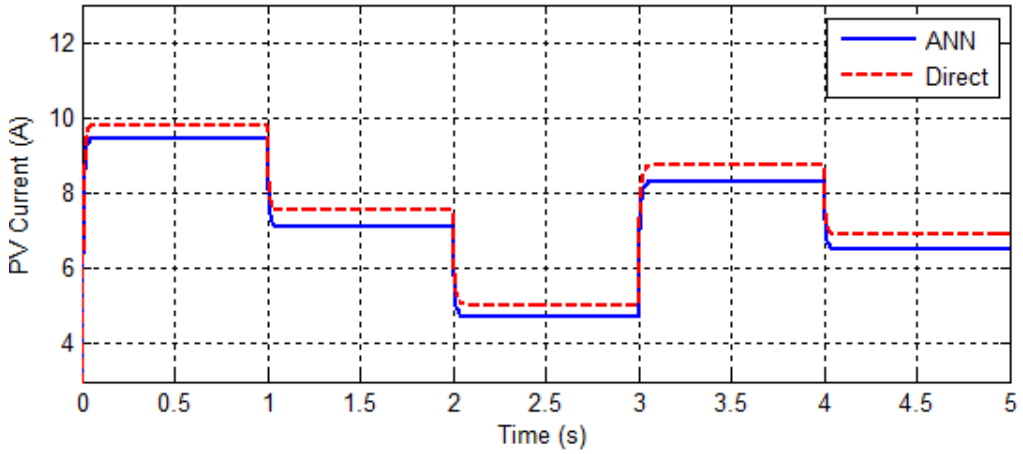

Fig. 7.52 PV array output current under varying irradiation levels for ANN MPPT.

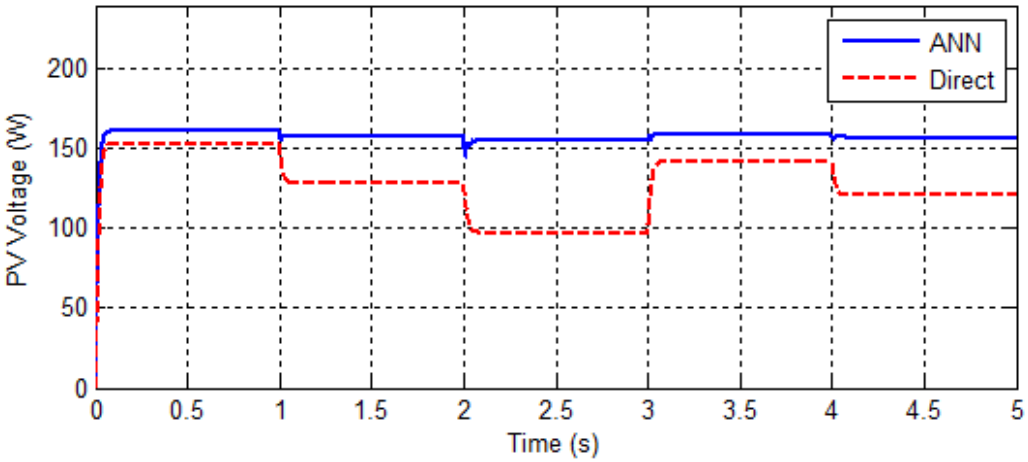

Fig. 7.53 PV array output voltage under varying irradiation levels for ANN MPPT.

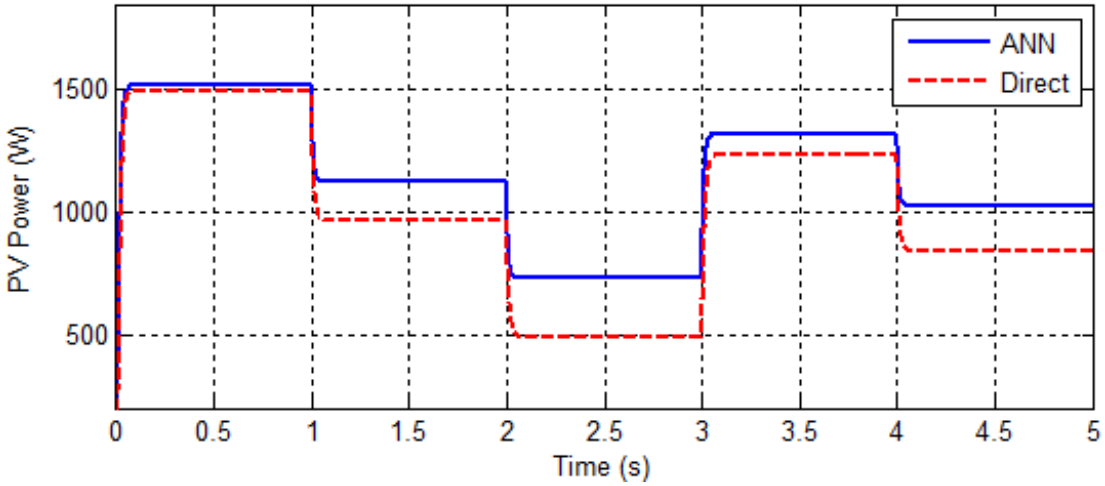

Fig. 7.54 PV array output power under varying irradiation levels for ANN MPPT.

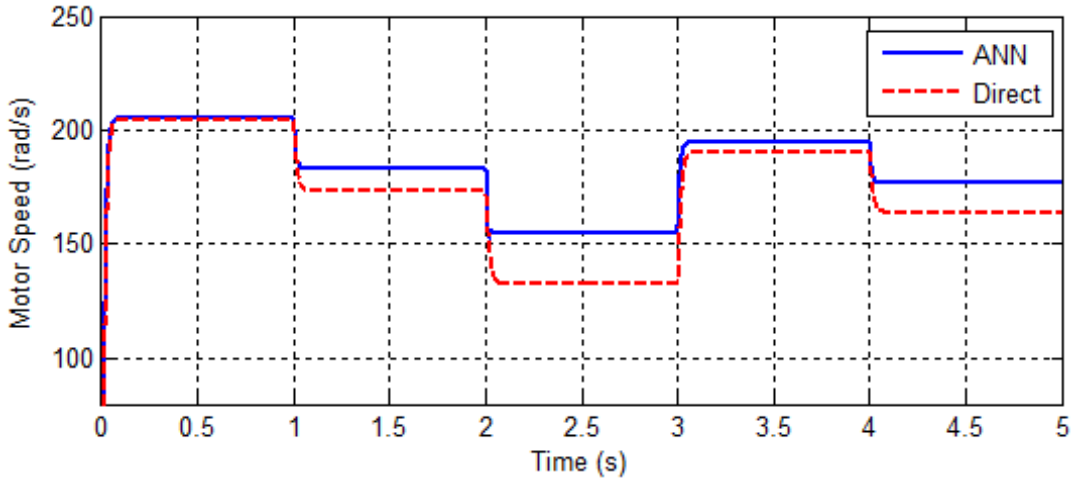

Fig. 7.55 Rotational speed under varying irradiation levels for ANN MPPT.

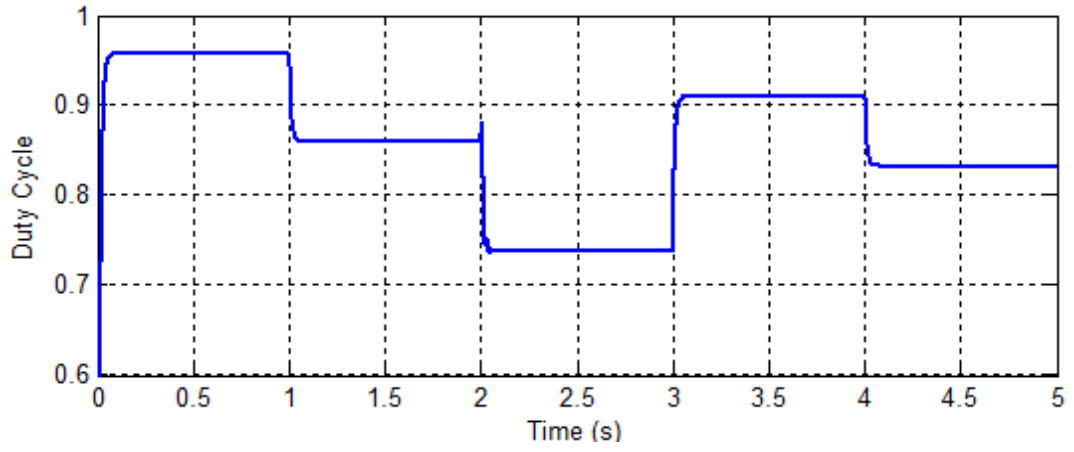

Fig. 7.56 Duty ratio waveform of ANN MPPT.

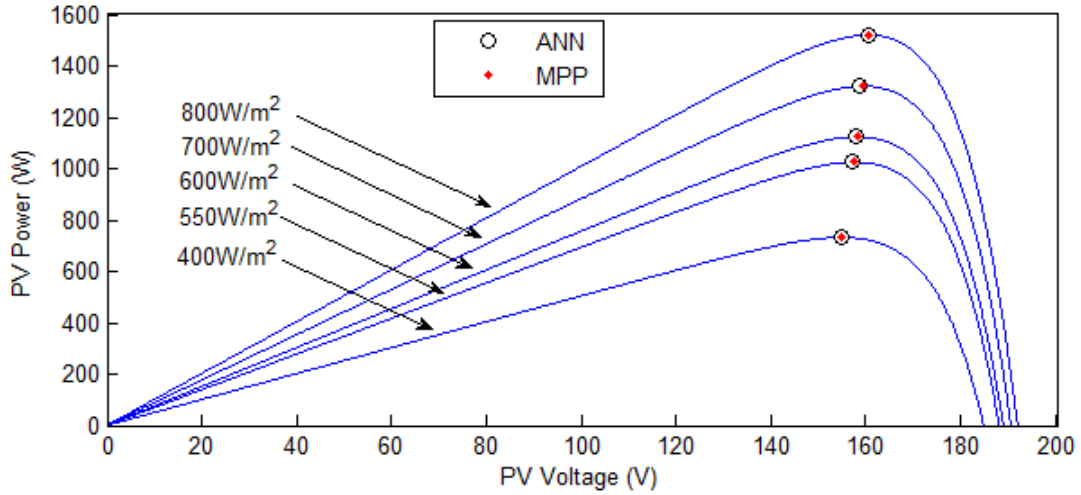

Fig. 7.57 The operating points of PV system using ANN MPPT controller on the *P-V* curves under different irradiation levels.

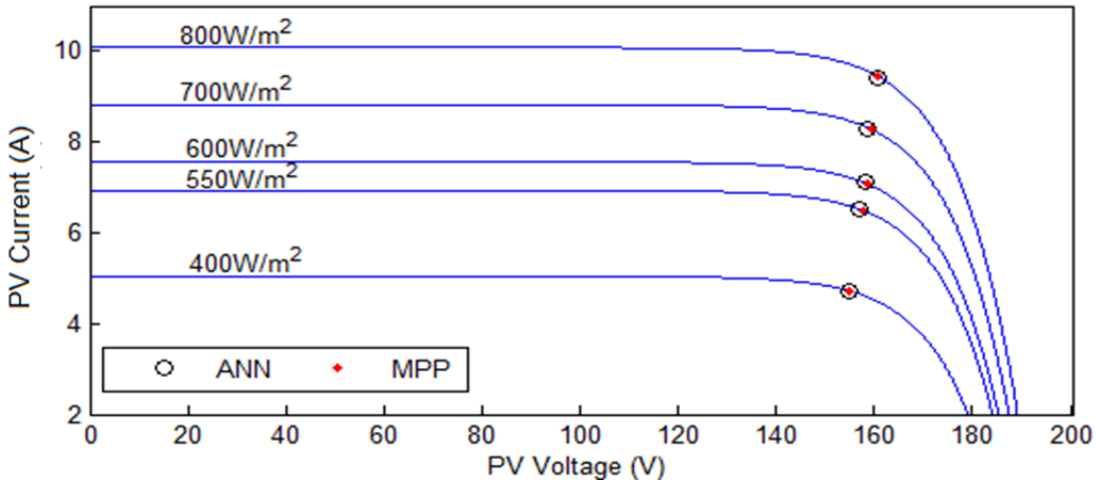

Fig. 7.58 The operating points of PV system using ANN MPPT controller on the *I-V* curves under different irradiation levels.

7.4.5 Comparison between MP&O, FLC and ANN MPPT techniques

The last four sections show the performance of the proposed MP&O, FLC and ANN MPPT techniques compared to the directly connected system under different solar irradiation levels. In this section, the comparison is carried out among the MP&O, FLC and ANN MPPT techniques in terms of dynamic response and efficiency. The comparison is performed by implementing the three MPPT controllers in the same PV water pumping system shown in Fig. 7.26 and under the same sunlight conditions. As explained in section 7.4, a sudden change in the solar radiation should be applied to the PV system to verify the functionality of the proposed MPPT techniques and to perform a good comparison between them. Therefore, the solar

irradiation was rapidly varied for each MPPT technique as displayed in Fig. 7.31. To better quantify performance of the proposed MPPT techniques, the optimum calculated results were used as a reference for the simulated results of MP&O, FLC and ANN MPPT techniques.

Fig. 7.59 to Fig. 7.63 show superimposed plots of the simulation result of the tested MPPT techniques under different solar radiation levels. The plots reveal that, the MPPT techniques show the same dynamic response to the change of solar radiation. Fig. 7.61 shows that, the output power of PV array varies as the irradiation level changes at the time intervals of 1s, 2s and 3s, and therefore result in a change in the maximum operating power point accordingly. These changes in the maximum operating power point must be detected by the MPPT controllers and the appropriate adjustment in the duty ratio made.

Fig. 7.62 shows the plot of the control signals of three MPPT techniques during the period of rapid change in the solar irradiation. The MPPT controllers start adjusting the duty ratio to reach the new MPP. Furthermore, the plot does not reveal any differences in terms of the dynamic response. The three techniques show the ability to quickly adjust to the rapid change in the irradiation level and avoid an associated deviation from the MPP.

The MP&O and ANN techniques produce almost identical duty ratio curve to the optimum calculated duty ratio, even though they use a different tracking approach However, the FLC MPPT technique shows a greater error than the MP&O and ANN MPPT techniques in comparison to the optimum calculated duty ratio. Furthermore, Fig. 7.59 and Fig. 7.60 clearly show that the PV current and voltage produced by FLC deviate slightly from the theoretically calculated results, especially at the levels of irradiation of 400 W/m^2, 600 W/m^2 and 700 W/m^2.

In general the three MPPT techniques show the ability to track the MPP and increase the performance of the PV system when the rapid change in the irradiation occurs. However, a comparison of the PV array output power plots achieved with the various MPPT techniques shown in Fig. 7.61 reveals that the MP&O MPPT method show a superior performance in tracking capability, since it yields slightly higher output power than the ANN and FLC MPPT techniques under randomly changing environmental conditions. Then the ANN MPPT technique comes after, since it produces an output power greater than that produced by the FLC MPPT technique.

A summary of the performance comparison between the directly connected system, MP&O, FLC, ANN MPPT, and theoretically expected result is shown in Table 7.5.

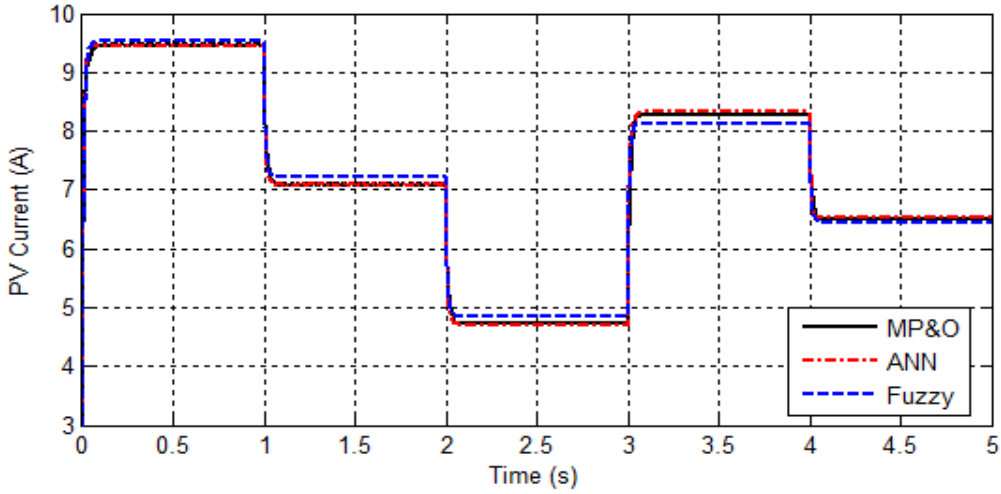

Fig. 7.59 PV output current: comparison between proposed MP&O MPPT, FLC MPPT and ANN MPPT.

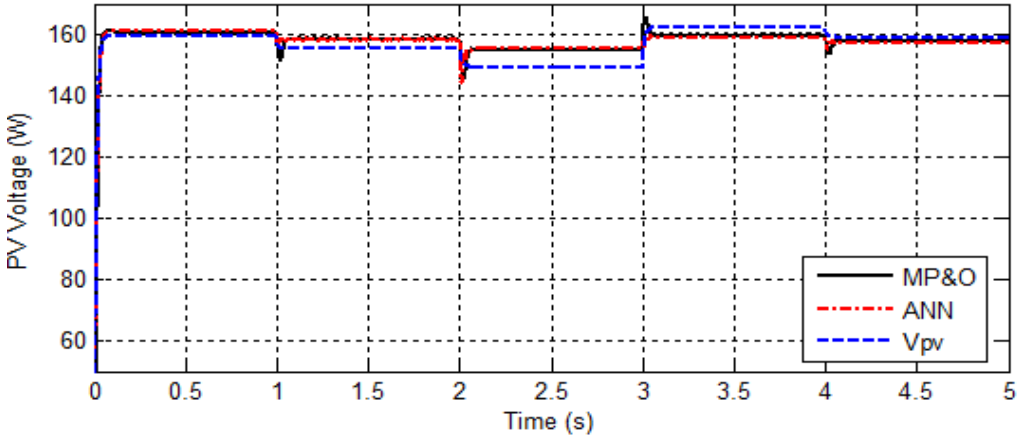

Fig. 7.60 PV output voltage: comparison between proposed MP&O MPPT, FLC MPPT and ANN MPPT.

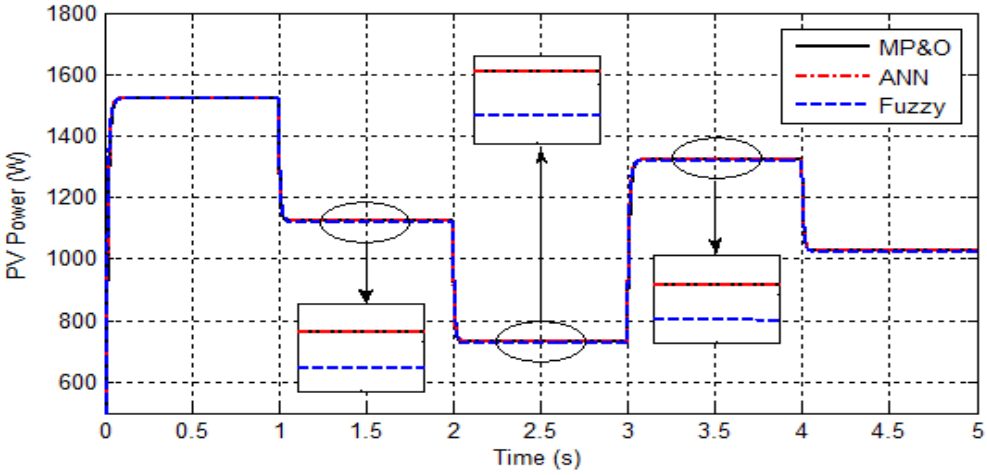

Fig. 7.61 PV output power: comparison between proposed MP&O MPPT, FLC MPPT and ANN MPPT.

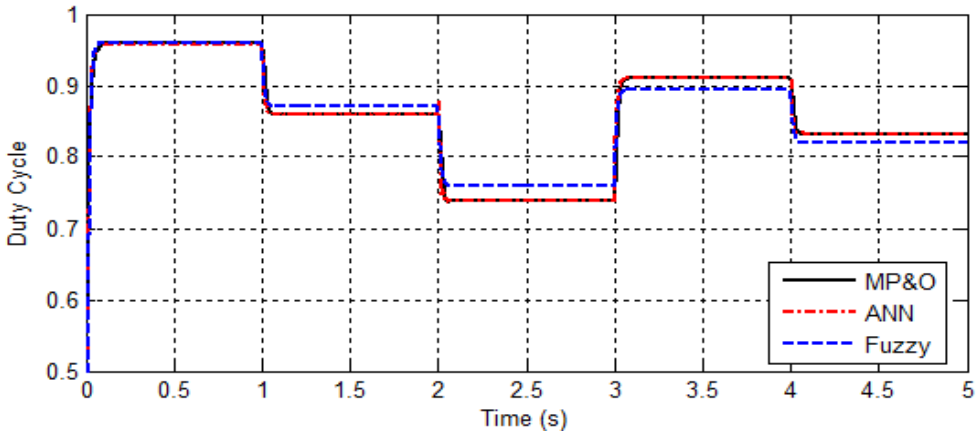

Fig. 7.62 Duty ratio waveform: comparison between proposed MP&O MPPT, FLC MPPT and ANN MPPT.

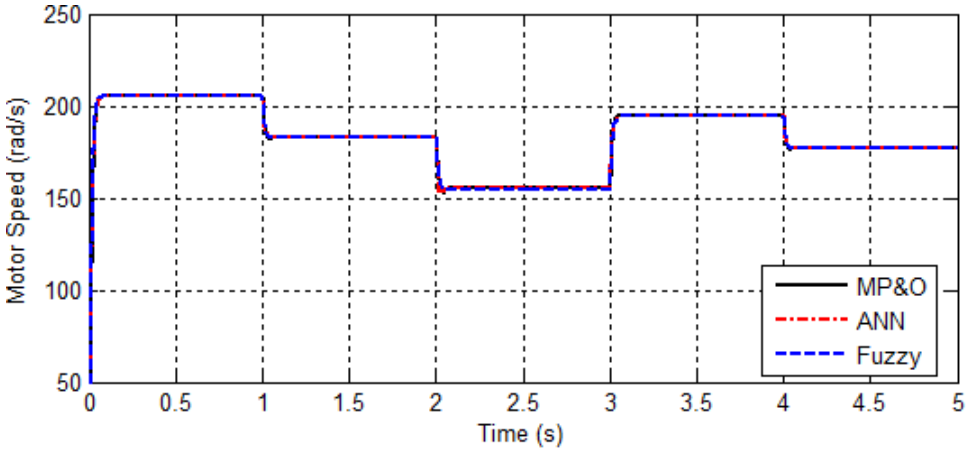

Fig. 7.63 Rotational speed: comparison between proposed MP&O MPPT, FLC MPPT and ANN MPPT.

Table 7.5 Tracking performance: a comparison between MPPT techniques, directly connected system without MPPT results.

Insolation	G (W/m^2)	800	600	400	700	550
Theory	P_{PV} (W)	1520.1	1123.4	732.0689	1321.3	1025
	I_{PV} (A)	9.5	7.1	4.7220	8.3	6.5
	V_{PV} (V)	160.7	158.4	155.035	159.7	157.7
	ω_m (rad/s)	205.704	183.491	155.602	195.132	177.186
	D	0.95762	0.86117	0.74027	0.91136	0.83377
Direct	P_{PV} (W)	1497	968.1	490.7	1236	839
	I_{PV} (A)	9.786	7.534	5.039	8.723	6.917
	V_{PV} (V)	152.9	128.5	97.39	141.7	121.3
	ω_m (rad/s)	204.5	173.4	132.9	190.3	164.1
	Efficiency η (%)	98.480	86.175	67.029	93.544	81.853
	Error %	1.52	13.8241	32.97	6.455	18.146
MP&O	P_{PV} (W)	1520.1	1123.3	732.03	1321.2	1024.9
	I_{PV} (A)	9.459	7.096	4.724	8.272	6.499
	V_{PV} (V)	160.704	158.300	154.959	159.719	157.701
	ω_m (rad/s)	205.2	183.2	155.3	194.9	176.8
	D	0.9596	0.8599	0.7394	0.9099	0.8316
	Efficiency η (%)	100	99.991	99.994	99.992	99.990
	Error %	0	0.0089	0.0053	0.0075	0.0097
Fuzzy	P_{PV} (W)	1519.5	1120	724.6	1318.8	1024.8
	I_{PV} (A)	9.533	7.207	4.86	8.13	6.443
	V_{PV} (V)	160.640	157.835	153.386	159.429	157.685
	ω_m (rad/s)	205.1	182.1	154.6	194.5	176.61
	D	0.9602	0.8702	0.7601	0.895	0.8202
	Efficiency η (%)	99.960	99.697	98.979	99.810	99.980
	Error %	0.0394	0.3026	1.0202	0.189	0.019
ANN	P_{PV} (W)	1520	1123.3	732.02	1321	1024.8
	I_{PV} (A)	9.449	7.112	4.703	8.321	6.524
	V_{PV} (V)	160.863	157.94	155.65	158.754	157.081
	ω_m (rad/s)	205.2	183.1	155.2	194.7	176.6
	D	0.9573	0.8606	0.7388	0.9108	0.8325
	Efficiency η (%)	99.993	99.991	99.993	99.977	99.980
	Error %	0.0066	0.0089	0.0066	0.022	0.019

Error calculation

The error indicates the absolute difference between the simulated maximum power and the theoretically calculated maximum power divided by the theoretically calculated maximum power as in the following equation:

$$Error = \frac{|P_{PV} - P_{max}|}{P_{max}} \times 100\% \quad (7.6)$$

Where P_{PV} is the simulated maximum power and P_{max} is the theoretically calculated maximum power.

7.4.6 Tracking efficiency of MPPT techniques

The tracking efficiency comparison process between the proposed MPPT techniques was performed in MATLAB/SIMULINK under rapidly changing irradiation.

Table 7.6 Tracking efficiency comparison between MPPT techniques and directly connected system.

Insolation	G (W/m^2)	800	600	400	700	550
Direct	Efficiency η (%)	98.48	86.17	67.029	93.544	81.85
	Total Efficiency η (%)	85.41				
MP&O	Efficiency η (%)	100	99.991	99.994	99.992	99.99
	Total Efficiency η (%)	99.99				
	Efficiency improvement by MP&O η (%)	1.52	13.821	32.965	6.448	18.14
	Total Efficiency improvement by MP&O η (%)	14.58				
Fuzzy	Efficiency η (%)	99.96	99.697	98.979	99.810	99.98
	Total Efficiency η (%)	99.68				
	Efficiency improvement by FLC η (%)	1.48	13.527	31.95	6.266	18.13
	Total Efficiency improvement by FLC η (%)	14.27				
ANN	Efficiency η (%)	99.993	99.991	99.993	99.977	99.98
	Total Efficiency η (%)	99.98				
	Efficiency improvement by ANN η (%)	1.513	13.821	32.964	6.433	18.13
	Total Efficiency improvement by ANN η (%)	14.57				

Table 7.6 presents a summary of the tracking efficiency of the proposed MPPT techniques with respect to the optimum calculated results and the tracking efficiency improvement in the proposed MPPT techniques with respect to the directly connected system. The three proposed MPPT methods present significant advantages over the directly connected systems under all irradiation levels. The total efficiency improvement achieved by MP&O is approximately 14.58% and the total efficiency improvement achieved by FLC and ANN is 14.27% and 14.57% respectively. Fig. 7.64 illustrates the total efficiency of the system controlled by the three MPPT techniques and the directly connected system with respect to the optimum calculated result. It is clear that the maximum efficiency gained was 99.99% when the system was controlled by MP&O; closely followed by ANN where the total efficiency gained by this technique was 99.98%, and the total efficiency gained by FLC was 99.68% which is the lowest efficiency among the three MPPT techniques. Furthermore, the bar chart shows that, the total efficiency of the directly connected system is poor: it was approximately 85.41%.

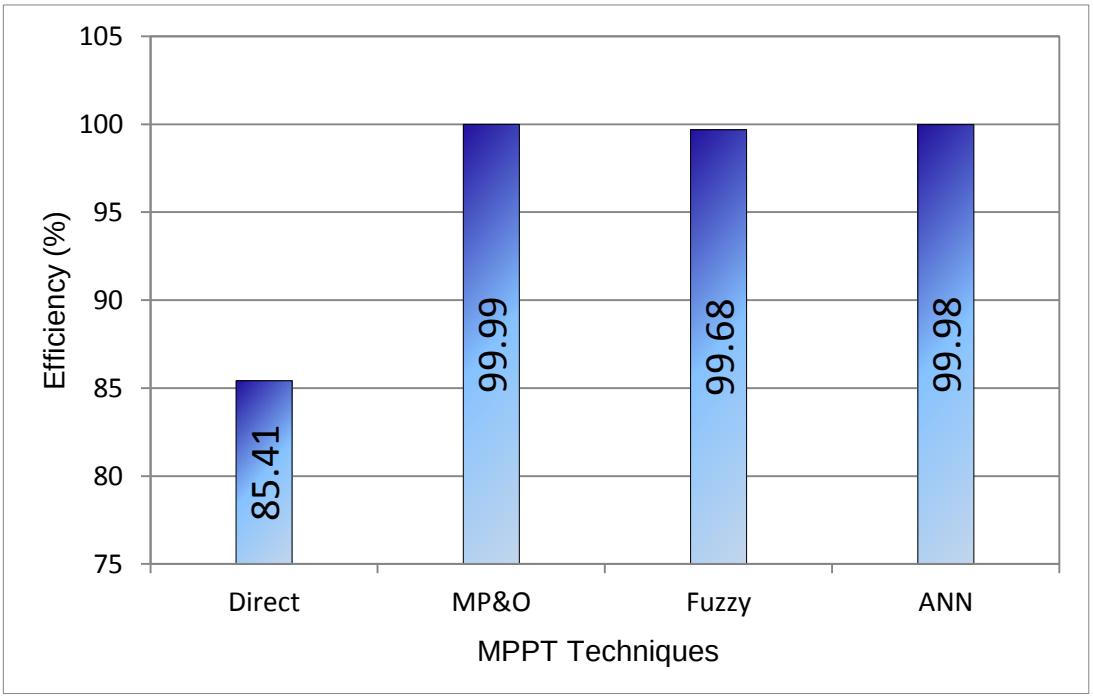

Fig. 7.64 Tracking efficiency: comparison between the proposed MPPT methods (MP&O, FLC and ANN).

7.5 Summary

This chapter provides the design and MATLAB simulation of the proposed PV water pumping system to test the performance of the proposed MPPT techniques and to verify their functionality. The system comprises of PV array, DC-DC buck converter, MPPT controller and DC motor load pump. Each of these components has simulated and masked in an individual subsystem so can be easily controlled and precisely monitored. Then, these subsystems are combined to form the complete system.

First, to verify the functionality of the proposed MP&O MPPT algorithm and compare its performance against the conventional P&O algorithm, they were implemented in MATLAB with a resistive load. The simulation was performed under rapidly varying solar irradiation levels starting at 1000 W/m^2 to be dropped down to 700 W/m^2 at the time of 1.0s, then increased to 900 W/m^2 at 2.0s, and then decreased back at 3.0s to reach 700 W/m^2 again. The results show that the MP&O has significant improvement compared with the P&O. The results proved that the MP&O has improved the tracking speed and has eliminated the oscillation around the MPP in steady state.

Second, the resistive load was replaced with a water pump load and the complete PV water pumping system was implemented in the MATLAB/SIMULINK to verify the performance of the proposed MPPT techniques: MP&O, FLC, ANN. To verify the functionality and benefits of the proposed MPPT techniques, the result of each MPPT technique was firstly compared to the result of directly coupled PV water pumping system without MPPT. Then a comparison was carried out between the proposed MPPT techniques to find the best performance and to quantify the most efficient one. The simulation was carried out under different levels of solar irradiation, and it was started at 800 W/m2 and then decreased to reach 600 W/m2 at the time of 1.0s, then further decreased at the time of 2.0s to reach 400 W/m2, then increased again to 700 W/m2 at the time of 3.0s, and then reduced to 550 W/m2 at 4.0s. The result shows that the directly coupled PV water pumping system without MPPT has poor efficiency of 85.41% because of the mismatching between the PV array and the DC pump motor load. However, the system with the proposed MPPT can utilize more than 99% of the PV capacity. The three proposed MPPT techniques can increase the overall efficiency of the system by more than 14%.

The other set of simulations which provides a performance comparison of the three proposed MPPT was carried out at the same irradiation levels. The best results show that PV water pumping shows higher overall efficiency with the three proposed MPPT techniques. However, the highest system efficiency obtained with the MP&O technique which was 99.99% then the ANN technique and then FLC with the overall system efficiency of 99.98% and 99.68% respectively.

CHAPTER 8 - CONCLUSION AND FUTURE WORK

8.1 Conclusion

In this research, a stand-alone photovoltaic water pumping system is presented to supply the water in remote location areas with a clean and sustainable source of energy. The main focuses of this research was how to improve the total system efficiency by implementing an efficient MPPT techniques to transfer the maximum available power to the load especially under rapidly changing atmospheric conditions.

The thesis reviewed and discussed some existing MPPT controller methods, including constant voltage method, P&O, INC, fractional short-circuit current, fractional open-circuit voltage, etc., and showed their ability to track the MPP under rapidly changing weather conditions. It illustrated the advantages and disadvantages of each individual MPPT technique tracking performance. Based on the outcome of this evaluation, three proposed MPPT techniques were identified which substantially address the disadvantages that most MPPT techniques suffer from.

The three more efficient MPPT controllers proposed were analysed and developed in more depth using new system simulations to clearly show improvements. The first proposed technique is a modified perturb and observe MP&O technique. The P&O MPPT method is very simple in comparison with other techniques, which makes it the easiest to design and implement. However, a P&O method with fixed perturbation step makes it difficult to achieve both a fast response and optimal steady-state operating conditions when atmospheric conditions are changeable. An adaptive P&O MPPT was developed using fuzzy logic control (FLC) to continually adjust the step-size according to the change of atmospheric conditions. The MP&O with variable step-size was shown to have a faster dynamic response and virtually eliminates the steady state oscillation around the MPP thereby; it improves the MPPT efficiency of the PV system. The design and results of the developed MP&O MPPT technique were presented and explained. Relatively simple operation of the FLC was achieved using as inputs the change in the PV power and current and the variable step-size of the P&O as the output.

The two other new developed MPPT methods, fuzzy logic controller FLC MPPT and artificial neural network ANN, were also presented in this thesis. Both the FLC and ANN were implemented and evaluated by simulation in the PV water pumping system MATLAB model. The design process for the operating concept of each controller was presented and explained in detail. Both the FLC and ANN MPPT techniques were shown to have relatively simple configurations comprising two input variables and one output: for the input variables they use the variation of the PV array power and the variation of the DC motor speed; and they produce one output signal, which is the duty ratio for the buck chopper. Moreover, an off-line ANN, trained using the Levenberg-Marquardt algorithm, was utilized for on-line estimation of duty ratio for a feedforward loop. Calculated data was used for the off-line training of the ANN, and the net was trained using MATLAB software. The accuracy of the estimation was evaluated from a graph of convergence error.

The simulation results were presented in order to show the benefits of MPPT and evaluate the performance and functionality of the proposed MPPT techniques. The simulations were performed using MATLAB/SIMULINK. A model of the complete PV systems was presented and discussed along with how all of the masked components have been combined to form this system. A more detailed SIMULINK model of each component was also presented, starting with the PV solar panels, buck converter, DC load and MPPT controllers, and then each component masked within a subsystem.

The simulation results were divided into two parts: in the first part the PV system is feeding a resistive load to evaluate and test the performance of the modified P&O algorithm against the more conventional P&O algorithm. The simulation results clearly showed that, the modified P&O has the ability to improve both the steady-state and dynamic performance of photovoltaic power generator systems. Performance was assessed with rapidly changing solar irradiation conditions. The output results of the MP&O were compared to the output results of the P&O with two different step-size values. The comparison figures were presented and the efficiency improvement in both steady-state and transient responses were also summarized in a table. The simulation results clearly showed that, the modified P&O

method has the ability to improve both the steady-state and dynamic performance of tracking the MPP and thereby increasing the total efficiency of the PV system.

In the second part, the resistive load was replaced with a DC water pump to validate the performance and functionality of the proposed MP&O, FLC and ANN MPPT methods under changing irradiation levels. The proposed techniques were firstly compared to the directly connected PV water pumping system without MPPT to verify the functionality and benefits of the proposed MPPT techniques. The simulations also make comparisons amongst the proposed techniques with optimum calculated results to evaluate the total efficiency of the PV water pumping system gained by using each MPPT technique and to quantify the most efficient technique under rapidly changing weather conditions.

The comparison figures were presented with a table summarising the performance of the proposed MPPT techniques and the efficiency improvement of the PV system gained by each technique. The simulation results showed that the directly connected PV water pumping system without MPPT has poor efficiency due to the mismatching between the PV array and the DC pump motor load. Whereas, the system with the three proposed MPPT techniques utilizes more than 99% of the available PV array energy. The proposed MPPT techniques were able to track the MPP deliver maximum power to the load with high efficiency under the dynamic and steady-state conditions. The results also confirm that the proposed MPPT methods have the potential to significantly increase the total efficiency of the PV water pumping system by more than 14.2% compared to the system without MPPT. In the last step of simulation evaluation, the performance of the three proposed MP&O, FLC and ANN MPPT methods were compared under rabidly changing irradiation levels. The results validate that the all of three proposed MPPT techniques can significantly increase the efficiency of energy production from PV and the performance of the PV water pumping system. The highest system efficiency was shown to be achieved by the MP&O, followed by the ANN, and then the FLC method with values of 99.99%, 99.98% and 99.68%, respectively.

8.2 Contributions

The major contributions of this thesis are:

1) The proposed modified perturb and observe (MP&O) MPPT method with a variable step-size. The conventional P&O was modified to overcome the drawbacks in the conventional P&O MPPT algorithm. This is done by combining the conventional P&O with the fuzzy logic control FLC. The FLC uses the change in the PV array power ΔP_{PV} and the change in the PV array current ΔI_{PV} as the input variables and outputs the step-size ΔS for the P&O algorithm. When a step change in the solar irradiation or temperature occurs, the FLC automatically tunes the step-size according to the change in the operating power. If the operating point is far from the MPP, the FLC increases the step-size to enable fast tracking of the MPP. A comparison with conventional P&O MPPT algorithm showed that the proposed MP&O algorithm has improved both the steady-state and dynamic performance of the photovoltaic power generator systems.

2) The proposed two-input Fuzzy logic controller for the MPPT of PV water pumping system. The PV array output power change, ΔP_{pv}, and the change in rotation speed of the pump, $\Delta \omega_m$, are used as inputs for this controller, which in turn adjusts the duty-ratio, ΔD, of the buck converter to track the MPP of the system. The FLC was proposed by making use of the relation between the PV array output power and the rotational speed to adjust the duty ratio of the buck converter which adapts online the PV array output power to maximize the rotational speed. At the time when output power of the PV array is at a maximum, the hydraulic power, $P_P = K_T \omega_m^3$, is at a maximum. Consequently, the rotational speed, ω_m, is at a maximum at the MPP. By maximizing the rotational speed, the daily volume of water discharge by the centrifugal water pump will be increased.

3) The proposed artificial neural network ANN control based MPPT of PV water pumping system. The controller adjusts the duty-ratio of the buck converter online to track the MPP of the system by using the PV array output power, P_{pv}, and the rotation speed of the pump, ω_m, as input variables.

4) The comparison carried out, using a representative water pumping system simulation model under the same atmospheric conditions, between the three proposed MPPT techniques MP&O, FLC and ANN. The results for three MPPT techniques quantifying performance under different solar insolation levels. Identification and quantification of the extent of the MP&O systems superior performance in comparison with the FLC and ANN techniques.

8.3 Future work

An adaptive Neuro-Fuzzy ANFIS MPPT controller, when implemented with the PV water pumping system, may allow a further improvement in overall efficiency under changing PV array conditions. The whole system could also be conducted and simulated in MATLAB/SIMULINK first to facilitate the system analysis. The ANFIS should be tested with different irradiation and temperature levels to verify and assess its functionality and performance compared to the proposed MPPT techniques.

In the current PV system, the buck converter is used as an interface to enable the MPPT process. Future research could investigate some other converters such as boost, cuk and buck-boost along with the proposed MPPT techniques to improve flexibility in the choice and configuration of PV array connection.

In this work, simulation models were developed and used to compare the performance of the proposed MPPT techniques. However, practical hardware tests at a representative power level and under the typical climatic conditions of an application need to be conducted to verify the simulation results. The simulation results achieved in this work will hopefully incentivise future investigations involving building prototype models to test experimentally the developed MPPT techniques for the PV water pumping system.

References

[1] UNEP, "Water Policy and Strategy viewed on," *www.unep.org/dpdl/water/* September 2015.

[2] UNESCO, "The UN World Water Development Report (2003)," *(viewed on www.unesco.org/water/wwap/wwdr/, September 2015).*

[3] UNESCO, "The UN World Water Development Report (2014)," *(viewed on www.unesco.org/water/wwap/wwdr/, September 2015).*

[4] A. Z. Sahin and S. Rehman, "Economical Feasibility of Utilizing Photovoltaics for Water Pumping in Saudi Arabia," *International Journal of Photoenergy,* vol. 2012, p. 9, 2012.

[5] A. Oi, "Design and simulation of photovoltaic water pumping system," Master Thesis, California Polytechnic State University, 2005.

[6] M. L. a. C. Greenwood, "Green investing: Towards a clean energy infrastructure," *World Economic Forum USA Inc,* January 2009.

[7] M. Thomson, "Reverse-osmosis desalination of seawater powered by photovoltaics without batteries," Doctoral Thesis, Loughborough University, 2003.

[8] E. Koutroulis, *et al.,* "Development of a microcontroller-based, photovoltaic maximum power point tracking control system," *Power Electronics, IEEE Transactions on,* vol. 16, pp. 46-54, 2001.

[9] T. M. Pavlović, *et al.*, "A review of concentrating solar power plants in the world and their potential use in Serbia," *Renewable and Sustainable Energy Reviews,* vol. 16, pp. 3891-3902, 2012.

[10] V. V. Tyagi, *et al.*, "Progress in solar PV technology: Research and achievement," *Renewable and Sustainable Energy Reviews,* vol. 20, pp. 443-461, 2013.

[11] F. R. Pazheri, *et al.*, "A review on global renewable electricity scenario," *Renewable and Sustainable Energy Reviews,* vol. 31, pp. 835-845, 2014.

[12] J. S. Ramos and H. M. Ramos, "Solar powered pumps to supply water for rural or isolated zones: A case study," *Energy for Sustainable Development,* vol. 13, pp. 151-158, 2009.

[13] P. Purohit and A. Michaelowa, "CDM potential of SPV pumps in India," *Renewable and Sustainable Energy Reviews,* vol. 12, pp. 181-199, 2008.

[14] D. P. Kaundinya, *et al.*, "Grid-connected versus stand-alone energy systems for decentralized power—A review of literature," *Renewable and Sustainable Energy Reviews,* vol. 13, pp. 2041-2050, 2009.

[15] M. A. Eltawil and Z. Zhao, "Grid-connected photovoltaic power systems: Technical and potential problems—A review," *Renewable and Sustainable Energy Reviews,* vol. 14, pp. 112-129, 2010.

[16] N. Argaw, "Renewable energy water pumping systems handbook," *Denver, Colorado, USA: National Renewable Energy Laboratory (NREL),* 2004.

[17] B. Eker, "Solar powered water pumping systems," *Trakia Journal of Sciences,* vol. 3, pp. 7-11, 2005.

[18] G. M. Masters, *Renewable and efficient electric power systems*: Wiley-Interscience, 2005.

[19] R. Illanes, *et al.*, "Comparative study by simulation of photovoltaic pumping systems with stationary and polar tracking arrays," *Progress in Photovoltaics: Research and Applications,* vol. 11, pp. 453-465, 2003.

[20] M. Dursun and S. Ozden, "Application of Solar Powered Automatic Water Pumping in Turkey," in *International Conference on Electrical Energy and Networks (ICEEN)*, 2011, pp. 52-57.

[21] J. Appelbaum, "Starting and steady-state characteristics of DC motors powered by solar cell generators," *Energy Conversion, IEEE Transactions on*, pp. 17-25, 1986.

[22] V. Badescu, "Dynamic model of a complex system including PV cells, electric battery, electrical motor and water pump," *Energy,* vol. 28, pp. 1165-1181, 2003.

[23] M. Kolhe, *et al.*, "Determination of magnetic field constant of DC permanent magnet motor powered by photovoltaic for maximum mechanical energy output," *Renewable Energy,* vol. 21, pp. 563-571, 2000.

[24] M. Kashyap, *et al.*, "Solar Powered PMDC Motor Drive," in *Proceedings of the Conference on Advances in Communication and Control Systems-2013*, 2013.

[25] H. Metwally and W. R. Anis, "Dynamic performance of directly coupled photovoltaic water pumping system using DC shunt motor," *Energy conversion and management,* vol. 37, pp. 1407-1416, 1996.

[26] P. Koner, "Optimization techniques for a photovoltaic water pumping system," *Renewable Energy,* vol. 6, pp. 53-62, 1995.

[27] K. Benlarbi, *et al.*, "A fuzzy global efficiency optimization of a photovoltaic water pumping system," *Solar energy,* vol. 77, pp. 203-216, 2004.

[28] S. S. Chandel, *et al.*, "Review of solar photovoltaic water pumping system technology for irrigation and community drinking water supplies," *Renewable and Sustainable Energy Reviews,* vol. 49, pp. 1084-1099, 2015.

[29] A. O. Omole, "Analysis, modeling and simulation of optimal power tracking of multiple-modules of paralleled solar cell systems," Master of Science Thesis, The Florida State University College of Engineering, 2006.

[30] K. H. Hussein, *et al.*, "Maximum photovoltaic power tracking: an algorithm for rapidly changing atmospheric conditions," *Generation, Transmission and Distribution, IEE Proceedings-,* vol. 142, pp. 59-64, 1995.

[31] L. Fangrui, *et al.*, "Comparison of P&O and hill climbing MPPT methods for grid-connected PV converter," in *Industrial Electronics and Applications, 2008. ICIEA 2008. 3rd IEEE Conference on*, 2008, pp. 804-807.

[32] T. Noguchi, *et al.*, "Short-current pulse-based maximum-power-point tracking method for multiple photovoltaic-and-converter module system," *Industrial Electronics, IEEE Transactions on,* vol. 49, pp. 217-223, 2002.

[33] J. Ahmad, "A fractional open circuit voltage based maximum power point tracker for photovoltaic arrays," in *Software Technology and Engineering (ICSTE), 2010 2nd International Conference on,* 2010, pp. V1-247-V1-250.

[34] T. Esram and P. L. Chapman, "Comparison of Photovoltaic Array Maximum Power Point Tracking Techniques," *Energy Conversion, IEEE Transactions on,* vol. 22, pp. 439-449, 2007.

[35] V. Salas, *et al.*, "Review of the maximum power point tracking algorithms for stand-alone photovoltaic systems," *Solar Energy Materials and Solar Cells,* vol. 90, pp. 1555-1578, 2006.

[36] T. Hiyama, *et al.*, "Identification of optimal operating point of PV modules using neural network for real time maximum power tracking control," *Energy Conversion, IEEE Transactions on,* vol. 10, pp. 360-367, 1995.

[37] R. M. Hilloowala and A. M. Sharaf, "A rule-based fuzzy logic controller for a PWM inverter in a stand alone wind energy conversion scheme," *Industry Applications, IEEE Transactions on,* vol. 32, pp. 57-65, 1996.

[38] R. Faranda and S. Leva, "Energy comparison of MPPT techniques for PV Systems," *WSEAS transactions on power systems,* vol. 3, pp. 446-455, 2008.

[39] L. Piegari and R. Rizzo, "Adaptive perturb and observe algorithm for photovoltaic maximum power point tracking," *Renewable Power Generation, IET,* vol. 4, pp. 317-328, 2010.

[40] N. Khaehintung, *et al.*, "FPGA implementation of MPPT using variable step-size P&O algorithm for PV applications," in *Communications and*

Information Technologies, 2006. ISCIT'06. International Symposium on, 2006, pp. 212-215.

[41] N. Fermia, *et al.*, "Predictive & adaptive MPPT perturb and observe method," *Aerospace and Electronic Systems, IEEE Transactions on*, vol. 43, pp. 934-950, 2007.

[42] H. Wang, *et al.*, "Adaptive maximum power point tracker in photovoltaic grid-connected system," in *Power Electronics for Distributed Generation Systems (PEDG), 2010 2nd IEEE International Symposium on*, 2010, pp. 374-377.

[43] D. Sera, *et al.*, "Optimized maximum power point tracker for fast changing environmental conditions," in *Industrial Electronics, 2008. ISIE 2008. IEEE International Symposium on*, 2008, pp. 2401-2407.

[44] W. Xiao and W. G. Dunford, "A modified adaptive hill climbing MPPT method for photovoltaic power systems," in *Power Electronics Specialists Conference, 2004. PESC 04. 2004 IEEE 35th Annual*, 2004, pp. 1957-1963.

[45] J. Xu, *et al.*, "ANN based on IncCond Algorithm for MPP Tracker," in *Bio-Inspired Computing: Theories and Applications (BIC-TA), 2011 Sixth International Conference on*, 2011, pp. 129-134.

[46] J. M. Enrique, *et al.*, "A reliable, fast and low cost maximum power point tracker for photovoltaic applications," *Solar energy*, vol. 84, pp. 79-89, 2010.

[47] C. Jaen, *et al.*, "Overview of maximum power point tracking control techniques used in photovoltaic systems," 2008, pp. 1099-1102.

[48] V. Salas, *et al.*, "Review of the maximum power point tracking algorithms for stand-alone photovoltaic systems," *Solar Energy Materials and Solar Cells*, vol. 90, pp. 1555-1578, 2006.

[49] B. Subudhi and R. Pradhan, "A comparative study on maximum power point tracking techniques for photovoltaic power systems," *Sustainable Energy, IEEE Transactions on*, vol. 4, pp. 89-98, 2013.

[50] P. Bhatnagar and R. Nema, "Maximum power point tracking control techniques: State-of-the-art in photovoltaic applications," *Renewable and Sustainable Energy Reviews*, vol. 23, pp. 224-241, 2013.

[51] M. A. Eltawil and Z. Zhao, "MPPT techniques for photovoltaic applications," *Renewable and Sustainable Energy Reviews*, vol. 25, pp. 793-813, 2013.

[52] X. Weidong and W. G. Dunford, "A modified adaptive hill climbing MPPT method for photovoltaic power systems," in *Power Electronics Specialists Conference, 2004. PESC 04. 2004 IEEE 35th Annual*, 2004, pp. 1957-1963 Vol.3.

[53] D. P. Hohm and M. E. Ropp, "Comparative study of maximum power point tracking algorithms using an experimental, programmable, maximum power point tracking test bed," in *Photovoltaic Specialists Conference, 2000. Conference Record of the Twenty-Eighth IEEE,* 2000, pp. 1699-1702.

[54] T. Tafticht, *et al.*, "A new MPPT method for photovoltaic systems used for hydrogen production," *COMPEL: The International Journal for Computation and Mathematics in Electrical and Electronic Engineering,* vol. 26, pp. 62-74, 2007.

[55] T. Tafticht, *et al.*, "An improved maximum power point tracking method for photovoltaic systems," *Renewable Energy,* vol. 33, pp. 1508-1516, 2008.

[56] N. Onat, "Recent developments in maximum power point tracking technologies for photovoltaic systems," *International Journal of Photoenergy,* vol. 2010, 2010.

[57] W. Xiao, "A modified adaptive hill climbing maximum power point tracking (MPPT) control method for photovoltaic power systems," Master Thesis The University of British Columbia, 2003.

[58] H. Knopf, "Analysis, Simulation, and evaluation of maximum power point tracking (MPPT) methods for a solar powered vehicle," Master Thesis, Portland State University, 1999.

[59] H. Yongji and L. Deheng, "A new method for optimal output of a solar cell array," in *Industrial Electronics, 1992., Proceedings of the IEEE International Symposium on,* 1992, pp. 456-459.

[60] C. Hua and C. Shen, "Comparative study of peak power tracking techniques for solar storage system," in *Applied Power Electronics Conference and Exposition, 1998. APEC'98. Conference Proceedings 1998., Thirteenth Annual,* 1998, pp. 679-685.

[61] H. Chihchiang and S. Chihming, "Study of maximum power tracking techniques and control of DC/DC converters for photovoltaic power system," in *Power Electronics Specialists Conference, 1998. PESC 98 Record. 29th Annual IEEE,* 1998, pp. 86-93 vol.1.

[62] T. Chee Wei, *et al.*, "Analysis of perturb and observe maximum power point tracking algorithm for photovoltaic applications," in *Power and Energy Conference, 2008. PECon 2008. IEEE 2nd International,* 2008, pp. 237-242.

[63] C. Dorofte, *et al.*, "A combined two-method MPPT control scheme for grid-connected photovoltaic systems," in *Power Electronics and Applications, 2005 European Conference on,* 2005, pp. 10 pp.-P.10.

[64] D. Sera, *et al.*, "Improved MPPT method for rapidly changing environmental conditions," in *Industrial Electronics, 2006 IEEE International Symposium on,* 2006, pp. 1420-1425.

[65] N. Femia, *et al.*, "Optimization of perturb and observe maximum power point tracking method," *Power Electronics, IEEE Transactions on,* vol. 20, pp. 963-973, 2005.

[66] A. Giustiniani, *et al.*, "Low-frequency current oscillations and maximum power point tracking in grid-connected fuel-cell-based systems," *Industrial Electronics, IEEE Transactions on,* vol. 57, pp. 2042-2053, 2010.

[67] C. Liu, *et al.*, "Advanced algorithm for MPPT control of photovoltaic systems," in *Canadian solar buildings conference, Montreal*, 2004, pp. 20-24.

[68] A. Yafaoui, *et al.*, "Implementation of maximum power point tracking algorithm for residential photovoltaic systems," in *2nd Canadian solar buildings conference Calgary*, 2007, pp. 10-14.

[69] G. J. Yu, *et al.*, "A novel two-mode MPPT control algorithm based on comparative study of existing algorithms," in *Photovoltaic Specialists Conference, 2002. Conference Record of the Twenty-Ninth IEEE*, 2002, pp. 1531-1534.

[70] O. Wasynezuk, "Dynamic Behavior of a Class of Photovoltaic Power Systems," *Power Apparatus and Systems, IEEE Transactions on,* vol. PAS-102, pp. 3031-3037, 1983.

[71] K. Kobayashi, *et al.*, "A study on a two stage maximum power point tracking control of a photovoltaic system under partially shaded insolation conditions," in *Power Engineering Society General Meeting, 2003, IEEE*, 2003, p. 2617 Vol. 4.

[72] S. Yuvarajan and X. Shanguang, "Photo-voltaic power converter with a simple maximum-power-point-tracker," in *Circuits and Systems, 2003. ISCAS '03. Proceedings of the 2003 International Symposium on*, 2003, pp. III-399-III-402 vol.3.

[73] M. Abou El Ela and J. A. Roger, "Optimization of the function of a photovoltaic array using a feedback control system," *Solar Cells,* vol. 13, pp. 107-119, 1984.

[74] M. A. S. Masoum, *et al.*, "Theoretical and experimental analyses of photovoltaic systems with voltageand current-based maximum power-point tracking," *Energy Conversion, IEEE Transactions on,* vol. 17, pp. 514-522, 2002.

[75] M. A. S. Masoum and H. Dehbonei, "Design, construction and testing of a voltage-based maximum power point tracker (VMPPT) for small satellite power supply," 1999.

[76] G. W. Hart, *et al.*, "Experimental tests of open-loop maximum-power-point tracking techniques for photovoltaic arrays," *Solar Cells,* vol. 13, pp. 185-195, 1984.

[77] Z. M. Salameh, *et al.*, "Step-down maximum power point tracker for photovoltaic systems," *Solar Energy,* vol. 46, pp. 279-282, 1991.

[78] D. Hohm and M. E. Ropp, "Comparative study of maximum power point tracking algorithms," *Progress in Photovoltaics: Research and Applications,* vol. 11, pp. 47-62, 2003.

[79] C. Cabal, *et al.*, "Adaptive digital MPPT control for photovoltaic applications," in *Industrial Electronics, 2007. ISIE 2007. IEEE International Symposium on*, 2007, pp. 2414-2419.

[80] X. Liu and L. A. Lopes, "An improved perturbation and observation maximum power point tracking algorithm for PV arrays," in *Power Electronics Specialists Conference, 2004. PESC 04. 2004 IEEE 35th Annual*, 2004, pp. 2005-2010.

[81] S. T. Buddha, "Topology Reconfiguration To Improve The Photovoltaic (PV) Array Performance," Master Thesis, Arizona State University, 2011.

[82] B. Tull, "Photovoltaic Cells: Science and Materials," 2004 http://www.molchem. science.ru.nl/rowan/Coll/caput-college/PhotovoltaicCells.pdf

[83] G. M. Masters, "Frontmatter," in *Renewable and Efficient Electric Power Systems*, ed: John Wiley & Sons, Inc., 2005, pp. i-xx.

[84] L. Castaner, *et al.*, *Modelling photovoltaic systems using PSpice*: Wiley Online Library, 2002.

[85] M. G. Villalva, *et al.*, "Comprehensive Approach to Modeling and Simulation of Photovoltaic Arrays," *Power Electronics, IEEE Transactions on,* vol. 24, pp. 1198-1208, 2009.

[86] T. Huan-Liang, "Insolation-oriented model of photovoltaic module using Matlab/Simulink," *Solar Energy,* vol. 84, pp. 1318-1326, 2010.

[87] G. Walker, "Evaluating MPPT converter topologies using a MATLAB PV model," *Journal of Electrical & Electronics Engineering, Australia,* vol. 21, pp. 49-56, 2001.

[88] E. M. Natsheh, *et al.*, "Modeling and control for smart grid integration of solar/wind energy conversion system," in *Innovative Smart Grid Technologies (ISGT Europe), 2011 2nd IEEE PES International Conference and Exhibition on*, 2011, pp. 1-8.

[89] S. R. Wenham, *Applied photovoltaics*: Earthscan/James & James, 2007.

[90] S. R. Wenham, *Applied photovoltaics*: Routledge, 2011.

[91] C. Wang, "Modeling and control of hybrid wind/photovoltaic/fuel cell distributed generation systems," 2006.

[92] G. Walker, "Evaluating MPPT converter topologies using a MATLAB PV model," *Journal of Electrical & Electronics Engineering,* vol. 21, pp. 49-56, 2001.

[93] T. Tafticht, *et al.*, "An improved maximum power point tracking method for photovoltaic systems," *Renewable Energy,* vol. 33, pp. 1508-1516, 2008.

[94] R. C. Neville, *Solar energy conversion: the solar cell*: Elsevier Science, 1995.

[95] Krismadinata, *et al.*, "Photovoltaic Module Modeling using Simulink/Matlab," *Procedia Environmental Sciences,* vol. 17, pp. 537-546, 2013.

[96] C. M. F. Santos, "Optimised Photovoltaic Solar Charger With Voltage Maximum Power Point Tracking," Master Thesis, Universidade Técnica de Lisboa, 2008.

[97] Y. T. Tan, "Impact on the power system with a large penetration of photovoltaic generation," PhD, Manchester, 2004.

[98] N. Mohan and T. M. Undeland, *Power electronics: converters, applications, and design*: Wiley-India, 2007.

[99] M. H. Rashid, *Power Electronics - Circuits, Devices, and Applications 3rd Edition Pearson Education*: Academic Pr, 2004.

[100] T. L. Skvarenina, *The power electronics handbook*: CRC, 2002.

[101] S. Kasat, "Analysis, design and modeling of DC-DC converter using simulink," Oklahoma State University, 2004.

[102] H. Sira-Ramirez and R. Silva-Ortigoza, *Control Design Techniques in Power Electronics Devices, Power Systems Series*: Springer-Verlag London, 2006.

[103] R. F. Coelho, *et al.*, "A study of the basic DC-DC converters applied in maximum power point tracking," in *Power Electronics Conference, 2009. COBEP '09. Brazilian*, 2009, pp. 673-678.

[104] R. F. Coelho, *et al.*, "A simplified analysis of DC-DC converters applied as maximum power point tracker in photovoltaic systems," in *Power Electronics for Distributed Generation Systems (PEDG), 2010 2nd IEEE International Symposium on*, 2010, pp. 29-34.

[105] E. Duran, *et al.*, "A New Application of the Buck-Boost-Derived Converters to Obtain the I-V Curve of Photovoltaic Modules," in *Power Electronics Specialists Conference, 2007. PESC 2007. IEEE*, 2007, pp. 413-417.

[106] E. Duran, *et al.*, "Comparative analysis of buck-boost converters used to obtain I-V characteristic curves of photovoltaic modules," in *Power Electronics Specialists Conference, 2008. PESC 2008. IEEE*, 2008, pp. 2036-2042.

[107] J. M. Enrique, *et al.*, "Theoretical assessment of the maximum power point tracking efficiency of photovoltaic facilities with different converter topologies," *Solar Energy*, vol. 81, pp. 31-38, 2007.

[108] E. Duran, *et al.*, "Comparative analysis of buck-boost converters used to obtain I–V characteristic curves of photovoltaic modules," in *Power Electronics Specialists Conference, 2008. PESC 2008. IEEE*, 2008, pp. 2036-2042.

[109] F. Mocci and M. Tosi, "Comparison of power converter technologies in photovoltaic applications," in *Electrotechnical Conference, 1989. Proceedings.'Integrating Research, Industry and Education in Energy and Communication Engineering', MELECON'89., Mediterranean*, 1989, pp. 11-15.

[110] R. Krishnan, *Electric motor drives: modeling, analysis, and control* vol. 626: Prentice Hall Upper Saddle River, NJ, 2001.

[111] J. Gonzalez-Llorente, *et al.*, "Analyzing the optimal matching of dc motors to photovoltaic modules via dc-dc converters," in *Applied Power Electronics Conference and Exposition (APEC), 2010 Twenty-Fifth Annual IEEE*, 2010, pp. 1062-1068.

[112] W. R. Anis and H. M. B. Metwally, "Dynamic performance of a directly coupled PV pumping system," *Solar energy*, vol. 53, pp. 369-377, 1994.

[113] A. Ghoneim, "Design optimization of photovoltaic powered water pumping systems," *Energy conversion and management*, vol. 47, pp. 1449-1463, 2006.

[114] M. veerachary, *et al.*, "Feedforward maximum power point tracking of PV systems using fuzzy controller," *Aerospace and Electronic Systems, IEEE Transactions on*, vol. 38, pp. 969-981, 2002.

[115] L. A. Zadeh, "A fuzzy-set-theoretic interpretation of linguistic hedges," *J. Cybern*, vol. 2, pp. 4-34, 1972.

[116] L. A. Zadeh, "Outline of a new approach to the analysis of complex systems and decision processes," *Systems, Man and Cybernetics, IEEE Transactions on*, pp. 28-44, 1973.

[117] E. H. Mamdani and S. Assilian, "An experiment in linguistic synthesis with a fuzzy logic controller," *International journal of man-machine studies,* vol. 7, pp. 1-13, 1975.

[118] L. P. Holmblad and J.-J. Østergaard, *Control of a cement kiln by fuzzy logic*: Smidth, 1982.

[119] Y. Bai and D. Wang, "Fundamentals of Fuzzy Logic Control—Fuzzy Sets, Fuzzy Rules and Defuzzifications," in *Advanced Fuzzy Logic Technologies in Industrial Applications,* ed: Springer, 2006, pp. 17-36.

[120] R. J. Machado and A. Freitas da Rocha, "A hybrid architecture for fuzzy connectionist expert systems," in *Hybrid architectures for intelligent systems,* 1992, pp. 135-152.

[121] Y. Bai, *et al.*, *Advanced fuzzy logic technologies in industrial applications*: Springer, 2007.

[122] M. Mobaied, "Fuzzy Logic Speed Controllers Using FPGA Technique for Three-Phase Induction Motor Drives," Master Thesis, The Islamic University – Gaza, 2008.

[123] M. S. El-Moghany, "Fuzzy controller design using FPGA for sun tracking in solar array system," 1 Master Thesis, The Islamic University – Gaza, 2011.

[124] N. S. D'Souza, "Variable perturbation size maximum power point tracking algorithms for photovoltaic systems," Master Thesis, Concordia University, 2006.

[125] I. Iancu, "A Mamdani type fuzzy logic controller," *Fuzzy Logic: Controls, Concepts, Theories and Applications, InTech Croatia, Rijeka,* pp. 55-54, 2012.

[126] C.-C. Lee, "Fuzzy logic in control systems: fuzzy logic controller. II," *Systems, Man and Cybernetics, IEEE Transactions on,* vol. 20, pp. 419-435, 1990.

[127] Y. Shi and P. Sen, "A new defuzzification method for fuzzy control of power converters," in *Industry Applications Conference, 2000. Conference Record of the 2000 IEEE,* 2000, pp. 1202-1209.

[128] M. Veerachary, *et al.*, "Neural-network-based maximum-power-point tracking of coupled-inductor interleaved-boost-converter-supplied PV system using fuzzy controller," *Industrial Electronics, IEEE Transactions on,* vol. 50, pp. 749-758, 2003.

[129] E. Cox, *Fuzzy modeling and genetic algorithms for data mining and exploration*: Morgan Kaufmann, 2005.

[130] A. Elgharbi, *et al.*, "AMaximum POWER POINT TRACKING METHOD BASED ON ARTIFICIAL NEURAL NETWORK FOR A PV SYSTEM," *International Journal,* vol. 5, 1963.

[131] S. A. Kalogirou, "Artificial intelligence for the modeling and control of combustion processes: a review," *Progress in Energy and Combustion Science,* vol. 29, pp. 515-566, 2003.

[132] Y. H. Hu and J.-N. Hwang, *Handbook of neural network signal processing*: CRC press, 2001.

[133] A. Mellit and S. A. Kalogirou, "Artificial intelligence techniques for photovoltaic applications: A review," *Progress in Energy and Combustion Science,* vol. 34, pp. 574-632, 2008.

[134] B. K. Bose, "Neural network applications in power electronics and motor drives—An introduction and perspective," *Industrial Electronics, IEEE Transactions on,* vol. 54, pp. 14-33, 2007.

[135] M. Veerachary and N. Yadaiah, "ANN based peak power tracking for PV supplied DC motors," *Solar energy,* vol. 69, pp. 343-350, 2000.

[136] H. Demuth, *et al.*, "Neural network toolbox™ 6," *User's guide, The MathWorks, Inc,* 2008.

[137] B. L. Kalman and S. C. Kwasny, "Why Tanh: choosing a sigmoidal function," in *Neural Networks, 1992. IJCNN., International Joint Conference on*, 1992, pp. 578-581.

[138] A. Hutchinson, *Algorithmic learning*: Oxford University Press, Inc., 1994.

[139] D. Scott, "The discovery of new functional oxides using combinatorial techniques and advanced data mining algorithms," UCL (University College London), 2008.

[140] F. d. O. Resende, "Contributions for microgrids dynamic modelling and operation," PhD Thesis, Porto University, 2012.

[141] R. Haque, "Transmission loss allocation using artificial neural networks," Master Thesis, University of Saskatchewan Saskatoon, 2006.

[142] E. Karatepe, *et al.*, "Neural network based solar cell model," *Energy conversion and management,* vol. 47, pp. 1159-1178, 2006.

[143] M. Beale, *et al.*, "Neural network toolbox," *Neural Network Toolbox, The Math Works,* vol. 5, p. 25, 1992.

[144] R. Reed, "Pruning algorithms-a survey," *Neural Networks, IEEE Transactions on,* vol. 4, pp. 740-747, 1993.

[145] B. Mutwali, "An Economic Analysis of Grid-tie Residential Photovoltaic System and Oil Barrel Price Forecasting: A Case Study of Saudi Arabia," 2013.

[146] Z. Yong, *et al.*, "The MPPT Control Method by Using BP Neural Networks in PV Generating System," in *Industrial Control and Electronics Engineering (ICICEE), 2012 International Conference on*, 2012, pp. 1639-1642.

[147] C. C. Lee, "Fuzzy logic in control systems: Fuzzy logic controller--part I," *IEEE Transactions on systems, man, and cybernetics,* vol. 20, pp. 404-418, 1990.

[148] The MathWorks, Inc "MATLAB User Guide," *Technical Manual,* 2015.

[149] M. Elgendy, *et al.*, "Dynamic behaviour of DC motor-based photovoltaic pumping systems under searching MPPT algorithms," in *Power Engineering, Energy and Electrical Drives, 2009. POWERENG'09. International Conference on*, 2009, pp. 413-418.

[150] M. Elgendy, *et al.*, "Operating Characteristics of the P&O Algorithm at High Perturbation Frequencies for Standalone PV Systems," *Energy Conversion, IEEE Transactions on,* vol. 30, pp. 189-198, 2015.

Appendix A

A.1MATLAB Functions and Scripts

A.1.1 MATLAB Function for Modelling HIT180-180W PV Module

This MATLAB function PV array is to simulate the current-voltage relationship of HIT180-180W PV module and used in simulations throughout of this thesis.

```
function Ia = PV array (G,TaC,Va)
% calculates module current under given voltage, irradiance and
temperature
% Out: Ia = Module operating current (A), vector or scalar
% In: Va = Module operating voltage (V), vector or scalar
% G = Irradiance (1G = 1000 W/m^2), scalar
% TaC = Module temperature in deg C, scalar
%////////////////////////////////////////////////////////////
% Define constants
k = 1.381e-23; % Boltzmann's constant
q = 1.602e-19; % Electron charge
% Following constants are taken from the datasheet of PV module
and
% curve fitting of I-V character (Use data for 1000W/m^2)
A = 1;                % Diode ideality factor (A),
                      % 1 (ideal diode) < A < 2
Eg = 1.12;            % Band gap energy; 1.12eV (Si), 1.42
(GaAs),
                      % 1.5 (CdTe), 1.75 (amorphous Si)
Ns = 36*4;            % # of series connected cells (BP SX150s,
72 cells)
                      %for TaC =0:25:75
Go=1000;
Tref = 298;           % Reference temperature (25C) in Kelvin
Voc_Tref = 21.6*4/Ns; % Voc (open circuit voltage per cell) @
temp TrK
Isc_Tref =2.4*5;      % Isc (short circuit current per cell) @
temp TrK
a = 0.65e-3;          % Temperature coefficient of Isc (0.065%/C)
```

```
                        % Define variables
TaK = 273 + TaC;        % Module temperature in Kelvin
Vc = Va / Ns;           % Cell voltage

% Calculate short-circuit current for TaK
Isc = Isc_Tref * (1 + (a * (TaK - Tref)));
% Calculate photon generated current @ given
irradiance
Iph = (G/Go) * Isc;
% Define thermal potential (Vt) at temp Tref
Vt_Tref = A * k * Tref / q;
                        % Define b = Eg * q/(A*k);
b = Eg * q /(A * k);
% Calculate reverse saturation current for given temperature
Io_Tref = Isc_Tref / (exp(Voc_Tref / Vt_Tref) -1);
Io = Io_Tref * (TaK / Tref)^(3/A) * exp(-b * (1 / TaK -1 /
Tref));

% Calculate series resistance per cell
dVdI_Voc = -1.07/Ns;    % Take dV/dI @ Voc from I-V curve of
datasheet
Xv = Io_Tref / Vt_Tref * exp(Voc_Tref / Vt_Tref);
Rs = - dVdI_Voc - 1/Xv;
% Define thermal potential (Vt) at temp Ta
Vt_Ta = A * k * TaK / q;
% Ia = Iph - Ir * (exp((Vc + Ia * Rs) / Vt_Ta) -1)
% f(Ia) = Iph - Ia - Ir * ( exp((Vc + Ia * Rs) / Vt_Ta) -1) = 0
% Solve for Ia by Newton's method: Ia2 = Ia1 - f(Ia1)/f'(Ia1)
Ia=3; %initial value pf Ia

% Perform 5 iterations
for j=1:5;

Ia = Ia - (Iph - Ia - Io .* ( exp((Vc + Ia .* Rs) ./ Vt_Ta) -
1))./ (-1 - Io * (Rs ./ Vt_Ta) .* exp((Vc + Ia .* Rs) ./ Vt_Ta));
end
```

A.1.2 MATLAB script for calculating the ω_m for a given value of P_{peak}.

```
%Motor parameters
%-----------------------------------------------------------------
%Speed Wm = 1500
La = 0.02;    %Armature inductance of the motor (H).
Ra = 1.5;     % Armature resistance of the motor (Ω).
K = 0.67609; % torque and back emf proportional constant (Nm.A^-1).
Bm = 0.002387  % Viscous torque constant of rotational losses
(Nm.s.rad^-1).
Ja = 0.02365;    % motor shaft iertia (kgm^2).
Kl = 0.00039;    % The proportional constant of the load
torque.(Nm.s.rad^-1)
Am = 0.2;          % motor friction (Nm).
Al = 0.3;          % Load friction (Nm).

%Tl = (Al+Kl*(Wm^1.8))
%Tm = Am + Bm*Wm +Tl
%Tm = Ia*K
%Ia = ((Am + Bm*Wm + Tl)/K)

%Va = Ia*Ra+ K*Wm

%P = ((Ia^2)*Ra)+(Ia)*K*Wm

%P = ((((Am + Bm*Wm + Tl)/K)^2)*Ra)+(((Am + Bm*Wm + Tl)/K))*K*Wm


%%Wm = solve ('((((0.2  + (0.002387*Wm) +
4)/0.67609)^2)*1.5)+((((0.2  +(0.002387*Wm) + 4)))*Wm) = 1440','Wm')

%solve
('(((Bm^2*Ra/K^2)+Bm)*Wm^2)+(((2*Bm*Tl*Ra/K^2)+Tl)*Wm)+(Tl^2*Ra/K^2)
-Ppeak =0','Wm')

%Wm = -(K^2*Tl + K*(4*Ppeak*Ra*Bm^2 + 4*Ppeak*Bm*K^2 +
K^2*Tl^2)^(1/2) + 2*Bm*Ra*Tl)/(2*(Ra*Bm^2 + Bm*K^2))

Wm=solve('(((Bm^2*Ra/K^2)+Bm)*Wm^2)+(((2*Bm*(Al+Kl*Wm^1.8)*Ra/K^2)+(
Al+Kl*Wm^1.8))*Wm)+((Al+Kl*Wm^1.8)^2*Ra/K^2)-Ppeak =0','Wm')
```

A.1.3 MATLAB script for calculating the *D* corresponding to MPP

```
% Duty Ratio Calculation corresponding to the maximum power points

%Motor parameters
%-------------------------------------------------------------------
-------
%Speed Wm = 1500
La = 0.02;          %Armture inductance of the motor (H).
Ra = 1.5;           % Armture resistance of the motor (?).
K = 0.67609;        % torque and back emf proportional constant
(Nm.A^-1).
Bm = 0.002387;      % Viscous torque constant of rotational losses
(Nm.s.rad^-1).
Ja = 0.02365;       % motor shaft iertia (kgm^2).
Kl = 0.00039;       % The proportional constant of the load
torque.(Nm.s.rad^-1)
Am = 0.2;           % motor friction (Nm).
Al = 0.3;           % Load friction (Nm).
%OOOOOOOOOOOOOOOOOOOOOOOOOOOOOOOOOOOOOOOOOOOOOOOOOOOOOOOOOOOOOOOOO
OOOOOOOOO
% Duty Ratio Calculation

%Wm = solve('((((0.2 + 0.002387*Wm +
((0.3+0.00039*(Wm^1.8))))/0.67609)^2)*1.5)+(((0.2 + 0.002387*Wm +
((0.3+0.00039*(Wm^1.8))))/0.67609))*0.67609*Wm = 650','Wm')

Wm =     13.4016

%Tl = (Al+Kl*(Wm^1.8))
Tl = (0.3+0.00039*( Wm^1.8))

%Tm = Am + Bm*Wm +Tl
Tm = Am + Bm*Wm +Tl

%Tm = Ia*K
%Ia = Tm / K
Ia = ((Am + Bm*Wm + Tl)/K)

%Va = Ia*Ra+ K*Wm
Va = Ia*Ra+ K*Wm

D =  Va / Vpv
```

A.1.4 MATLAB Functions script for P&O Algorithm

```
function D_k = fun (D_k2,D_k1,V_k,V_k1,I_k,I_k1,ds)
P_k1=I_k1*V_k1;
P_k=I_k*V_k;
dP=P_k1-P_k;
dD=D_k2-D_k1;
if dP>0
    if dD>0
        D_k=D_k2+ds;
    Else
        D_k=D_k2-ds;
    End
else
        if dD>0
            D_k=D_k2-ds;
        else
            D_k=D_k2+ds;
        end
end
%P_k=P_k1
%D_k2=D_k1
```

Appendix B

B.1 FIS of Fuzzy logic based variable step-size of P&O algorithm

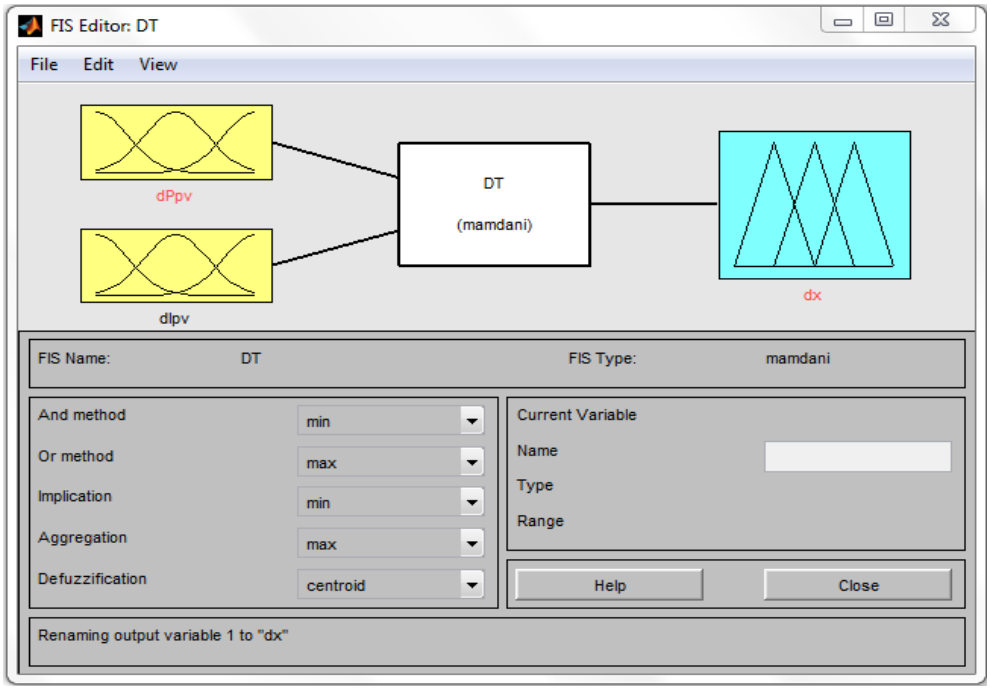

Fig. B.1 FIS editor.

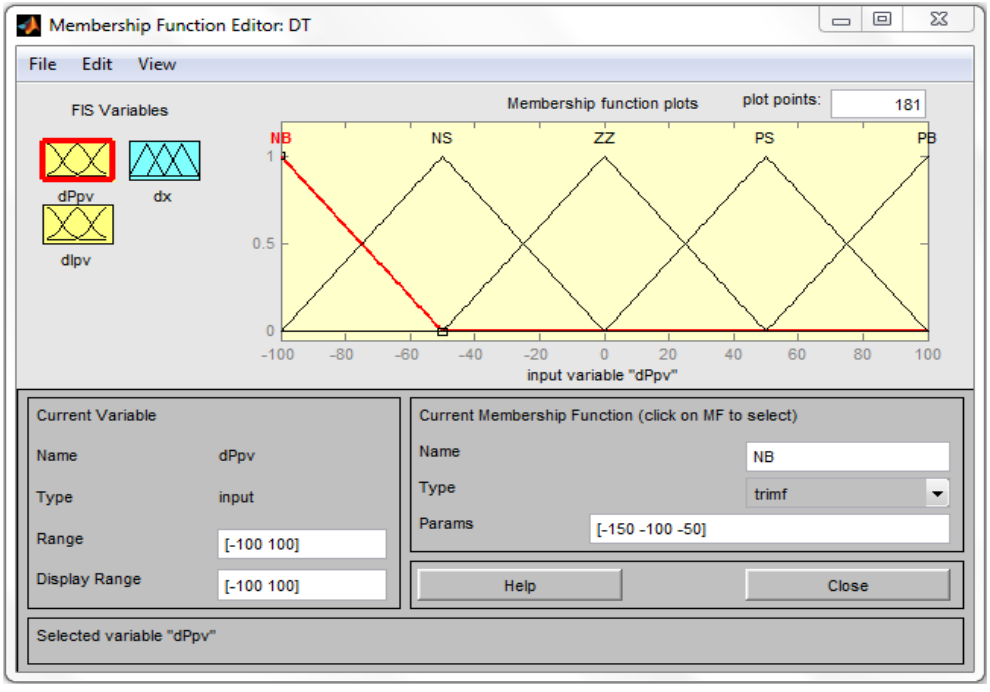

Fig. B.2 Membership function editor.

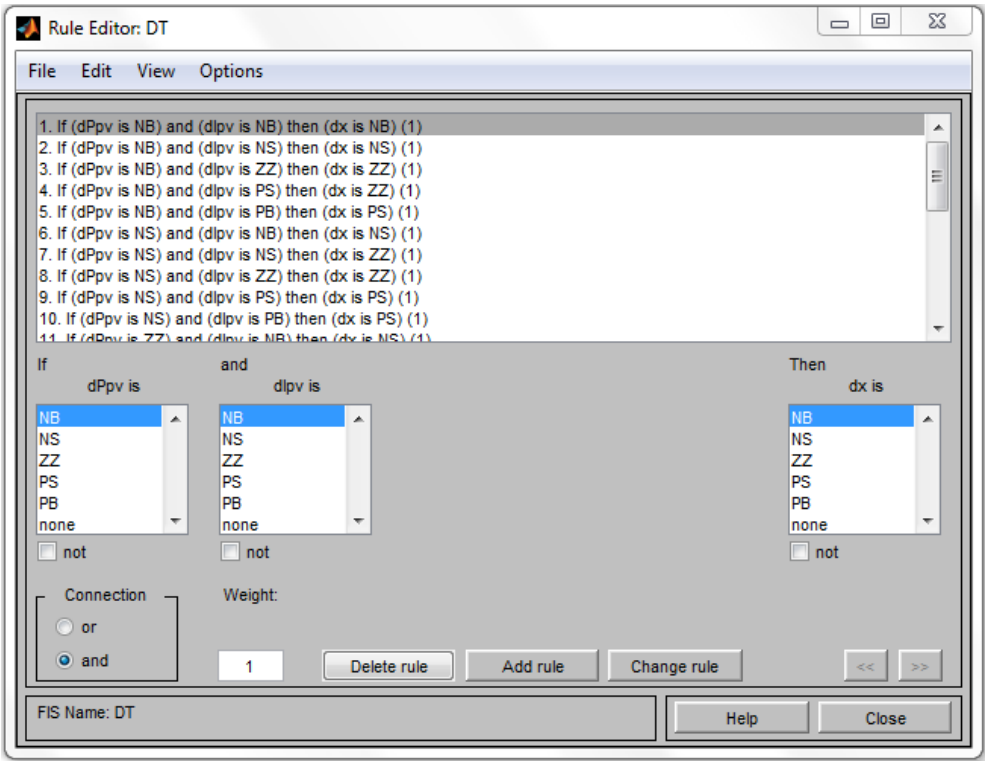

Fig. B.3 Rule-base editor.

Appendix C

Table C.1 The data set collected for training the ANN.

Solar Insolation (W/m^2)	PV array Current (A)	PV array Voltage (V)	PV array Power (W)	Rotational Speed (rad/s)	Duty Ratio
10	0.1160	120.4100	13.9694	19.981	0.12385
20	0.2330	127.0450	29.6011	34.109	0.19558
30	0.3503	130.9300	45.8602	44.348	0.24535
40	0.4677	133.6800	62.5251	52.535	0.28416
50	0.5853	135.8100	79.4902	59.448	0.31637
60	0.7030	137.5450	96.6933	65.486	0.34416
70	0.8208	139.0100	114.0933	70.880	0.36874
80	0.9386	140.2750	131.6608	75.778	0.39090
90	1.0565	141.3900	149.3739	80.281	0.41114
100	1.1744	142.3850	167.2157	84.460	0.42982
110	1.2923	143.2850	185.1724	88.368	0.44721
120	1.4104	144.1000	203.2330	92.044	0.46352
130	1.5284	144.8500	221.3883	95.521	0.47889
140	1.6465	145.5400	239.6303	98.824	0.49346
150	1.7646	146.1850	257.9524	101.973	0.50730
160	1.8827	146.7850	276.3487	104.986	0.52052
170	2.0008	147.3450	294.8141	107.875	0.53318
180	2.1190	147.8750	313.3442	110.653	0.54532
190	2.2372	148.3700	331.9349	113.330	0.55702
200	2.3554	148.8400	350.5827	115.916	0.56830
210	2.4736	149.2900	369.2843	118.417	0.57918
220	2.5918	149.7150	388.0368	120.839	0.58972
230	2.7101	150.1200	406.8376	123.190	0.59994
240	2.8284	150.5050	425.6843	125.474	0.60986
250	2.9466	150.8750	444.5746	127.696	0.61950
260	3.0649	151.2300	463.5065	129.859	0.62888
270	3.1832	151.5700	482.4782	131.968	0.63802
280	3.3015	151.8950	501.4878	134.026	0.64694
290	3.4198	152.2100	520.5338	136.036	0.65565
300	3.5382	152.5100	539.6146	138.000	0.66416
310	3.6566	152.8000	558.7289	139.921	0.67248
320	3.7749	153.0850	577.8753	141.802	0.68060
330	3.8933	153.3550	597.0526	143.644	0.68858

Table C.2 The data set collected for training the ANN

Solar Insolation (W/m^2)	PV array Current (A)	PV array Voltage (V)	PV array Power (W)	Rotational Speed (rad/s)	Duty Ratio
340	4.0116	153.6200	616.2596	145.449	0.69637
350	4.1299	153.8750	635.4952	147.219	0.70402
360	4.2484	154.1200	654.7585	148.957	0.71155
370	4.3667	154.3600	674.0484	150.662	0.71891
380	4.4852	154.5900	693.3640	152.337	0.72616
390	4.6036	154.8150	712.7044	153.984	0.73328
400	4.7220	155.0350	732.0689	155.602	0.74027
410	4.8403	155.2500	751.4566	157.194	0.74714
420	4.9588	155.455	770.8667	158.761	0.75393
430	5.0772	155.655	790.2987	160.302	0.76060
440	5.1955	155.855	809.7517	161.821	0.76715
450	5.3140	156.045	829.2252	163.316	0.77362
460	5.4325	156.230	848.7185	164.790	0.78000
470	5.5510	156.410	868.2310	166.242	0.78629
480	5.6693	156.590	887.7622	167.674	0.79247
490	5.7877	156.765	907.3115	169.087	0.79857
500	5.9063	156.930	926.8784	170.480	0.80462
510	6.0248	157.095	946.4624	171.855	0.81058
520	6.1431	157.260	966.0630	173.212	0.81643
530	6.2617	157.415	985.6798	174.553	0.82226
540	6.4	157.6	1005.3	175.875	0.82782
550	6.5	157.7	1025	177.186	0.83377
560	6.6	157.9	1044.6	178.473	0.83907
570	6.7	158	1064.3	179.751	0.84485
580	6.9	158.2	1084	181.013	0.85001
590	7	158.3	1103.7	182.259	0.85563
600	7.1	158.4	1123.4	183.491	0.86117
610	7.2	158.6	1143.1	184.709	0.86609
620	7.3	158.7	1162.9	185.918	0.87151
630	7.4	158.8	1182.6	187.108	0.87683
640	7.6	158.9	1202.4	188.291	0.88212
650	7.7	159.1	1222.2	189.460	0.88677
660	7.8	159.2	1242	190.617	0.89192

Table C.3 The data set collected for training the ANN

Solar Insolation (W/m^2)	PV array Current (A)	PV array Voltage (V)	PV array Power (W)	Rotational Speed (rad/s)	Duty Ratio
670	7.9	159.3	1261.8	191.762	0.89701
680	8	159.4	1281.6	192.895	0.90203
690	8.2	159.5	1301.4	194.016	0.90699
700	8.3	159.7	1321.3	195.132	0.91136
710	8.4	159.8	1341.1	196.231	0.91620
720	8.5	159.9	1361	197.324	0.92101
730	8.6	160	1380.8	198.401	0.92575
740	8.7	160.1	1400.7	199.474	0.93045
750	8.9	160.2	1420.6	200.536	0.93511
760	9	160.3	1440.5	201.588	0.9397
770	9.1	160.4	1460.4	202.631	0.94426
780	9.2	160.5	1480.3	203.665	0.94876
790	9.3	160.6	1500.2	204.689	0.95322
800	9.5	160.7	1520.1	205.704	0.95762
810	9.6	160.8	1540.1	206.715	0.96201
820	9.7	160.9	1560	207.712	0.96632
830	9.8	161	1579.9	208.701	0.9705
840	9.9	161	1599.9	209.687	0.9754
850	10.1	161.1	1619.9	210.664	0.9796
860	10.2	161.2	1639.8	211.629	0.9838
870	10.3	161.3	1659.8	212.590	0.9879
880	10.4	161.4	1679.8	213.544	0.9920
890	10.5	161.5	1699.8	214.491	0.9960
900	10.6	161.5	1719.8	215.430	1.0006
910	10.8	161.6	1739.8	216.361	1.0046
920	10.9	161.7	1759.8	217.286	1.0085
930	11	161.8	1779.8	218.203	1.0124
940	11.1	161.9	1799.8	219.114	1.0163
950	11.2	161.9	1819.8	220.018	1.0208
960	11.4	162	1839.9	220.920	1.0246
970	11.5	162.1	1859.9	221.810	1.0283
980	11.6	162.2	1879.9	222.695	1.0320
990	11.7	162.2	1900	223.577	1.0364

Table C.4 The data set collected for training the ANN

Solar Insolation (W/m^2)	PV array Current (A)	PV array Voltage (V)	PV array Power (W)	Rotational Speed (rad/s)	Duty Ratio
1000	11.8	162.3	1920	224.449	1.0401
1010	11.9	162.4	1940.1	225.320	1.0437
1020	12.1	162.4	1960.2	226.184	1.0480
1030	12.2	162.5	1980.2	227.038	1.0515
1040	12.3	162.6	2000.3	227.891	1.0551
1050	12.4	162.6	2020.4	228.738	1.0593
1060	12.5	162.7	2040.4	229.575	1.0627
1070	12.7	162.8	2060.5	230.410	1.0662
1080	12.8	162.8	2080.6	231.241	1.0703
1090	12.9	162.9	2100.7	232.066	1.0737
1100	13	163	2120.8	232.886	1.0771
1110	13.1	163	2140.9	233.700	1.0811
1120	13.3	163.1	2161	234.510	1.0844
1130	13.4	163.1	2181.1	235.314	1.0884
1140	13.5	163.2	2201.2	236.114	1.0917
1150	13.6	163.2	2221.3	236.909	1.0956
1160	13.7	163.3	2241.4	237.699	1.0988
1170	13.8	163.4	2261.6	238.488	1.1020
1180	14	163.4	2281.7	239.268	1.1059
1190	14.1	163.5	2301.8	240.044	1.1090
1200	14.2	163.5	2321.9	240.816	1.1128
1210	14.3	163.6	2342.1	241.587	1.1159
1220	14.4	163.6	2362.2	242.349	1.1197
1230	14.6	163.7	2382.3	243.108	1.1228

Appendix D

D.1PV water pumping system MPPT controls simulation

D.1.1 FIS of FLC based MPPT of PV water pumping system Matlab SIMULINK

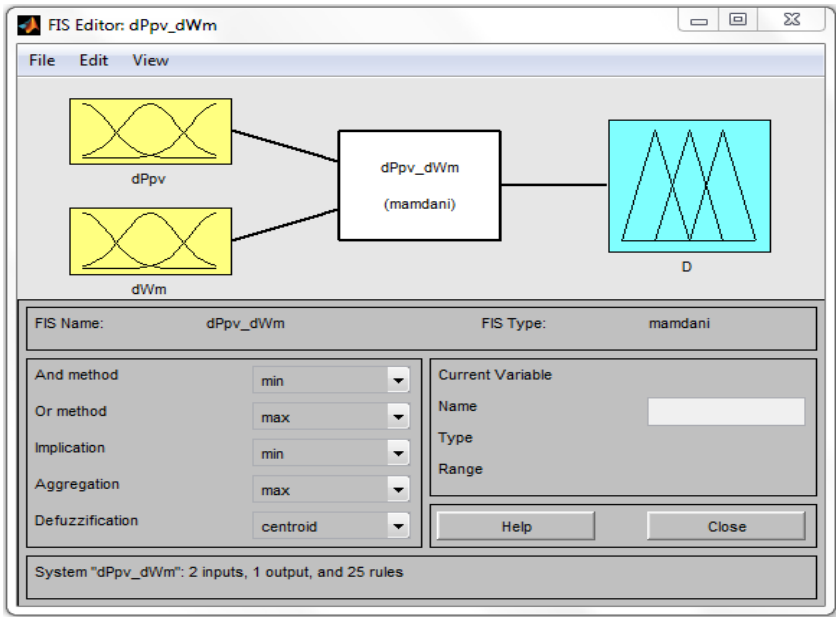

Fig. D.4 FIS editor.

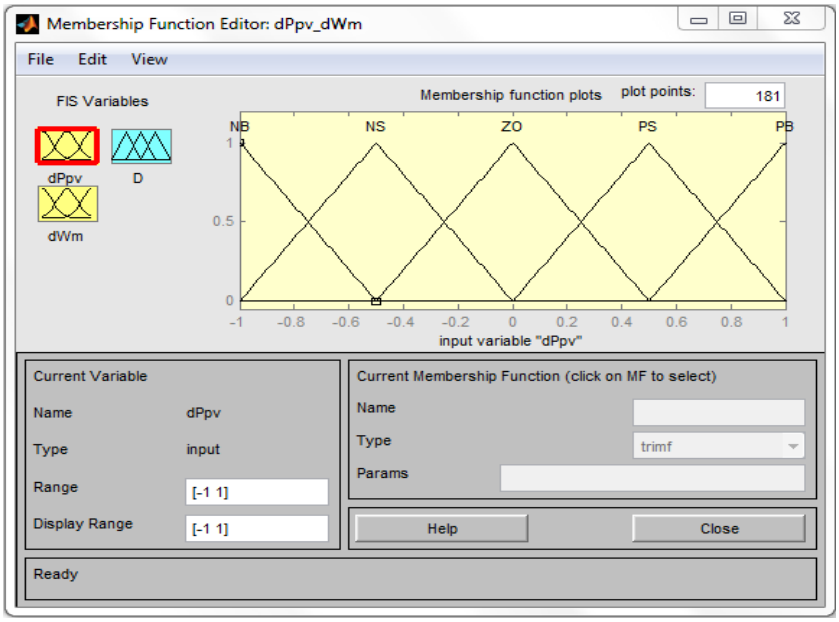

Fig. D.5 Membership function editor of the input variable (dP_{pv}).

Fig. D.6 Membership function editor of the input variable ($d\omega_m$).

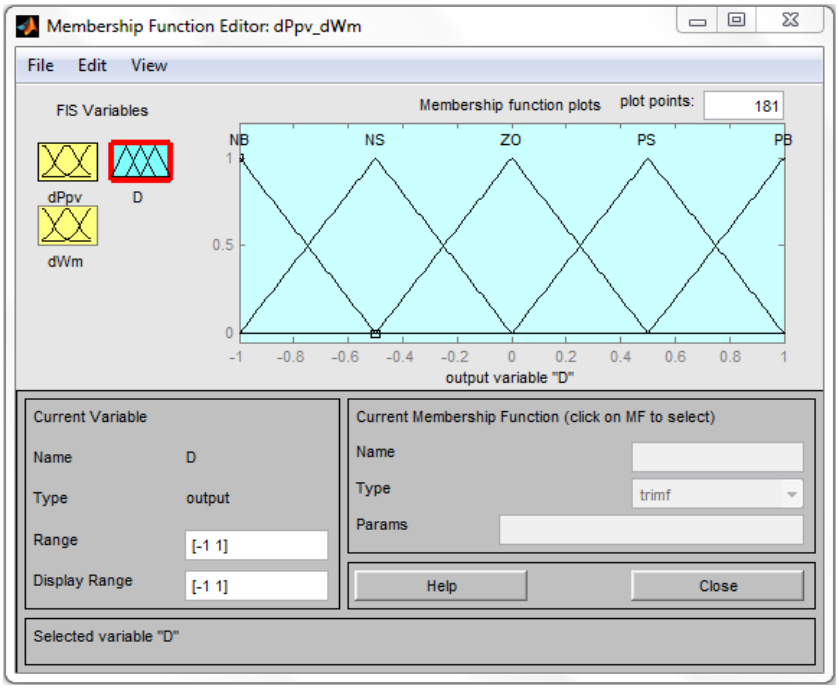

Fig. D.7 Membership function editor of the output variable (D).

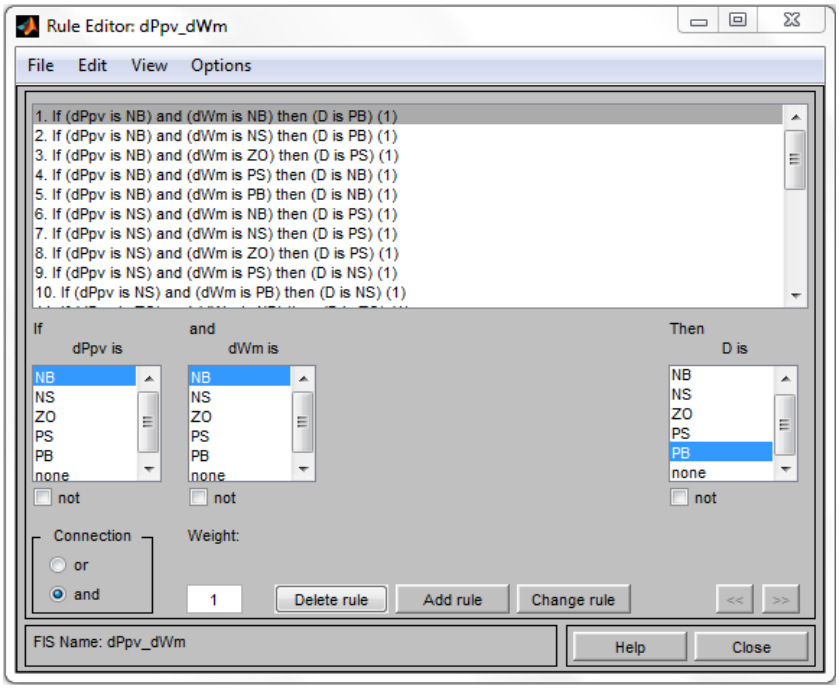

Fig. D.8 Rule-base editor.

Appendix E

E.1.1 ANN based MPPT of PV water pumping system MATLAB SIMULINK

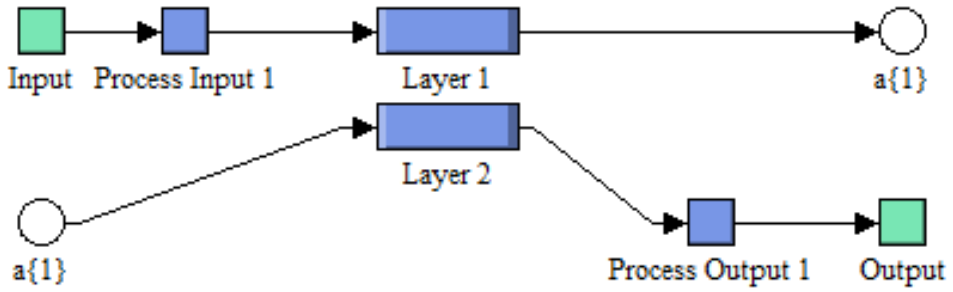

Fig. E.9 Layers of Neural Network of Controller.

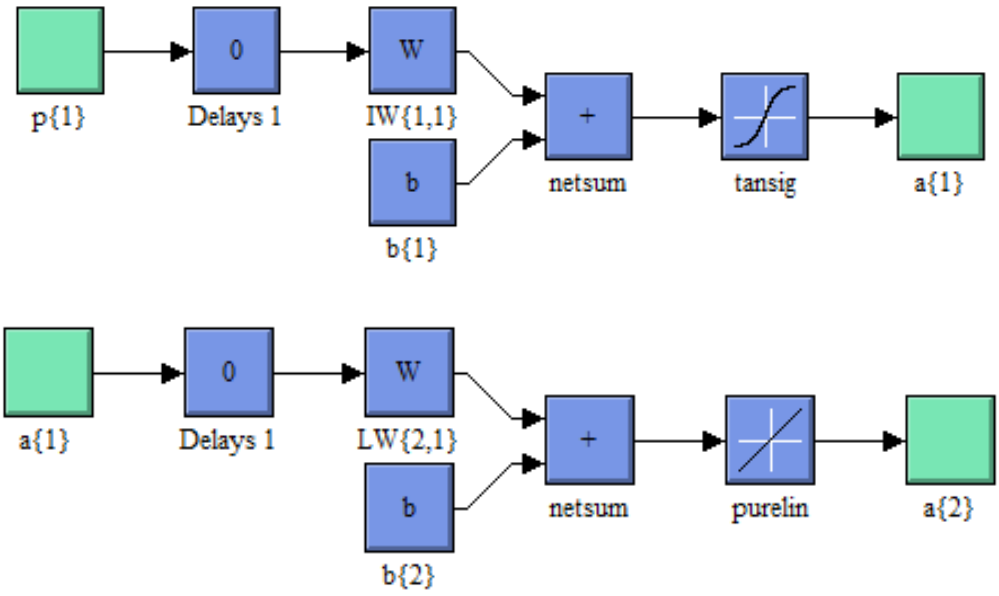

Fig. E.10 Structure of Neural Network Layer.

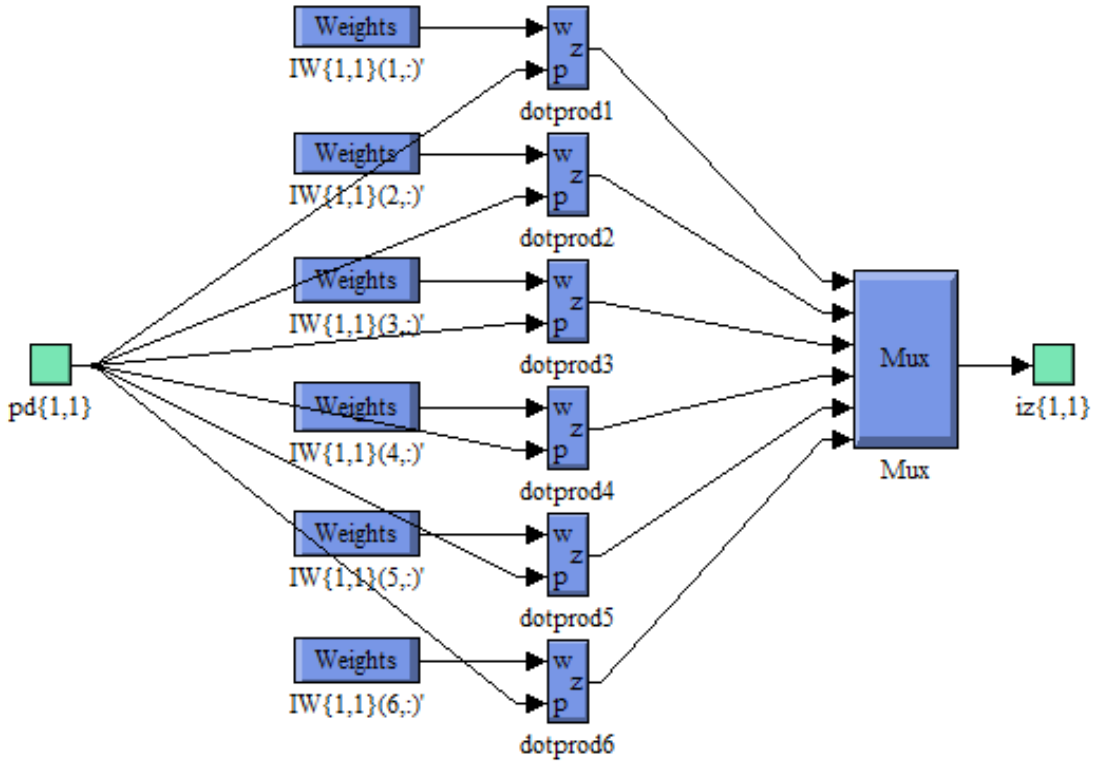

Fig. E.11 Structure of Hidden Layer Neuron.

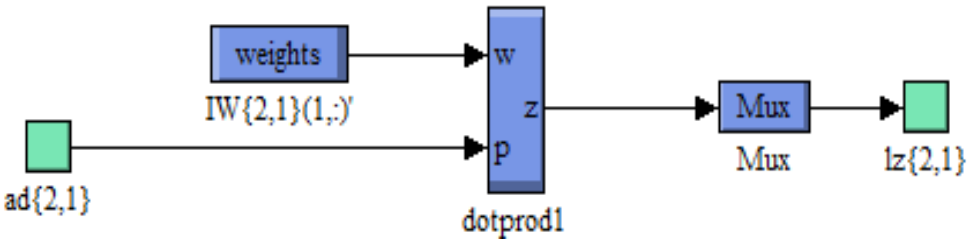

Fig. E.12 Structure of Output Layer Neuron.

PUBLICATIONS

F. A. O. Aashoor and F. V. P. Robinson, "A variable step size perturb and observe algorithm for photovoltaic maximum power point tracking," in *Universities Power Engineering Conference (UPEC), 2012 47th International*, 2012, pp. 1-6.

F. A. O. Aashoor and F. V. P. Robinson, "Maximum power point tracking of photovoltaic water pumping system using fuzzy logic controller," in *Power Engineering Conference (UPEC), 2013 48th International Universities'*, 2013, pp. 1-5.

F. A. O. Aashoor and F. V. P. Robinson, " Maximum power point tracking of PV water pumping system using artificial neural based control," in *Renewable Power Generation Conference (RPG 2014), 3rd*, 2014, pp. 1-6.

A Variable Step Size Perturb and Observe Algorithm for Photovoltaic Maximum Power Point Tracking

F. A. O. Aashoor
University of Bath, UK
F.A.O.Aashoor@bath.ac.uk

F.V.P. Robinson
Member IEEE
University of Bath, UK
F.V.P.Robinson@bath.ac.uk

***Abstract*—Photovoltaic (PV) panels are devices that convert sun light into electrical energy and are considered to be one of the major ways of producing clean and inexhaustible renewable energy. However, these devices do not always naturally operate at maximum efficiency due to the nonlinearity of their output current-voltage characteristic which is affected by the panel temperature and irradiance. Hence, the addition of a high-performance maximum-power-point tracking, MPPT, power-converter interface is the key to keeping the PV system operating at the optimum power point which then gives maximum efficiency. Many MPPT power-converters and different types of control techniques have been considered in the past. This paper primarily considers the MPPT power-converter control method or algorithm. A so called perturb and observe (P&O) technique is considered in this work. This technique is widely used due to its low cost and ease of implementation. With conventional P&O algorithms using fixed iteration step-size, it is impossible to satisfy both performance requirements of fast dynamic response and good accuracy during the steady state at the same time. This is because, if the step-size is set to be big enough for a fast dynamic response, the oscillation around the maximum-power operating point will increase during the steady state leading to lost power generation, and if the step size is too small optimum generation is not quickly restored during changing operating conditions. To overcome these limitations a new adaptive P&O method with variable step size has been investigated which has been implemented using fuzzy logic control. The proposed method has been evaluated by simulation using MATLAB and compared with the conventional P&O under different insolation, or sun-light intensity, levels. The obtained results illustrate the effectiveness of the proposed technique and its ability for practical and efficient tracking of maximum power.**

***Index Terms*—Fuzzy Logic Control, Maximum Power Point Tracking (MPPT), Photovoltaic (PV), Perturb and Observe algorithm (P&O), Variable step size.**

I. INTRODUCTION

Over the past two decades renewable energy sources have gained more attention in contributing to power production due to the increase of power demand in the world. Especially as there is much concern with the world's energy crises, oil shortage and environmental problems caused by conventional power generation sources such as fossil (i.e. oil, natural gas, coal) and nuclear fuels. Renewable energy sources such as wind energy, wave energy and solar energy may be the right solution for these problems. Solar energy is a very attractive renewable source amongst all the aforementioned renewable sources due to relative small system size, free and sustainable generation source or fuel, noise free operation due to the absence of moving parts, the possibility to put it close to the user, ease of installation and systems require relatively little regular maintenance. However the efficiency of solar panels is not very high. Their ability to transfer sunlight to electrical power is relatively inefficient, with conversion efficiency typically in the range 12 ~ 20%. The range of efficiency can drop further during varying solar irradiation, panel temperature and load conditions. Therefore, if the load is directly coupled to the PV array, the PV array must usually be oversized to supply the required power to the load. This leads to an over-sized expensive system. The overall system cost can be reduced and operation is possible at increased efficiency if the solar panel is constantly used to extract as much power as possible during the day-light hours by ensuring that the panel is always operating under optimal power delivery conditions, rather like impedance matching allows maximum power to be extracted from a voltage source with internal resistance. To accomplish this, maximum power point tracker (MPPT) systems are employed. A typical MPPT system consists of a switch-mode power-converter inserted between the PV source and the load, and the duty cycle of the converter is controlled by a control algorithm to enable tracking of the MPP [1]. A large amount of research work has been carried out by different researchers and designers to investigate power converter and control methods to track the MPP of a photovoltaic module [1-5]. In recent years, many techniques for automatically identifying and operating at the maximum power point have been published and implemented with different variations. In [6, 7] at least 19 distinct techniques are discussed, analyzed to determine their advantages and disadvantages, and summarized in a table as a helpful guide in choosing the appropriate MPPT method for specific PV system.

The maximum power point tracking techniques can be classified as incremental conductance (IncCond) [3], fractional short-circuit current [4], fractional open-circuit voltage [5], load current voltage maximization, ripple

correlation control, hill climbing/perturb and observe (P&O) [2], neural network [8], fuzzy logic control and other MPPT methods [6, 9].

In practice, the P&O method is the most commonly used technique, owing to its low cost, ease of implementation and its relatively good tracking performance, when compared to the other techniques. Nevertheless the P&O method fails to track the MPP when the atmospheric conditions change rapidly. And oscillates around the MPP or near to it when the atmospheric conditions change slowly or constant. Consequently, part of available energy is wasted. Many authors have proposed different improvements of the basic P&O algorithm as in [10-15].

In this work, a P&O algorithm with variable step size is proposed for further improvement in the tracking speed and steady state accuracy, which may be implemented using a fuzzy logic controller.

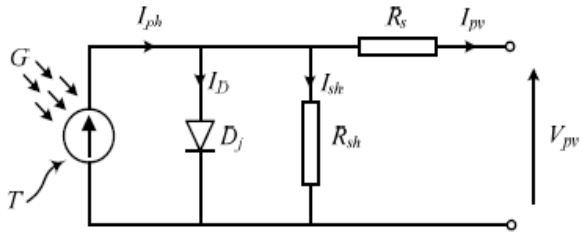

Fig.1.The electric equivalent circuit of a solar cell.

II. SOLAR ARRAY MODEL

The basic solar cell is usually represented by a p-n junction diode connected in parallel with a current source and modeled by equations (1) to (5) as in [16]. This conventional equivalent circuit as illustrated in figure (1). The current source in the circuit represents the photocurrent produced by the sunlight and the diode models the current-voltage characteristic of the cell. The current-voltage characteristic function can be gained by applying Kirchhoff's current law to the circuit. According to Kirchhoff's current law,

$$I_{PV} = I_{ph} - I_D \tag{1}$$

D_j represents the ideal p-n diode, I_D the diode internal diffusion current, R_{sh} and R_s are shunt and series resistance and I_{ph} expressed as the photocurrent or light generated current and it is proportional to the radiation and surface temperature. The output current and voltage of the solar cell is represented by I_{PV} and V_{PV} respectively. The diode internal diffusion current is defined by equation (2).

$$I_D = I_S \cdot \left[\exp\left(\frac{q \cdot V_{PV}}{A \cdot K \cdot T_C} \right) - 1 \right] \tag{2}$$

q is the charge of electron ($=1.61*10^{-19}C$), A is the diode ideality factor, K is Boltzmann's constant of $1.38*10^{-23}$ J/K and T_C is the cell's operating temperature in Kelvin (K). The cell dark saturation current (I_S) varies with the temperature according to equation (3).

$$I_S = I_{RS} \cdot \left(\frac{T_C}{T_{Ref}} \right)^3 \cdot \exp\left[\frac{q \cdot E_{gap}}{A \cdot K} \left(\frac{1}{T_{Ref}} - \frac{1}{T_C} \right) \right] \tag{3}$$

T_{Ref} is the cell reference temperature in Kelvin (K), I_{RS} is the cell reverse saturation current in ampere (A) at reference temperature (T_{Ref}) and solar radiation (G). E_{gap} is the band-gap energy of the semiconductor used in the cell. The photocurrent (I_{ph}) mostly depends on the cell's operating temperature and solar intensity as in equation (4).

$$I_{Ph} = \left[I_{SC} + K_I \cdot \left(T_C - T_{Ref} \right) \right] \cdot \frac{G}{1000} \tag{4}$$

Where I_{SC} is the short-circuit current at reference temperature 25^o C and solar radiation of 1kW/m^2, K_I is the temperature coefficient of the cell's short circuit, and G is the solar insolation in kW/m^2 [16-18]. For the most practical applications the solar cells are connected in series and parallel to produce enough power voltage and current.

$$I_{PV} = I_{Ph} - I_S \cdot \left[\exp\left(\frac{q \cdot (V_{PV} + I_{PV} \cdot R_S)}{A \cdot K \cdot T_C} \right) - 1 \right] \tag{5}$$

Equation (5) was used in Matlab/Simulink to set up the PV electrical characteristics of SANYO HIT180W module model as well as to simulate the I-V and P-V characteristics for different irradiation levels at fixed temperature of 25°C. The test PV module used in this work is 96 SANYO HIT180 180W panels connected in 12×8 matrix. Table I shows the characteristic values and performance of the PV panel with respect to STC and are obtained from module datasheet. Figure 2 shows the variation of output I-V and P-V characteristics of the simulated PV module as function of irradiation. I-V and P-V from the simulated model correlates well with the characteristics provided by the module manufacture. Therefore the model can be used for testing MPPT algorithms.

Table I

Electrical Characteristics of SANYO HIT180W	
Parameter	**Value**
Rated Power (Pmax)	180 W
Maximum Power Voltage (Vpm)	54.0 V
Maximum Power Current (Ipm)	3.33 A
Open Circuit Voltage (Voc)	66.4 V
Short Circuit Current (Isc)	3.65 A
Temperature Coefficient (Voc)	-0.173 V / °C
Temperature Coefficient (Isc)	1.10 mA / °C

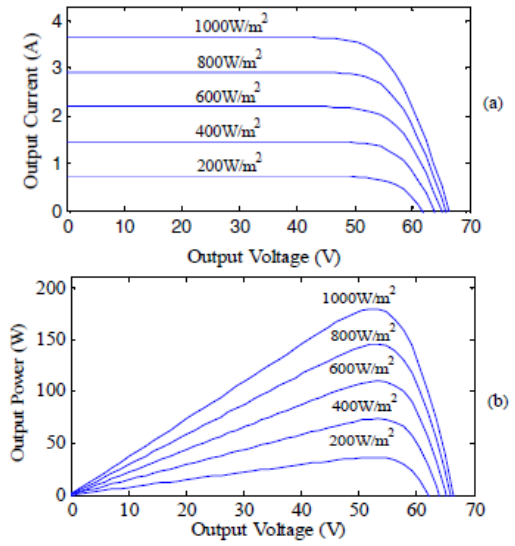

Fig.2. Effect of irradiance on (a) *I-V* curve and (b) *P-V* curve at constant temperature.

III. Conventional Perturb and Observe Algorithm (P&O)

The Perturb and Observe algorithm is considered to be the most commonly used MPPT algorithm of all the techniques because of its simple structure and ease of implementation. It is based on the concept that on the power-voltage curve dP/dV goes to zero at the top of the curve as illustrated in figure 2b [1, 2, 10, 19]. The P&O operates by periodically perturbing (incrementing or decrementing) the PV array terminal voltage or current and comparing the corresponding output power of PV array $P(n+1)$ with that at the previous perturbation $P(n)$. If the perturbation in terminal voltage leads to an increase in power ($dP/dV > 0$), the perturbation should be kept in the same direction otherwise the perturbation is moved to the opposite direction. The perturbation cycle is repeated until the maximum power is reached at the $dP/dV=0$ point . The flowchart of P&O algorithm is shown in figure (3)

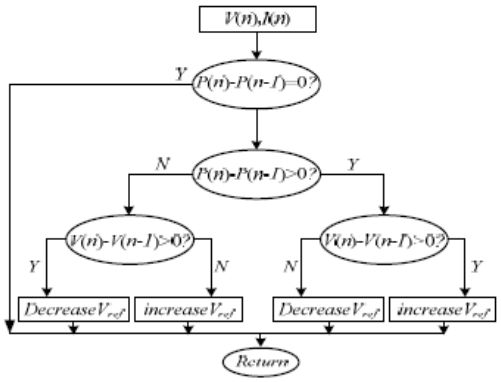

Fig.3.Flowchart of the P&O algorithm.

The advantages of this technique as mentioned before are simplicity; ease of implementation and it does not require a prior knowledge of the PV generator. However, the P&O will not stop perturbing when the MPP is reached and will oscillate around it resulting in power loss. The P&O algorithm can be implemented using two different approaches. Either using direct duty-ratio control where the power is measured every PWM cycle [2, 20], or reference voltage control, where a reference voltage is used as a perturbation parameter and a PI controller is needed to adjust the duty ratio [10, 15, 21]

IV. Modified Variable Step-Size Perturb and Observe Algorithm (MP&O)

Generally the P&O MPPT algorithm is run with a fixed step-size. If this step-size is set to be large the algorithm will have a faster response to dynamics to track the MPP. However, the algorithm with a large step-size results in excessive steady state oscillation, which reduces power efficiency. This performance situation is reversed when the P&O MPPT is running with a small step-size. Therefore, P&O MPPT with fixed step-size does not allow a good tradeoff between steady-state oscillation and dynamic response to changing operating conditions. Therefore, in this work a modified P&O MPPT algorithm with variable step-size is proposed, which may be implemented using fuzzy logic control as shown in figure (4).

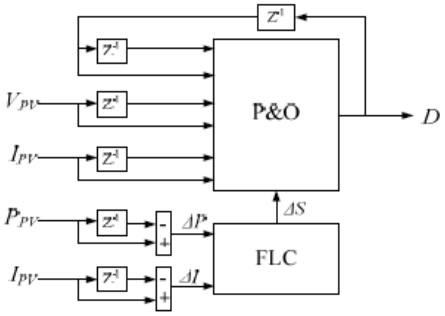

Fig.4.Block diagram of the proposed P&O algorithm with variable step-size.

A. *Fuzzy logic control (FLC)*

A fuzzy logic controller (FLC) is used to vary the step-size. The proposed fuzzy logic controller is based on prior expert knowledge of the system. The main elements of the FLC systems are shown in figure 5. It consists of four sections, Fuzzification, Inference engine, Defuzzification and Rule-Base. The input variables of the FLC are (ΔP_{PV}) and (ΔI_{PV}) the change in PV power and the change of PV current, respectively, whereas the output of the FLC is the variable step-size (ΔS) of the P&O algorithm

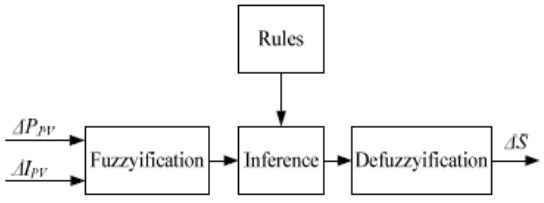

Fig.5.General diagram of fuzzy logic controller.

Where the input variables (ΔP_{PV}) and (ΔI_{PV}) can be calculated by equations (6) to (8).

$$P_{PV}(k) = V_{PV}(k) * I_{PV}(k) \quad (6)$$

$$\Delta P_{PV}(k) = P_{PV}(k) - P_{PV}(k-1) \quad (7)$$

$$\Delta I_{PV}(k) = I_{PV}(k) - I_{PV}(k-1) \quad (8)$$

Quantities $P_{PV}(k)$ and $I_{PV}(k)$ are the PV array power and current, respectively, and $V_{PV}(k)$ is the PV array voltage. The membership function of the input and the output variables are shown below in figures 6-8. All the membership functions are expressed by triangular functions. They consist of five fuzzy subsets which are denoted by NB (negative big), NS (negative small), ZZ (zero), PS (positive small) and PB (positive big).

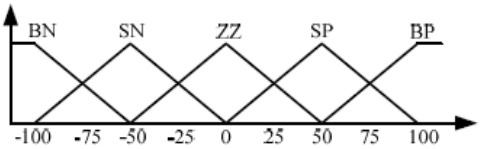

Fig.6. Membership functions of the 1st input variable (ΔP_{PV}).

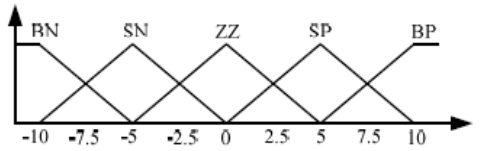

Fig.7. Membership functions of the 2nd input variable (ΔI_{PV}).

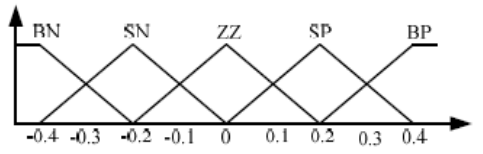

Fig.8. Membership functions of the output variable (ΔS).

The fuzzy inference rules of the FLC consist of 25 rules as illustrated in table II, which determine the output of the controller. The fuzzy logic rules are expressed in terms of IF-THEN and are written as:

IF $\Delta P_{PV}(k)$ is NB and $\Delta I_{PV}(k)$ is NB THEN ΔS is NB.

The defuzzification stage is required to calculate the crisp output value. Hence the output of the FLC defuzzified using centre of gravity (COG) method to calculate ΔS [22].

TABLE II
FUZZY RULES BASE TABLE I

ΔI_{PV}	ΔP_{PV}				
	NB	NS	ZZ	PS	PB
NB	NB	NS	NS	ZZ	ZZ
NS	NS	ZZ	ZZ	ZZ	PS
ZZ	ZZ	ZZ	ZZ	PS	PS
PS	ZZ	PS	PS	PS	PB
PB	PS	PS	PB	PB	PB

V. SIMULATION RESULTS

A block diagram of the proposed system is illustrated in figure (9). A DC/DC buck converter is used to interface PV output to the resistive load to track the maximum power of the PV array. To perform the tracking of maximum power, a modified perturbation and observation algorithm has been implemented. The system has been modeled and operation simulated in MATLAB/Simulink.

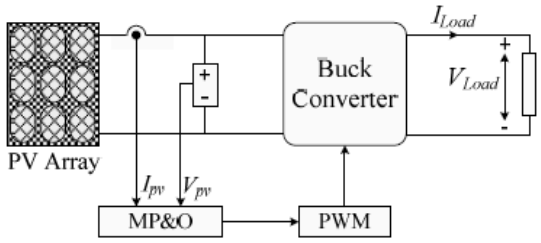

Fig.9. Photovoltaic module output current using P&O algorithm.

The buck converter is conducted in MATLAB and simulated using SimPowerSystems blocks. The converter consists of an IGBT switch and freewheeling diode. Additionally, input and output filters are included. The input capacitance C_{in} of the buck converter is 172µF, output capacitance C_{out} is 40µF and its inductance L is 444µH. The simulations allow verification of the feasibility and the performance of the proposed modified variable step-size P&O algorithm. Additionally, a comparison is carried out between the performance of the modified P&O algorithm and the conventional P&O algorithm by simulating both MPPT methods under exactly the same conditions. The main focus is on how fast the MPP is being tracked during the dynamic state and the level of power ripple caused by oscillations around the MPP under steady state conditions.

In reality, the output power of a photovoltaic cell is mainly influenced by ambient temperature and solar irradiation. Though the change in ambient temperature has a slow influence on the PV cell and it is not directly related to the dynamic response. Therefore the cell working temperature is fixed at the value of 25°C in all simulations. In practice, clouds sometimes move very quickly leading to a sudden change in the PV panel output power, consequently, the algorithm has to be tested under different irradiation levels to verify the speed of tracking. The PV panel is configured to produce 180W with an open-circuit voltage of 66.4V at 1000 W/m^2 solar irradiance. The irradiation was abruptly decreased from 1000 W/m^2 to 400 W/m^2 at 0.3s and increased back to 800 W/m^2 at 0.6s.

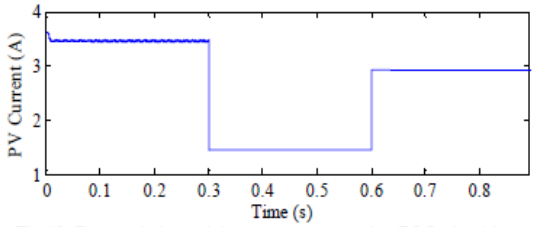

Fig.10. Photovoltaic module output current using P&O algorithm.

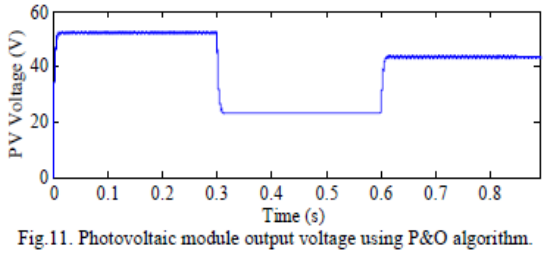

Fig.11. Photovoltaic module output voltage using P&O algorithm.

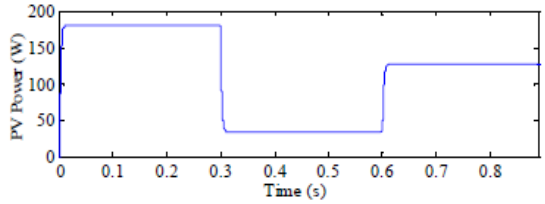

Fig.12. Photovoltaic module output power using P&O algorithm.

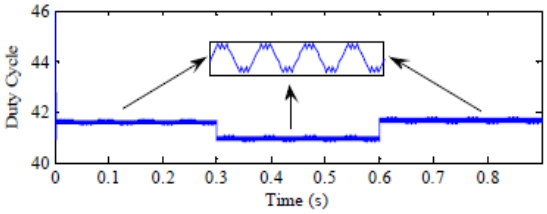

Fig.13. Duty ratio waveform of P&O algorithm.

The simulation results illustrated in figures 10-13 represent the performance of the maximum power point tracking using (P&O) control with fixed a step-size of 0.01. Figures 14-17 show the simulation results performance and effectiveness of the modified maximum power point tracking method (MP&O). The simulation waveform for both algorithms can be described as following. The duty ratio *D* adjusted quickly by MPPT until a stable maximized output power is reached. When the irradiation abruptly changes from 1000 W/m^2 to 400 W/m^2 and then increases again to 800 W/m^2 at 0.3s and 0.6s, the operating power points deviate from the optimal power point. The MPPT tracks again at that time to force the system to work at the new maximum operating point.

Figure 13 shows the duty cycle response of P&O algorithm to

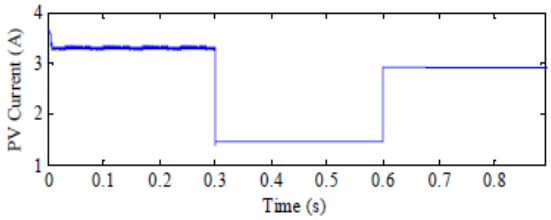

Fig.14. Photovoltaic module output current using MP&O algorithm.

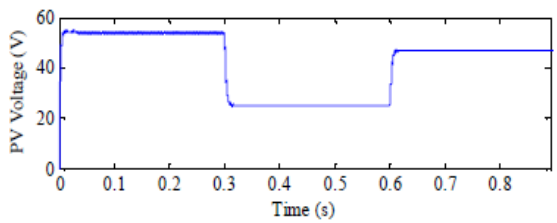

Fig.15. Photovoltaic module output voltage using MP&O algorithm.

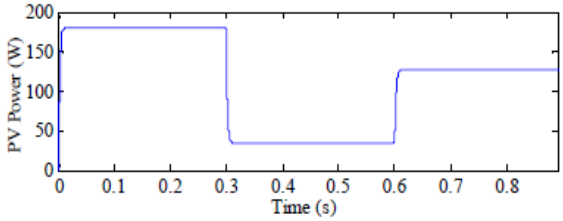

Fig.16. Photovoltaic module output power using MP&O algorithm.

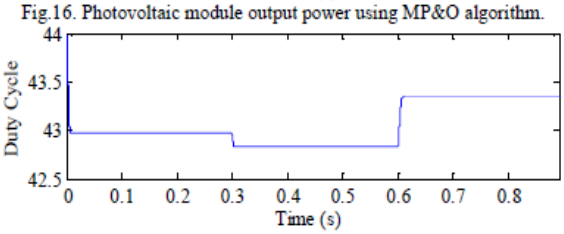

Fig.17. Duty ratio waveform of MP&O algorithm.

the change of irradiation levels. As the irradiation changes the duty cycle changes as well to track the new MPP. However during the steady state the duty cycle keeps swinging around the MPP instead of settling, which leads to some power loss. In contrast, if the perturbation step size is smaller the system will be more stable but slows down the response. However, According to the simulation results the proposed method shows better performance over conventional P&O technique. Figure 17 shows duty cycle waveform of the proposed method. This figure illustrates that, the algorithm stops oscillating in the steady-state as the maximum power point is reached. In addition, the proposed method shows faster dynamic performance than that of fixed step-size as illustrated in figures 18.

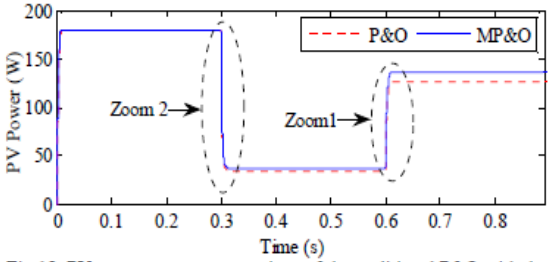

Fig.18. PV output power: comparison of the traditional P&O with the proposed algorithm.

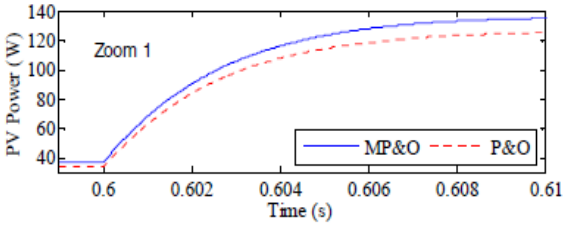

Zoomed image of figure (18)

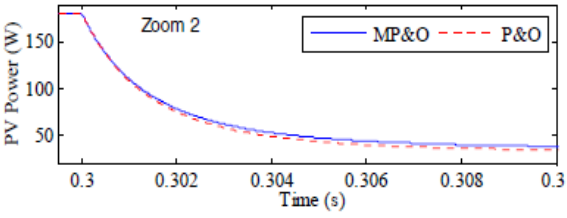

Zoomed image of figure (18)

VI. Conclusion

The output current-voltage characteristics of solar arrays are nonlinear, and the operating conditions of the optimum PV power gained from the PV array is affected by solar irradiation, cell temperature and loading conditions. Therefore, a maximum power point tracking control is needed to continually match the PV internal resistance with the loading effect, hence ensuring that maximum power is transferred to the load.

In this work, the photovoltaic panel has been modelled using a moderate complexity equivalent circuit, and the result compared with manufacture's datasheet characteristics. The simulated results match the characteristics given by the datasheet under different irradiation and cell temperature conditions. The effect of cell temperature and irradiation on the PV panel output characteristics have been investigated with varying load conditions. An adaptive P&O MPPT has been proposed and evaluated using fuzzy logic control to give variable step-size convergence to improve the efficiency of the PV system. To set up the complete PV system simulation model a Buck DC-DC converter was included with a PWM controller. The performance of modified P&O algorithm is evaluated and compared with traditional P&O algorithm using MATLAB simulation. The simulation results clearly show that, the modified P&O has the ability to improve both the steady state and dynamic performance of the photovoltaic power generator system.

References

[1] Koutroulis, E., K. Kalaitzakis, and N.C. Voulgaris, Development of a microcontroller-based, photovoltaic maximum power point tracking control system. Power Electronics, IEEE Transactions on, 2001. 16(1): p. 46-54.

[2] Fangrui, L., et al. Comparison of P&O and hill climbing MPPT methods for grid-connected PV converter. in Industrial Electronics and Applications, 2008. ICIEA 2008. 3rd IEEE Conference on. 2008.

[3] Hussein, K.H., et al., Maximum photovoltaic power tracking: an algorithm for rapidly changing atmospheric conditions. Generation, Transmission and Distribution, IEE Proceedings-, 1995. 142(1): p. 59-64.

[4] Noguchi, T., S. Togashi, and R. Nakamoto, Short-current pulse-based maximum-power-point tracking method for multiple photovoltaic-and-converter module system. Industrial Electronics, IEEE Transactions on, 2002. 49(1): p. 217-223.

[5] Ahmad, J. A fractional open circuit voltage based maximum power point tracker for photovoltaic arrays. in Software Technology and Engineering (ICSTE), 2010 2nd International Conference on. 2010.

[6] Esram, T. and P.L. Chapman, Comparison of Photovoltaic Array Maximum Power Point Tracking Techniques. Energy Conversion, IEEE Transactions on, 2007. 22(2): p. 439-449.

[7] Salas, V., et al., Review of the maximum power point tracking algorithms for stand-alone photovoltaic systems. Solar Energy Materials and Solar Cells, 2006. 90(11): p. 1555-1578.

[8] Hiyama, T., S. Kouzuma, and T. Imakubo, Identification of optimal operating point of PV modules using neural network for real time maximum power tracking control. Energy Conversion, IEEE Transactions on, 1995. 10(2): p. 360-367.

[9] Hilloowala, R.M. and A.M. Sharaf, A rule-based fuzzy logic controller for a PWM inverter in a stand alone wind energy conversion scheme. Industry Applications, IEEE Transactions on, 1996. 32(1): p. 57-65.

[10] Piegari, L. and R. Rizzo, Adaptive perturb and observe algorithm for photovoltaic maximum power point tracking. Renewable Power Generation, IET, 2010. 4(4): p. 317-328.

[11] Khaehintung, N., T. Wiangtong, and P. Sirisuk. FPGA Implementation of MPPT Using Variable Step-Size P&O Algorithm for PV Applications. in Communications and Information Technologies, 2006. ISCIT '06. International Symposium on. 2006.

[12] Fermia, N., et al., Predictive & Adaptive MPPT Perturb and Observe Method. Aerospace and Electronic Systems, IEEE Transactions on, 2007. 43(3): p. 934-950.

[13] Wang, H., et al. Adaptive maximum power point tracker in photovoltaic grid-connected system. in Power Electronics for Distributed Generation Systems (PEDG), 2010 2nd IEEE International Symposium on. 2010.

[14] Sera, D., et al. Optimized Maximum Power Point Tracker for fast changing environmental conditions. in Industrial Electronics, 2008. ISIE 2008. IEEE International Symposium on. 2008.

[15] Weidong, X. and W.G. Dunford. A modified adaptive hill climbing MPPT method for photovoltaic power systems. in Power Electronics Specialists Conference, 2004. PESC 04. 2004 IEEE 35th Annual. 2004.

[16] Villalva, M.G., J.R. Gazoli, and E.R. Filho, Comprehensive Approach to Modeling and Simulation of Photovoltaic Arrays. Power Electronics, IEEE Transactions on, 2009. 24(5): p. 1198-1208.

[17] Huan-Liang, T., Insolation-oriented model of photovoltaic module using Matlab/Simulink. Solar Energy, 2010. 84(7): p. 1318-1326.

[18] Walker, G., Evaluating MPPT converter topologies using a MATLAB PV model. Journal of Electrical & Electronics Engineering, Australia, 2001. 21(1): p. 49-56.

[19] Jaen, C., et al. Overview of maximum power point tracking control techniques used in photovoltaic systems. 2008: IEEE.

[20] Chee Wei, T., T.C. Green, and C.A. Hernandez-Aramburo. Analysis of perturb and observe maximum power point tracking algorithm for photovoltaic applications. in Power and Energy Conference, 2008. PECon 2008. IEEE 2nd International. 2008.

[21] Chihchiang, H. and S. Chihming. Study of maximum power tracking techniques and control of DC/DC converters for photovoltaic power system. in Power Electronics Specialists Conference, 1998. PESC 98 Record. 29th Annual IEEE. 1998.

[22] Lee, C.C., Fuzzy logic in control systems: Fuzzy logic controller--part I. IEEE Transactions on systems, man, and cybernetics, 1990. 20(2): p. 404-418.

[23] SANYO HIT180-180W Photovoltaic Module. Datasheet, 2008.

[24] Abou El Ela, M. and J.A. Roger, Optimization of the function of a photovoltaic array using a feedback control system. Solar Cells, 1984. 13(2): p. 107-119.

Maximum Power Point Tracking of Photovoltaic Water Pumping System Using Fuzzy Logic Controller

F. A. O. Aashoor
Department of Electronic and Electrical Engineering
University of Bath, UK
F.A.O.Aashoor@bath.ac.uk

F.V.P. Robinson
Member IEEE
Department of Electronic and Electrical Engineering
University of Bath, UK
F.V.P.Robinson@bath.ac.uk

***Abstract*-Diode junction photovoltaic (PV) generators exhibit nonlinear V-I characteristics and the maximum power extractable varies with the intensity of solar radiation, temperature and load conditions. A maximum power point tracking (MPPT) controller is therefore usually employed in PV-generator applications to automatically extract maximum power irrespective of the instantaneous conditions of the PV system. This paper presents a fuzzy logic control (FLC) scheme for extracting the maximum power from a stand-alone PV generator for use in a water pumping system. The PV-generator system comprises a solar panel, DC-DC buck chopper, fuzzy MPP tracker and permanent DC-motor driving a centrifugal pump. The fuzzy controller generates a control signal for the pulse-width-modulation generator which in turn adjusts the duty ratio of the buck chopper to match the load impedance to the PV generator, and consequently maximizes the motor speed and the water discharge rate of a coupled centrifugal pump. The control method has been modelled in Matlab/Simulink and simulation results are presented to confirm its significantly improved power extraction performance under different sunlight conditions, when compared with a directly-connected PV-generator energized pumping system operating.**

***Index Terms*--DC/DC buck converter, fuzzy logic controller, maximum power point tracking, photovoltaic water pumping system**

I. INTRODUCTION

Solar energy generation using arrays of photovoltaic–cells is an attractive source of renewable energy, especially, for energizing relatively small stand-alone systems. Solar energy is often considered the best power source for applications, such as water pumping in rural areas in developing countries, where many people have no access to an AC power grid. Previous studies on photovoltaic-generator driven water pumping systems have previously considered a number of suitable pumps and motors [1]-[5]. Two types of pumps are widely employed in PV water pumping systems: the centrifugal pump and volumetric pump. The centrifugal pump is capable of pumping a high volume of water and operating at relatively high efficiency. Volumetric pumps are usually used when a low flow rate is required [1]. As the energy obtained from solar panels is in the form of DC, the pumps are mostly driven by DC motors to minimize system complexity since they can be directly connected to the PV panel or array [2]. Separately-excited and permanent magnet (PM) brushed DC motors are often recommended for PV pumping system [3]-[5]. Other types of DC brushed and AC motors have also been investigated, such as shunt [6] and series DC motors [7], permanent magnet synchronous motors (brushless DC motors) and AC induction motors [8]. AC motors have attractive features such as high efficiency, brushless configuration, simpler geometry and rugged construction; and initial cost can be lower in the case of the cage induction motor. However, an inverter is required to convert the DC output of the PV generator to AC power to drive the motor. Consequently, the cost and complexity of the overall system significantly increases.

In this work, the new fuzzy logic MPPT controller will be applied and evaluated using a minimal complexity, low-cost, robust system comprising a DC-motor pump drive. The system is simulated and analysed using Matlab/Simulink and the energy utilization efficiency is calculated for different levels of irradiation and temperature.

II. SYSTEM DESCRIPTION

A schematic of the photovoltaic generator and water pumping system used to investigate the fuzzy logic controller performance is shown in Fig.1. The system comprises a PV generator, buck converter, fuzzy based MPPT control unit and DC motor coupled to a centrifugal pump. The power produced by the PV generator is supplied to the DC motor through a buck converter. The output power of the PV generator and the rotation speed of the pump are used as input variables of the fuzzy control unit to determine the duty-ratio control signal for the buck converter.

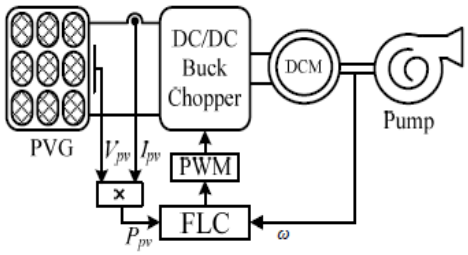

Fig.1. Schematic diagram of the proposed water pumping system.

Solar Array Mode

The solar-cell array is modeled using the cell equivalent circuit shown in Fig.2. The current source connected in parallel with a p-n junction diode models the current-voltage characteristic of the cell [9]. The output current of the equivalent circuit can be expressed as a function of the cell's voltage as in (1).

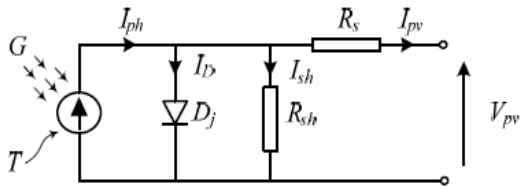

Fig.2. Equivalent circuit a solar cell.

$$I_{PV} = I_{Ph} - I_D \tag{1}$$

D_j represents the ideal p-n diode internal diffusion current, I_D; R_{sh} and R_s model the shunt and series connected resistance effects; and I_{ph} models the photocurrent or light generated current and is proportional to the incident radiation and surface temperature. The output current and voltage of the solar cell are represented by I_{PV} and V_{PV} respectively. The diode internal diffusion current is defined by (2).

$$I_D = I_S \cdot \left[exp\left(\frac{q.V_{PV}}{A \cdot K \cdot T_C}\right) - 1\right] \tag{2}$$

In (2), q is electron charge, $1.61\times10^{-19}C$, A is diode ideality factor, K is Boltzmann's constant, 1.38×10^{-23} J/K, and T_C is the cell's operating temperature in Kelvin (K). The cell dark saturation current (I_S) varies with the temperature according to (3).

$$I_S = I_{RS} \cdot \left(\frac{T_C}{T_{Rrf}}\right)^3 . exp\left[\frac{q \cdot E_{gap}}{A \cdot K}\left(\frac{1}{T_{Ref}} - \frac{1}{T_C}\right)\right] \tag{3}$$

T_{Ref} is the cell's reference temperature in Kelvin, I_{RS} is the cell reverse saturation current in ampere at reference temperature T_{Ref} and G is solar insulation in kW/m^2. E_{gap} is the band-gap energy of the semiconductor used in the cell. The photocurrent I_{ph} mostly depends on the cell's operating temperature and solar intensity as in (4).

$$I_{Ph} = \left[I_{SC} + K_I \cdot (T_C - T_{Rrf})\right] \cdot \frac{G}{1000} \tag{4}$$

In (4), I_{SC} is the short-circuit current at reference temperature 25^o C and K_I is the temperature coefficient of short circuit current [9]-[11].

For most practical applications the solar cells are connected in series strings which are then connected in parallel to produce the required voltage and current, or power.

$$I_{PV} = I_{Ph} - I_S \cdot \left[exp\left(\frac{q \cdot (V_{PV} + I_{PV} \cdot R_S)}{A \cdot K \cdot T_C}\right) - 1\right] \tag{5}$$

Equation (5) was used in Matlab/Simulink to model the electrical characteristics of a Mono Crystalline, PP1237, 37Wp PV module. Simulated output characteristics were found to be in good agreement with the manufacturer's experimental data.

A. Electric Motor Model

Employing DC motors in PV pumping systems instead of AC motors has been the subject of previous investigations which have generally concluded that DC motors can be usefully operated when directly coupled to the PV generators when minimal overall system cost and complexity is required. However, the objective here is to improve the utilization of the PV system and introduce greater control flexibility by interposing a DC/DC power converter.

A permanent magnet DC motors is proposed for this application since it does not require a separate field power supply and gives relatively efficient and low- maintenance operation. In addition, the PMDCM coupled with centrifugal pump has a low starting torque compared to the other PV electro-mechanical systems and may be relatively easily matched with the output characteristics with the PV array. The equivalent circuit of the permanent magnet DC motor is shown in Fig.3. The dynamic equation of the motor at constant flux is given by [12].

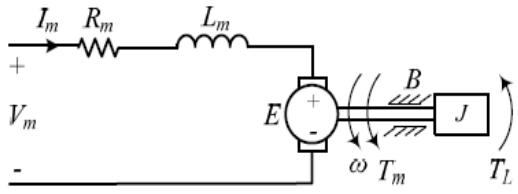

Fig.3. Circuit model for DC permanent magnet motor with pump load.

$$V_a = I_m R_m + L_m \frac{dI_m}{dt} + E \tag{6}$$

$$\text{Where } E = K_e \omega$$

In (6), V_m is the applied voltage, R_m is the armature winding resistance, L_m is the armature self-inductance, I_m is the motor armature current, E is the motor back e.m.f., K_e is the back e.m.f. constant and ω is the angular speed of the rotor.

$$T_m = K_m I_m = J\frac{d\omega}{dt} + B\omega + C + T_L \tag{7}$$

In (7), K_m is the torque constant, J is the moment of inertia, B is the viscous torque constant for rotational losses, C is the torque constant for rotational losses and T_m and T_L are the electromagnetic torque and the load torque, respectively.

B. *Centrifugal Pump Model*

Although the volumetric pump and the centrifugal pump are widely used in PV pumping systems, it was found in [13] that the PV generator energy utilized by the centrifugal pump is much higher than by the volumetric pump because the centrifugal pump works for longer periods even for low insolation levels and its load characteristic is well matched to the maximum power locus of the PV generator. Also centrifugal pumps are inexpensive, simple, require low maintenance and are available in a wide range of flow rates and heads. Therefore a centrifugal pump is considered in this work.

The driving torque for centrifugal pump is proportional to the square of the rotational speed as given by [14]. Hence,

$$T_p = T_L = K_p \omega^2 \tag{8}$$

T_p is the torque required to drive the pump and K_p is the constant for given centrifugal pump.

III. FUZZY LOGIC CONTROLLER

Fuzzy logic controllers have been widely used for industrial processes in the resent years due to their heuristic nature associated with simplicity and effectiveness for both linear and nonlinear systems [15]. The control objective is to track maximum power, will lead consequently to maximize the dc motor speed and the water discharge rate of the coupled centrifugal pump. At the time when output power of the PV generator is maximum at a given condition the hydraulic power $P_P = K_T\, \omega$ is maximum. Consequently the rotational speed ω is a maximum at the maximum power point. By making use of the relation between the PVG output power and the rotational speed, a fuzzy logic controller has been proposed to adjust the buck converter ratio which adapts online the PVG output power to maximize the rotational speed.

A. *Fuzzification*

In the fuzzification stage, numerical input variables are calculated or converted into linguistic variables based on subsets called membership function [8], [16]. The fuzzy logic controller proposed has two input variables as illustrated in Table I which are the rotation speed variation $\Delta\omega(k)$ and PVG output power variation $\Delta P(k)$ at sampling instant k and they are expressed as a follows:

$$\Delta\omega(k) = G_\omega\, (\omega(k) - \omega(k\text{-}1)) \tag{9}$$

$$\Delta P(k) = G_P\, (P(k) - P(k\text{-}1)) \tag{10}$$

In (9) and (10), G_ω and G_P are scaling factors used to normalize the $\Delta\omega$(k) and $\Delta P(k)$, respectively. The scaling factors play an important role in optimizing performance and can be chosen using trial and error method. The membership functions of the both inputs and output variables are represented by symmetric triangular functions and defined in common normalized range of (-1, 1) as shown in Fig.4. The membership function of both inputs and output variables are assigned five sets, including positive big (PB), positive small (PS), zero (ZO), negative big (NS), and negative small (NB).

B. *Fuzzy Rule Algorithm*

Fuzzy rules comprise a set of rules in linguistic form which associate the fuzzy inputs with the fuzzy output. These are based on an expert knowledge and understanding of the system behavior that is required to achieve the control objectives. The fuzzy control rules have been set up using a set of IF-THEN statements as described in Table I. The fuzzy rules are designed to incorporate the following considerations keeping in view the overall tracking performance.

1. If a positive variation in the rotation speed is accompanied with a positive variation of PVG output power, then the chopper duty ratio should be increased. Otherwise if the variation of PVG output power is negative, then chopper ratio should be decreased.

2. If the rotation speed variation is zero or sufficiently close to zero which means that its maximum is reached, then there should be no change in the chopper ratio.

3. If a negative variation in the rotation speed is accompanied with a positive variation in PVG output power, then the chopper duty ratio should be decreased. Otherwise if the variation of PVG output power is positive, then chopper ratio should be increased.

C. *Defuzzification*

In the defuzzification stage and inference mechanism the output of fuzzy logic control is converted from linguistic variables to numerical variables. The inference mechanism determines the matching degree of the current fuzzy input with respect to each rule and the controller has to resolve the conflict between different rules being fired at the same time and decides which rules are to be fired according to the input field. Then the fired rules are combined to form the control actions. There are different methods of defuzzifying an outcome fuzzy set. The method used in this paper is called Center of Gravity (CoG) or centroid. The idea of (CoG) is to find the variable value of the center of gravity of the composite membership function for the fuzzy value [17]. The crisp value of the output variable $D(k+1)$ is computed by the following equation:

$$\Delta D = \frac{\sum_{i=1}^{n} \mu_i x_i s_i \Delta D_i}{\sum_{i=1}^{n} \mu_i s_i\, \Delta D_i} \tag{11}$$

Where n is the maximum number of effective rules, μ_i is the ith rule degree of fulfillment at the kth sampling period, x_i the gravity Centre abscissa of the output fuzzy logic membership function corresponding to the ith rule and S_i is its surface. The final duty ratio change is obtained by adding this change to the previous value of the control duty ratio as a follows:

$$D(k+1) = D(k) - G_D\,\Delta D(k-1) \qquad (12)$$

Where G_D is the output scaling factor of the fuzzy logic controller and $D(k+1)$ is the final output signal sent to the system.

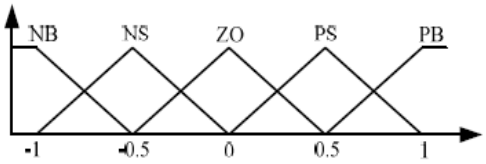

Fig.4. Membership functions of Δω, ΔP and ΔD.

TABLE I. RULE BASE TABLE FOR THE FUZZY LOGIC CONTROLLER.

If Δ□ > 0 If ΔP > 0 D(K)=D(K-1)+ΔD Else D(K)=D(K-1)- ΔD End	If Δ□ is PB and ΔP is PB then ΔD is PB
	If Δ□ is PB and ΔP is PS then ΔD is PB
	If Δ□ is PB and ΔP is NB then ΔD is NB
	If Δ□ is PB and ΔP is NS then ΔD is NB
	If Δ□ is PB and ΔP is ZO then ΔD is NS
	If Δ□ is PS and ΔP is PB then ΔD is PS
	If Δ□ is PS and ΔP is PS then ΔD is PS
	If Δ□ is PS and ΔP is NB then ΔD is NS
	If Δ□ is PS and ΔP is NS then ΔD is NS
	If Δ□ is PS and ΔP is ZO then ΔD is NS
If Δ□ = 0 D(K) = D(K-1)	If Δ□ is ZO and ΔP is PB then ΔD is PB
	If Δ□ is ZO and ΔP is PS then ΔD is PB
	If Δ□ is ZO and ΔP is ZO then ΔD is ZO
	If Δ□ is ZO and ΔP is NB then ΔD is NB
	If Δ□ is ZO and ΔP is NS then ΔD is NB
If Δ□ < 0 If ΔP > 0 D(K)=D(K-1)-ΔD Else D(K)=D(K-1)+ ΔD End	If Δ□ is NB and ΔP is PB then ΔD is NB
	If Δ□ is NB and ΔP is PS then ΔD is NB
	If Δ□ is NB and ΔP is NB then ΔD is PB
	If Δ□ is NB and ΔP is NS then ΔD is PB
	If Δ□ is NB and ΔP is ZO then ΔD is PS
	If Δ□ is NS and ΔP is PB then ΔD is NS
	If Δ□ is NS and ΔP is PS then ΔD is NS
	If Δ□ is NS and ΔP is NB then ΔD is PS
	If Δ□ is NS and ΔP is NS then ΔD is PS
	If Δ□ is NS and ΔP is ZO then ΔD is PS

IV. SIMULATION RESULTS

In order to verify the performance of the proposed technique of fuzzy logic control, a comparison has been made between a directly connected system and the proposed method under different ambient temperature and solar insolation levels. The solar insolation level is assumed to undergo an abrupt change from 400 W/m^2 to 800 W/m^2 and then to 200 W/m^2 as shown in Fig.5. Then the temperature is abruptly increased from 45 C° to 65 C° and then decreased again to 45 C° as shown in Fig.9. Fig.6 to Fig.8 present the variation of PV voltage, PV power and rotation speed under different irradiation levels for both proposed FLC method and the directly connected system. The effect of the temperature change on PV voltage, PV power and motor speed of both the proposed FLC method and the directly connected system are shown in Fig10 to Fig.12.

From the simulation results it is evident that the proposed FLC technique gives improved performance over the directly connected system in both cases, of rapid change in temperature and insolation. As a result the quantity of the daily pumped water gained by the proposed method is higher than that pumped by directly connected system. Table III summarizes the comparison between the proposed method and the directly connected system.

TABLE II. PARAMETERS OF PM DC MOTOR, LOAD, AND PV ARRAY [5].

DC PM Motor data Manufactured by Kirloskar Electric company	
Rated motor voltage	60V
Rated motor current	16.5A
Rated motor speed	272.3 (rad/sec)
Armature resistance	0.8Ω
Armature inductance	0.04H
Voltage and torque constant	0.175 (rad/sec)
Load data	
Moment of inertia (J)	0.024kg-m^2
Torque constant for rotational losses (C)	0.08 N-m
Viscose friction coefficient (B)	0.0010 N-m (read/sec)
Centrifugal pump load torque (T_L)	0.15+1.6532×10^{-5}□^{2}
PV array data (Mono Crystalline, PP1237, 37Wp module)	
Rated Power (Pmax)	37 W
Maximum Power Voltage (Vpm)	16.4 V
Maximum Power Current (Ipm)	2.24 A
Open Circuit Voltage (Voc)	21.6 V
Short Circuit Current (Isc)	2.54 A

TABLE III

SIMULATION RESULT FOR GIVEN IRRADIATION AND TEMPERATURE.

Temperature (C°)	25	25	25	45	65	45
Solar Insolation (W/m^2)	200	600	200	600	600	600
PVG Power (W) Fuzzy	75.18	440.2	75.18	265.2	194.4	265.2
PVG Power (W) Direct	55.28	347.6	55.27	225.9	162.9	225.9
PVG Voltage(V) Fuzzy	34.49	61.71	34.49	49.98	44.18	49.98
PVG Voltage (V) Direct	22.29	51.09	22.27	42.81	37.99	42.81
Rotational Speed (rad/s) Fuzzy	130.4	272.5	130.4	232.4	216.2	232.4
Rotational Speed (rad/s) Direct	120.8	248	120.8	213.4	185.7	213.4

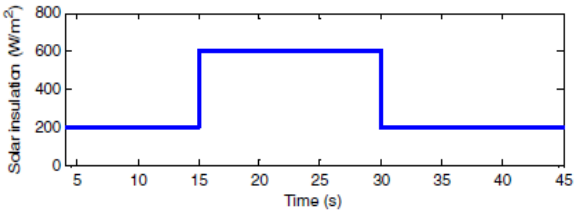

Fig.5. The change of solar irradiation.

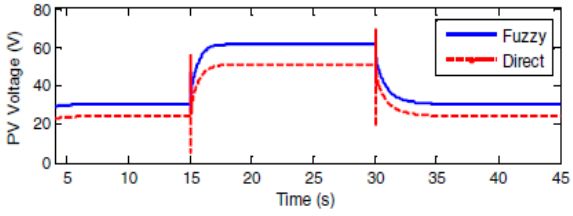

Fig.6. Variation of the PV output voltage as the irradiation level changes.

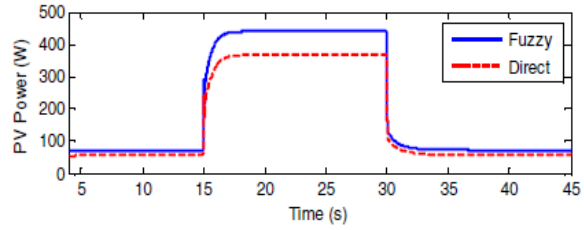

Fig.7. Variation of the PV output power as the irradiation level changes.

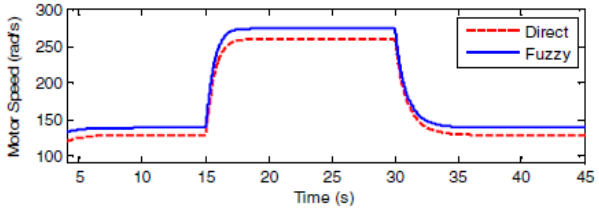

Fig.8. Variation of the rotational speed as the irradiation level changes.

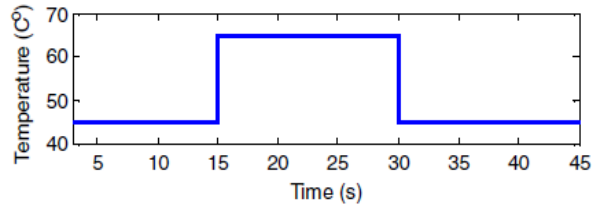

Fig.9. The change of temperature.

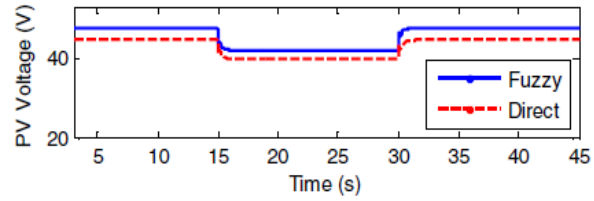

Fig.10. Variation of the PV output voltage as the temperature changes.

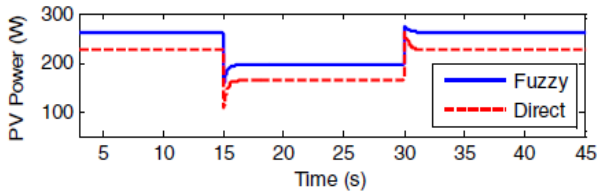

Fig.11. Variation of the PV output power as the temperature changes.

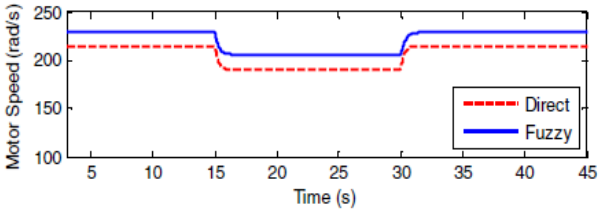

Fig.12. Variation of the rotational speed as the temperature changes.

V. CONCLUSION

A fuzzy logic controller has been proposed and implemented in a PV water pumping system. The design process of the FLC was thoroughly discussed. The whole system has been simulated in Matlab/Simulink. The performance of the FLC was studied and compared with a directly connected system under the same insolation and temperatures levels. The simulation results confirm the likely benefits of the proposed FLC which increases and better maximizes the level of energy produced by the PVG, and gives greater PV water pumping system capacity in comparison with a system without MPPT. The only measurements required to implement the proposed technique are the PV voltage and current, i.e. power, and the motor speed.

VI. REFERENCES

[1] Illanes, R., et al., *Comparative study by simulation of photovoltaic pumping systems with stationary and polar tracking arrays.* Progress in Photovoltaics: Research and Applications, 2003. 11(7): p. 453-465.

[2] Dursun, M. and S. Ozden. *Application of Solar Powered Automatic Water Pumping in Turkey*. 2011.

[3] Appelbaum, J., *Starting and Steady-State Characteristics of DC Motors Powered by Solar Cell Generators.* Energy Conversion, IEEE Transactions on, 1986. EC-1(1): p. 17-25.

[4] Badescu, V., *Dynamic model of a complex system including PV cells, electric battery, electrical motor and water pump.* Energy, 2003. 28(12): p. 1165-1181.

[5] Kolhe, M., S. Kolhe, and J. Joshi, *Determination of magnetic field constant of DC permanent magnet motor powered by photovoltaic for maximum mechanical energy output.* Renewable Energy, 2000. 21(3): p. 563-571.

[6] Metwally, H. and W.R. Anis, *Dynamic performance of directly coupled photovoltaic water pumping system using DC shunt motor.* Energy conversion and management, 1996. 37(9): p. 1407-1416.

[7] Koner, P., *Optimization techniques for a photovoltaic water pumping system.* Renewable Energy, 1995. 6(1): p. 53-62.

[8] Benlarbi, K., L. Mokrani, and M. Nait-Said, *A fuzzy global efficiency optimization of a photovoltaic water pumping system.* Solar Energy, 2004. 77(2): p. 203-216.

[9] Villalva, M.G., J.R. Gazoli, and E.R. Filho, *Comprehensive Approach to Modeling and Simulation of Photovoltaic Arrays.* Power Electronics, IEEE Transactions on, 2009. 24(5): p. 1198-1208.

[10] Walker, G., *Evaluating MPPT converter topologies using a MATLAB PV model.* Journal of Electrical & Electronics Engineering, Australia, 2001. 21(1): p. 49-56.

[11] Huan-Liang, T., *Insolation-oriented model of photovoltaic module using Matlab/Simulink.* Solar Energy, 2010. 84(7): p. 1318-1326.

[12] Krishnan, R., *Electric motor drives: modeling, analysis, and control.* Vol. 626. 2001: Prentice Hall Upper Saddle River, NJ.

[13] Anis, W.R. and H. Metwally, *Dynamic performance of a directly coupled PV pumping system.* Solar Energy, 1994. 53(4): p. 369-377.

[14] Braunstein, A. and A. Kornfeld, *Analysis of solar powered electric water pumps.* Solar Energy, 1981. 27(3): p. 235-240.

[15] Veerachary, M., T. Senjyu, and K. Uezato, *Feedforward maximum power point tracking of PV systems using fuzzy controller.* Aerospace and Electronic Systems, IEEE Transactions on, 2002. 38(3): p. 969-981.

[16] Veerachary, M., T. Senjyu, and K. Uezato, *Neural-network-based maximum-power-point tracking of coupled-inductor interleaved-boost-converter-supplied PV system using fuzzy controller.* Industrial Electronics, IEEE Transactions on, 2003. 50(4): p. 749-758.

[17] Cox, E., *Fuzzy modeling and genetic algorithms for data mining and exploration*2005: Morgan Kaufmann.

Maximum power point tracking of PV water pumping system using artificial neural based control

F A O Aashoor, F V P Robinson†

Dept of Electronic & Electrical Engineering, University of Bath,UK, F.A.O.Aashoor@bath.ac.uk
F.V.P.Robinson@bath.ac.uk

Keywords: Artificial Neural Network (ANN), DC/DC buck converter, maximum power point tracking, photovoltaic water pumping system

Abstract

In photovoltaic (PV) water pumping systems, a maximum power point tracking (MPPT) controller is extremely important. Since PV generators exhibit nonlinear *I-V* characteristics and their maximum power point varies with solar insolation. Therefore, the MPPT controller optimises the solar energy conversion by ensuring that the PV generator runs at the maximum power point at all times under different illumination conditions. In this paper, a new artificial neural network (ANN) based searching algorithm is proposed for maximum power point tracking (MPPT). The system is composed of solar array, buck converter and centrifugal pump load driven by a permanent magnet DC motor. The proposed ANN controller uses the output power of the PV generator and speed of the DC motor as input signals and generates the pulse width modulation (PWM) control signal to adjust the operating duty ratio of a buck converter to match the load impedance to the internal impedance of the PV array; thus maximizing the motor speed and the water discharge rate of a centrifugal pump. A complete dynamic simulation of the system is developed in MATLAB/SIMULINK to demonstrate the feasibility of the ANN control scheme under different sunlight insolation levels. The results obtained verify that the proposed ANN controller shows a significant improvement in the power extraction performance under different sunlight conditions, when compared with a directly-connected PV-generator energized pumping system. Moreover, the simulation results match the calculated improvement.

1 Introduction

The standalone photovoltaic (PV) water pumping system has received increasing attention in the last 20 years because of the ongoing cost reductions in PV arrays. It is important to operate the PV energy conversion systems at the MPP or near to it to increase the efficiency of the PV system. The PV array has non-linear. The output current and power of the PV array depends on its operating terminal voltage. Also, the output power of PV array is fluctuating with the change in the ambient temperature and solar irradiation. Therefore, for most of the time under varying irradiation levels the DC motor and pump are operating the PV array far from the MPP. Due to non-linear voltage-current characteristic of the PV array it is challenging to track the MPP. To overcome these problems, many algorithms have been developed to provide maximum PV power. These vary in complexity, computation burden, range of effectiveness, hardware implementation, popularity, convergence speed, and in other respects [1] and [2]. The perturb and observe (P&O) algorithm is the most commonly used algorithm, due to its ease of implementation. However, the (P&O) algorithm suffers from oscillation around the MPP during steady state operation, leading to some waste of available energy, and the system accuracy is low [2]. The incremental conductance method is used to overcome the oscillation problem by comparing the incremental and instantaneous conductance of the PV array. However, system implementation is more complex and increases the cost to the whole system [3]. The fractional short-circuit current and fractional open-circuit voltage methods are simple, but both techniques share the same drawbacks, such as error due to linearization approximation and temporary power loss caused by the ongoing short-circuit or open-circuit calibration cycles of the PV array [1].

2 The proposed MPPT scheme

The complete combined system of artificial neural network ANN controller with a PV water pumping system is illustrated in Figure (1). The system mainly consists of a PV array, DC-DC buck converter and permanent magnet DC motor driving a centrifugal pump.

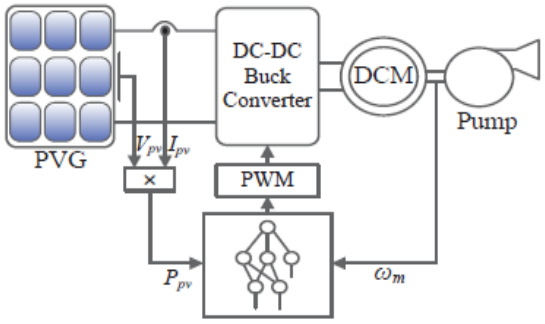

Figure 1: Block diagram of MPPT controller.

The schematic diagram in Figure 1the inputs of the proposed ANN controller are the PV array output power P_{pv} and the motor rotational speed ω_m, and the output of ANN controller is the buck converter control signal. Maximum power is delivered by the PV array at different solar insolation levels

by using the ANN controller to adjust the duty ratio of the buck converter. The ANN controller design and training will be discussed in more detail in the coming sections.

2.1 The solar cell model

The operation and behaviour of the photovoltaic generator has been mathematically described and modelled in different ways in the literature. These models differ in some aspect such as accuracy, calculation procedures and the number of parameters included in calculating the current-voltage characteristic. However, the one diode electrical equivalent circuit is the most commonly used circuit for cell based analysis as shown in Figure (2). [4] The equivalent circuit of a solar cell mainly consist of a current source connected in parallel with a diode and two resistors shunt R_{sh} and series R_s to represent the losses [5].

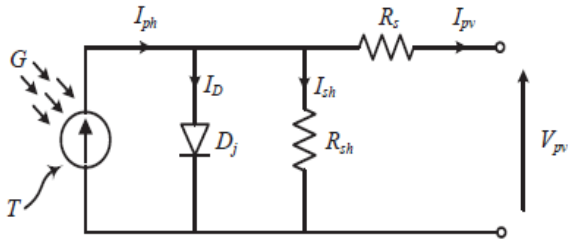

Figure 2: PV cell equivalent circuit.

The current-voltage characteristic function can be gained by applying Kirchhoff's current law in the circuit above, which yields Equation (1).

$$I_{PV} = I_{Ph} - I_D \qquad (1)$$

In the circuit above, D_j is the ideal p-n junction diode, I_D the diode internal diffusion current and I_{ph} the photocurrent, or light generated current, which is proportional to the radiation and surface temperature. The output current and voltage of the solar cell is represented by I_{PV} and V_{PV}, respectively. The diode internal diffusion current is modelled by Equation (2).

$$I_D = I_S \cdot \left[exp\left(\frac{q \cdot V_{PV}}{A \cdot K \cdot T_C} \right) - 1 \right] \qquad (2)$$

As q is the charge of electron, 1.6×10^{-19} C, A is diode ideality factor, K is Boltzmann's constant, 1.38×10^{-23} J/K, and T_C is the cell's operating temperature in kelvin. The cell dark saturation current, I_S , varies with temperature according to Equation (4). The photocurrent, I_{ph}, is related to the cell's operating temperature and solar intensity as shown in Equation (3).

$$I_{Ph} = \left[I_{SC} + K_I \cdot (T_C - T_{Rrf}) \right] \cdot \frac{G}{G_r} \qquad (3)$$

Where I_{SC} is the short-circuit current, K_I is the temperature coefficient of the cell's short circuit (Amperes/ ^oK), T_{Ref} is the cell reference temperature in kelvin, $T_{Ref} = 298$ ^oK (25 ^oC), G is the solar insolation in W/m^2 and G_r represents the reference solar radiation W/m^2, G_r = 1kW/m^2. Short-circuit current is always measured under standard test conditions of reference temperature 25^oC and solar radiation of 1kW/m^2 [4] and [5-7]

$$I_S = I_{RS} \cdot \left(\frac{T_C}{T_{Rrf}} \right)^3 \cdot exp\left[\frac{q \cdot E_{gap}}{A \cdot K} \left(\frac{1}{T_{Ref}} - \frac{1}{T_C} \right) \right] \qquad (4)$$

In Equation (4), I_{RS} is the cell reverse saturation current in ampere at T_{Ref}, and the solar radiation 1kW/m^2. E_{gap} is the band-gap energy of the semiconductor used in the cell.
A higher power range is required in most practical applications, so the solar cells are connected in series and parallel to meet the demand described in Equation (4). However, only R_s is included in the equation, because the PV cell is relatively insensitive to the variation of R_{sh} .Therefore R_{sh} is neglected for simplicity with little loss in accuracy.

$$I_{PV} = N_P \cdot I_{Ph} - N_P \cdot I_S \cdot \left[exp\left(\frac{q}{AKT_C} \left(\frac{V_{PV}}{N_S} + I_{PV} \cdot \frac{R_S}{N_P} \right) \right) - 1 \right] \qquad (5)$$

Where N_P is the number of cells in parallel and N_S is the number of cells in series. Eequation is used to simulate the output characteristic of PV panel.

The simulation is based on the datasheet of (Mono Crystalline, PP1237, 37Wp) photovoltaic module and the parameters of this solar module are listed in Table (1).

PV panel data Mono Crystalline, PP1237, 37Wp module	
Quantity	Value
Rated Power (Pmax)	37 W
Maximum Power Voltage (Vpm)	16.4 V
Maximum Power Current (Ipm)	2.24 A
Open Circuit Voltage (Voc)	21.6 V
Short Circuit Current (Isc)	2.54 A

Table 1: Main parameters of the solar panel.

2.2 Motor model

Since the output produced by PV generators is DC power, a DC motor is usually employed instead of AC motors in the PV pumping systems, because DC motors can be more easily interfaced with PV generators without using DC to AC power conversion. Therefore, the overall system cost and complexity will significantly reduce. In this work, a permanent magnet DC motor is used to drive a centrifugal pump load. The permanent magnet DC motor has some advantages such as reliability, high efficiency and relatively infrequent maintenance [8]. Moreover, the PMDC motor coupled with centrifugal pump has suitable matching characteristics with the PV array characteristics and its starting low torque is low compared to other PV electro-mechanical systems [8] and [9]. Figure (2) illustrates the equivalent circuit of the permanent magnet DC motor with the pump load.

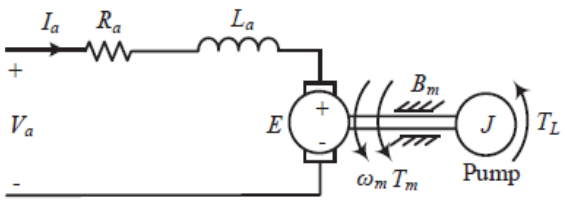

Figure 2: Circuit model for PMDC motor with pump load.

In Figure 2, R_a is the armature winding resistance (Ω), L_a is the armature self-inductance (H), I_a is the motor armature current (A) and V_a is the applied voltage (V).

According to the equivalent circuit shown in Figure 2 the armature DC voltage can be calculated using Equation (6).

$$V_a = R_a I_a + L_a \frac{dI_a}{dt} + e \qquad (6)$$

e is the induced voltage when the motor is turning, and is known as a back emf. The induced voltage e is proportional to the angular speed of the rotor (ω_m) and the back emf constant proportionality (K_e) as given by ($e = K_e \omega_m$)

The torque balance equation is given by Equation (7).

$$T_e = K_t I_a = J \frac{d\omega_m}{dt} + B_m \omega_m + T_L \qquad (7)$$

Where K_t is the torque constant, J is the moment of inertia, B_m is the viscose torque constant for rotational losses, T_e and T_L are the electromagnetic torque and the load torque respectively.

2.3 Centrifugal pump load

There are two types of pump widely used in PV pumping systems: volumetric pump and the centrifugal pump. However, it was reported in [10] that, a load composed of a DC motor driving a constant volumetric pump represents a non-matched load for a PV generator because the motor driving a constant volumetric pump requires a nearly constant current. Conversely, it was found in [11] that the PV sourced energy utilized by the centrifugal pump is much higher than with the volumetric pump, because the centrifugal pump works for longer periods even for low insolation levels. Moreover, the characteristics of the DC motor and centrifugal pump combination are well matched with the maximum power locus of the PV generator. Centrifugal pumps are inexpensive, simple, require low maintenance and are available in a wide range of flow rates and heads. Therefore a centrifugal pump is considered in this work.

The centrifugal pump load develops speed-dependant torque. The speed-torque relationship for a centrifugal pump including friction torque is given by Equation (8) [12].

$$T_p = T_L = A_L K_L \omega_m^{1.8} \qquad (8)$$

T_p is the torque required to drive the pump, A_L is the load friction (Nm) and K_L the proportional constant of the load torque N.m/(rad/sec)^2.

2.4 Neural network MPPT controller architecture

The structure of multilayer feedforward networks are mostly determined by experience, and according to previous studies there is no valid formula that is appropriate for different situations [13]. There are two methods of selecting the architecture of the ANN techniques as in [13, 14]. The first method begins with a small network and then proceeds by gradually adding connections or nodes as needed. In the second method, a big network is selected, and then proceeds by gradually eliminating the unnecessary connections or nodes. The first method was used in this study to map the relationship between the duty ratio and the PV power and the motor speed. Finally, after selecting an appropriate neural network size, a satisfactory result was obtained with a three layer feed-forward backpropagation neural network, comprising (input, hidden and output layers) as shown in Figure 3.

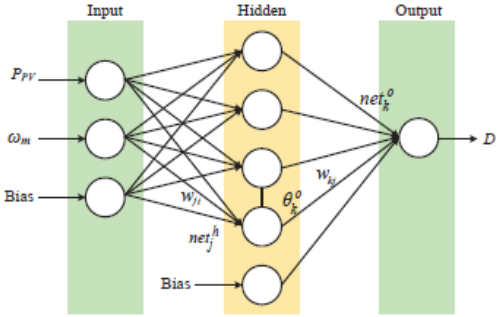

Figure 3: Feedforward neural network.

The number of nodes in the hidden layer is determined empirically as indicated above in the first method. It was found that, the 6 hidden nodes gave the most precise estimation and the result of this case as shown in Figure 4. This illustrates the neural network construction in MATALB/SIMULINK environment, the input layer has 2 nodes, the hidden layer has 6 nodes and the output layer has 1 node. Accordingly, the input layer consists of a two dimensional vector, PV generator output power and the DC motor speed. The output layer of the proposed ANN comprises only, a one dimensional vector which is the controlling signal of the buck chopper. The outputs of the input layer are weighted and summed together, and then a bias is added to the sum of the weighted inputs. Finally the summation of the weighted inputs and the bias are passed through the transfer function f. There are different types of transfer function that are used as activation functions, such as sigmoid, Gaussian, tangent, hyperbolic constant etc. Two of the most commonly used functions, tangent and linear function are used in this work.

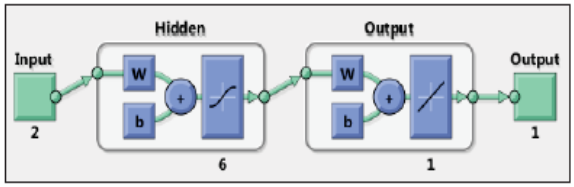

Figure 4: The training network model in MATLAB.

A tangent function is used as an activation function to calculate the hidden layer output and a linear function to calculate the output [15] and [16]. An example of linear transfer function and tangent transfer function are shown in Figure 5 (a) and (b) respectively.

The tangent function was used as transfer function of the single hidden layer that is described by Equation (9) and directed in Figure (5) (b) [17].

$$f(x) = \frac{1}{1 + exp^{-x}} \quad (9)$$

For the neurons of the output layer of the neural network, the pure linear transfer function $f(x) = x$ was used to provide a wide range of solutions as shown in Figure (5) (a) [18].

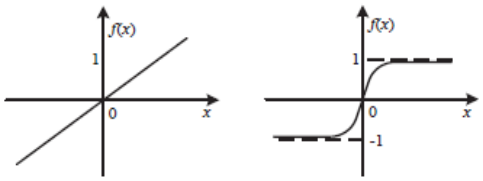

(a) Linear function (b) Tangent function

Figure 5: Transfer function.

The collected data for training should be first normalized before being applied to the input layer as the input vector, $x = (x_1, x_2, x_3, \ldots, x_n\, x)^T$.

The normalizing function is $x = (x - x_{min}) / (x_{max} - x_{min})$. When the weight vectors of the input layer are multiplied to the hide layer and adding the bias vector, the net input to the hidden layer j is

$$net_j^h = \sum_{i=1}^{n} \left(w_{ji}\, x_i + \theta_j^h \right) \quad (10)$$

In Equation (10), w_{ji} is the weight on the connection from the ith input unit and θ_j^h is the bias for each joint from the input layer to the output layer, which is mainly used to improve the learning speed during network training process. Now the output value from the hidden layer is

$$y_j^h = f_1 \left(\sum_{i=1}^{n} w_{ji}\, x_i + \theta_j^h \right) \quad (11)$$

The net input to the neurons in the output layer becomes

$$net_k^0 = \sum_{j=1}^{N_h} w_{kj}\, y_j^h + \theta_k^0 \quad (12)$$

In Equation (12), θ_k^0 is the threshold value for neuron in the output layer. The output of the neurons in the output layer is

$$y_k^0 = f_2 \left(\sum_{j=1}^{N_h} w_{kj}\, y_j^h + \theta_k^0 \right) \quad (13)$$

The training process is the process of determining the connection weights of the neural network. A set of input output pairs of the training patterns or training data are needed to accomplish the training process. The input data set is PV generator maximum output power P_{max} and the rotational speed of the motor ω_m, whereas the output data set is the corresponding duty ratio of the buck chopper. The training data has been obtained by varying the solar radiation level from 50W/m^2 to 1200W/m^2 with incremental value of 10W/m^2. While the PV surface temperature is incremented by 2 °C per step from 0 to 70 °C, and the corresponding duty cycle is calculated for each case.

A neural network toolbox in MATLAB\SIMULINK has been used to achieve the training process. During the network training, all the computations are offline. The back-propagation algorithm is used in this work; this type is considered one of the most widely used algorithms because of the ease of implementation, robustness and stability. The learning stage of the network is performed by updating the weights and biases using a backpropagation algorithm with the gradient descent method in order to minimize a mean squared error performance index E by using Equation (15). The smaller the mean square error is the better performance and the accuracy of the network in real life will achieve.

$$E_p = \frac{1}{2} \cdot \sum_{j} \left(t_{pj} - o_{pj} \right)^2 \quad (14)$$

$$E = \sum_{p=1}^{m} E_p \quad (15)$$

Where P is the index of the output neurons, o_{pj} is the measured output of the outputs and t_{pj} is the desired output of the output neurons. In this work, the connection weights are updated by the following formula:

3 Simulation results

The MATLAB\SIMULINK software is used for simulation of the photovoltaic water pumping system. The system was simulated to verify the functionality and performance of the proposed ANN controller based on MPPT of water pumping system and to quantify how the proposed controller increased the system efficiency compared with directly connected system under different solar insolation levels. The complete simulation model of the system consists of a PV model

connected through a controlled buck chopper to PM DCM driving centrifugal pump load, also the ANN MPPT control unit is included.

However the buck converter is implemented without the output filter because it is feeding an inductive load. The parameters of each block used in this system are listed in Table (2). The effect of solar insolation level was given by two different stepwise cases, decrements and increments on the solar insolation. In the first case the solar insolation was decreased from 650 W/m^2 to 550 W/m^2 to 450 W/m^2 to 250 W/m^2 at the time instants 1s, 2s and 3s as shown in Figure 6. In the second case the solar insolation started from 200 W/m^2 and then stepped up to 600 W/m^2 with 100 W/m^2 steps at the time instants 1s, 2s, 3s and 4s, respectively, as shown in Figure 10. Figures 8 and 12, Figures 7 and 11 and Figures 9 and 13 The cases show the good matching between the motor speed ω_m, the PV power P_{pv} and the duty cycle control D of the ANN controller with the theoretical results when solar insolation is increasing or decreasing. The same figures indicate that the directly connected system is operating far from the MPP in both cases under all insolation conditions.

DC PM motor and the load pump data	
Rated motor voltage (V_a)	120V
Rated motor current (I_a)	9.2A
Rated motor speed (ω)	157.079 (rad/sec)
Armature resistance (R_a)	1.5Ω
Armature inductance (L_a)	0.2H
Voltage constant (K_e)	0.67609 V/(rad/sec)
Torque constant (K_T)	0.67609 Nm/A
Motor friction (A_m)	0.2 Nm
Moment of inertia (J)	0.02365 Kg.m2
Viscose friction coefficient (B)	0.002387 Nm/(read/sec)
Load torque constant (K_e)	0.00039 Nm/(read/sec)
Load friction (A_L)	0.3 Nm

Table 2: Parameters of the PM DC motor and the load pump.

When the solar insolation varies, the ANN control is seen to adjust the duty cycle to its optimal value. Hence the motor speed converges to an optimal value which corresponding to PV generation at the MPP, leading to maximization in the water pump discharge rate. A summary of the comparison between the ANN MPPT, directly connected system and theoretically expected result is shown in Table (3) and Table (4).

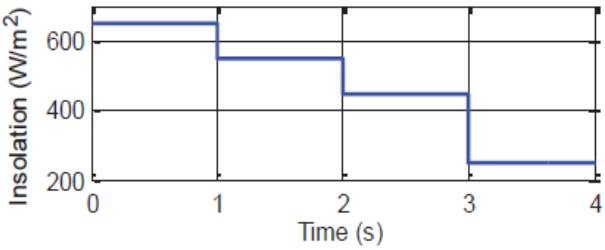

Figure 6: Change of solar irradiation case 1.

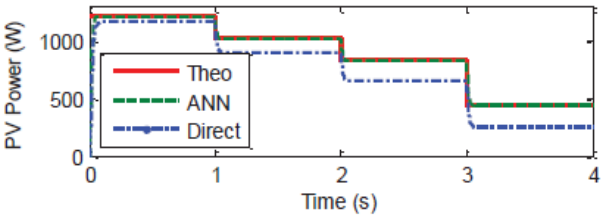

Figure 7: Variation of the P_{pv} as the G level changes case 1.

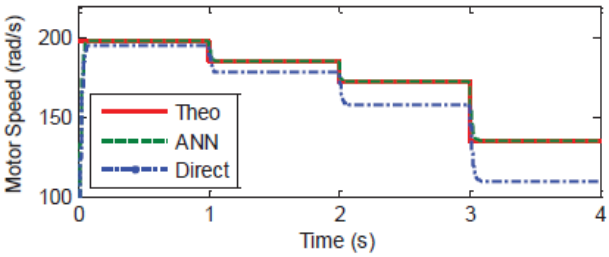

Figure 8: Variation of the ω_m as the G level changes case1.

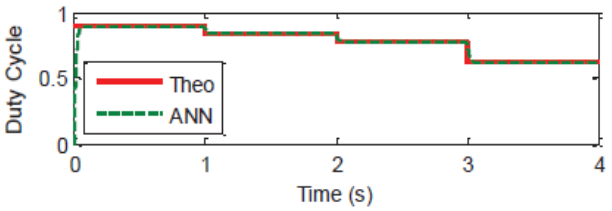

Figure 9: Variation of the D as the G level changes case1.

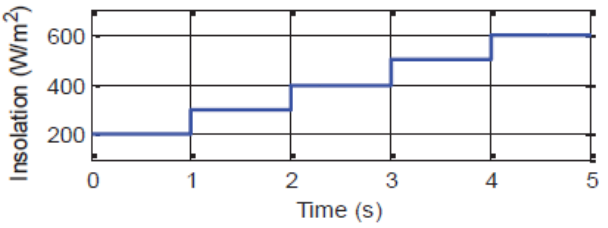

Figure 10: Change of solar irradiation case 2.

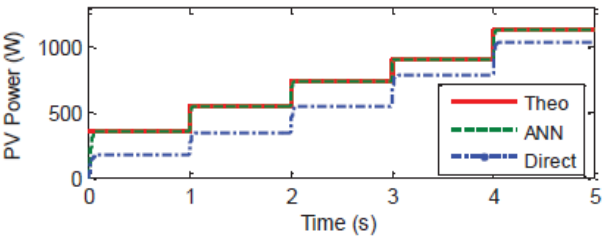

Figure 11: Variation of the P_{pv} as the G level changes case 2.

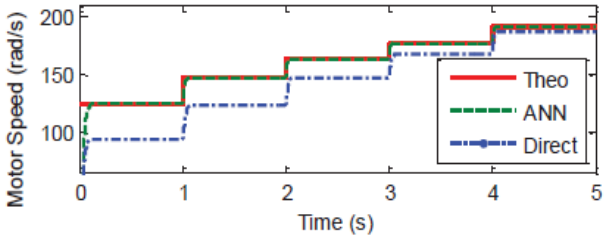

Figure 12: Variation of the ω_m as the G level changes case 2.

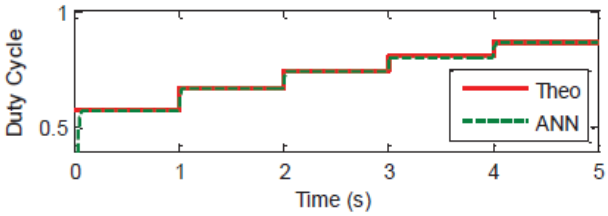

Figure 13: Variation of *D* as the *G* level changes case 2.

	G (W/m)	650	550	450	250
Direct	*Ppv* (W)	1165	903.1	654.9	249.1
	Wm (rad/s)	195	177.7	157.9	109.6
	Error %	0.042	0.114	0.207	0.425
ANN	*Ppv* (W)	1216	1019	829.0	433.9
	Wm (rad/s)	197.6	185.2	171.8	135.1
	D	0.889	0.83	0.777	0.618
	Error %	0	0.0002	0.00006	0
Theo	*Ppv* (W)	1216.0	1019.2	829.05	433.9
	Wm (rad/s)	197.6	185.3	171.8	135.1
	D	0.888	0.835	0.774	0.620

Table 3: Simulation results for given irradiation case 1.

	G (W/m)	200	300	400	500	600
Direct	*Ppv* (W)	171.2	337.1	540.7	776.1	1034
	Wm (rad/s)	94.59	123.1	147.1	168.1	186.7
	Error %	0.512	0.376	0.259	0.137	0.081
ANN	*Ppv* (W)	350.7	540.7	729.9	898.9	1125
	Wm (rad/s)	124.7	146.8	164	177.1	192.0
	D	0.573	0.667	0.742	0.800	0.866
	Error %	0.0003	0	0	0.00011	0.00044
Theo	*Ppv* (W)	350.8	540.7	729.9	899	1125.5
	Wm (rad/s)	124.6	146.8	164.0	177.2	192.2
	D	0.569	0.665	0.741	0.806	0.862

Table 4: Simulation results for given irradiation case 2.

4 Conclusion

This paper proposes an ANN-based MPPT controller for standalone PV water pumping systems. The proposed ANN-based MPPT controller has been simulated using MATLAB/SIMULINK. The optimized values of PV power and the corresponding motor speed values for various irradiation and temperature levels was used to train the ANN. Then, the trained ANN was used as the means to provide duty cycle *D* corresponding to the PV maximum power for any environmental variations. To verify the performance of the proposed ANN controller, a comparison has been carried out by means of Matlab simulation between the PV water pumping system with ANN MPPT control and the directly connected system under different solar irradiation levels. The simulation results show that the proposed ANN controller has excellent convergence MPP and the results show a good marching with the theoretical MPP under different insolation and weather conditions. The method allows the overall efficiency of the PV system to be improved.

References

[1] T. Esram and P. L. Chapman, "Comparison of Photovoltaic Array Maximum Power Point Tracking Techniques," *Energy Conversion, IEEE Transactions on*, vol. 22, pp. 439-449, 2007.

[2] V. Salas, *et al.*, "Review of the maximum power point tracking algorithms for stand-alone photovoltaic systems," *Solar Energy Materials and Solar Cells*, vol. 90, pp. 1555-1578, 2006.

[3] J. Xu, *et al.*, "ANN based on IncCond Algorithm for MPP Tracker," in *Bio-Inspired Computing: Theories and Applications (BIC-TA), 2011 Sixth International Conference on*, 2011, pp. 129-134.

[4] M. G. Villalva and J. R. Gazoli, "Comprehensive approach to modeling and simulation of photovoltaic arrays," *Power Electronics, IEEE Transactions on*, vol. 24, pp. 1198-1208, 2009.

[5] H.-L. Tsai, "Insolation-oriented model of photovoltaic module using Matlab/Simulink," *Solar energy*, vol. 84, pp. 1318-1326, 2010.

[6] G. Walker, "Evaluating MPPT converter topologies using a MATLAB PV model," *Journal of Electrical & Electronics Engineering*, vol. 21, pp. 49-56, 2001.

[7] S. R. Wenham, *Applied photovoltaics*: Routledge, 2011.

[8] M. H. Rashid, *Power Electronics - Circuits, Devices, and Applications 3rd Edition Pearson Education*: Academic Pr, 2004.

[9] R. Krishnan, *Switched reluctance motor drives: modeling, simulation, analysis, design, and applications*: CRC press, 2001.

[10] W. R. Anis and H. M. B. Metwally, "Dynamic performance of a directly coupled PV pumping system," *Solar energy*, vol. 53, pp. 369-377, 1994.

[11] A. Ghoneim, "Design optimization of photovoltaic powered water pumping systems," *Energy conversion and management*, vol. 47, pp. 1449-1463, 2006.

[12] J. Appelbaum, "Starting and steady-state characteristics of DC motors powered by solar cell generators," *Energy Conversion, IEEE Transactions on*, pp. 17-25, 1986.

[13] E. Karatepe, *et al.*, "Neural network based solar cell model," *Energy conversion and management*, vol. 47, pp. 1159-1178, 2006.

[14] R. Reed, "Pruning algorithms-a survey," *Neural Networks, IEEE Transactions on*, vol. 4, pp. 740-747, 1993.

[15] M. Veerachary and N. Yadaiah, "ANN based peak power tracking for PV supplied DC motors," *Solar energy*, vol. 69, pp. 343-350, 2000.

[16] H. Demuth, *et al.*, "Neural network toolbox™ 6," *User's guide*, 2008.

[17] B. L. Kalman and S. C. Kwasny, "Why Tanh: choosing a sigmoidal function," in *Neural Networks, 1992. IJCNN., International Joint Conference on*, 1992, pp. 578-581.

[18] B. Mutwali, "An Economic Analysis of Grid-tie Residential Photovoltaic System and Oil Barrel Price Forecasting: A Case Study of Saudi Arabia," 2013.